

HU ISSN 1586–2070

JOURNAL OF COMPUTATIONAL AND APPLIED MECHANICS

An Open Access International Journal

Published by the University of Miskolc

VOLUME 10, NUMBER 2 (2015)



MISKOLC UNIVERSITY PRESS

HU ISSN 1586–2070

JOURNAL OF COMPUTATIONAL AND APPLIED MECHANICS

An Open Access International Journal

Published by the University of Miskolc

VOLUME 10, NUMBER 2 (2015)



MISKOLC UNIVERSITY PRESS

EDITORS

László **BARANYI**, Institute of Energy Engineering and Chemical Machinery, University of Miskolc, H-3515 MISKOLC, Hungary, e-mail: arambl@uni-miskolc.hu

István **PÁCZELT**, Institute of Applied Mechanics, University of Miskolc, H-3515 MISKOLC, Hungary e-mail: mechpacz@uni-miskolc.hu

György **SZEIDL**, Institute of Applied Mechanics, University of Miskolc, H-3515 MISKOLC, Hungary e-mail: Gyorgy.SZEIDL@uni-miskolc.hu

EDITORIAL BOARD

Edgár **BERTÓTI**, Institute of Applied Mechanics, University of Miskolc, H-3515 MISKOLC, Hungary, e-mail: edgar.bertoti@uni-miskolc.hu

Attila **BAKSA**, Institute of Applied Mechanics, University of Miskolc, H-3515 MISKOLC, Hungary, attila.baksa@uni-miskolc.hu

István **ECSEDI**, Institute of Applied Mechanics, University of Miskolc, H-3515 MISKOLC, Hungary, mechecs@uni-miskolc.hu

Ulrich **GABBERT**, Institut für Mechanik, Otto-von-Guericke-Universität Magdeburg, Universitätsplatz 2, 39106 MAGDEBURG, Germany, ulrich.gabbert@mb.uni-magdeburg.de

Zsolt **GÁSPÁR**, Department of Structural Mechanics, Budapest University of Technology and Economics, Műegyetem rkp. 3, 1111 BUDAPEST, Hungary, gaspar@ep-mech.me.bme.hu

Robert **HABER**, Department of Theoretical and Applied Mechanics, University of Illinois at Urbana-Champaign, 216 Talbot Lab., 104 S. Wright Str., URBANA, IL 61801, USA, r-haber@uiuc.edu

Csaba **HÓS**, Department of Hydraulic Machines, Budapest University of Technology and Economics, Műegyetem rkp. 3, 1111 BUDAPEST, Hungary, HOSCSABA@vizgep.bme.hu

Károly **JÁRMAI**, Institute of Logistics, University of Miskolc, H-3515 MISKOLC, Hungary, altjar@uni-miskolc.hu

László **KOLLÁR**, Department of Strength of Materials and Structures, Budapest University of Technology and Economics, Műegyetem rkp. 3. K.II.42., 1521 BUDAPEST, Hungary, lkollar@eik.bme.hu

József **KÖVECSÉS**, Mechanical Engineering Department 817 Sherbrooke Street West, MD163 Montreal, Quebec H3A 2K6 jozsef.kovecses@mcgill.ca

Márta **KURUTZ**, Department of Structural Mechanics, Budapest University of Technology and Economics, Műegyetem rkp. 3, 1111 BUDAPEST, Hungary, kurutzm@eik.bme.hu

Herbert **MANG**, Institute for Strength of Materials, University of Technology, Karlsplatz 13, 1040 VIENNA, Austria, Herbert.Mang@tuwien.ac.at

Sanjay **MITTAL**, Department of Aerospace Engineering, Indian Institute of Technology Kanpur, UP 208 016, India, smittal@iitk.ac.in

Zenon **MRÓZ**, Polish Academy of Sciences, Institute of Fundamental Technological Research, Swietokrzyska 21, WARSAW, Poland zmroz@ippt.gov.pl

Gyula **PATKÓ**, Institute of Machine Tools and Mechatronics, University of Miskolc, H-3515 MISKOLC, Hungary, patko@uni-miskolc.hu

Jan **SLADEK**, Ústav stavbeníctva a architektúry, Slovenskej akadémie vied, Dubróvska cesta 9, 842 20 BRATISLAVA, Slovakia, usarslad@savba.sk

Gábor **STÉPÁN**, Department of Applied Mechanics, Budapest University of Technology and Economics, Műegyetem rkp. 3, 1111 BUDAPEST, Hungary, stepan@mm.bme.hu

Barna **SZABÓ**, Department of Mechanical Engineering and Materials Science, Washington University, Campus Box 1185, ST. LOUIS, MO 63130, USA, szabo@wustl.edu

Balázs **TÓTH**, Institute of Applied Mechanics, University of Miskolc, 3515 MISKOLC, Hungary, balazs.toth@uni-miskolc.hu

HONORARY EDITORIAL BOARD MEMBERS

Imre **KOZÁK**, Institute of Applied Mechanics, University of Miskolc, H-3515 Miskolc-Egyetemváros, Hungary

Tibor **CZIBERE**, Department of Fluid and Heat Engineering, University of Miskolc, H-3515 Miskolc-Egyetemváros, Hungary

R. Ivan **LEWIS**, Room 2-16 Bruce Building, Newcastle University, NEWCASTLE UPON TYNE, NE1 7RU, UK

Gábor **HALÁSZ**, Department of Hydraulic Machines, Budapest University of Technology and Economics, Műegyetem rkp. 3, 1111 BUDAPEST, Hungary,

PREFACE

1. INTRODUCTION

The present issue of JCAM is dedicated to two excellent scientists: Professor Barna Szabó, who turned 80 in 2015 and Professor Imre Kozák, who is 85 this year. For political reasons Professor Szabó had to leave Hungary in 1956 – he was a student of the University of Miskolc between 1954 and 1956. He has made a scientific career and did and still does his best to provide help and support to the University of Miskolc, more precisely to the Institute of Applied Mechanics (which was called the Department of Mechanics until 2014).

Professor Kozák graduated from the University of Miskolc in 1954 and has been working for the university since then. He chaired the Department of Mechanics from 1971 till 1993 and had a very significant influence on the scientific activity of the department in various ways: as a scientific leader of promising young PhD students and by starting a separate track in applied mechanics.

Further information about their scientific and educational activities are presented in Sections 1 and 2 of this Preface.

With this and the next issue their former and present students, co-workers and friends wish them many more productive years in good health.

2. A PROFESSIONAL LIFE DEDICATED TO COMPUTATIONAL MECHANICS PROFESSOR BARNA SZABÓ 80 YEARS OLD

Barna Szabó was born in Martonvásár, Hungary in 1935. After graduating from the Franciscan High School in Esztergom in 1954, he was admitted to the Faculty of Mining Engineering of the Technical University of Heavy Industry in Miskolc (now University of Miskolc). Following the failed Hungarian uprising in 1956 he emigrated to Canada, where he resumed his undergraduate studies at the University of Toronto.

He was employed as Mining Engineer by the International Nickel Company of Canada (INCO) in Thompson, Manitoba between 1960 and 1962. In 1962 he joined H. G. Acres Ltd., a large civil engineering firm located in Niagara Falls, Ontario, where he was employed in the Department of Applied Mechanics. He worked on the design of major hydroelectric power stations, such as the Jean-Lesage Generating Station in Quebec and the Churchill Falls Generating Station in Labrador, as well as on a variety of interdisciplinary projects. In the following year he began part-time studies at the State University of New York at Buffalo where he received the degree



Master of Science in Civil Engineering in 1966. Recognizing that digital computers would play an increasingly important role in the practice of engineering, he decided to continue his graduate studies in that area. He received his Ph.D. degree in 1968.

From 1968 until his retirement in 2014 he was a member of the Faculty of Engineering and Applied Science of Washington University in St. Louis, Missouri. He was named The Albert P. and Blanche Y. Greensfelder Professor of Mechanics in 1975 and appointed Director of the Center for Computational Mechanics in 1977.

From the very beginning his research activities were guided by the idea that engineering decisions cannot be based on computed information unless procedures for the estimation and control of the errors of approximation are available.

An experimental computer code, called COMET-X, was developed under his direction at the Center for Computational Mechanics. The distinguishing feature of this code was that converging sequences of finite element solutions could be generated based on hierarchic sequences of finite element spaces. This allowed investigation of the convergence characteristics of what is known today as the p -version of the finite element method.

He observed that increasing the polynomial degree of elements on a fixed mesh results in a rate of convergence in energy norm that is faster than if fixed p and uniform or quasi-uniform mesh refinement, known as the h -version, were used, even when the solution being approximated contained singular points. This result was surprising because it contradicted the then generally accepted interpretation of a key mathematical theorem concerning the asymptotic rate of convergence of the finite element method. This contradiction was demonstrated in a paper published 1978 [1].

The practical importance of the early results obtained by Szabó and his research team was recognized by the Istituto Sperimentale Modelli e Strutture (ISMES) in Bergamo, Italy, where the first industrial-scale implementation of the p -version was undertaken with the goal to perform numerical simulation of the mechanical response of arch dams in the Italian Alps as part of a safety monitoring system mandated by the government of Italy. The justification for early adoption of the new methodology was based on the fact that solution verification was a technical requirement which could not be met by conventional methods. The code developed at ISMES is called FIESTA.

The term " p -version of the finite element method" first appeared in a publication 1981 [2] in which the theoretical foundations were established of a discretization strategy whereby the finite element mesh is fixed and the polynomial degree p of the elements is progressively increased. The results presented in this paper motivated research in the applied mathematics community on the properties of high order finite element methods, which continues to this day.

Today the distinction between the h - and p -versions exists primarily for historical and theoretical reasons. Conceptually the h -version is a subset of the p -version, in the sense that any implementation of the p -version can be used in such a way that p is fixed and the mesh is progressively refined. In practical applications the design of the mesh and the choice polynomial degrees are both important. In fact, it is possible to realize exponential rates of convergence when the p -version is used in combination with proper mesh design. This point was first discussed from the engineering perspective [3] and from the theoretical perspective [4] in 1986. Details are available in a textbook published in 1991 [5].

The first industrial-scale implementation of the p -version in the United States was undertaken by Noetic Technologies Corporation in St. Louis in 1984, which produced

the FEA software PROBE. The first release of PROBE (1985) featured a number of innovations, which included posteriori error estimation, the realization of exponential convergence rates and superconvergent extraction of stress intensity factors. The first applications of PROBE were in the aerospace industry in support of mechanical fatigue and damage tolerance modeling. Other large implementations of the p -version were MECHANICA¹ by the Rasna Corporation in 1987 and STRIPE by the Aeronautical Research Institute of Sweden² in 1988.

Szabó recognized that while solving mathematical problems by approximate methods, subject to estimation and control of the errors of approximation, was fundamentally important, it is also of fundamental importance from the engineering and scientific perspectives to formulate mathematical problems that simulate some specific aspects of a physical reality with sufficient reliability to justify basing engineering decisions on them. He outlined the concept of hierarchic sequences of mathematical models with reference to structural plates and shells at a conference in 1986³ which was published two years later [6]. In this view any mathematical model is understood to be a special case of a more comprehensive model, one with fewer limitations imposed by the assumptions incorporated in the model. Szabó published a textbook, co-authored by Professor Ivo Babuška, on the formulation, verification and validation of mathematical models in 2011 [7]. The Chinese translation of this book was published in 2013.

In order to make development of a computational framework designed to support hierarchic modeling and discretization strategies possible, it was necessary to assemble a professional team of engineers and programmers. To this end Szabó co-founded a company, called Engineering Software Research and Development, Inc. (ESRD) in 1989. The mission of this company is “to create and market software tools for the advancement of the quality, reliability and timeliness of information that serves the engineering decision-making process⁴”. ESRD produces and markets the software StressCheck, which is the only finite element analysis software tool designed to meet the technical requirements of simulation governance [8]. It is used primarily in the aerospace sector. ESRD received the Boeing Gold Performance Excellence Award in 2014.

Szabó has published over 150 papers and two textbooks. He is a founding member and Fellow of the US Association for Computational Mechanics. Among his honors are election to the Hungarian Academy of Sciences as External Member in 1995 and Doctor Honoris Causa, University of Miskolc in 1998.

Szabó was honored on the occasion of his 65th birthday by an international conference held in St. Louis in 2000⁵. Two journals issued special editions in connection with that conference^{6, 7}.

¹Now called Creo Simulate.

²Now called the Aeronautics Division of the Swedish Defense Research Agency.

³The Impact of Mathematical Analysis on the Numerical Solution of Engineering Problems. University of Maryland, College Park, MD September 17–19, 1986.

⁴www.esrd.com

⁵International Conference on p and hp Finite Element Methods: Mathematics and Engineering Practice.

⁶Int. J. Numer. Meth. Engng. **53**(1) (2002), Guest Editors: Z. Yosibash and M. Suri

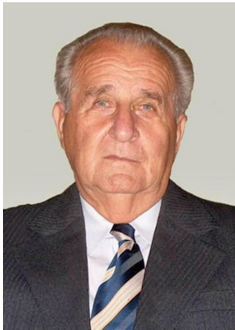
⁷Computers and Mathematics with Applications, **46**(1), (2003), Guest Editors: Z. Yosibash and M. Suri.

The Council of his hometown, Martonvásár, awarded him honorary citizenship in 2015.

REFERENCES

- [1] B. Szabó and A. Mehta. “Convergent finite element approximations in fracture mechanics.” In: *Int. J. Numer. Meth. Engng.* 12 (1978), pp. 551–560.
- [2] I. Babuška, B. Szabó, and N. Katz. “The p -version of the finite element method.” In: *SIAM J. Numer. Anal.* 12 (1981), pp. 515–545.
- [3] B. Szabó. “Mesh design for the p -version of the finite element method.” In: *Computer Methods in Applied Mechanics and Engineering* 55.1 (1986), pp. 181–197.
- [4] B. Guo and I. Babuška. “The hp -version of the finite element method.” In: *Computer Methods in Applied Mechanics and Engineering* 1.1 (1986), pp. 21–41.
- [5] B. Szabó and I. Babuška. *Finite Element Analysis*. John Wiley & Sons Inc., New York, 1991.
- [6] B. Szabó and G. J. Sahrman. “Hierarchic plate and shell models based on p -extension.” In: *Int. J. Numer. Meth. Engng.* 26 (1988), pp. 1855–1881.
- [7] B. Szabó and I. Babuška. *Introduction to Finite Element Analysis: Formulation, Verification and Validation*. John Wiley & Sons Inc., New York, 2011.
- [8] B. Szabó and R. Actis. “Simulation governance: Technical requirements for mechanical design.” In: *Computer Methods in Applied Mechanics and Engineering* 249 (2012), pp. 158–168.

3. A PROFESSIONAL LIFE DEDICATED TO MECHANICS OF SOLID BODIES PROFESSOR IMRE KOZÁK 85 YEARS OLD



Imre Kozák was born in Gór, a small village in Western Hungary, in 1930. After graduating from the grammar school Nagy Lajos in Szombathely in 1949 he was admitted to the Faculty of Mechanical Engineering of the Technical University of Heavy Industry in Miskolc – today’s University of Miskolc. In 1953 he obtained an M.Sc. degree in Mechanical Engineering. He began his graduate studies at the Department of Mechanics of the same university with the then Department Head István Sályi as his scientific supervisor, in 1953. This work later culminated in a Ph.D. thesis entitled *Small elastic plastic deformations of a thin walled cylindrical shell subjected to internal pressure*. This thesis was the first in which the Prandtl-Reuss equations were applied to bent cylindrical shells. The main difficulty of the problem raised lay in the fact that the solution required large amounts of computations before the advent of computers [1]. He was awarded his Ph.D. degree in 1961 and was appointed Associate Professor at the Department of Mechanics.

In 1967 he took part in the organization of the first Colloquium on Plasticity held in Miskolc in honor of Professor Endre Reuss, who was a well-known specialist in this field. This was the first scientific meeting of mechanical nature in Hungary after

World War II.

From 1967 to 1970 he was the Prorektor responsible for scientific matters.

In 1968 Kozák was appointed Full Professor. Three years later, in 1971 he took over leadership at the Department of Mechanics and held the post of Head of Department till 1993.

Since 1971 the Hungarian Conference on Engineering Mechanics has been organized at the University of Miskolc every four years. He has taken part in the preparations and organization of the conferences on each occasion.

From 1966 to 1969 he greatly contributed in cooperation with Professor Béda (Technical University of Budapest) and Professor Sályi to a new initiative by launching academic programs for mechanical engineers specialized in theoretical and applied mechanics. The students who chose the new program of theoretical and applied mechanics graduated from the university with an M.Sc. degree. He took part in designing the new curriculum and gave lectures, for the first time in the academic programs for mechanical engineers in Hungary on such subjects as Theory of Shells, Mechanics of Continua, Differential Geometry with Indicical Notations etc. It is worthy of mention that eight of his former students are Full Professors today.

In the years 1972 to 1978 he was appointed General Prorektor of the University of Miskolc. After office hours he devoted time to updating the materials of the fundamental courses of engineering mechanics (Statics, Strength of Materials, Dynamics, Theory of Vibration).

In 1978 he received the Gold Medal of the Order of Labor.

As regards his research, his aim was to work out a linear shell theory in terms of stresses. Because of the unresolved problems in connection with the compatibility of strain fields – what the independent, necessary and sufficient conditions are the strains should meet in order to be compatible if the displacements are not variables of the governing equations, what the solution to the Southwell paradox is⁸, – he had to do some supplementary research.

As regards his results, it is worthy of mention that he modified and supplemented the dual formulation of linear elasticity and the system of dual variational principles by solving the aforementioned Southwell paradox, i.e., by pointing out that only three of the six Saint-Venant compatibility conditions are independent, provided that the so-called compatibility boundary conditions are satisfied, and showing that the independent compatibility conditions and independent stress functions should be chosen according to the same rule [2, 3, 4]. Based on these results he was able to establish a general theory of shells in dual system regarding the stresses as fundamental variables [5]. This work led to the thesis *Theory of thin shells in terms of stresses*. After its defense the Committee of Scientific Qualifications at the Hungarian Academy of

⁸It was Southwell (1936, 1938) who first derived the compatibility conditions from the principle of minimum complementary energy as a variational principle. He pointed out that, by utilizing Maxwell's (1870) and Morera's (1892) solutions, only three of the six Saint-Venant compatibility conditions follow from the principle of minimum complementary energy. Since any stress condition can be given in terms of three stress functions chosen appropriately, he arrived at a contradiction, because for the displacements to be single-valued all the six Saint-Venant compatibility conditions should be satisfied. This contradiction was named Southwell's paradox after him. After Southwell's papers the following problems remained unresolved. Is it sufficient for the strains to satisfy three Saint-Venant compatibility equations? If so, which three? If so, are there further conditions to satisfy?

Sciences awarded him the degree Doctor of Science in 1981.

From 1980 to 1983 he was again the Prorector responsible for scientific matters.

Between 1983 and 1985 Kozák wrote the textbooks *Continuum Mechanics* (in Hungarian)] and *Mechanics of Elastic Bodies* [6] (in Hungarian)] with co-authors. The book *Continuum Mechanics* contains his most important results concerning the investigations he carried out in a dual system.

In the late 80s Kozák began to deal with the relative motion of continua. By relative motion we mean the motion of a solid body (continuum) with respect to an arbitrary curvilinear coordinate system, which is also in motion and therefore is capable of deformation (one can regard it as if it were a fictitious body). This motion is distinguished from the motion of the solid body (continuum) relative to an arbitrary but fixed curvilinear coordinate system (absolute motion). Within the framework of these investigations he set up the necessary formalism. In headwords: relative and absolute velocity fields, relative and absolute deformations, deformation gradients, strain tensors, volume and surface elements, material time derivatives (for the deformation gradients, volume and surface elements), some questions of the physically objective material time derivatives of the strain tensors, principle of virtual power and work in each configuration with special regard to the case of follower loads. One of his major results was the derivation of some new and known materially objective (invariant under any coordinate transformation) time derivatives with a systematic method [7, 8, 9].

In 1988 he won the Apáczai Csere János Prize. In 1990 and 1993 he was awarded the medals Pro Unversitate and Pro Urbe of Miskolc.

The graduate education that leads to the degree of Doctor of Philosophy had earlier been controlled formally by the Hungarian Academy of Sciences (Russian system) but was taken over by the hungarian universities in 1990. He took part in establishing new curricula for the graduate students at the Faculty of Mechanical Engineering of the University of Miskolc.

A revised and supplemented English edition of his book *Continuum Mechanics* [10] was published in 1995. This edition contains, among others, Kozák's method of deriving materially objective time derivatives.

He was elected corresponding member of the Hungarian Academy of Sciences in 1995. He gave his inaugural lecture with the title *Continuum Mechanics and Geometry* at the Seat of the Miskolc Committee of the Hungarian Academy of Sciences in 1996.

In 1996 the City Council of Miskolc awarded Kozák honorary citizenship.

In the '90s he proceeded with his research in continuum mechanics. The results are applicable to investigating geometrically non-linear static stability problems and postcritical equilibrium paths. Some of the results are listed below very briefly:

- The incremental form of the principle of virtual displacements for follower loads and the derivation of the formulae for the Newton–Raphson iteration procedure that solves the corresponding non-linear problem. When applying a finite element discretization it is reasonable to introduce, in addition to the usual linear and geometric stiffness matrices, the load-correction stiffness matrix which is symmetric if the follower loads have a potential and is asymmetric if the follower loads have no potential.

- The Newton-Raphson iteration can be initiated not only from an equilibrium configuration under the given load but from an arbitrary non-equilibrium configuration provided that the latter is appropriately chosen, independently of the loads. In this way both fundamental equilibrium paths and bifurcation paths as well as complementary paths and limit points can be investigated. The critical load can be determined by the path following method and the determinant search algorithm. The equilibrium surfaces due to the geometrical imperfections and the load parameter(s), their stable and unstable regions and the critical loads can be determined numerically [8].
- It has been shown that linear eigenvalue problems for follower loads cannot be investigated properly if the load correction matrix is left out of consideration.

In 1999 Kozák won, together with his colleague István Páczelt, the Széchenyi Prize which is the highest scientific award in Hungary.

He was elected an ordinary member of the Hungarian Academy of Sciences in 2001. He gave his inaugural lecture with the title *3D Stability Analysis of the Equilibrium States of Solid Bodies for Deformation Dependent Loads* at the Seat of the Miskolc Committee of the Hungarian Academy of Sciences in the same year.

Since 2000 he has been working for the Institute of Applied Mechanics as a professor emeritus.

In 2013 he was awarded the Hungarian Decoration With Cross.

Kozák participated actively in the work of a number of scientific associations and societies. Since 1966 he has been a member of the today's Committee of Theoretical and Applied Mechanics of the Hungarian Academy of Sciences. Since 1973 he has also been a member of the Hungarian National Committee of the International Union of Theoretical and Applied Mechanics. From 1984 to 1996 he was a member of the Committee of Scientific Qualifications at the Hungarian Academy of Sciences.

Kozák has been taking part in the work of the Miskolc Committee of the Hungarian Academy of Sciences since it came into existence in 1979. Since its foundation he has been a member of the Expert Committee of Mechanical Engineering. Between 1984-96 he was the Chair of the Club Council. In 1990 he was elected a member of the Committee. From 1993 to 1996 he was the vice chairman of the Committee. From 1996 till 2002 he was the Chairman of the Committee.

Kozák has visited a number of foreign cities (Vienna, Graz, Leoben, Prague, Brno, Bratislava, Kosice, Cracow, Berlin, Magdeburg, Dresden, St. Petersburg, Moscow, Kharkov, Frunze, Detroit, Algir, Oran, Constantine).

He is an excellent lecturer. He has the gift to present very complicated things – relationships, lines of thoughts – in an elegant and simple manner and to make his audience understand what at first seems difficult. Those who have had the privilege to attend his courses will remember these lectures fondly.

He has written altogether 17 university textbooks for his students on Statics, Strength of Materials, Dynamics, Elasticity, Plasticity, Theory of Shells etc. These books came out in Hungarian.

He has published a total of 61 scientific papers so far.

Kozák has been the scientific supervisor of 8 Ph.D. dissertations and a number of M.Sc. theses. Four of his PhD students (Edgár Bertóti, Béla Csizmadia, György Szeidl and Károly Váradi) are full professors.

REFERENCES

- [1] I. Kozák. “Small Elastic-Plastic Plastic Deformation (Caused by Internal Pressure) of a Thin-Walled Tube.” In: *Acta Technica Hungarorum* 55.1-3 (1966), pp. 7–26.
- [2] I. Kozák. “Notes on the field equations with stresses and the boundary conditions in the linearized theory of elastostatics.” In: *Acta Technica Hungarorum* 90.3-4 (1980), pp. 221–245.
- [3] I. Kozák. “Determination of compatibility boundary conditions in linear elastostatics with the aid of the principle of minimum complementary energy.” In: *Publ. Techn. Univ. Heavy Industry, Miskolc, Ser. D. Natural Sciences* 34.2 (1980), pp. 83–98.
- [4] I. Kozák. “Remarks and contributions to the variational principles of the linearized theory of elasticity in terms of the stress functions.” In: *Acta Technica Hungarorum* 92.1-2 (1981), pp. 45–65.
- [5] I. Kozák. “Construction of an approximate linear shell theory by asymptotic integration of the equations of elasticity in terms of stresses.” In: *Advances in Mechanics* 6.1-2 (1983), pp. 91–110.
- [6] G. Béda and I. Kozák. *Mechanics of Elastic Bodies*. (in Hungarian). Műszaki Könyvkiadó, Budapest, 1987.
- [7] I. Kozák. “Relative motion of continua and the principle of virtual displacements.” In: *Publ. Univ. of Miskolc, Series D. Natural Sciences, Mathematics* 37 (1997), pp. 59–75.
- [8] I. Kozák. “Time rates of tensors in continuum mechanics under arbitrary time dependent transformations, Part i. Material time rates.” In: *Journal of Computational and Applied Mechanics* 2.2 (2001), pp. 205–221.
- [9] I. Kozák. “Time rates of tensors in continuum mechanics under arbitrary time dependent transformations, Part ii. Systems of materially objective time rates of tensors.” In: *Journal of Computational and Applied Mechanics* 3.2 (2002), pp. 141–156.
- [10] G. Béda, I. Kozák, and J. Verhás. *Continuum Mechanics*. ISBN:963-05-6758-X. Academic Publisher, Budapest, 1995.

NUMERICAL SOLUTION TO BOUNDARY LAYER PROBLEM OF NON-NEWTONIAN FLUID FLOW OVER A MOVING SURFACE

GABRIELLA BOGNÁR AND ZOLTÁN CSÁTI

Department of Machine and Product Design, University of Miskolc
3515 Miskolc, Miskolc–Egyetemváros, Hungary
v.bognar.gabriella@uni-miskolc.hu, machcsz@uni-miskolc.hu

[Received: June 01, 2015, Accepted: October 26, 2015.]

Dedicated to Professor Barna Szabó on the occasion of his eightieth birthday

Abstract. The paper generalizes the classical Sakiadis problem for non-Newtonian power law fluids. Applying the similarity method the governing partial differential equations are transformed to one ordinary differential equation. The resulting boundary value problem is solved by Chebyshev spectral collocation on a truncated domain. The effect of the power-law exponent on the numerical solutions is investigated.

Mathematical Subject Classification: 34B40, 65N35

Keywords: non-Newtonian fluid, boundary layer, similarity method, spectral method

1. INTRODUCTION

The study of a flow generated by a moving surface in an otherwise quiescent fluid plays a significant role in many material processing applications such as hot rolling, metal forming and continuous casting (see e.g., Altan et al. [1], Fisher [2], Tadmor and Kline [3]). Boundary layer flow induced by the uniform motion of a continuous plate in a Newtonian fluid has been analytically studied by Sakiadis [4] and experimentally by Tsou et al. [5]. A polymer sheet extruded continuously from a die travelling between a feed roll and a wind-up roll was investigated by Sakiadis [6], [4]. For the laminar velocity field of a Newtonian fluid Tsou et al. [5] showed in their analytical and experimental study that the obtained analytical results are in excellent agreement with the measured data, therefore it proves that the mathematical model for boundary layer on a continuous moving surface describes a physically realizable flow.

Recently, a number of researchers are motivated to investigate the problem of boundary layer flow due to its application in engineering processes. Flows along a continuously moving surface are encountered in several processes, for example the thermal and moisture treatment of materials, particularly in processes involving continuous pulling of a sheet through a reaction zone, in metallurgy, the paper industry,

and in the manufacture of polymeric sheets. Fluids for which the relationship between the shear stress and the rate of strain is non-linear at given temperature and pressure are said to be non-Newtonian. Most fluids such as molten plastics, artificial fibres, petroleum, blood and polymer solutions are considered as non-Newtonian fluids. Schowalter [7] introduced the concept of the boundary layer in the theory of non-Newtonian power-law fluids. Acrivos, Shah and Petersen [8] have investigated the steady laminar flow of non-Newtonian fluids over a plate.

Our aim is to examine the solutions to the boundary layer problem of a power-law non-Newtonian fluid along an impermeable flat surface moving with a constant velocity in an otherwise quiescent fluid environment. In the absence of an exact solution in closed form, numerical solutions for the velocity distribution in the boundary layer for different power-law exponents will be presented, and the dependence of the skin friction parameter and the boundary layer thickness on the power-law exponent n are examined.

In this paper, we apply a spectral method for the solution to the boundary value problem (BVP). Spectral methods were first applied in the 1970s but their mathematical foundation were endowed by Gottlieb and Orszag in 1977. By the 1990s, spectral methods had become attractive tools for scientists dealing with fluid mechanics and meteorological modeling [9]. In contrast to the finite difference or the finite element methods which are local in character, spectral methods are global methods. With the advent of the spectral element method, complicated domains can be handled. In spite of being mainly used in fluid mechanics, nowadays, they are more and more frequently utilized in biomechanics, astrophysics and the study of electromagnetic waves.

The text is organized into four sections. In Section 2 the governing equations describing the phenomenon are introduced. In Section 3 a BVP of nonlinear ordinary differential equations is derived by applying the similarity method. Section 4 is devoted to the numerical solution of the BVP using a spectral collocation method. Finally, we summarize the consequences of our investigations in Section 5.

2. GOVERNING EQUATIONS

Consider a steady, two-dimensional, laminar boundary layer flow of viscous, incompressible power-law fluid past a continuously moving plate passing through with constant velocity U_w in an otherwise quiescent fluid. The x -axis extends parallel to the plate and the y -axis is perpendicular to the x -axis. The flat surface is placed at $y = 0$. The boundary layer equations for a flow over a flat plate neglecting pressure gradient and body forces can be described by the following continuity and momentum equations [5]:

$$\frac{\partial u}{\partial x} + \frac{\partial v}{\partial y} = 0, \quad (2.1)$$

$$u \frac{\partial u}{\partial x} + v \frac{\partial u}{\partial y} = \frac{1}{\rho} \frac{\partial \tau_{yx}}{\partial y}, \quad (2.2)$$

where u and v denote the horizontal and vertical fluid velocity component, respectively, and τ_{yx} is the shear stress. Hereafter, we apply the Ostwald–de Waele power-law constitutive equation for the non-Newtonian model [10]:

$$\tau_{yx} = K \left| \frac{\partial u}{\partial y} \right|^{n-1} \frac{\partial u}{\partial y}, \tag{2.3}$$

where K is the consistency and n is the power-law exponent. If $n < 1$, the fluid is pseudoplastic, if $n > 1$ it is dilatant while the fluid is Newtonian for $n = 1$. Substituting Eq. (2.3) into (2.2), the fundamental equation is obtained for the velocity field. Equation (2.1) can identically be satisfied when the stream function ψ is introduced as $u = \partial\psi/\partial y$, $v = -\partial\psi/\partial x$. Then from (2.3) we get a third order nonlinear partial differential equation:

$$\psi_y \psi_{yx} - \psi_x \psi_{yy} = \gamma (|\psi_{yy}|^{n-1} \psi_{yy})_y, \tag{2.4}$$

where $\gamma = K/\rho$ and the subscripts denote the partial differentiation with respect to the appropriate variable. The wall is impermeable and no-slip boundary condition is supposed. Furthermore, the ambient fluid velocity is zero and we suppose that the plate is moving at a constant velocity; therefore the boundary conditions can be formulated as follows:

$$u(x, 0) = U_w, \quad v(x, 0) = 0, \quad \lim_{y \rightarrow \infty} u(x, y) = 0. \tag{2.5}$$

3. SIMILARITY SOLUTION

The similarity method is applied for the transformation of (2.4) to an ordinary differential equation. Let us introduce similarity variables η and $f(\eta)$ as

$$\eta = a \frac{y}{x^\beta}, \quad \psi = bx^{-\alpha} f(\eta), \tag{3.1}$$

where a, b, α, β are constants, which will be determined from the invariance condition for the differential equation and the three boundary conditions. Substituting (3.1) into Eq. (2.4) one obtains

$$a^2 b^2 x^{-2\alpha-2\beta-1} [a f f'' - (\alpha + \beta) f'^2] = \gamma (a^2 b)^n x^{(-\alpha-2\beta)n} \frac{a}{x^\beta} [|f''|^{n-1} f'']',$$

where the primes denote differentiation with respect to η . One can observe that the differential equation remains invariant if

$$(2n - 1)\beta + (n - 2)\alpha = 1 \tag{3.2}$$

and

$$a^2 b^2 = \gamma (a^2 b)^n a \tag{3.3}$$

hold.

Rewriting the boundary conditions by applying the stream function, one may establish other connections among the parameters. According to (3.1), in the third condition of (2.5) if $y \rightarrow \infty$, i.e. $\eta \rightarrow \infty$, for fixed x we get

$$\lim_{y \rightarrow \infty} \psi_y(x, y) = \lim_{\eta \rightarrow \infty} f'(\eta) = abx^{-\alpha-\beta} f'(\eta) = 0.$$

Let us choose $f'(\infty) = \lim_{\eta \rightarrow \infty} f'(\eta) = 0$, then

$$\alpha + \beta = 0. \quad (3.4)$$

At $\eta = 0$ setting

$$f'(0) = 1$$

implies

$$ab = U_w \quad (3.5)$$

from the first condition in (2.5). On the other hand, from Eq. (3.2) and from Eq. (3.4) it follows that

$$\beta = -\alpha = \frac{1}{n+1}.$$

The second condition in (2.5) is expressed as

$$-\psi_x(x, 0) = \frac{b}{n+1} x^{-\frac{n}{n+1}} [\eta f'(\eta) - f(\eta)] = 0,$$

which is satisfied for $\eta = 0$ if

$$f(0) = 0.$$

Consequently, the parameter values are the following:

$$\begin{aligned} \alpha &= -\frac{1}{n+1}, & \beta &= \frac{1}{n+1}, \\ a &= \gamma^{-\frac{1}{n+1}} U_w^{\frac{2-n}{n+1}}, & b &= \gamma^{\frac{1}{n+1}} U_w^{\frac{2n-1}{n+1}}. \end{aligned}$$

The connection among the dimensionless similarity variables and the original velocity is

$$u(x, y) = U_w f'(\eta), \quad (3.6)$$

$$v(x, y) = \frac{U_w}{n+1} Re_x^{-\frac{1}{n+1}} (\eta f'(\eta) - f(\eta)), \quad (3.7)$$

$$\eta = Re_x^{\frac{1}{n+1}} \frac{y}{x}, \quad Re_x = \frac{U_w^{2-n} x^n}{\gamma}, \quad (3.8)$$

where Re_x is the local Reynolds number. Instead of the BVP of partial differential equations (2.1), (2.2), (2.3) and (2.5) we obtained by the similarity analysis the BVP of a nonlinear ODE (3.9) and (3.10)

$$\left(|f''|^{n-1} f'' \right)' + \frac{1}{n+1} f f'' = 0 \quad (3.9)$$

$$f(0) = 0, \quad f'(0) = 1, \quad \lim_{\eta \rightarrow \infty} f'(\eta) = 0. \quad (3.10)$$

Since the velocity field can be calculated from $f(\eta)$ using (3.6)-(3.7), our goal is to determine the solution to (3.9)-(3.10). We also want to examine the boundary layer thickness and $f''(0)$. The latter one is necessary for computation of the drag coefficient

$$C_D = (n+1)^{\frac{1}{n+1}} Re^{-\frac{n}{n+1}} (-f''(0))^n \quad (3.11)$$

and the wall shear stress

$$\tau_w(x) = \left[\frac{\rho^n K U_w^{3n}}{x^n} \right] (-f''(0))^n. \quad (3.12)$$

4. NUMERICAL SOLUTION

We use a spectral method for the determination of the solution to (3.9)–(3.10). Spectral methods are able to provide very accurate results when the solution is smooth enough. More precisely, if the solution is differentiable to all orders, an exponential (or infinite order or spectral) convergence is achieved. However, if the solution is m -times continuously differentiable, the rate of convergence is algebraic: $\mathcal{O}(k^{-m})$, where k is the k -th expansion mode [11]. Superior convergence can be achieved for entire functions. For periodic problems, Fourier spectral methods are straightforward; however, in our case the domain is non-periodic, therefore we are going to use the Chebyshev method. All three versions of spectral methods (collocation, Galerkin and tau) belong to the method of weighted residuals and the main classification is carried out according to the type of trial functions used. Trial functions in the Galerkin method are the same as the weight functions and satisfy some of the boundary conditions. In spectral collocation, trial functions are Dirac-delta functions located at the collocation points while the tau method, similarly to the Galerkin method, operates in the weak form but the trial functions generally do not satisfy the boundary conditions [9]. In our calculations the collocation method is used. During collocation we determine the function values of the interpolating polynomial at the collocation points (nodal approximation) as opposed to the other two methods, which give results for the coefficients of the truncated approximating series (modal approximation). For other aspects of the method, we refer to [9].

The n -th order Chebyshev polynomial of the first kind, $T_n(\bar{x})$ is defined on $[-1, 1]$ and can be expressed by the recursion

$$T_0(\bar{x}) = 1, \quad T_1(\bar{x}) = \bar{x}, \quad T_n(\bar{x}) = 2\bar{x}T_{n-1}(\bar{x}) - T_{n-2}(\bar{x}), \quad n > 1.$$

The modal approximation of a function $w(\bar{x})$ is

$$I_N w(\bar{x}) = \sum_{j=0}^N a_j T_j(\bar{x}), \tag{4.1}$$

where a_j are the Chebyshev coefficients. The nodal approximation of $w(\bar{x})$ can be evaluated in the Lagrange base as

$$p_N w(\bar{x}) = \sum_{j=0}^N w_j \ell_j(\bar{x}), \tag{4.2}$$

where ℓ_j are the Lagrange basis polynomials. The spectral differentiation for Chebyshev polynomials can be carried out either by a matrix-vector product or by using the Fast Fourier Transform (FFT). We implement the matrix-vector multiplication method because of the relatively low number of collocation points. The first derivative of w is approximated as

$$w'(\bar{x}_i) \approx \sum_{j=0}^N D_{ij} w_j, \quad i = 0, \dots, N,$$

where \mathbf{D} is the first differentiation matrix. Similarly, the p -th order derivative is calculated as

$$\frac{d^p w(\bar{x}_i)}{d\bar{x}^p} \approx \sum_{j=0}^N D_{ij}^{(p)} w_j, \quad i = 0, \dots, N, \quad (4.3)$$

with $\mathbf{D}^{(p)}$ standing for the p -th differentiation matrix. For \mathbf{D} and $\mathbf{D}^{(2)}$ exact formulas exist.

One of the methods for solving a BVP on an infinite or semi-infinite interval is the so-called domain truncation [11]. Performing the truncation and the linear mapping we have

$$\eta \in [0, \infty) \longrightarrow \xi \in [0, L] \xrightarrow{\zeta = \frac{\xi}{L}} \zeta \in [0, 1] \xrightarrow{\bar{x} = 2\zeta - 1} \bar{x} \in [-1, 1]. \quad (4.4)$$

Introducing $\bar{f}(\bar{x}) = f(\eta(\bar{x}))$, BVP (3.9)–(3.10) reads

$$\frac{8}{L^3} \bar{f}''' - \frac{1}{n(n+1)} \left(\frac{4}{L^2} \right)^{2-n} \bar{f} |\bar{f}''|^{2-n}, \quad (4.5)$$

$$\bar{f}(-1) = 0, \quad \bar{f}'(-1) = L/2, \quad \bar{f}'(1) = 0. \quad (4.6)$$

After the discretization of \bar{f} , $N + 2$ number of algebraic equations are at our disposal. The differential equation (4.5) is approximated at the $N - 1$ inner nodes and the three boundary conditions (4.6). However, the number of unknowns are only $N + 1$, therefore the resulting system is overdetermined. One possible solution is to take an interpolant that already satisfies some of the boundary conditions [12]. Let us seek function g such that

$$\bar{f}(\bar{x}) = P(\bar{x})g(\bar{x}), \quad P(\bar{x}) = a\bar{x}^2 + b\bar{x} + c.$$

In case of $P(-1) = 0$, $P'(-1) = L/2$ and $P'(1) = 0$ are satisfied, a , b , c are obtained as

$$a = -L/8, \quad b = L/4, \quad c = 3L/8.$$

Now the differential equation is reformulated by

$$\begin{aligned} & \frac{8}{L^3} [6ag' + (6a\bar{x} + 3b)g'' + (a\bar{x}^2 + b\bar{x} + c)g'''] - \frac{1}{n(n+1)} \left(\frac{4}{L^2} \right)^{2-n} (a\bar{x}^2 + b\bar{x} + c)g \\ & |2ag + (4a\bar{x} + 2b)g' + (a\bar{x}^2 + b\bar{x} + c)g''|^{2-n} = 0 \end{aligned} \quad (4.7)$$

under boundary conditions

$$g(-1) = 1, \quad g'(1) = 0. \quad (4.8)$$

The BVP (4.7)–(4.8) can be solved with the Chebyshev spectral technique.

After the discretization of $g(\bar{x})$ and its derivatives according to (4.2) and (4.3), the resulting system of nonlinear equations is solved by the Levenberg–Marquardt algorithm in MATLAB. Table 1 contains the essential values of $f''(0)$ for various number of collocation points and for different interval length L and power-law exponent n .

The numerical results for different power-law exponents are depicted in Fig. 1, where $f'(\eta)$ is shown which is proportional to $u(x, y)$ (see Eq. (3.6)). The figure shows that with larger values of n the boundary layer thickness decreases and shorter

Table 1. Values of $f''(0)$ for different power-law exponents

	$n = 0.5$ ($L = 30, N = 23$)	$n = 0.7$ ($L = 25, N = 25$)	$n = 0.8$ ($L = 20, N = 20$)	$n = 1$ ($L = 20, N = 30$)
$f''(0)$	-0.468917	-0.443623	-0.441151	-0.443748
	$n = 1.1$ ($L = 10, N = 20$)	$n = 1.3$ ($L = 6, N = 20$)	$n = 1.5$ ($L = 6, N = 10$)	
$f''(0)$	-0.447283	-0.45624	-0.466919	

interval is enough for the truncation. Because $f''(0) < 0$, both the drag coefficient in

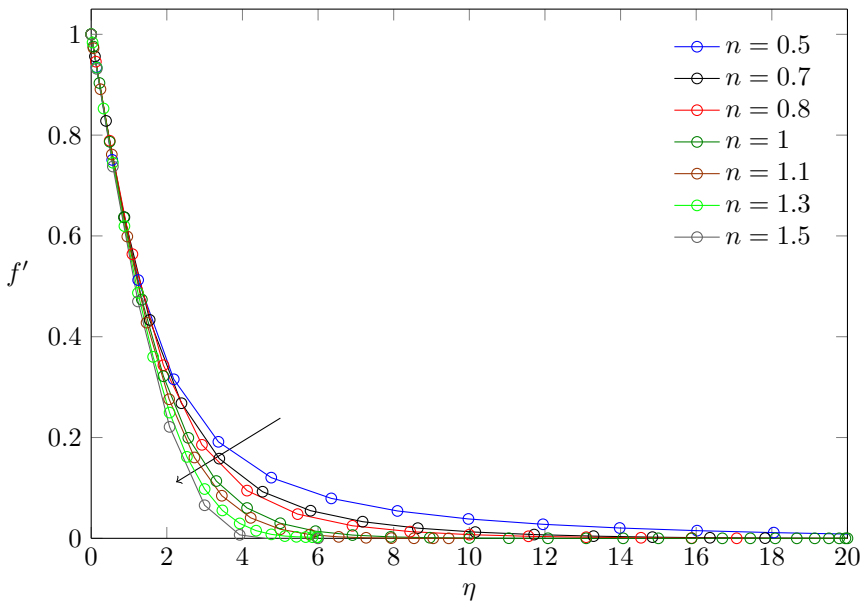


Figure 1. Velocity profiles for different values of n

Eq. (3.11) and the wall shear stress in Eq. (3.12) are influenced by $(-f''(0))^n$ and this is described in Fig. 2.

Table 2 collects the calculated function values for some n .

Error estimation is based on the monotonic decrease of the absolute value of the Chebyshev coefficients a_j . Namely, if the coefficients before a_N tend to a_N smoothly in absolute value, then the solution is supposed to be correct [11]. The last retained coefficient a_N in (4.1) is proportional to the truncation error. We also performed the calculations for different numbers of collocation points. For the calculated values of

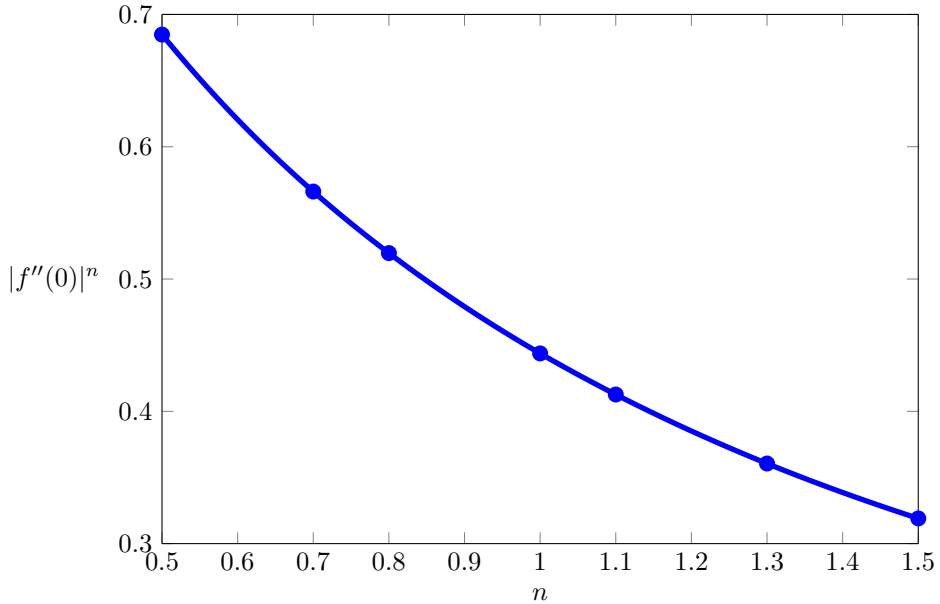


Figure 2. The values of $|f''(0)|^n$ for $n \in [0.5, 1.5]$

Table 2. The values of $|f''(0)|^n$ for some values of n

n	0.5	0.7	0.8	1
$ f''(0) ^n$	0.684775	0.566122	0.519601	0.443763
n	1.1	1	1.5	
$ f''(0) ^n$	0.412706	0.360538	0.319053	

n , using the values of L and N given in Table 1, the worst estimated error is obtained for $n = 0.5$ as $1.55\text{e-}6$ and the best one is $3.70\text{e-}11$ for $n = 1$.

5. CONCLUSIONS

The paper deals with the solutions to the generalized Sakiadis problem for non-Newtonian power-law fluids. The boundary layer assumption is taken into account, then a similarity transformation is used in order to solve an ordinary differential equation instead of the system of partial differential equations. Chebyshev spectral collocation is applied after domain truncation and the appropriate treatment of the boundary conditions. From the solutions achieved, we found that the boundary layer thickness decreases as the power-law exponent increases, while the drag coefficient and the wall shear stress increase with larger n exponents.

REFERENCES

1. ALTAN, T., OH, S., and GEGEL, H.: *Metal Forming Fundamentals and Applications*. Asm. Intl., 1979.
2. FISHER, E. G.: *Extrusion of Plastics*. Wiley, New York, 1976.
3. TADMOR, Z. and KLEIN, I.: *Engineering Principles of Plasticating Extrusion*. Polymer Science and Engineering Series, Van Nostrand Reinhold, New York, 1970.
4. SAKIADIS, B. C.: Boundary layer behavior on continuous solid surfaces. II: The boundary layer on a continuous flat surface. *AIChE*, **7**(2), (1961), 221–225.
5. TSOU, F., SPARROW, E., and GOLDSTEIN, R.: Flow and heat transfer in the boundary layer on a continuous moving surface. *Int. J. Heat Mass Transfer*, **10**(2), (1967), 219–235.
6. SAKIADIS, B. C.: Boundary-layer behavior on continuous solid surfaces: I. Boundary-layer equations for two-dimensional and axisymmetric flow. *AIChE*, **7**(1), (1961), 26–28.
7. SCHOWALTER, W.: *Mechanics of Non-Newtonian fluids*. Pergamon Press, 1st edn., 1978.
8. ACRIVOS, A., SHAH, M., and PETERSEN, E.: Momentum and heat transfer in laminar boundary flow of non-Newtonian fluids past external surfaces. *AIChE Journal*, **6**(2), (1960), 312–317.
9. CANUTO, C., HUSSAINI, M. Y., QUARTERONI, A., and ZANG, T. A.: *Spectral Methods: Fundamentals in Single Domains*. Springer, 1st edn., 2006.
10. POP, I. and GORLA, R.: Mixed convection similarity solutions of a non-newtonian fluid on a horizontal surface. *Wärme-und Stoffübertragung*, **26**, (1990), 57–63.
11. BOYD, J. P.: *Chebyshev and Fourier Spectral Methods*. Dover Publications, 2000.
12. FORNBERG, B.: A pseudospectral fictitious point method for high order initial-boundary value problems. *SIAM J. Sci. Comput.*, **28**(5), (2006), 1716–1729.

COMPARATIVE STUDY OF PRIMAL- AND DUAL-MIXED FINITE ELEMENT MODELS FOR CYLINDRICAL SHELLS

EDGÁR BERTÓTI

Institute of Applied Mechanics, University of Miskolc
H-3515 Miskolc, Miskolc–Egyetemváros, Hungary
edgar.bertoti@uni-miskolc.hu

[Received: October 4, 2015, Accepted: November 10, 2015.]

*Dedicated to Professor Barna Szabó on the occasion of his eightieth birthday
and to Professor Imre Kozák on the occasion of his eighty-fifth birthday*

Abstract. Analytical and numerical comparisons of a primal-mixed, a dual-mixed and a consistent primal-dual mixed finite element formulation are presented for cylindrical shells using the lowest possible order, constant and linear, polynomial approximations within the framework of the Naghdi shell model. The stiffness matrices and the load vectors of the mixed elements are explicitly derived and compared to each other and to that of the standard displacement-based shell element for axisymmetric deformations. It is pointed out that the stiffness matrices of the dual-mixed and the primal-dual mixed elements can be related to that of the standard shell element through two geometry-, material- and mesh-dependent coefficients. One of these coefficients turns out to be a reliable shear locking indicator which can be used to transform the standard displacement-based shell element into a shear locking-free dual-mixed one, independently of the thickness and the loading of the shell. The numerical comparisons indicate that the dual-mixed element is the only element that gives second-order rates of asymptotic convergence for all the variables, including the bending moment and shear force computations.

Mathematical Subject Classification: 05C38, 15A15

Keywords: primal-mixed, dual-mixed, finite element, cylindrical shell, shear locking indicator

1. INTRODUCTION

Reliable numerical analysis of structural shells represents one of the biggest challenges in computational mechanics. During the past decades, a large variety of shell formulations and shell finite element models have been developed, investigated and analyzed, both numerically and analytically. Due to the enormously huge number of publications on shell formulations and shell finite elements, it is almost impossible to give a brief overview within a short introduction, even on the most significant contributions. The reader is rather referred to the excellent review of [1] and the textbooks of [2, 3, 4, 5]. Among the current possibilities, the higher-order displacement-based shell

elements and the low-order mixed shell finite elements seem to be the most reliable ones for thin shells [5, 6, 7].

The appearance of, and the remedies for, the different types of locking phenomenon, including shear and membrane locking, in finite element analyses of beams, plates and shells have been the subject of many research papers as well. Regarding Naghdi-type first-order shear deformation models for shells [8, 9, 10, 11], several shear locking-free elements have been developed and different techniques for avoiding locking problems have also been widely analyzed [12, 13, 4, 5].

Regarding mixed variational formulations and finite element models, the primal-mixed elements with continuous displacement approximations and discontinuous surface tractions are more popular than the dual-mixed elements, but they lead to the same low-order rates of convergence for the stresses as the conventional displacement-based models [14]. In contrast, the dual-mixed elements require surface traction continuity at the element interfaces and apply discontinuous approximations for the displacements, i.e., a standard stiffness matrix equation with conforming nodal displacements cannot directly be derived from them. However, as the local equilibrium of the surface tractions at the element interfaces is satisfied by the stress approximation of the dual-mixed elements, they result in better rates of asymptotic convergence for the stress variables than those obtained by primal-mixed elements.

The locking-free property of a shell finite element is understood in the sense that no degradation in the rates of convergences of the displacement and stress variables appears when the thickness of the shell approaches zero. The analytical investigation and explanation of the locking-free behavior of different, displacement-based or mixed, shell elements would require explicit comparisons of their closed form stiffness matrices and load vectors. This, however, seems to be rather hopeless for general shells, due to the complexity of their geometry, the related variational formulations and finite element models. In addition, the discontinuous approximation of the displacements in dual-mixed finite element formulations makes their analytical comparisons to primal- and primal-mixed elements rather difficult. This is true even for those cases when the surface traction continuity at the element interfaces is enforced by applying the λ -multiplier technique, a method often called hybridization [15, 16], as the λ -multipliers usually correspond to non-conforming nodal displacements. Special exceptions to that rule are the one-dimensional problems like beams and, regarding shells, the cylindrical shell with axisymmetric deformations, where the λ -multipliers turn out to be the nodal displacements. This fact enables direct analytical comparisons of the element stiffness matrices and load vectors of the dual-mixed formulation to those obtained with the displacement-based and the primal-mixed approaches.

The main goal of the present work is to perform analytical and numerical comparisons of different finite element formulations for cylindrical shells in the framework of the dimensionally reduced Naghdi shell model. The formulations investigated in this paper have much similarity and analogy to those presented for the Timoshenko beam in [17]. The strong and the (Galerkin-type) weak formulations of the governing equations for axisymmetric deformations are summarized in Section 2. Among the several

possibilities, a primal-mixed, a dual-mixed and a consistent primal-dual mixed formulation are investigated in detail, deriving the corresponding stiffness matrices and load vectors analytically, using the lowest possible order of polynomial approximations the formulations permit.

The derivation and comparison of the stiffness matrices and the load vectors of the different finite element models have been performed using the computer algebra system Maple(TM) and the results are summarized in Section 3. The relationships between the element stiffness matrices suggest the introduction of two geometry-, material- and mesh-dependent coefficients denoted by C_m and C_s that can easily be computed for each element in the mesh. To show and compare the approximation capabilities of the formulations and elements considered, Section 4 presents a demonstrative numerical example, a clamped-clamped shell subjected to uniform load. In the concluding remarks a recipe is given for how the stiffness matrices of the standard and primal-mixed formulations can be transformed, applying the shear locking indicator C_s , to obtain shear locking-free finite element solutions with second-order rates of asymptotic convergences in all the variables, i.e., in the displacements, bending moments and shear forces, independently of the thickness of the shell.

2. STRONG AND WEAK FORMULATIONS FOR THE CYLINDRICAL SHELL MODEL

A homogeneous circular cylindrical shell of length L and uniform thickness d is investigated in a Cartesian xyz coordinate system. The axis x coincides with the axis of the shell, the middle surface of which is a cylinder of radius R (see Figure 1). The orthonormal basis vectors of the local cylindrical coordinate system, attached to the middle surface, are denoted by e_i , $i = 1, 2, 3$, the cylindrical coordinates of an arbitrary point P on the middle surface are $x_1 \equiv x$, x_2 and x_3 , each of them has a dimension of length. The middle surface of the shell is given by $S_0 := \{\mathbf{x} \mid x \in (0, L), x_2 \in [0, 2R\pi), x_3 = 0\}$. We assume that the shell is loaded axisymmetrically, i.e., all the variables used for describing the shell problem are independent of the coordinate x_2 . The torsion problem of the shell is not investigated.

2.1. Strong forms of the governing equations. Applying the main kinematical assumptions of the Naghdi shell model [8, 5], the displacement field of the 3D shell is approximated through the thickness as

$$u_1(x, x_3) = u(x) + \phi(x) x_3, \tag{2.1}$$

$$u_3(x, x_3) = w(x), \tag{2.2}$$

where $u(x)$ and $w(x)$ are the displacements of the middle surface in axial and transverse directions, respectively, and $\phi(x) \equiv \phi_2(x)$ is the (small) rotation of the normal to the middle surface at $x \equiv x_1$ around the local base vector e_2 . The displacement component u_2 is identically zero. The non-zero strain components of the shell are given by

$$e_{11}(x, x_3) = \varepsilon_{11}(x) + \kappa_{11}(x) x_3, \tag{2.3}$$

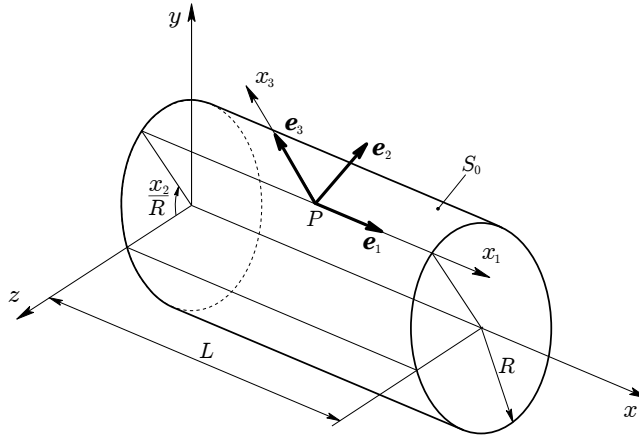


Figure 1. Middle surface of the cylindrical shell

$$2e_{13}(x, x_3) = \gamma_{13}(x), \quad (2.4)$$

$$e_{22}(x, x_3) = \varepsilon_{22}(x), \quad (2.5)$$

where

$$\varepsilon_{11}(x) = u_{,x}, \quad (2.6)$$

$$\gamma_{13}(x) = w_{,x} + \phi, \quad (2.7)$$

$$\kappa_{11}(x) = \phi_{,x}, \quad (2.8)$$

$$\varepsilon_{22}(x) = w/R \quad (2.9)$$

are, respectively, the axial membrane strain, the transverse shear strain, the curvature of the middle surface in the $x_1 x_3$ plane and the circumferential membrane strain (a comma followed by the index x in the subscript denotes differentiation with respect to $x \equiv x_1$). Relations (2.6)-(2.9) are the kinematic equations of the dimensionally reduced shell model with Reissner-Mindlin-type kinematics. Note that (2.9) is not a differential equation.

Assuming linearly elastic and isotropic materials and identically zero transverse normal stresses, i.e., $\sigma_{33} = 0$, the constitutive relations for the 3D shell are given by

$$\sigma_{11}(x, x_3) = E_1(\varepsilon_{11} + \nu\varepsilon_{22}) + E_1 \kappa_{11} x_3, \quad (2.10)$$

$$\sigma_{22}(x, x_3) = E_1(\varepsilon_{22} + \nu\varepsilon_{11}) + \nu E_1 \kappa_{11} x_3, \quad (2.11)$$

$$\sigma_{13}(x, x_3) = k_s 2G \varepsilon_{13} = k_s G \gamma_{13}(x), \quad (2.12)$$

where $E_1 = E/(1 - \nu^2)$ with elasticity modulus E and Poisson ratio ν , G is the shear modulus and k_s is the shear correction factor. Introducing the stress resultants and couples as

$$\begin{Bmatrix} N_{11}(x) \\ N_{22}(x) \\ N_{13}(x) \end{Bmatrix} = \int_{-\frac{d}{2}}^{+\frac{d}{2}} \begin{Bmatrix} \sigma_{11} \\ \sigma_{22} \\ \sigma_{13} \end{Bmatrix} dx_3, \quad \begin{Bmatrix} M_{11}(x) \\ M_{22}(x) \end{Bmatrix} = \int_{-\frac{d}{2}}^{+\frac{d}{2}} x_3 \begin{Bmatrix} \sigma_{11} \\ \sigma_{22} \end{Bmatrix} dx_3, \quad (2.13)$$

the stress-strain relations of the shell model can be given in the form

$$N_{11}(x) = E_1 d (\varepsilon_{11} + \nu \varepsilon_{22}), \tag{2.14}$$

$$N_{22}(x) = E_1 d (\varepsilon_{22} + \nu \varepsilon_{11}), \tag{2.15}$$

$$N_{13}(x) = k_s G d \gamma_{13}, \tag{2.16}$$

$$M_{11}(x) = E_1 I_1 \kappa_{11}, \tag{2.17}$$

$$M_{22}(x) = \nu E_1 I_1 \kappa_{11}, \tag{2.18}$$

where $I_1 = d^3/12$. Due to the assumptions employed, the geometrical and material parameters I_1 , E , G and ν , as well as k_s are all constants. Note that the above constitutive equations are uniquely invertible and the membrane strains, for example, can be computed from the membrane forces according to the inverse stress-strain relations

$$\varepsilon_{11}(x) = \frac{1}{Ed} (N_{11} - \nu N_{22}), \tag{2.19}$$

$$\varepsilon_{22}(x) = \frac{1}{Ed} (N_{22} - \nu N_{11}). \tag{2.20}$$

The equilibrium equations of the shell model are

$$N_{11,x} + p_1 = 0, \tag{2.21}$$

$$N_{13,x} - \frac{1}{R} N_{22} + p_3 = 0, \tag{2.22}$$

$$M_{11,x} - N_{13} + m_2 = 0, \tag{2.23}$$

where $p_1(x)$, $p_3(x)$ and $m_2(x)$ are distributed (known) external loads. For thin shells, the distributed moment load $m_2(x)$ is usually neglected, as we do so in this paper.

Displacement and stress boundary conditions can be prescribed for the variables u , w , ϕ and N_{11} , N_{13} , M_{11} , respectively, at both ends of the shell, $x = 0$ and $x = L$, by paying attention to the fact that $\{u, N_{11}\}$, $\{w, N_{13}\}$ and $\{\phi, M_{11}\}$ are work-conjugate variables.

2.2. Weak forms of the governing equations. In the subsequent analysis, the constitutive equations (2.14)-(2.18) will be satisfied in a strong sense. In addition, to simplify the finite element formulation and to obtain comparable 4×4 stiffness matrices, the kinematic equation (2.6) and the equilibrium equation (2.21) will also be satisfied in a strong sense. This means that the solution for the axial membrane force $N_{11}(x)$ is obtained by direct integration from (2.21) as

$$N_{11}(x) = N_{11}(0) - \int_{\xi=0}^x p_1(\xi) d\xi, \tag{2.24}$$

and the axial displacement $u(x)$ will be obtained from (2.6) by integration as well:

$$u(x) = u(0) + \int_{\xi=0}^x \varepsilon_{11}(\xi) d\xi. \tag{2.25}$$

The computation of the strain component $\varepsilon_{11}(x)$ for (2.25) is based on (2.19), which requires a solution for $N_{22}(x)$. The method of computing the membrane force $N_{22}(x)$ depends on the weak formulation applied, as discussed in Section 3.

2.2.1. *Kinematic equations.* The first weak forms of the kinematic equations (2.7)-(2.8) of the shell model are

$$\int_0^L (\gamma_{13} - w_{,x} - \phi) \delta N_{13} \, dx = 0, \quad (2.26)$$

$$\int_0^L (\kappa_{11} - \phi_{,x}) \delta M_{11} \, dx = 0, \quad (2.27)$$

where $\delta N_{13}(x)$ and $\delta M_{11}(x)$ are arbitrary weighting functions (virtual shear force and bending moment). The second weak forms of the kinematic equations are obtained from (2.26)-(2.27) by applying the divergence theorem:

$$\int_0^L (\gamma_{13} \delta N_{13} + w \delta N_{13,x} - \phi \delta N_{13}) \, dx - [w \delta N_{13}]_0^L = 0, \quad (2.28)$$

$$\int_0^L (\kappa_{11} \delta M_{11} + \phi \delta M_{11,x}) \, dx - [\phi \delta M_{11}]_0^L = 0. \quad (2.29)$$

The kinematic equation (2.9) is not a differential equation, it has only one weak form:

$$\int_0^L (\varepsilon_{22} - \frac{w}{R}) \delta N_{22} \, dx = 0, \quad (2.30)$$

where $\delta N_{22}(x)$ is an arbitrary weighting function (virtual membrane force).

2.2.2. *Equilibrium equations.* The first weak forms of the equilibrium equations (2.22)-(2.23) are

$$\int_0^L (N_{13,x} - \frac{1}{R} N_{22} + p_3) \delta w \, dx = 0, \quad (2.31)$$

$$\int_0^L (M_{11,x} - N_{13}) \delta \phi \, dx = 0, \quad (2.32)$$

where $\delta w(x_1)$ and $\delta \phi(x_1)$ are arbitrary functions (virtual displacements and rotation). The second weak forms of the equilibrium equations are obtained from (2.31)-(2.32) by applying the divergence theorem:

$$\int_0^L (-N_{13} \delta w_{,x} - \frac{1}{R} N_{22} \delta w + p_3 \delta w) \, dx + [N_{13} \delta w]_0^L = 0, \quad (2.33)$$

$$\int_0^L (-M_{11} \delta \phi_{,x} - N_{13} \delta \phi) \, dx + [M_{11} \delta \phi]_0^L = 0. \quad (2.34)$$

2.3. Variational formulations – a brief overview of the possibilities. Depending on which forms, strong or weak, of the governing equations in Sections 2.1 and 2.2 are selected, different types of variational formulations and finite element models for the shell problem can be constructed, as shown in Table 1. The displacement boundary conditions for $w(x)$ and $\phi(x)$, as well as the stress/force boundary conditions for $N_{13}(x)$ and $M_{11}(x)$ at $x = 0$ and/or $x = L$ can be either essential or natural, depending on the formulation considered. The quality of the finite element solution, as is well known, can largely depend on the variational formulation employed, especially when low-order polynomial approximations are used.

Table 1. An overview of variational formulations

	Variational formulation			
	primal	primal-mixed	dual-mixed	dual
Kinematic equations	strong	1st weak	2nd weak	2nd weak
Constitutive equations	strong	strong	strong	strong
Equilibrium equations	2nd weak	2nd weak	1st weak	strong
Displacement b.c.	essential	essential	natural	natural
Stress/force b.c.	natural	natural	essential	essential

Note that there exist two other *primal-dual mixed* formulations for the shell problem that are not included in Table 1. They can be obtained by mixing the weak forms of the governing equations in such a way that one of the kinematic equations is considered in its first weak form, the other in its second weak form, and the corresponding equilibrium equations are taken into account in their second and first weak forms, respectively. Out of the two possibilities, a consistent primal-dual mixed formulation and the related shell finite element are presented in Section 3.4. Note also that additional mixed variational formulations and finite element models can be constructed by taking into account the constitutive equations in their weak forms.

3. FINITE ELEMENT FORMULATIONS

In this section, the derivation of the stiffness matrices and the load vectors of one shell element denoted by e will be summarized for displacement-based, primal-mixed, dual-mixed and a consistent primal-dual mixed variational formulations, employing Bubnov-Galerkin-type approximations of the lowest possible order.

The mapping between the master element $\hat{e} := \{\xi \mid -1 \leq \xi \leq 1\}$ and the actual element $e := \{x \mid x_a \leq x \leq x_b\}$ with nodal coordinates $x_a < x_b$ is given by

$$x = x(\xi) = x_a \mathcal{N}_1(\xi) + x_b \mathcal{N}_2(\xi), \tag{3.1}$$

where

$$\mathcal{N}_1(\xi) = \frac{1}{2}(1 - \xi), \quad \mathcal{N}_2(\xi) = \frac{1}{2}(1 + \xi) \tag{3.2}$$

are the standard linear interpolation functions. The Jacobian of the mapping (3.1) is $J = h/2$ with element length $h = x_b - x_a$. All the symbolic computations presented in this section have been performed using the computer algebra system MapleTM.

3.1. Displacement-based (primal) formulation. This is the simplest and most known formulation, found in many textbooks and papers and reviewed briefly here for notational reasons. The axial membrane force $N_{11}(x)$ is assumed to be known, according to (2.24), and the membrane force $N_{22}(x)$ will be computed from the inverse stress-strain relation (2.20):

$$N_{22}(x) = \frac{Ed}{R} w(x) + \nu N_{11}(x), \quad (3.3)$$

where the kinematic equation (2.9) has also been used. Inserting (3.3), as well as (2.16)-(2.17) in (2.33)-(2.34) and taking into account (2.7)-(2.8), the second weak forms of the equilibrium equations for the shell element e can be written as

$$\int_{x_a}^{x_b} [-k_s G d (w_{,x}^e + \phi^e) \delta w_{,x}^e - \frac{Ed}{R^2} w^e \delta w^e + \hat{p}_3^e \delta w^e] dx + [N_{13} \delta w]_{x_a}^{x_b} = 0, \quad (3.4)$$

$$\int_{x_a}^{x_b} [-E_1 I_1 (\phi_{,x}^e \delta \phi_{,x}^e) - k_s G d (w_{,x}^e + \phi^e) \delta \phi^e] dx + [M_{11} \delta \phi]_{x_a}^{x_b} = 0, \quad (3.5)$$

where $\hat{p}_3^e = p_3^e - \nu N_{11}^e/R$. Employing linear approximation for both $w(x)$ and $\phi(x)$ on element e , we can write:

$$w^e(\xi) = w_a \mathcal{N}_1(\xi) + w_b \mathcal{N}_2(\xi), \quad (3.6)$$

$$\phi^e(\xi) = \phi_a \mathcal{N}_1(\xi) + \phi_b \mathcal{N}_2(\xi), \quad (3.7)$$

where $w_i = w(x_i)$ and $\phi_i = \phi(x_i)$, $i = a, b$ are the nodal displacements and rotations. This is the lowest possible order (though inconsistent) C^0 -continuous approximation for $w(x)$ and $\phi(x)$. Introducing the matrix of nodal displacements

$$[\mathbf{u}]^T = [w_a \ w_b \ \phi_a \ \phi_b] \quad (3.8)$$

and approximating the weighting functions $\delta w^e(x)$ and $\delta \phi^e(x)$ by piece-wise linear functions as well (Bubnov-Galerkin method), the principle of virtual work with variational equations (3.4)-(3.5) leads to the matrix equation

$$[\mathbf{K}^{\text{ST}}] [\mathbf{u}] = [\mathbf{F}^{\text{ST}}], \quad (3.9)$$

where

$$\begin{aligned} [\mathbf{K}^{\text{ST}}] &= [\mathbf{K}_m^{\text{ST}}] + [\mathbf{K}_b^{\text{ST}}] + [\mathbf{K}_s^{\text{ST}}] = \frac{Ed}{h} \frac{h^2}{R^2} \begin{bmatrix} 1/3 & 1/6 & 0 & 0 \\ 1/6 & 1/3 & 0 & 0 \\ 0 & 0 & 0 & 0 \\ 0 & 0 & 0 & 0 \end{bmatrix} \\ &+ \frac{E_1 I_1}{h} \begin{bmatrix} 0 & 0 & 0 & 0 \\ 0 & 0 & 0 & 0 \\ 0 & 0 & 1 & -1 \\ 0 & 0 & -1 & 1 \end{bmatrix} + \frac{k_s G d}{h} \begin{bmatrix} 1 & -1 & -h/2 & -h/2 \\ -1 & 1 & h/2 & h/2 \\ -h/2 & h/2 & h^2/3 & h^2/6 \\ -h/2 & h/2 & h^2/6 & h^2/3 \end{bmatrix} \end{aligned} \quad (3.10)$$

is the standard stiffness matrix of the shell element (indicated by the letters ST in the superscript) and

$$[\mathbf{F}^{\text{ST}}] = \begin{bmatrix} F_1 \\ F_2 \\ F_3 \\ F_4 \end{bmatrix}, \quad \begin{aligned} F_j &= \frac{h}{2} \int_{-1}^{+1} \hat{p}_3^e \mathcal{N}_j(\xi) \, d\xi + \tilde{Q}_j, \\ F_{j+2} &= \tilde{M}_j, \quad j = 1, 2 \end{aligned} \quad (3.11)$$

is its load vector with \tilde{Q}_j and \tilde{M}_j , $j = 1, 2$ representing known external loads (edge forces and moments) at the nodes. For the sake of subsequent comparisons, the stiffness matrix in (3.10) is given as the sum of three matrices: $[\mathbf{K}_m^{\text{ST}}]$, $[\mathbf{K}_b^{\text{ST}}]$ and $[\mathbf{K}_s^{\text{ST}}]$ are called, respectively, the membrane, bending and shear part of the stiffness matrix of the shell element.

3.2. Primal-mixed formulation. In the primal-mixed formulation, the equilibrium equations are considered in their second weak forms (2.33)-(2.34), just like in the pure displacement-based formulation: the kinematic equations are, however, taken into account in their first weak forms (2.26)-(2.27) and (2.30). This allows independent approximations for the stress variables $N_{22}(x)$, $N_{13}(x)$ and $M_{11}(x)$. The membrane force $N_{11}(x)$ is assumed to be known from (2.24). Taking into account the constitutive relations (2.16)-(2.17) and (2.20), the corresponding variational equations for element e read:

$$\int_{x_a}^{x_b} \left(\frac{1}{k_s G d} N_{13}^e - w^e_{,x} - \phi^e \right) \delta N_{13}^e \, dx = 0, \quad (3.12)$$

$$\int_{x_a}^{x_b} \left(\frac{1}{E_1 I_1} M_{11}^e - \phi^e_{,x} \right) \delta M_{11}^e \, dx = 0, \quad (3.13)$$

$$\int_{x_a}^{x_b} \left[\frac{1}{E d} (N_{22}^e - \nu N_{11}^e) - \frac{w^e}{R} \right] \delta N_{22}^e \, dx = 0, \quad (3.14)$$

$$\int_{x_a}^{x_b} \left[-N_{13}^e \delta w^e_{,x} - \frac{1}{R} N_{22}^e \delta w^e + p_3^e \delta w^e \right] dx + [N_{13} \delta w]_{x_a}^{x_b} = 0, \quad (3.15)$$

$$\int_{x_a}^{x_b} \left(-M_{11}^e \delta \phi^e_{,x} - N_{13}^e \delta \phi^e \right) dx + [M_{11} \delta \phi]_{x_a}^{x_b} = 0. \quad (3.16)$$

As the displacement boundary conditions are still essential, the primal-mixed formulation requires C^0 continuous approximation for the displacement variables $w(x)$ and $\phi(x)$, and their lowest possible order approximation is linear. The stress boundary conditions are still natural, there is no continuity requirement for the variables $N_{13}(x)$ and $M_{11}(x)$, their lowest possible order approximation is constant. The membrane force $N_{22}(x)$ is considered now as an independent variable and, as no boundary condition exists for it, its lowest order approximation is constant:

$$w^e(\xi) = w_a \mathcal{N}_1(\xi) + w_b \mathcal{N}_2(\xi), \quad N_{22}^e(\xi) = N_0, \quad (3.17)$$

$$\phi^e(\xi) = \phi_a \mathcal{N}_1(\xi) + \phi_b \mathcal{N}_2(\xi), \quad N_{13}^e(\xi) = Q_0, \quad M_{11}^e(\xi) = M_0. \quad (3.18)$$

Introducing the matrices of nodal displacements $w_i = w(x_i)$ and $\phi_i = \phi(x_i)$, $i = a, b$ and element stresses N_0, Q_0, M_0 , as

$$[\mathbf{u}]^T = [w_a \ w_b \ \phi_a \ \phi_b], \quad [s_0]^T = [N_0 \ Q_0 \ M_0] \quad (3.19)$$

and applying the Bubnov-Galerkin method, i.e., $\delta w^e(x)$ and $\delta \phi^e(x)$ are approximated by linear functions, while $\delta N_{22}^e(x) = \delta N_0$, $\delta N_{13}^e(x) = \delta Q_0$ and $\delta M_{11}^e(x) = \delta M_0$ are arbitrary constants, the stress parameters in $[s_0]$ can be eliminated at element level and variational equations (3.12)-(3.16) lead to the matrix equation

$$[\mathbf{K}^{\text{PM}}] [\mathbf{u}] = [\mathbf{F}^{\text{PM}}], \quad (3.20)$$

where

$$\begin{aligned} [\mathbf{K}^{\text{PM}}] &= [\mathbf{K}_m^{\text{PM}}] + [\mathbf{K}_b^{\text{PM}}] + [\mathbf{K}_s^{\text{PM}}] = \frac{Ed}{h} \frac{h^2}{R^2} \begin{bmatrix} \boxed{1/4 \quad 1/4} & 0 & 0 \\ 1/4 \quad 1/4 & 0 & 0 \\ 0 & 0 & 0 & 0 \\ 0 & 0 & 0 & 0 \end{bmatrix} \\ &+ \frac{E_1 I_1}{h} \begin{bmatrix} 0 & 0 & 0 & 0 \\ 0 & 0 & 0 & 0 \\ 0 & 0 & 1 & -1 \\ 0 & 0 & -1 & 1 \end{bmatrix} + \frac{k_s G d}{h} \begin{bmatrix} 1 & -1 & -h/2 & -h/2 \\ -1 & 1 & h/2 & h/2 \\ -h/2 & h/2 & \boxed{h^2/4} & \boxed{h^2/4} \\ -h/2 & h/2 & h^2/4 & h^2/4 \end{bmatrix} \end{aligned} \quad (3.21)$$

is the stiffness matrix of the primal-mixed element (indicated by the letters PM in the superscript) and

$$[\mathbf{F}^{\text{PM}}] = \begin{bmatrix} F_1 \\ F_2 \\ F_3 \\ F_4 \end{bmatrix}, \quad \begin{aligned} F_j &= \frac{h}{2} \int_{-1}^{+1} [p_3^e \mathcal{N}_j(\xi) - \frac{\nu}{2R} N_{11}^e(\xi)] d\xi + \tilde{Q}_j, \\ F_{j+2} &= \tilde{M}_j, \end{aligned} \quad j = 1, 2 \quad (3.22)$$

is its load vector with external nodal forces and moments \tilde{Q}_j and \tilde{M}_j , $j = 1, 2$.

Remark. If $N_{22}(x)$ is not considered as an independently approximated variable but computed from (3.3), then variational equation (3.14) is identically satisfied and the membrane part of the primal-mixed stiffness matrix will be equal to that of the standard displacement-based element, and the equality of the load vectors holds true as well, i.e.,

$$[\mathbf{K}_m^{\text{PM}}] = [\mathbf{K}_m^{\text{ST}}] \quad \text{and} \quad [\mathbf{F}^{\text{PM}}] = [\mathbf{F}^{\text{ST}}].$$

The shear part of the primal-mixed stiffness matrix does not change, i.e., $[\mathbf{K}_s^{\text{PM}}]$ is computed according to (3.21) and, thus, it always differs from that of the standard element, $[\mathbf{K}_s^{\text{ST}}]$.

3.3. Dual-mixed formulation. In the dual-mixed formulation, the kinematic equations are taken into account in their second weak forms (2.28)-(2.29) and the equilibrium equations are considered in their first weak forms (2.31)-(2.32). The axial

membrane force $N_{11}(x)$ is assumed to be known, according to (2.24), and the membrane force $N_{22}(x)$ will be computed from (3.3). Taking into account the constitutive equations (2.16)-(2.17), the corresponding variational equations for element e read:

$$\int_{x_a}^{x_b} \left(\frac{1}{k_s G d} N_{13}^e \delta N_{13}^e + w^e \delta N_{13,x}^e - \phi^e \delta N_{13}^e \right) dx - [w \delta N_{13}]_{x_a}^{x_b} = 0, \quad (3.23)$$

$$\int_{x_a}^{x_b} \left(\frac{1}{E_1 I_1} M_{11}^e \delta M_{11}^e + \phi^e \delta M_{11,x}^e \right) dx - [\phi \delta M_{11}]_{x_a}^{x_b} = 0, \quad (3.24)$$

$$\int_{x_a}^{x_b} \left(N_{13,x}^e - \frac{E d}{R^2} w^e + \hat{p}_3^e \right) \delta w^e dx = 0, \quad (3.25)$$

$$\int_{x_a}^{x_b} (M_{11,x}^e - N_{13}^e) \delta \phi^e dx = 0. \quad (3.26)$$

As the displacement boundary conditions are natural in this case, the displacement variables $w(x)$ and $\phi(x)$ can be approximated discontinuously, and their lowest-order approximation is constant. The stress boundary conditions are now essential and C^0 -continuous approximation is required for the stress variables $N_{13}(x)$ and $M_{11}(x)$, i.e., their lowest possible order approximation is linear:

$$w^e(\xi) = w_0, \quad N_{13}^e(\xi) = Q_a \mathcal{N}_1(\xi) + Q_b \mathcal{N}_2(\xi), \quad (3.27)$$

$$\phi^e(\xi) = \phi_0, \quad M_{11}^e(\xi) = M_a \mathcal{N}_1(\xi) + M_b \mathcal{N}_2(\xi). \quad (3.28)$$

The matrices of the unknowns, the element displacements w_0, ϕ_0 and the nodal stresses $Q_i = N_{13}(x_i), M_i = M_{11}(x_i), i = a, b$, appearing in (3.27)-(3.28), are given by

$$[u_0]^T = [w_0 \ \phi_0], \quad [s]^T = [Q_a \ Q_b \ M_a \ M_b]. \quad (3.29)$$

The element stiffness matrix of the dual-mixed formulation will be derived applying the λ -multiplier technique, a method often called hybridization [15, 16]. This technique involves the introduction of additional nodal variables as unknowns that turn out to be the nodal values of the displacement $w(x)$ and rotation $\phi(x)$ of element e :

$$[u]^T = [w_a \ w_b \ \phi_a \ \phi_b], \quad (3.30)$$

where $w_i = w(x_i)$ and $\phi_i = \phi(x_i), i = a, b$. Note that these nodal displacements and rotations are, at least at approximation level, independent from w_0 and ϕ_0 , which are approximations for $w^e(x)$ and $\phi^e(x)$ in the element domain. In view of (3.29) and (3.30), the last terms on the left-hand side of (3.23)-(3.24) can be written as

$$- [w \delta N_{13}]_{x_a}^{x_b} = w_a \delta Q_a - w_b \delta Q_b, \quad (3.31)$$

$$- [\phi \delta M_{11}]_{x_a}^{x_b} = \phi_a \delta M_a - \phi_b \delta M_b, \quad (3.32)$$

and, in order to ensure the continuity of $N_{13}(x)$ and $M_{11}(x)$ at the nodes, variational equations (3.23)-(3.26) should be supplemented by equations

$$\delta w_a Q_a - \delta w_b Q_b = 0, \quad (3.33)$$

$$\delta \phi_b M_b - \delta \phi_a M_a = 0, \quad (3.34)$$

where $\delta w_i = \delta w(x_i)$ and $\delta \phi_i = \delta \phi(x_i)$, $i = a, b$ are arbitrary nodal values. Equations (3.33)-(3.34) are parts of the global variational equations that ensure the continuity of the shear force $N_{13}(x)$ and bending moment $M_{11}(x)$ at all the nodes (see Appendix A).

Using the variational equations (3.23)-(3.26) together with (3.31)-(3.34) and applying the Bubnov-Galerkin method, all the variables of (3.29) can be eliminated at element level and, as w_i and ϕ_i , $i = a, b$ are the nodal displacements and rotations, the stiffness matrix and the load vector of the dual-mixed element can be derived. After performing all the (symbolic) computations, the following matrix equation is obtained:

$$[\mathbf{K}^{\text{DM}}] [\mathbf{u}] = [\mathbf{F}^{\text{DM}}], \quad (3.35)$$

where

$$\begin{aligned} [\mathbf{K}^{\text{DM}}] &= [\mathbf{K}_m^{\text{DM}}] + [\mathbf{K}_b^{\text{DM}}] + [\mathbf{K}_s^{\text{DM}}] = \frac{Ed}{h} \frac{h^2}{R^2} \begin{bmatrix} 1/4 & 1/4 & 0 & 0 \\ 1/4 & 1/4 & 0 & 0 \\ 0 & 0 & 0 & 0 \\ 0 & 0 & 0 & 0 \end{bmatrix} \frac{1}{C_m} \\ &+ \frac{E_1 I_1}{h} \begin{bmatrix} 0 & 0 & 0 & 0 \\ 0 & 0 & 0 & 0 \\ 0 & 0 & 1 & -1 \\ 0 & 0 & -1 & 1 \end{bmatrix} + \frac{k_s G d}{h} \begin{bmatrix} 1 & -1 & -h/2 & -h/2 \\ -1 & 1 & h/2 & h/2 \\ -h/2 & h/2 & h^2/4 & h^2/4 \\ -h/2 & h/2 & h^2/4 & h^2/4 \end{bmatrix} \frac{1}{C_s} \end{aligned} \quad (3.36)$$

is the stiffness matrix of the dual-mixed element (indicated by the letters DM in the superscript) and

$$[\mathbf{F}^{\text{DM}}] = \begin{bmatrix} F_1 \\ F_2 \\ F_3 \\ F_4 \end{bmatrix}, \quad \begin{aligned} F_j &= \frac{1}{C_m} \frac{h}{4} \int_{-1}^{+1} \hat{p}_3^e(\xi) d\xi + \tilde{Q}_j, \\ F_{j+2} &= \tilde{M}_j, \quad j = 1, 2 \end{aligned} \quad (3.37)$$

is its load vector with \tilde{Q}_j and \tilde{M}_j , $j = 1, 2$ representing known external loads at the nodes. The material- and mesh-dependent constants C_m and C_s appearing in (3.36) and (3.37) are given by

$$C_m = 1 + \frac{1}{12} \frac{E}{k_s} \frac{h^2}{G R^2}, \quad \text{with} \quad \lim_{h/R \rightarrow 0} C_m = 1, \quad (3.38)$$

$$C_s = 1 + k_s \frac{G}{E_1} \frac{h^2}{d^2}, \quad \text{with} \quad \lim_{h/d \rightarrow 0} C_s = 1. \quad (3.39)$$

The role of these constants is discussed in Section 3.5. Note that for isotropic materials C_m and C_s depend on the Poisson ratio only, as $E/G = 2(1+\nu)$ and $G/E_1 = (1-\nu)/2$.

Remark. If variational equations (3.23)-(3.26) are supplemented by the weak form of the kinematic equation (2.30) or, equivalently, by (3.14), then $N_{22}(x)$ can be approximated as an independent variable. A dual-mixed formulation of this type with piece-wise constant approximation for $N_{22}(x)$ yields, however, the same stiffness matrix as given by (3.36). This is due to the fact that in the above formulation $N_{22}(x)$ is

expressed by $w(x)$ using (3.3), and $w(x)$ has been approximated by an element-wise constant function.

3.4. A consistent primal-dual mixed formulation. In view of the strong forms of the kinematic equation (2.7) and the equilibrium equation (2.23) of the shell model, a consistent finite element approximation would require that the polynomial degree of the displacement $w(x)$ be higher by one than that of the rotation $\phi(x)$, and the same applies to the bending moment $M_{11}(x)$ and shear force $N_{13}(x)$. In this sense, none of the three finite element formulations and models considered in Sections 3.1–3.3 is consistent, since both $w(x)$ and $\phi(x)$ are approximated by the same degree of polynomials (by either constant, or linear functions) and this is true for $M_{11}(x)$ and $N_{13}(x)$ as well.

A consistent approximation of the lowest possible order, i.e., constant for $\phi(x)$ and $N_{13}(x)$ and linear for $w(x)$ and $M_{11}(x)$, can easily be derived for the shell model investigated by mixing the weak forms (2.26)-(2.29) and (2.31)-(2.34) of the governing equations in such a way that one of the kinematic equations is considered in its first weak form, the other in its second weak form, and the equilibrium equations are taken into account accordingly. The corresponding consistent primal-dual mixed weak formulation, out of the two possible formulations of this type, is described by the following variational equations:

$$\int_{x_a}^{x_b} \left(\frac{1}{k_s G d} N_{13}^e - w_{;x}^e - \phi^e \right) \delta N_{13}^e dx = 0, \quad (3.40)$$

$$\int_{x_a}^{x_b} \left(\frac{1}{E_1 I_1} M_{11}^e \delta M_{11}^e + \phi^e \delta M_{11,x}^e \right) dx - [\phi \delta M_{11}]_{x_a}^{x_b} = 0, \quad (3.41)$$

$$\int_{x_a}^{x_b} \left[-N_{13}^e \delta w_{;x}^e - \frac{E d}{R^2} w^e \delta w^e + \hat{p}_3^e \delta w^e \right] dx + [N_{13} \delta w]_{x_a}^{x_b} = 0, \quad (3.42)$$

$$\int_{x_a}^{x_b} (M_{11,x}^e - N_{13}^e) \delta \phi^e dx = 0. \quad (3.43)$$

These equations can be considered as a special combination of the weak forms of the primal- and dual-mixed formulations of Sections 3.2 and 3.3. As the displacement boundary condition for $w(x)$ and the stress boundary condition for $M_{11}(x)$ are now essential, C^0 -continuous approximation is required for them. The boundary conditions for $\phi(x)$ and $N_{13}(x)$ are natural, they can be approximated discontinuously. The lowest possible order approximation of the variables is given as follows:

$$w^e [\xi(x)] = w_a \mathcal{N}_1(\xi) + w_b \mathcal{N}_2(\xi), \quad \phi^e(x) = \phi_0, \quad (3.44)$$

$$M_{11}^e [\xi(x)] = M_a \mathcal{N}_1(\xi) + M_b \mathcal{N}_2(\xi), \quad N_{13}^e(x) = Q_0. \quad (3.45)$$

This approximation is consistent with the strong form of the kinematic equation (2.7) and the equilibrium equation (2.23), as the polynomial degree of $w(x)$ is higher by one than $\phi(x)$, and the same applies to $M_{11}(x)$ and $N_{13}(x)$.

The element stiffness matrix for the present case can be obtained by introducing the nodal rotations ϕ_a and ϕ_b as Lagrangian multipliers to ensure the continuity of

$M_{11}(x)$ at the nodes. The corresponding variational equations are equivalent to (3.32) and (3.34) of the dual-mixed formulation of Section 3.3 and, therefore, they are not repeated here. After eliminating the element unknowns ϕ_0, Q_0, M_a, M_b , the matrix equation for the nodal variables $[u]^T = [w_a \ w_b \ \phi_a \ \phi_b]$ is obtained, which can be given briefly as

$$([K_m^{ST}] + [K_b^{ST}] + [K_s^{DM}]) [u] = [F^{ST}]. \quad (3.46)$$

According to the indices in the superscripts, the stiffness matrix of the primal-dual mixed element is obtained as the sum of the membrane and bending parts of the displacement-based (standard) stiffness matrix of (3.10) and the shear part of the dual-mixed stiffness matrix (3.36). The element load vector is equivalent to that of the displacement-based formulation given by (3.11).

Remark. In the above formulation, $N_{22}(x)$ is computed from $w(x)$ according to (3.3) and will be C^0 continuous and piece-wise linear (provided that $N_{11}(x)$ is at most a linear function). If $N_{22}(x)$ is considered as an independent variable and approximated by piece-wise constant function, just like in the case of the primal-mixed formulation of Section 3.2, then the membrane and bending parts of the primal-dual mixed stiffness matrix will be equal to those of the primal-mixed element and the same applies to the load vectors, i.e.,

$$([K_m^{PM}] + [K_b^{PM}] + [K_s^{DM}]) [u] = [F^{PM}].$$

Note, however, that neither constant nor linear approximation of the membrane force $N_{22}(x)$ is consistent with the strong form of the corresponding equilibrium equation (2.22).

3.5. Relationships between stiffness matrices and load vectors of different variational formulations and finite elements. In view of the results of Sections 3.1–3.4, the analytical comparison of the stiffness matrices and the load vectors gives the following results.

3.5.1. Comparison of the displacement-based and primal-mixed formulations. On comparing the stiffness matrices in (3.10) and (3.21), it can be seen that no difference exists between the bending parts, i.e., $[K_b^{ST}] = [K_b^{PM}]$. Four components in the membrane, as well as in the shear parts of the stiffness matrices are different; these terms are indicated by frames in (3.21). The load vectors (3.11) and (3.22) of the two formulations are equivalent, provided the membrane force N_{11}^e is zero.

The difference in the membrane stiffness matrices has no significant effect on the performance of the elements, which is due to the coefficient h^2/R^2 and to the fact, that in practical finite element computations the relation $h \ll R$ applies. The rather small difference in the shear parts results, however, in a dramatic change in the approximation properties of the elements for thin shell problems and, as is well known, the primal-mixed formulation leads to shear locking-free displacement computations, just like in the case of the Timoshenko beam element (see, e.g., [2, 18] and [17]). Note that the primal-mixed element of Section 3.2 can also be obtained by the reduced integration technique applied in the standard displacement formulation.

3.5.2. *Comparisons with respect to the dual-mixed formulation.* On comparing the element stiffness matrices in (3.21) and (3.36), it can be seen that no difference exists between their bending parts. The membrane and shear parts of the stiffness matrices of the primal- and dual-mixed formulations are related through the constants C_m and C_s , respectively, defined by (3.38) and (3.39). The relationships are given briefly by

$$[\mathbf{K}_m^{\text{DM}}] = \frac{1}{C_m}[\mathbf{K}_m^{\text{PM}}], \quad [\mathbf{K}_b^{\text{DM}}] = [\mathbf{K}_b^{\text{PM}}], \quad [\mathbf{K}_s^{\text{DM}}] = \frac{1}{C_s}[\mathbf{K}_s^{\text{PM}}]. \quad (3.47)$$

The load vectors (3.22) and (3.37) for arbitrary distributed load $p_3(x)$ are different and they are equivalent only in those cases when the shell element is subjected to concentrated shear forces and bending moments \tilde{Q}_i and \tilde{M}_i , $i = 1, 2$ at the nodes.

After some algebraic manipulation it can also be pointed out that the relationship between the sum of the bending and shear parts of the standard (displacement-based) element's stiffness matrix and that of the dual-mixed element can be written as

$$[\mathbf{K}_b^{\text{DM}}] + [\mathbf{K}_s^{\text{DM}}] = \frac{1}{C_s}([\mathbf{K}_b^{\text{ST}}] + [\mathbf{K}_s^{\text{ST}}]). \quad (3.48)$$

The sum of the above element stiffness matrices will be equal only when $C_s = 1$, i.e., in the limiting case of $h/d \rightarrow 0$. The above relation indicates that the results of the standard displacement formulation can, theoretically, never be equivalent to those of the dual-mixed formulation and, as is well known, the standard element cannot lead to shear locking-free results for shells, no matter how thin or thick the shell is.

3.5.3. *Comparisons with respect to the primal-dual mixed formulation.* Taking into account the results of Subsection 3.4 and making use of relations (3.47)-(3.48), the matrix equation (3.46) can be rewritten as

$$\{[\mathbf{K}_m^{\text{ST}}] + \frac{1}{C_s}([\mathbf{K}_b^{\text{ST}}] + [\mathbf{K}_s^{\text{ST}}])\}[\mathbf{u}] = [\mathbf{F}^{\text{ST}}]. \quad (3.49)$$

This equation suggests that the solution of the primal-dual mixed element for the nodal displacements $[\mathbf{u}]$ can be directly computed with the knowledge of the stiffness matrix and load vector of the standard shell element using the mesh-dependent constant C_s . The bending moment and shear force computation will, however, become equivalent to that of the primal-dual mixed element only in that case when they are computed from the nodal displacement vector $[\mathbf{u}]$ without differentiation, according to equations (B.5)-(B.6) and (B.9) of Appendix B.

Assuming that the primal-dual mixed formulation is locking-free, equation (3.49) suggests that either the mesh-dependent constant C_s , defined by (3.39), or its reciprocal

$$0 < \mathcal{L}_s = \frac{1}{C_s} \leq 1 \quad (3.50)$$

can be considered as a shear locking indicator for the standard shell element and its displacement solution. The closer \mathcal{L}_s is to zero, the more serious the shear locking is. $\mathcal{L}_s = C_s = 1$ would indicate absolutely locking-free behavior; it could be attained, however, only when the length h of the element is zero. The function $\mathcal{L}_s = \mathcal{L}_s(h/d)$, depicted in Figure 2 for $\nu = 0.3$ and $k_s = 5/6$, clearly indicates that only a sufficiently

refined mesh, when h/d is (much) smaller than unity and the corresponding \mathcal{L}_s value is close to 1, can lead to acceptable numerical results in the case of the standard element. For example, if the element size h is chosen to be equal to the thickness d , the error in the displacements is around 20%, with respect to the primal-dual mixed solution, no matter how thin or thick the shell is. Using (3.39), the required mesh size and element number for a given locking-error tolerance in the displacement computation can *a priori* be determined.

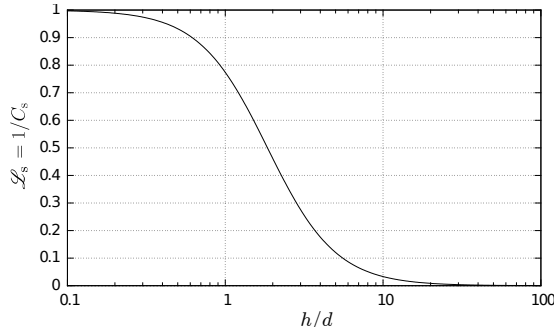


Figure 2. Locking indicator $\mathcal{L}_s = 1/C_s$ versus h/d

Remark. The coefficient C_m defined by (3.38) has a very similar structure to C_s in terms of h/R and the function $1/C_m$ versus h/R is practically the same as that of $1/C_s$ versus h/d in Figure 2. The relevance of C_m in the finite element computations is, however, not as significant as that of C_s , which is primarily due to the fact that relations $h \ll R$ and, thus, $h/R \ll 1$ usually hold true. In addition, the membrane part of the stiffness matrices contains the term $h^2/R^2 \lll 1$ as well.

4. NUMERICAL EXAMPLE AND COMPARISONS

The analytical comparisons of different variational formulations and finite element matrices, presented in the previous sections, are supplemented here by numerical comparisons through the solution of a simple demonstrative example, a clamped-clamped cylindrical shell subjected to uniform load $p_3(x) = p_0$ (Figure 3). The numerical solutions are computed and compared for shells with thickness to radius ratios $d/R = 10^{-2}$, 10^{-3} , 10^{-4} and 10^{-6} employing uniform mesh refinement. The decay length of the cylindrical shell is defined by [19]

$$\ell = \frac{2\pi}{\beta} \quad \text{with} \quad \beta = \sqrt[4]{\frac{3(1-\nu^2)}{R^2d^2}}. \quad (4.1)$$

In order to approximate the boundary layer correctly, $L = 4\ell$ is chosen for each shell investigated, and only half the length of the shell is discretized with symmetry conditions prescribed at $x = L/2 = 2\ell$. The radius of the mid-surface is $R = 1000$ mm, $E = 2 \cdot 10^5$ MPa, $\nu = 0.3$, $k_s = 5/6$, and the load value is $p_0 = 1$ MPa. The finite

element computations were performed using research codes written in MapleTM and Octave.

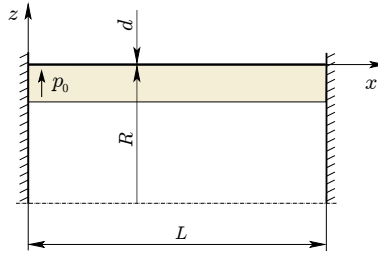


Figure 3. Clamped-clamped shell with uniform load

The decay lengths, as well as the analytical solutions for the central displacement, the maximum bending moment and shear force are listed in Table 2. Scaled values according to the expressions

$$\bar{w} = w d \quad \bar{M} = \frac{M_{11}}{d}, \quad \bar{Q} = \frac{N_{13}}{\beta d} \quad (4.2)$$

are also listed in Table 2. Note that these analytical solutions, based on the Naghdi shell model including shear deformations, are slightly different from that of the Koiter shell model which relies on the Kirchhoff-Love kinematical hypothesis and, thus, excludes shear deformations.

Table 2. Analytical solutions for clamped-clamped shell (Naghdi-model, scaled values)

d/R	ℓ [mm]	$\bar{w} _{L/2}$	\bar{M}_{\max}	\bar{Q}_{\max}
10^{-1}	1.545750e+03	4.999982	-2.765072e+02	5.659172e+02
10^{-2}	4.888090e+02	4.999967	-2.997833e+02	6.009802e+02
10^{-3}	1.545750e+02	4.999965	-3.023283e+02	6.047993e+02
10^{-4}	4.888090e+01	4.999965	-3.025852e+02	6.051847e+02
10^{-5}	1.545750e+01	4.999965	-3.026109e+02	6.052223e+02
10^{-6}	4.888090e+00	4.999965	-3.026135e+02	6.052271e+02

The convergence of the central displacement at $L/2$ is shown in Figure 4 (using logarithmic scale) for the formulations considered in Section 3. The well-known shear locking phenomenon for the standard displacement-based shell element is clearly seen from the figures. None of the mixed elements are sensitive to the d/R ratio and the asymptotic rate of convergence of the relative error in the displacements is of order two, independently of the mixed formulation employed.

Figure 5 shows the convergence curves of the relative error in the maximum bending moment (at $x = 0$) on a log-log scale. The error amplification due to shear locking

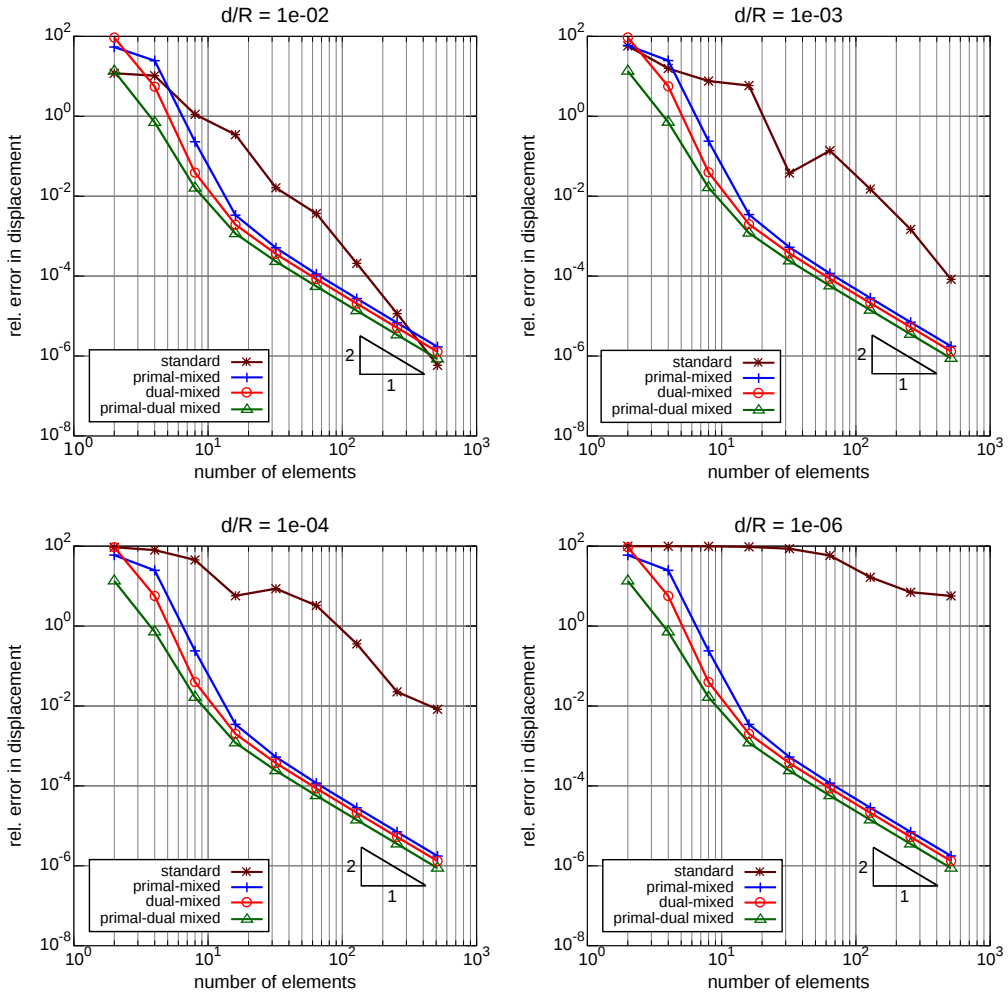


Figure 4. Convergence of the central displacement $w(L/2)$

of the standard element is apparent again as d/R decreases. The mixed elements are locking-free in the bending moment computations as well; the asymptotic rates of their convergences are, however, significantly different: while the primal-mixed element (equivalent, in this case, with the reduced integration displacement element) gives first-order rates, the dual-mixed and the primal-dual mixed elements give second-order rates of asymptotic convergence (3% error, for instance, in the bending moment requires about 30 dual-mixed elements and more than 500 primal-mixed elements). This property is clearly the main advantage in the application of the dual-mixed and the primal-dual mixed elements.

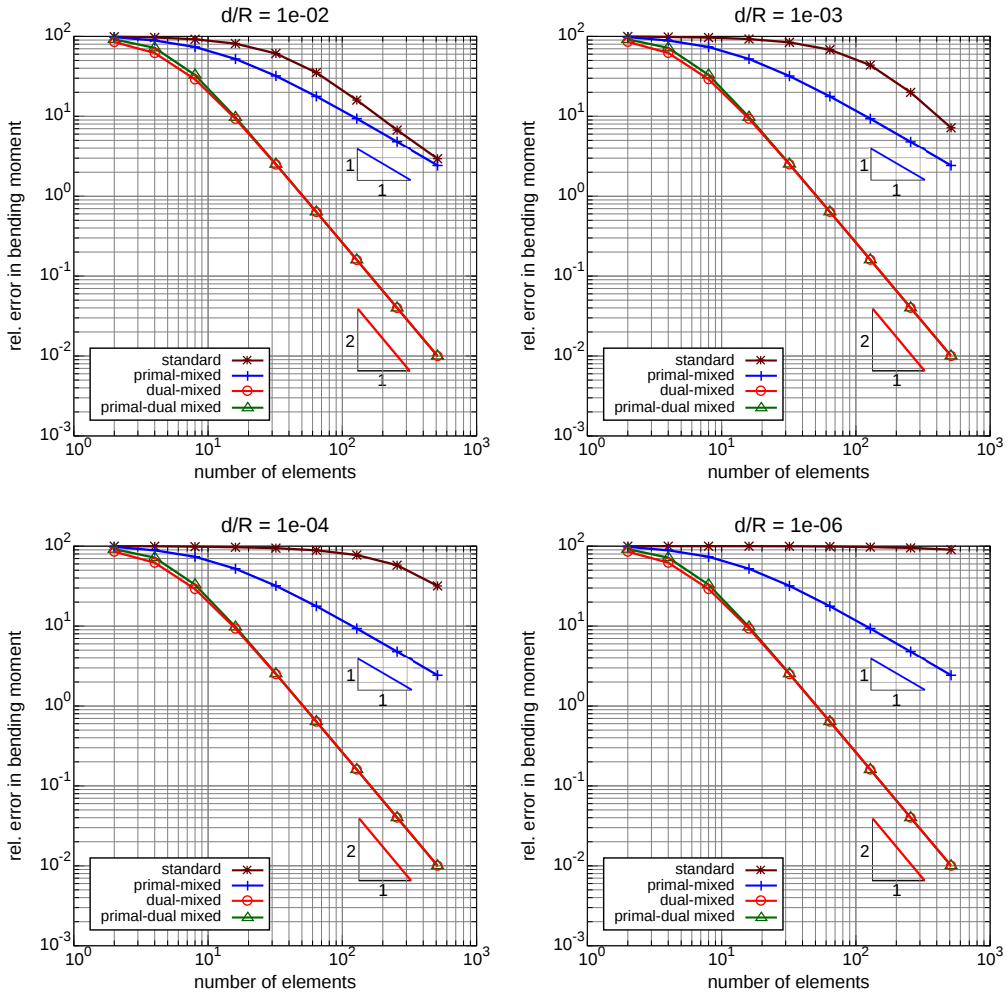


Figure 5. Convergence of the maximum bending moment

The convergence curves of the relative error in the maximum shear force (at $x = 0$) are depicted in Figure 6. To obtain comparable results for displacement-based and primal-mixed elements, the average nodal values of the first element have been taken as the shear force value at $x = 0$. The discretization error due to shear locking of the standard displacement element is the most serious in the shear force computation; the mixed elements are, again, locking-free. Only the dual-mixed element gives second-order rates of asymptotic convergence for the shear force, whereas the primal-mixed and the primal-dual mixed elements provide first-order rates of convergence only, as indicated in Figure 6. Note that the order of convergence is strongly related to the approximation order of the shear force: in the dual-mixed formulation the

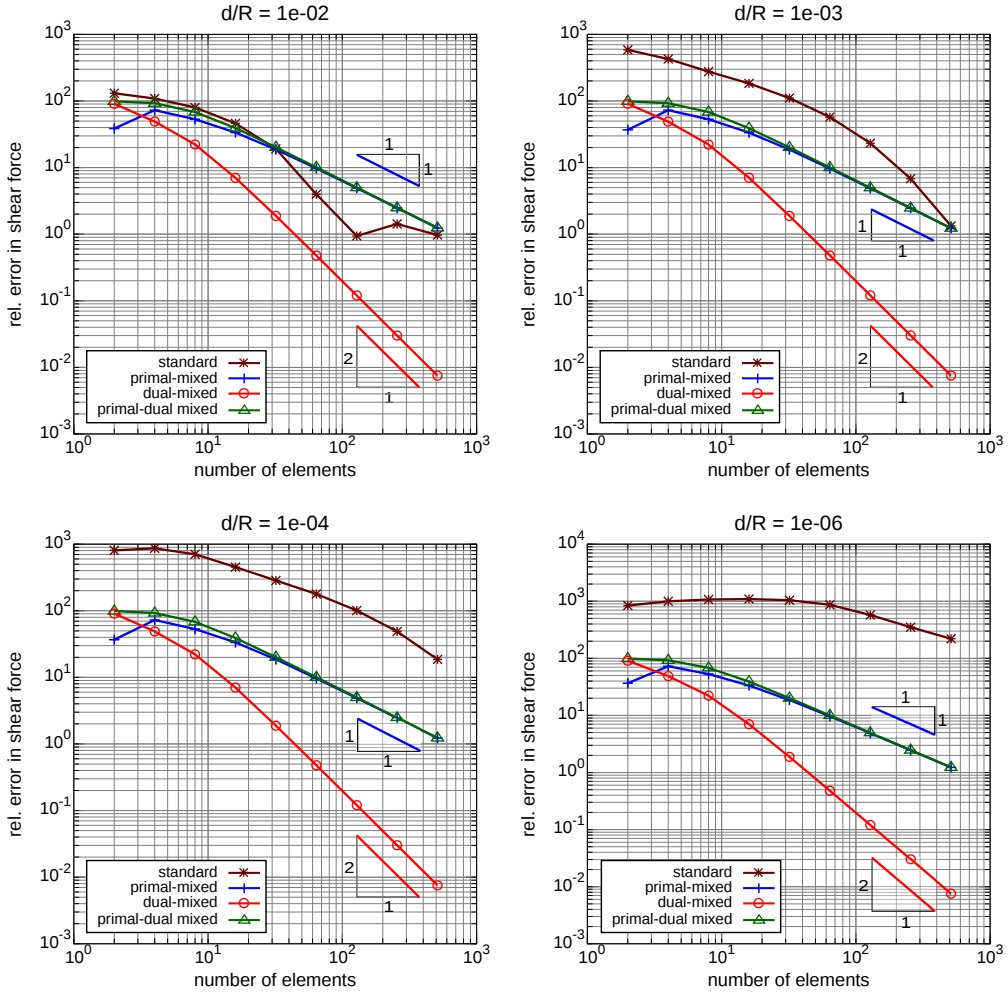


Figure 6. Convergence of the maximum shear force

shear force approximation is element-wise linear and obtained according to (B.7)-(B.8) of Appendix B. In the primal-dual-mixed formulation, the shear force is piece-wise constant and obtained according to (B.9).

5. CONCLUDING REMARKS

Considering the Naghdi shell model for axisymmetric deformations of cylindrical shells, the stiffness matrices and the load vectors of three different mixed finite elements have been derived and compared analytically and explicitly to each other and to those of the standard displacement element, using the lowest possible order

of polynomial approximations the formulations permit. The shear locking-free behavior of the mixed finite elements has been demonstrated through a simple model problem. The numerical results and comparisons clearly demonstrated that out of the four finite element models investigated in this paper, the dual-mixed element is the only one that gives second-order rates of asymptotic convergence for both the bending moment and shear force computations. This property is considered as the main advantage of the dual-mixed elements over the standard displacement-based and primal-mixed elements.

The analytical investigations of the relationships between the element stiffness matrices resulted in the introduction of two geometry-, material- and mesh-dependent coefficients denoted by C_m and C_s which can easily be computed for each element in the mesh. The effect of C_m is usually insignificant, the coefficient C_s , or its reciprocal denoted by \mathcal{L}_s turned out, however, to be a reliable shear locking indicator which can have a significant impact on the behavior of either the displacement-based, or the primal-mixed element. The structure of C_s , together with equation (3.49) and the presented numerical results, confirms the well-known fact that locking-free behavior can theoretically never be obtained using the original, unmodified, displacement-based shell element.

The results of the paper provide variational support for the transformability of the standard displacement-based shell element into a shear locking-free dual-mixed one, independently of the thickness and the loading of the shell. The recipe for obtaining shear locking-free solutions for cylindrical shells with second-order rates of convergence in all the variables (displacement, bending moment and shear force) from the knowledge of the stiffness matrix and load vector of the standard displacement formulation and the shear locking indicator C_s of (3.39) is the following:

- compute the standard element stiffness matrix and load vector for each element, according to Subsection 3.1 and equations (3.10)-(3.11);
- compute the mesh-dependent constant C_s according to (3.39) for each element of size h in the mesh;
- modify the element stiffness matrices according to (3.48)-(3.49) and, after assembling them, compute the solution for the nodal displacements and rotations;
- in the post-processing phase, compute the element bending moments and shear forces according to (B.5)-(B.6) and (B.7)-(B.8) of Appendix B.

Similar transformation steps can be applied to the element matrices of the primal-mixed formulations, according to equation (3.47), in order to obtain second-order rates of asymptotic convergence in the bending moment and shear force computations.

Acknowledgements. This research was carried out in the framework of the Center of Excellence of Innovative Engineering Design and Technologies at the University of Miskolc and was supported by the New Hungarian Development Plan and jointly financed by the European Union and European Social Fund (TÁMOP-4.2.1.B-10/2/KONV-2010-0001 project).

REFERENCES

1. BISHOFF, M., WALL, W. A., BLETZINGER, K.-U., and RAMM, E.: Models and finite elements for thin walled structures. In *The Encyclopedia of Computational Mechanics Vol. II* (E. Stein, R. de Borst and T. J. R. Hughes, Eds.). John Wiley & Sons, New York, 2004. pp. 59–137.
2. HUGHES, T. J. R.: *The Finite Element Method, Linear Static and Dynamic Finite Element Analysis*. Prentice-Hall, Englewood Cliffs, New Jersey, 1987.
3. BATHE, K.-J.: *Finite Element Procedures*. Prentice-Hall, Upper Saddle River, New Jersey, 1996.
4. REDDY, J. N.: *Theory and Analysis of Elastic Plates and Shells*. 2nd edn., CRC Press, Boca Raton, 2007.
5. CHAPELLE, D. and BATHE, K.-J.: *The Finite Element Analysis of Shells – Fundamentals*. Springer-Verlag, Berlin, 2nd edn., 2011.
6. ARCINIEGA, R. A. and REDDY, J.: Tensor-based finite element formulations for geometrically nonlinear analysis of shells. *Computer Methods in Applied Mechanics and Engineering*, **196**, (2007), 1048–1073.
7. ECHTER, R., OESTERLE, B., and BISCHOFF, M.: A hierarchic family of isogeometric shell finite elements. *Computer Methods in Applied Mechanics and Engineering*, **254**, (2013), 170–180.
8. NAGHDI, P. M.: Foundations of Elastic Shell Theory. In *Progress in Solid Mechanics, Vol. IV* (I. N. Sneddon and R. Hill, Eds.). North-Holland, Amsterdam, 1963. Pp. 1–90.
9. KRAUS, H.: *Thin Elastic Shells*. John Wiley & Sons, New York, 1967.
10. NAGHDI, P. M.: The Theory of Shells and Plates. In *Handbuch der Physik, Band VIa/2* (S. Flügge and C. Truesdell, Eds.). Springer-Verlag, Berlin, 1972. Pp. 425–640.
11. CIARLET, P. G.: *Mathematical Elasticity. Volume III: Theory of Shells*. North-Holland, Amsterdam, 2000.
12. PITKÄRANTA, J.: The problem of membrane locking in finite element analysis of cylindrical shells. *Numerische Mathematik*, **61**, (1992), 523–542.
13. ARNOLD, D. N. and BREZZI, F.: Locking-free finite element methods for shells. *Mathematics of Computation*, **66**, (1997), 1–14.
14. KLAAS, O., J. SCHRÖDER, STEIN, E., and MIEHE, C.: A regularized dual mixed element for plane elasticity. Implementation and performance of the BDM element. *Computer Methods in Applied Mechanics and Engineering*, **121**, (1995), 201–209.
15. ROBERTS, J. E. and THOMAS, J.-M.: Mixed and Hybrid Methods. In *Handbook of Numerical Analysis, Vol. II* (P. G. Ciarlet and J. L. Lions, Eds.). North-Holland, Amsterdam, 1991, pp. 523–639.
16. BOFFI, D., BREZZI, F., and FORTIN, M.: *Mixed and Hybrid Finite Element Methods and Applications*. Springer-Verlag, New York, 2013.
17. BERTÓTI, E.: A comparison of primal- and dual-mixed finite element formulations for Timoshenko beams. *Engineering with Computers*, **31(1)**, (2015), 99–111.
18. REDDY, J. N.: *Energy Principles and Variational Methods in Applied Mechanics*. 2nd edn., John Wiley & Sons, New York, 2002.

19. TIMOSHENKO, S. P. and WOINOWSKY-KRIEGER, S.: *Theory of Plates and Shells*. McGraw-Hill, New-York, 2nd edn., 2007.

APPENDIX A.

In the dual-mixed variational formulation and finite element model presented in Section 3.3, the continuity of the shear force $N_{13}(x)$ and bending moment $M_{11}(x)$ at the element nodes with labels $i = 0, 1, 2, \dots, n_e$ is enforced by the following variational equations:

$$\sum_{i=0}^{n_e} \delta w_i \llbracket Q_i \rrbracket = 0, \tag{A.1}$$

$$\sum_{i=0}^{n_e} \delta \phi_i \llbracket M_i \rrbracket = 0, \tag{A.2}$$

where n_e is the number of the elements, δw_i and $\delta \phi_i$ are arbitrary virtual nodal displacements and rotations, and

$$\llbracket Q_i \rrbracket = Q_i^{i+1} - Q_i^i, \tag{A.3}$$

$$\llbracket M_i \rrbracket = M_i^{i+1} - M_i^i \tag{A.4}$$

denote the jumps in the shear force and bending moment at node i , where i and $i + 1$ in the superscript refer to two neighboring elements with common node i in the subscript. Note that (A.1)-(A.2) represent $2 \times (n_e + 1)$ independent equations.

In Section 3.3, the virtual displacements at the nodes of element e , with nodal coordinates x_a and x_b , have been denoted by $\delta w_a \equiv \delta w_{e-1}$, $\delta w_b \equiv \delta w_e$, and the nodal values of the element shear force $Q^e(x)$ have been denoted by $Q_a \equiv Q_{e-1}^e \equiv Q^e(x_a)$ and $Q_b \equiv Q_e^e \equiv Q^e(x_b)$. Employing this simplified notation, equation (A.1) for element e takes the form

$$\delta w_a Q_a - \delta w_b Q_b = 0, \tag{A.5}$$

which proves (3.33). Applying a similar procedure and notation simplification with respect to equation (A.2), variational equation (3.34) is obtained for element e .

When concentrated external loads \tilde{Q}_i and \tilde{M}_i are given at node i , the jumps in the shear force and bending moment should be equal to these prescribed values. In this case, instead of (A.1)-(A.2), the modified variational equations

$$\delta w_i \llbracket Q_i \rrbracket = \delta w_i \tilde{Q}_i, \quad \delta \phi_i \llbracket M_i \rrbracket = \delta \phi_i \tilde{M}_i \tag{A.6}$$

hold at node i . For completeness it is noted that when displacement boundary conditions are prescribed for the nodal values w_i and ϕ_i at node i , then $\delta w_i = 0$ and $\delta \phi_i = 0$ in equations (A.1)-(A.2) and (A.6).

APPENDIX B.

The dual-mixed formulation of Section 3.3 leads to an equation system of the form

$$[A] [q] + [B] [u] + [f] = [0], \tag{B.1}$$

$$[\mathbf{B}]^T[\mathbf{q}] + [\mathbf{g}] = [\mathbf{0}] \quad (\text{B.2})$$

for each element, where, using (3.29), $[\mathbf{q}]^T = [[\mathbf{u}_0]^T [\mathbf{s}]^T]$. An equation system for the nodal variables $[\mathbf{u}]$, defined by (3.30), can be obtained performing static condensation: expressing the unknowns $[\mathbf{q}]$ from (B.1) as

$$[\mathbf{q}] = -[\mathbf{A}]^{-1}([\mathbf{B}][\mathbf{u}] + [\mathbf{f}]) \quad (\text{B.3})$$

and substituting (B.3) into (B.2) leads to equation (3.35) with the following matrix expressions:

$$\begin{aligned} [\mathbf{K}^{\text{DM}}][\mathbf{u}] &= [\mathbf{F}^{\text{DM}}], & [\mathbf{K}^{\text{DM}}] &= [\mathbf{B}]^T[\mathbf{A}]^{-1}[\mathbf{B}], \\ & & [\mathbf{F}^{\text{DM}}] &= [\mathbf{g}] - [\mathbf{B}]^T[\mathbf{A}]^{-1}[\mathbf{f}]. \end{aligned} \quad (\text{B.4})$$

When the solution for $[\mathbf{u}]$ is known, the bending moment and shear force of the element can be computed using (B.3). For the dual-mixed element of Section 3.3, the nodal bending moments and shear forces are obtained as

$$M_a = \frac{1}{C_s} \left[\frac{k_s G d}{2} (w_a - w_b) + \frac{E_1 I_1}{h} (\phi_b - \phi_a) - \frac{k_s G h d}{6} (2\phi_a + \phi_b) \right], \quad (\text{B.5})$$

$$M_b = \frac{1}{C_s} \left[\frac{k_s G d}{2} (w_b - w_a) + \frac{E_1 I_1}{h} (\phi_b - \phi_a) + \frac{k_s G h d}{6} (\phi_a + 2\phi_b) \right], \quad (\text{B.6})$$

$$Q_a = -\frac{1}{C_m} \frac{E h d}{4 R^2} (w_a + w_b) + \frac{1}{C_s} k_s G d \left(\frac{w_b - w_a}{h} + \frac{\phi_a + \phi_b}{2} \right) + \frac{1}{C_m} \frac{h}{4} \int_{-1}^{+1} \hat{p}_3^e(\xi) d\xi, \quad (\text{B.7})$$

$$Q_b = \frac{1}{C_m} \frac{E h d}{4 R^2} (w_a + w_b) + \frac{1}{C_s} k_s G d \left(\frac{w_b - w_a}{h} + \frac{\phi_a + \phi_b}{2} \right) - \frac{1}{C_m} \frac{h}{4} \int_{-1}^{+1} \hat{p}_3^e(\xi) d\xi. \quad (\text{B.8})$$

For the primal-dual mixed element in Section 3.4, the nodal bending moments can be computed according to (B.5)-(B.6) and the constant element shear force is

$$Q_0 = \frac{1}{C_s} k_s G d \left(\frac{w_b - w_a}{h} + \frac{\phi_a + \phi_b}{2} \right). \quad (\text{B.9})$$

The mesh-dependent constants C_m and C_s are given by (3.38)-(3.39).

ON THE DIRECT BEM FORMULATION IN THE DUAL SYSTEM OF PLANE ELASTICITY FOR ORTHOTROPIC BODIES

JUDIT DUDRA

Institute of Logistics and Production Systems
H-3519 Miskolctapolca, Iglói út 2. Hungary
judit.dudra@gmail.com

GYÖRGY SZEIDL

Institute of Applied Mechanics, University of Miskolc
H-3515 Miskolc, Miskolc–Egyetemváros, Hungary
gyorgy.szeidl@uni-miskolc.hu

[Received: February 28, 2015, Accepted: September 18, 2015.]

*Dedicated to Professor Barna Szabó on the occasion of his eightieth birthday
and to Professor Imre Kozák on the occasion of his eighty-fifth birthday*

Abstract. The paper is devoted to plane problems of orthotropic bodies in a dual formulation. After presenting the governing equations in terms of stress functions of order one, we determine the two fundamental solutions and set up the dual Somigliana relations both for inner and exterior regions. These include the boundary integral equations of the direct method. A constant stress state at infinity is part of the formulation established for exterior regions. We also derive an integral representation of the stresses. The numerical examples presented illustrate the applicability of the direct boundary integral equations.

Mathematical Subject Classification: 74S15, 45F15

Keywords: Plane problems, orthotropic bodies, stress functions of order one, the dual Somigliana formulae, direct boundary element method

1. INTRODUCTION

According to the famous TONTI scheme [1], in the primal system of elasticity the displacement field is the basic variable while the strains and stresses are the intermediate variables of the first and second kind. Body forces are referred to as the source variable. Problems in the primal system are governed by the primal kinematic equations, which relate the strains to the displacements; HOOKE's law, which connects the primal intermediate variables of the second kind to those of the first kind; and the equilibrium or primal balance equations, written in terms of the intermediate variables of the second kind.

In the dual system of elasticity, stress functions are the basic variables, and stresses and strains constitute the intermediate variables of the first and second kind. A prescribed incompatibility, which is in general zero, is the source variable. Problems in the dual system are governed by the dual kinematic equations, which express the stresses in terms of stress functions; the inverse form of HOOKE's law, which relates the dual intermediate variables of the second kind to that of the first kind; and the compatibility equations (dual balance equations).

In a classical paper, RIZZO and SHIPPY [2] solve plane problems by the direct boundary element method for which physical quantities (in the primal system the displacements and the stress vector) are the unknowns on the boundary. These authors assume that the body is orthotropic and focus on an inner region. The most important relations are presented for anisotropic bodies as well. As in earlier work by RIZZO [3], the numerical solution is based on a constant approximation of the displacements and the stress vector over boundary elements.

A number of subsequent papers study the boundary value problems of plane elasticity using the boundary element method under the assumption that the material is orthotropic or anisotropic. VABLE and SIKARSKIE apply the indirect method for which the solution is sought in terms of appropriately chosen potential functions [4]. SHIAH and TAN transform 2D and 3D anisotropic field problems in such a way that the Laplace operator becomes the operator of the basic equation, a procedure known as direct domain mapping [5, 6]. However, these results can only be applied to problems of elasticity when it is possible to define a displacement potential which satisfies the basic equation investigated by SHIAH and TAN. HUNG, SAN, LIU and ZEN [7] also study orthotropic bodies and provide additional references. We emphasize that all these papers [2, 3, 4, 7] as well as the books [8, 9] and the references they cite use the primal system of plane elasticity.

While many papers study plane problems in the primal system, there are only a few which use the dual system and treat the real stress functions of order one as the basic variables. One advantage of using stress functions of order one is that calculating stresses only requires determining first derivatives, while with stress functions of order two the stresses are obtained in terms of the second derivatives. First derivatives are more convenient in boundary element applications, although an additional equation is needed to ensure that the stresses are symmetric. Assuming homogenous and isotropic materials and using stress functions of order one, SZEIDL investigated the plane problem with the direct boundary element method in the dual system of elasticity [10, 11].

Our goal in this paper is to extend the results presented in [10, 11] as well as those in the thesis [12] for homogenous but orthotropic materials. We develop the fundamental solutions and the Somigliana relations in the dual system of plane elasticity for an orthotropic body provided that the stress functions of order one are the basic variables. We then set up a direct boundary element formulation and present an algorithm for numerical solutions. The examples shown illustrate the applicability of the algorithm.

The paper is organized into eight sections. Section 2 presents the governing equation of the problem in a dual formulation. The fundamental solutions of order one and two are determined in Section 3. The dual Somigliana relations for inner and outer regions are derived in Sections 4 and 5. Section 6 deals with the determination of the stresses on the boundary. The last two sections present two numerical examples and a conclusion.

2. GOVERNING EQUATIONS

Throughout this paper $x_1 = x$ and $x_2 = y$ are rectangular Cartesian coordinates, referred to an origin O . For vectorial and tensorial quantities indicial notations are used. {Greek}[Latin subscripts] are assumed to have the range $\{(1,2)\}[(1,2,3)]$, summation over repeated indices is implied, $\delta_{\kappa\lambda}$ is the Kronecker delta, ε_{pqr} is the permutation symbol. If an index in a summation is repeated more than twice, we also typeset the summation symbol to avoid misunderstanding (see for instance equation (3.9) below).

The inner and outer regions shown in Figure 1 are denoted by A_i and A_e . They are bounded by the contour

$$\mathcal{L}_0 = \mathcal{L}_{t1} \cup \mathcal{L}_{u2} \cup \mathcal{L}_{t3} \cup \mathcal{L}_{u4} .$$

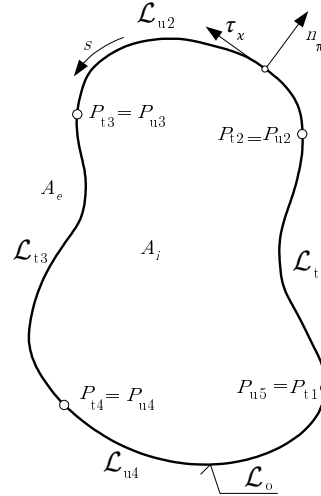


Figure 1.

We assume that [displacements]{tractions} are imposed on the arc $[\mathcal{L}_u = \mathcal{L}_{u2} \cup \mathcal{L}_{u4}]\{\mathcal{L}_t = \mathcal{L}_{t1} \cup \mathcal{L}_{t3}\}$. We stipulate that the contour has a unit tangent τ_κ and admits an appropriate parametrization in terms of its arc length s . The outer unit normal is denoted by n_π . In accordance with the notations introduced ∂_α stands for the derivatives taken with respect to x_α . Assuming plane problems let u_κ , $e_{\kappa\lambda}$ and $t_{\kappa\lambda}$ be the displacement field and the in plane components of strain and stress, respectively. The stress functions of order one are denoted by \mathcal{F}_ρ .

We shall assume that there are no body forces.

For homogenous and orthotropic material the plane problem of classical elasticity in the dual system of elasticity is governed by

1. the dual kinematic equations

$$t_{11} = \mathcal{F}_1 \partial_2, \quad t_{12} = \mathcal{F}_2 \partial_2, \quad (2.1a)$$

$$t_{21} = -\mathcal{F}_1 \partial_1, \quad t_{22} = -\mathcal{F}_2 \partial_1, \quad (2.1b)$$

which express the stresses in terms of stress functions of order one,

2. the inverse form of HOOKE's law

$$e_{11} = u_1 \partial_1 = s_{11} t_{11} + s_{12} t_{22}, \quad e_{22} = u_2 \partial_2 = s_{21} t_{11} + s_{22} t_{22}, \quad (2.2a)$$

$$e_{12} = \frac{1}{2} (u_1 \partial_2 + u_2 \partial_1) = \frac{s_{66}}{4} (t_{12} + t_{21}); \quad (2.2b)$$

where s_{11}, s_{12}, s_{21} and s_{22} stand for the constants of elasticity¹,

3. the compatibility conditions

$$e_{11} \partial_2 - e_{12} \partial_1 + \varphi_3 \partial_1 = 0, \quad e_{21} \partial_2 - e_{22} \partial_1 + \varphi_3 \partial_2 = 0 \quad (2.3)$$

in which φ_3 is the rotation field

4. and the symmetry condition

$$t_{12} = t_{21}. \quad (2.4)$$

If this equation is fulfilled then either equation (2.1a)₂ or equation (2.1b)₁ can be omitted. Thus we have nine equations for the nine unknowns $\mathcal{F}_1, \mathcal{F}_2, t_{11}, t_{12} = t_{21}, t_{22}, e_{11}, e_{12} = e_{21}, e_{22}$ and φ_3 .

Field equations (2.1a,b), (2.2a,b), (2.3) and (2.4) should be associated with appropriate boundary conditions. If the contour is not divided into parts then either tractions or displacements can be imposed on it. In the opposite case the contour is assumed to be divided into arcs of even number on which displacements and tractions are imposed alternately. As mentioned earlier, in Figure 1 {tractions}[displacements] are prescribed on the arc $\{\mathcal{L}_t\}[\mathcal{L}_u]$. Variables with hats stand for the values prescribed: $\hat{u}_\kappa, \hat{t}_\rho$ and $\hat{\mathcal{F}}_\rho$ are the prescribed displacements, tractions (stress vector) and stress functions, respectively.

For the sake of a formal similarity of the boundary integral equations regarded in primal and dual formulations we introduce the notation

$$\mathbf{t}_\lambda = -n_\kappa (\varepsilon_{\kappa\rho 3} e_{\rho\lambda} - \delta_{\kappa\lambda} \varphi_3) \quad s \in \mathcal{L}_o, \quad (2.5a)$$

where on the other hand

$$\mathbf{t}_\lambda = -\frac{du_\kappa}{ds} \quad s \in \mathcal{L}_o. \quad (2.5b)$$

We refer to \mathbf{t}_λ as the dual stress vector and to its elements as dual stresses. Observe that the same letter denotes both the stresses and the dual stresses; we distinguish between them by typesetting the dual stresses in calligraphic fonts. The same notational convention will be used for the dual displacements defined by equation (3.2)₂.

The dual field equations (2.1a), ..., (2.4) should be associated with the strain boundary conditions of the form

$$\mathbf{t}_\kappa = -\frac{d\hat{u}_\kappa}{ds} \quad s \in \mathcal{L}_u, \quad (2.6)$$

¹The strain energy density u should be strictly positive:

$$2u = t_{11} (s_{11} t_{11} + s_{12} t_{22}) + t_{22} (s_{21} t_{11} + s_{22} t_{22}) + \frac{s_{66}}{4} (t_{12} + t_{21}) (t_{12} + t_{21}) > 0.$$

(note that one can not prescribe boundary conditions directly on the displacements since they do not belong to the set of dual variables) and a set of boundary conditions imposed on the stress functions

$$\mathcal{F}_\rho(s) - \underbrace{\mathcal{F}_\rho(P_{ti})}_{C_{(ti)\rho}} = \underbrace{\int_{P_{ti}}^s \hat{t}_\rho(\sigma) d\sigma}_{\hat{\mathcal{F}}_\rho(s)}, \quad s \in \mathcal{L}_{ti}, \quad i = 1, 3 \quad (2.7)$$

where the integral with value $\hat{\mathcal{F}}_\rho(s)$ on the right side is the resultant of the tractions prescribed on the arc $[P_{ti}, s]$ while $C_{(ti)\rho}$ is an undetermined constant of integration.

The supplementary conditions of single valuedness can easily be obtained from equation (2.6). These conditions express displacement continuity at the endpoints of the arcs \mathcal{L}_{ti} regarded on the contour and have the form

$$\int_{\mathcal{L}_{ti}} n_\kappa (\varepsilon_{\kappa\rho 3} e_{\rho\lambda} - \delta_{\kappa\lambda} \varphi_3) ds - \hat{u}_\lambda|_{P_{ti}^{t,i+1}} = 0 \quad (i = 1, 3). \quad (2.8)$$

Observe that we have as many undetermined constants of integration as there are supplementary conditions of single valuedness.

One undetermined constant of integration $C_{(ti)\rho}$ can be set to zero without loss of generality, since the equations (2.1b,c) contain only the derivatives of the stress functions. It can also be shown that the supplementary conditions of single valuedness (2.8) are not independent, i.e., one condition can always be omitted. A proof for the latter statement assuming isotropic bodies and plane problems can be found in the thesis [13] by Szeidl.

3. BASIC EQUATION AND FUNDAMENTAL SOLUTIONS

After eliminating the intermediate variables $e_{\kappa\lambda}$ and $t_{\kappa\lambda}$ from the compatibility conditions (2.3) and the symmetry condition (2.4) we obtain the basic equation in the form

$$\mathfrak{D}_{ik} u_k = 0 \quad i = 1, 2, 3 \quad (3.1)$$

where \mathfrak{D}_{ik} is a differential operator and u_k is the vector of fundamental variables (the stress functions u_κ – see below – will be referred to as dual displacements):

$$[\mathfrak{D}_{ik}] = \begin{bmatrix} s_{11} \partial_2 \partial_2 + \frac{s_{66}}{4} \partial_1 \partial_1 & - \left(s_{12} + \frac{s_{66}}{4} \right) \partial_1 \partial_2 & -\partial_1 \\ - \left(s_{21} + \frac{s_{66}}{4} \right) \partial_1 \partial_2 & s_{22} \partial_1 \partial_1 + \frac{s_{66}}{4} \partial_2 \partial_2 & -\partial_2 \\ -\partial_1 & -\partial_2 & 0 \end{bmatrix}, \quad u_k = \underbrace{(\mathcal{F}_1, \mathcal{F}_2, -\varphi_3)}_{u_\kappa}. \quad (3.2)$$

Let $Q(\xi_1, \xi_2)$ and $M(x_1, x_2)$ be two points in the plane of strain: the source point and the field point. We shall assume temporarily that the point Q is fixed. The distance between Q and M is R , the position vector of M relative to Q is r_κ . We refer to the

solution of the differential equation

$$\overset{M}{\mathfrak{D}}_{ik} \mathbf{u}_k + \delta(M - Q) e_i(Q) = 0, \quad i = 1, 2, 3 \quad (3.3)$$

as the fundamental solution. Here $\delta(M - Q)$ stands for the Dirac function, $e_\kappa(Q)$ is a prescribed incompatibility and $e_3(Q)$ is a couple perpendicular to the plane of strain. We determine the fundamental solution following the approach of KUPRADZE [14], here we only present the main steps in the derivation.

Let D_{kl} be the cofactor of \mathfrak{D}_{ik}

$$\mathfrak{D}_{ik} D_{kl} = \det(\mathfrak{D}_{mn}) \delta_{il}. \quad (3.4)$$

We seek the fundamental variables \mathbf{u}_k in the form

$$\mathbf{u}_k = D_{kl} \chi_l, \quad (3.5)$$

where $\chi_l = \chi e_l(Q)$ and χ is the Galjorkin function. If we substitute (3.5) into (3.3) and take (3.4) into account we get

$$\det(\mathfrak{D}_{mn}) \chi + \delta(M - Q) = 0 \quad (3.6)$$

where

$$\det(\mathfrak{D}_{mn}) = - [s_{11} \partial_2^4 + (2s_{21} + s_{66}) \partial_1^2 \partial_2^2 + s_{22} \partial_1^4]. \quad (3.7)$$

For the sake of later calculations we introduce the following quantities

$$\alpha_{1,2}^2 = -\frac{2s_{21} + s_{66}}{2s_{11}} \pm \sqrt{\left(\frac{2s_{21} + s_{66}}{2s_{11}}\right)^2 - \frac{s_{22}}{s_{11}}}, \quad \beta_\kappa^2 = -1/\alpha_\kappa \quad (3.8a)$$

$$\rho_\kappa = (x_1 - \xi_1) + \beta_\kappa(x_2 - \xi_2), \quad (3.8b)$$

$$d_1 = - \begin{vmatrix} 1 & \tilde{\beta}_1 & \tilde{\beta}_1^2 \\ 1 & \beta_2 & \beta_2^2 \\ 1 & \tilde{\beta}_2 & \tilde{\beta}_2^2 \end{vmatrix}, \quad d_2 = - \begin{vmatrix} 1 & \beta_1 & \beta_1^2 \\ 1 & \tilde{\beta}_1 & \tilde{\beta}_1^2 \\ 1 & \tilde{\beta}_2 & \tilde{\beta}_2^2 \end{vmatrix}, \quad (3.8c)$$

($\tilde{\beta}_\kappa$ is the complex conjugate of β_κ)

$$\mathcal{K} = -\frac{1}{I_1 + I_2}, \quad I_\kappa = 4\pi \frac{d_\kappa}{b_\kappa + 1} (b_\kappa^3 s_{11} + b_\kappa^2 (s_{21} + s_{66}) - b_\kappa s_{12} - s_{22}), \quad (3.8d)$$

$$b_1 = \sqrt{D_1 - \sqrt{D}}, \quad b_2 = \sqrt{D_1 + \sqrt{D}} \quad (3.8e)$$

$$D = \left(\frac{2s_{21} + s_{66}}{2s_{11}}\right)^2 - \frac{s_{22}}{s_{11}}, \quad D_1 = \frac{2s_{21} + s_{66}}{2s_{11}} \quad (3.8f)$$

$$a_{33} = s_{11} s_{22} + \left(\frac{s_{66}}{4}\right)^2 - \left(s_{21} + \frac{s_{66}}{4}\right)^2. \quad (3.8g)$$

Using the quantities introduced it can be shown that the solution for χ takes the form

$$\chi(M, Q) = \mathcal{K} \operatorname{Im} \sum_{\kappa=1}^2 d_\kappa \rho_\kappa^2 \ln \rho_\kappa. \quad (3.9)$$

With the GALERKIN function χ it follows from equation (3.5) that

$$\mathbf{u}_k = D_{kl}\chi_l = \underbrace{D_{kl}\chi}_{\mathfrak{U}_{kl}} e_l = \mathfrak{U}_{kl}(M, Q)e_l(Q), \quad (3.10)$$

where $\mathfrak{U}_{kl}(M, Q)$ is the matrix of the fundamental solution of order one. Omitting the long formal transformations we find that

$$[\mathfrak{U}_{pq}(Q, M)] = \text{Im} \sum_{k=1}^2 \mathcal{K} \times \begin{bmatrix} d_k (2 \ln \rho_k + 3) \beta_k^2 & d_k (2 \ln \rho_k + 3) \beta_k & \frac{2d_k}{\rho_k} \left[-(s_{21} + \frac{s_{66}}{2}) \beta_k^2 + s_{22} \right] \\ d_k (2 \ln \rho_k + 3) \beta_k & d_k (2 \ln \rho_k + 3) & \frac{2d_k \beta_k}{\rho_k} \left[(s_{12} + \frac{s_{66}}{2}) - s_{11} \beta_k^2 \right] \\ \frac{2d_k}{\rho_k} \left[s_{22} - (s_{21} + \frac{s_{66}}{2}) \beta_k^2 \right] & \frac{2d_k \beta_k}{\rho_k} \left[(s_{21} + \frac{s_{66}}{2}) - s_{11} \beta_k^2 \right] & \left\{ s_{21} s_{66} + \frac{s_{66}^2}{2} - 2a_{33} \right\} \beta_k^2 \frac{d_k}{\rho_k} \end{bmatrix} \quad (3.11)$$

Recalling the dual kinematic equations (2.1a,b) we obtain the fundamental solutions for the stresses t_{11} , $t_{12} = t_{21}$ and t_{22} by calculating from the following equations:

$$t_{11} = \mathcal{F}_1 \overset{M}{\partial}_2 = \mathbf{u}_1 \overset{M}{\partial}_2 = \overset{M}{\partial}_2 \mathfrak{U}_{1l}(M, Q)e_l(Q), \quad (3.12)$$

$$t_{12} = \mathcal{F}_2 \overset{M}{\partial}_2 = \overset{M}{\partial}_2 \mathfrak{U}_{2l}(M, Q)e_l(Q) = t_{21} = -\mathcal{F}_1 \overset{M}{\partial}_1 = -\overset{M}{\partial}_1 \mathfrak{U}_{1l}(M, Q)e_l(Q), \quad (3.13)$$

$$t_{22} = -\mathcal{F}_2 \overset{M}{\partial}_1 = -\mathbf{u}_2 \overset{M}{\partial}_1 = -\overset{M}{\partial}_1 \mathfrak{U}_{2l}(M, Q)e_l(Q). \quad (3.14)$$

After performing the necessary calculations we have

$$\begin{bmatrix} t_{11} \\ t_{12} \\ t_{22} \end{bmatrix} = \mathcal{K} \text{Im} \sum_{k=1}^2 \frac{2d_k}{\rho_k} \begin{bmatrix} -\beta_k^3 & \beta_k^2 & -\frac{\beta_k}{\rho_k} \left[(s_{21} + \frac{s_{66}}{2}) \beta_k^2 + s_{22} \right] \\ \beta_k^2 & -\beta_k & \frac{1}{\rho_k} \left[(s_{21} + \frac{s_{66}}{2}) \beta_k^2 + s_{22} \right] \\ -\beta_k & 1 & \frac{\beta_k}{\rho_k} \left[(s_{12} + \frac{s_{66}}{2}) + s_{11} \beta_k^2 \right] \end{bmatrix} \begin{bmatrix} e_1 \\ e_2 \\ e_3 \end{bmatrix}. \quad (3.15)$$

With the knowledge of the stresses, the strains can be obtained from the HOOKE law (2.2a,b):

$$\begin{bmatrix} e_{11} \\ e_{12} \\ e_{22} \end{bmatrix} = \mathcal{K} \text{Im} \sum_{k=1}^2 \frac{2d_k}{\rho_k} \times \begin{bmatrix} -s_{11} \beta_k^3 - s_{12} \beta_k & s_{11} \beta_k^2 + s_{12} & -\frac{\beta_k}{\rho_k} \left[(s_{12} + \frac{s_{66}}{2})(s_{11} \beta_k^2 - s_{12}) + s_{11}(s_{22} - s_{12} \beta_k^2) \right] \\ \frac{1}{2} s_{66} \beta_k^2 & -\frac{1}{2} s_{66} \beta_k & \frac{s_{66}}{2 \rho_k} \left[(s_{21} + \frac{s_{66}}{2}) \beta_k^2 + s_{22} \right] \\ -s_{21} \beta_k^3 - s_{22} \beta_k & s_{21} \beta_k^2 + s_{22} & -\frac{\beta_k}{\rho_k} \left[(s_{21} + \frac{s_{66}}{2})(s_{21} \beta_k^2 - s_{22}) + s_{22}(s_{21} - s_{11} \beta_k^2) \right] \end{bmatrix} \begin{bmatrix} e_1 \\ e_2 \\ e_3 \end{bmatrix}. \quad (3.16)$$

The dual stress vector is defined by equation (2.5a). We can compute the dual stress vector from the fundamental solution of order one to obtain

$$\mathbf{t}_\kappa = -\frac{du_\kappa}{ds} = e_l(Q)\mathcal{T}_{l\kappa}(\overset{o}{M}, Q), \quad (3.17)$$

where $\mathcal{T}_{l\kappa}$ is referred to as fundamental solution of order two. The formal calculations are based on equation (2.5a,b), which can be rewritten in a matrix form:

$$-\frac{d}{ds} \begin{bmatrix} u_1 \\ u_2 \end{bmatrix} = \begin{bmatrix} n_2 & -n_1 & 0 \\ 0 & n_2 & -n_1 \end{bmatrix} \begin{bmatrix} e_{11} \\ e_{12} \\ e_{22} \end{bmatrix} + \begin{bmatrix} n_1 \\ n_2 \end{bmatrix} \varphi_3 \quad (3.18)$$

We remark that these calculations require the use of equation (3.16) and $e_l(Q)\mathcal{U}_3(M_o, Q)$ – the latter provides φ_3 . Omitting the details, we obtain for $\mathcal{T}_{l\kappa}$:

$$\begin{aligned} \mathfrak{T}_{11}(M_o, Q) = \mathcal{K} \operatorname{Im} \sum_{\kappa=1}^2 \frac{2d_\kappa}{\rho_\kappa} \left\{ n_2 (-s_{11}\beta_\kappa^3 - s_{12}\beta_\kappa) - \frac{n_1}{2} s_{66}\beta_\kappa^2 - \right. \\ \left. - n_1 \left[s_{22} + \left(s_{21} + \frac{s_{66}}{2} \right) \beta_\kappa^2 \right] \right\}, \quad (3.19a) \end{aligned}$$

$$\begin{aligned} \mathfrak{T}_{21}(M_o, Q) = \mathcal{K} \operatorname{Im} \sum_{\kappa=1}^2 \frac{2d_\kappa}{\rho_\kappa} \left\{ n_2 (s_{11}\beta_\kappa^2 + s_{12}) + \frac{n_1}{2} s_{66}\beta_\kappa - \right. \\ \left. - n_1\beta_\kappa \left[\left(s_{12} + \frac{s_{66}}{2} \right) + s_{11}\beta_\kappa^2 \right] \right\}, \quad (3.19b) \end{aligned}$$

$$\begin{aligned} \mathfrak{T}_{12}(M_o, Q) = \mathcal{K} \operatorname{Im} \sum_{\kappa=1}^2 \frac{2d_\kappa}{\rho_\kappa} \left\{ \frac{n_2}{2} s_{66}\beta_\kappa^2 + n_1 (s_{21}\beta_\kappa^3 + s_{22}\beta_\kappa) - \right. \\ \left. - n_2 \left[s_{22} + \left(s_{21} + \frac{s_{66}}{2} \right) \beta_\kappa^2 \right] \right\}, \quad (3.19c) \end{aligned}$$

$$\begin{aligned} \mathfrak{T}_{22}(M_o, Q) = \mathcal{K} \operatorname{Im} \sum_{\kappa=1}^2 \frac{2d_\kappa}{\rho_\kappa} \left\{ -\frac{n_2}{2} s_{66}\beta_\kappa - n_1 (s_{21}\beta_\kappa^2 + s_{22}) - \right. \\ \left. - n_2\beta_\kappa \left[\left(s_{12} + \frac{s_{66}}{2} \right) + s_{11}\beta_\kappa^2 \right] \right\}, \quad (3.19d) \end{aligned}$$

$$\begin{aligned} \mathfrak{T}_{31}(M_o, Q) = \mathcal{K} \operatorname{Im} \sum_{\kappa=1}^2 \frac{2d_\kappa}{\rho_\kappa} \left\{ -\frac{n_2\beta_\kappa}{\rho_\kappa} \left[\left(s_{12} + \frac{s_{66}}{2} \right) (s_{11}\beta_\kappa^2 - s_{12}) + s_{11}(s_{22} - s_{12}\beta_\kappa^2) \right] - \right. \\ \left. - \frac{n_1 s_{66}}{2\rho_\kappa} \left[\left(s_{21} + \frac{s_{66}}{2} \right) \beta_\kappa^2 + s_{22} \right] + n_1 \frac{\beta_\kappa^2}{\rho_\kappa} \left[a_{33} - \frac{s_{21}s_{66}}{2} - \frac{s_{66}^2}{4} \right] \right\}, \quad (3.19e) \end{aligned}$$

$$\begin{aligned} \mathfrak{T}_{32}(M_o, Q) = \mathcal{K} \operatorname{Im} \sum_{\kappa=1}^2 \frac{2d_\kappa}{\rho_\kappa} \left\{ \frac{n_2 s_{66}}{2\rho_\kappa} \left[\left(s_{21} + \frac{s_{66}}{2} \right) \beta_\kappa^2 + s_{22} \right] + \right. \\ \left. + \frac{n_1\beta_\kappa}{\rho_\kappa} \left[\left(s_{21} + \frac{s_{66}}{2} \right) (s_{21}\beta_\kappa^2 - s_{22}) \right] + s_{22}(s_{21} - s_{11}\beta_\kappa^2) \right\} + \end{aligned}$$

$$+n_2 \frac{\beta_\kappa^2}{\rho_\kappa} \left[a_{33} - \frac{s_{21}s_{66}}{2} - \frac{s_{66}^2}{4} \right] \} . \quad (3.19f)$$

It can also be shown by long hand made calculations that every column of the fundamental solutions \mathfrak{U}_{kl} and $\mathfrak{T}_{k\lambda}$ satisfies the basic equations if $Q \neq M$.

4. DUAL SOMIGLIANA FORMULAE FOR INNER REGIONS

The functions \mathcal{F}_ψ , $t_{\kappa\lambda}$, $e_{\kappa\lambda}$ and φ_3 are called an elastic state of the region A_i if they satisfy the corresponding field equations. Let

$$\mathcal{F}_\psi, t_{\kappa\lambda}, e_{\kappa\lambda}, \varphi_3 \quad \text{and} \quad \mathcal{F}_\psi^*, t_{\kappa\lambda}^*, e_{\kappa\lambda}^*, \varphi_3^*$$

be two elastic states of the region A_i . Integrating by parts, one can show that the relation

$$\begin{aligned} & \int_{A_i} \mathcal{F}_\lambda \underbrace{\left[\epsilon_{\kappa\rho 3} e_{\kappa\lambda}^* \partial_\rho + \varphi_3^* \partial_\lambda \right]}_{\mathbf{u}_\lambda(\mathfrak{D}_{\lambda l} \mathbf{u}_l^*)} dA - \int_{A_i} \varphi_3 \underbrace{\left(\mathcal{F}_\psi^* \partial_\psi \right)}_{-\mathbf{u}_3 \mathfrak{D}_{3 l} \mathbf{u}_l^*} dA - \\ & \quad - \int_{A_i} \left[\epsilon_{\kappa\rho 3} e_{\kappa\lambda} \partial_\rho + \varphi_3 \partial_\lambda \right] \mathcal{F}_\lambda^* dA + \int_{A_i} (\mathcal{F}_\psi \partial_\psi) \varphi_3^* dA = \\ & = \oint_{\mathcal{L}_o} \mathcal{F}_\lambda n_\pi \underbrace{\left[\epsilon_{\pi\kappa 3} e_{\kappa\lambda}^* - \delta_{\pi\lambda} \varphi_3^* \right]}_{\mathbf{u}_\lambda^* t_\lambda} ds - \oint_{\mathcal{L}_o} n_\pi \left[\epsilon_{\pi\kappa 3} e_{\kappa\lambda} - \delta_{\pi\lambda} \varphi_3 \right] \mathcal{F}_\lambda^* ds \quad (4.1) \end{aligned}$$

is an identity, referred to as the dual Somigliana identity. We can also write this identity in a more concise form

$$\int_A \left[\mathbf{u}_r \left(\mathfrak{D}_{r l} \mathbf{u}_l^* \right) - \mathbf{u}_r^* \left(\mathfrak{D}_{r l} \mathbf{u}_l \right) \right] dA = \oint_{\mathcal{L}_o} \left[\mathbf{u}_\lambda^* t_\lambda - \mathbf{u}_\lambda t_\lambda \right] ds . \quad (4.2)$$

Henceforward let $\mathbf{u}_l(M)$ be an elastic state of the region A_i . Suppose that the other elastic state, denoted by * , is the one which belongs to the fundamental solutions:

$$\mathbf{u}_l^*(M) = e_k(Q) \mathfrak{U}_{kl}(M, Q)$$

The latter is singular at the point Q . Consequently depending on the position of point Q relative to the region A_i we distinguish three cases – two of them are shown in Figure 2.

1. If $Q \in A_i$, then the neighborhood of Q with radius R_ε , which is denoted by A_ε and is assumed to lie wholly in A_i , is removed from A_i and we apply the dual Somigliana identity to the double connected domain $A' = A_i \setminus A_\varepsilon$. Note that the contour \mathcal{L}_ε of A_ε and the arc \mathcal{L}'_ε , which is assumed to be the part of the contour \mathcal{L}_ε lying within A_i , coincide with each other.

2. If $Q = \overset{\circ}{Q} \in \partial A = \mathcal{L}_o$, then the part $A_i \cap A_\varepsilon$ of the neighborhood A_ε of Q is removed from A_i and we apply the dual Somigliana identity to the simply connected region $A' = A_i \setminus (A_i \cap A_\varepsilon)$. In this case, the contour of the simply

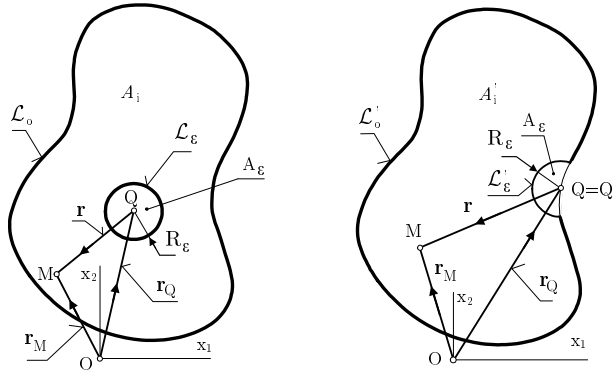


Figure 2.

connected region just obtained consists of two arcs, the arc \mathcal{L}'_o left from \mathcal{L}_o after the removal of A_ε and the arc \mathcal{L}'_ε , i.e., the part of \mathcal{L}_ε that lies within A_i .

3. If $Q \notin (A_i \cup \mathcal{L}_o)$ we apply the dual Somigliana identity to the original region A_i .

Since both $\overset{*}{\mathbf{u}}_k$ and \mathbf{u}_k are elastic states the surface integrals in (4.2) are identically equal to zero.

We now consider each of these three cases, focusing on the main steps of the argument.

1. If $Q \in A_i$ it follows from equation (4.2)

$$\oint_{\mathcal{L}_o} \left[\mathbf{u}_\lambda(\overset{\circ}{M}) \overset{*}{\mathbf{t}}_\lambda(\overset{\circ}{M}) - \overset{*}{\mathbf{u}}_\lambda(\overset{\circ}{M}) \mathbf{t}_\lambda(\overset{\circ}{M}) \right] ds_{\overset{\circ}{M}} + \oint_{\mathcal{L}_\varepsilon} \left[\mathbf{u}_\lambda(\overset{\circ}{M}) \overset{*}{\mathbf{t}}_\lambda(\overset{\circ}{M}) - \overset{*}{\mathbf{u}}_\lambda(\overset{\circ}{M}) \mathbf{t}_\lambda(\overset{\circ}{M}) \right] ds_{\overset{\circ}{M}} \tag{4.3}$$

$$= e_k(Q) \left\{ \oint_{\mathcal{L}_o} \left[\mathfrak{T}_{k\lambda}(\overset{\circ}{M}, Q) \mathbf{u}_\lambda(\overset{\circ}{M}) - \mathfrak{U}_{k\lambda}(\overset{\circ}{M}, Q) \mathbf{t}_\lambda(\overset{\circ}{M}) \right] ds_{\overset{\circ}{M}} + \oint_{\mathcal{L}_\varepsilon} \left[\mathfrak{T}_{k\lambda}(\overset{\circ}{M}, Q) \mathbf{u}_\lambda(\overset{\circ}{M}) - \mathfrak{U}_{k\lambda}(\overset{\circ}{M}, Q) \mathbf{t}_\lambda(\overset{\circ}{M}) \right] ds_{\overset{\circ}{M}} \right\} = 0.$$

Since equation (4.3) holds for arbitrary $e_k(Q)$ we have

$$\oint_{\mathcal{L}_o} \left[\mathfrak{T}_{k\lambda}(\overset{\circ}{M}, Q) \mathbf{u}_\lambda(\overset{\circ}{M}) - \mathfrak{U}_{k\lambda}(\overset{\circ}{M}, Q) \mathbf{t}_\lambda(\overset{\circ}{M}) \right] ds_{\overset{\circ}{M}} + \oint_{\mathcal{L}_\varepsilon} \left[\mathfrak{T}_{k\lambda}(M, Q) \mathbf{u}_\lambda(M) - \mathfrak{U}_{k\lambda}(M, Q) \mathbf{t}_\lambda(M) \right] ds_M = 0. \tag{4.4}$$

To obtain the final form of the above equation, we need to use the integrals detailed below:

- In spite of the singularity of the fundamental solution of order two we can prove that

$$\lim_{R_\varepsilon \rightarrow 0} \oint_{\mathcal{L}_\varepsilon} \mathfrak{T}_{\kappa\lambda}(M, Q) [\mathbf{u}_\lambda(M) - \mathbf{u}_\lambda(Q)] ds_M = 0. \quad (4.5)$$

- We can also show by performing formal transformations that

$$\lim_{R_\varepsilon \rightarrow 0} \oint_{\mathcal{L}_\varepsilon} \mathfrak{U}_{\kappa\lambda}(M, Q) \mathbf{t}_\lambda(M) ds_M = 0. \quad (4.6)$$

- It can be proved by relatively long hand calculations that

$$\lim_{R_\varepsilon \rightarrow 0} \oint_{\mathcal{L}_\varepsilon} \mathfrak{U}_{3\lambda}(M, Q) \mathbf{t}_\lambda(M) ds_M = \varphi_3|_Q = -\mathbf{u}_3|_Q. \quad (4.7)$$

Making use of the integrals (4.5), (4.6) and (4.7) from equation (4.4) we obtain

$$\begin{aligned} & \oint_{\mathcal{L}_o} \dots + \lim_{R_\varepsilon \rightarrow 0} \oint_{\mathcal{L}_\varepsilon} \dots = \\ & = \mathbf{u}_k(Q) - \oint_{\mathcal{L}_o} \mathfrak{U}_{k\lambda}(\overset{\circ}{M}, Q) \mathbf{t}_\lambda(\overset{\circ}{M}) ds_{\overset{\circ}{M}} + \oint_{\mathcal{L}_o} \mathfrak{T}_{k\lambda}(\overset{\circ}{M}, Q) \mathbf{u}_\lambda(\overset{\circ}{M}) ds_{\overset{\circ}{M}} = 0 \end{aligned} \quad (4.8)$$

which is, in fact, the first dual Somigliana formula:

$$\mathbf{u}_k(Q) = \oint_{\mathcal{L}_o} \mathfrak{U}_{k\lambda}(\overset{\circ}{M}, Q) \mathbf{t}_\lambda(\overset{\circ}{M}) ds_{\overset{\circ}{M}} - \oint_{\mathcal{L}_o} \mathfrak{T}_{k\lambda}(\overset{\circ}{M}, Q) \mathbf{u}_\lambda(\overset{\circ}{M}) ds_{\overset{\circ}{M}}. \quad (4.9)$$

2. If $Q = \overset{\circ}{Q}$ our starting point is the formula

$$\begin{aligned} & \int_{\mathcal{L}'_o} \left[\mathfrak{T}_{\kappa\lambda}(\overset{\circ}{M}, \overset{\circ}{Q}) \mathbf{u}_\lambda(\overset{\circ}{M}) - \mathfrak{U}_{\kappa\lambda}(\overset{\circ}{M}, \overset{\circ}{Q}) \mathbf{t}_\lambda(\overset{\circ}{M}) \right] ds_{\overset{\circ}{M}} + \\ & + \int_{\mathcal{L}'_\varepsilon} \left[\mathfrak{T}_{\kappa\lambda}(M, \overset{\circ}{Q}) \mathbf{u}_\lambda(M) - \mathfrak{U}_{\kappa\lambda}(M, \overset{\circ}{Q}) \mathbf{t}_\lambda(M) \right] ds_M = 0. \end{aligned} \quad (4.10)$$

Using the limit

$$\lim_{R_\varepsilon \rightarrow 0} \int_{\mathcal{L}'_\varepsilon} \mathfrak{T}_{\kappa\lambda}(M, \overset{\circ}{Q}) ds_M = c_{\kappa\lambda}(\overset{\circ}{Q}), \quad (4.11)$$

where $c_{\kappa\lambda}(\overset{\circ}{Q}) = \delta_{\kappa\lambda}/2$, if the contour is smooth at $\overset{\circ}{Q}$ and repeating the line of thought resulting in equation (4.9), we arrive at the second dual Somigliana formula, i.e. the integral equation of the direct method:

$$c_{\kappa\lambda}(\overset{\circ}{Q}) \mathbf{u}_\lambda(\overset{\circ}{Q}) = \oint_{\mathcal{L}_o} \mathfrak{U}_{\kappa\lambda}(\overset{\circ}{M}, \overset{\circ}{Q}) \mathbf{t}_\lambda(\overset{\circ}{M}) ds_{\overset{\circ}{M}} - \oint_{\mathcal{L}_o} \mathfrak{T}_{\kappa\lambda}(\overset{\circ}{M}, \overset{\circ}{Q}) \mathbf{u}_\lambda(\overset{\circ}{M}) ds_{\overset{\circ}{M}}. \quad (4.12)$$

3. If $Q \notin (A \cup \mathcal{L}_o)$ it is not too difficult to check that the third dual Somigliana formula takes the form:

$$0 = \oint_{\mathcal{L}_o} \mathfrak{U}_{\kappa\lambda}(\overset{\circ}{M}, Q) \mathbf{t}_\lambda(\overset{\circ}{M}) ds_{\overset{\circ}{M}} - \oint_{\mathcal{L}_o} \mathfrak{T}_{\kappa\lambda}(\overset{\circ}{M}, Q) \mathbf{u}_\lambda(\overset{\circ}{M}) ds_{\overset{\circ}{M}}. \quad (4.13)$$

Upon substitution of the first dual Somigliana formula (4.9) into the dual kinematic equations (2.1a,b) and taking into account that $\mathcal{F}_\kappa = \mathbf{u}_\kappa$ we get the stresses $\mathfrak{s}_m = (t_{11}, t_{12}, t_{22})$ in the form

$$\mathfrak{s}_m(Q) = \oint_{\mathcal{L}_o} S_{m\lambda}(\overset{\circ}{M}, Q) \mathbf{t}_\lambda(\overset{\circ}{M}) ds_{\overset{\circ}{M}} - \oint_{\mathcal{L}_o} D_{m\lambda}(\overset{\circ}{M}, Q) \mathbf{u}_\lambda(\overset{\circ}{M}) ds_{\overset{\circ}{M}}, \quad Q \in A_i \tag{4.14}$$

where the matrices of $S_{m\lambda}$ and $D_{m\lambda}$ are

$$[S_{m\lambda}] = -2\mathcal{K} \operatorname{Im} \sum_{k=1}^2 \frac{d_k}{\rho_k} \begin{bmatrix} -\beta_k^3 & \beta_k^2 \\ \beta_k^2 & -\beta_k \\ -\beta_k & 1 \end{bmatrix}, \tag{4.15}$$

and

$$[D_{m\lambda}] = \mathcal{K} \operatorname{Im} \sum_{k=1}^2 \frac{2d_k}{\rho_k^2} \times \begin{bmatrix} D_{11} & D_{12} \\ D_{21} & D_{22} \\ D_{31} & D_{32} \end{bmatrix},$$

in which

$$D_{11} = n_2 (-s_{11}\beta_k^4 - s_{12}\beta_k^2) - \frac{n_1}{2} s_{66}\beta_k^3 - n_1 \left[s_{22}\beta_k + \left(s_{21} + \frac{s_{66}}{2} \right) \beta_k^3 \right],$$

$$D_{21} = \frac{n_2}{2} s_{66}\beta_k^3 + n_1 (s_{21}\beta_k^4 + s_{22}\beta_k^2) + n_2 \left[s_{22}\beta_k + \left(s_{21} + \frac{s_{66}}{2} \right) \beta_k^3 \right],$$

$$D_{12} = n_2 (s_{11}\beta_k^3 + s_{12}\beta_k) + \frac{n_1}{2} s_{66}\beta_k^2 - n_1\beta_k^2 \left[\left(s_{12} + \frac{s_{66}}{2} \right) + s_{11}\beta_k^2 \right],$$

$$D_{22} = -\frac{n_2}{2} s_{66}\beta_k^2 - n_1 (s_{21}\beta_k^3 + s_{22}\beta_k) - n_2\beta_k^2 \left[\left(s_{12} + \frac{s_{66}}{2} \right) + s_{11}\beta_k^2 \right],$$

$$D_{13} = -n_2 (s_{11}\beta_k^2 + s_{12}) - \frac{n_1}{2} s_{66}\beta_k + n_1\beta_k \left[\left(s_{12} + \frac{s_{66}}{2} \right) + s_{11}\beta_k^2 \right],$$

$$D_{23} = \frac{n_2}{2} s_{66}\beta_k + n_1 (s_{21}\beta_k^2 + s_{22}) + n_2\beta_k \left[\left(s_{12} + \frac{s_{66}}{2} \right) + s_{11}\beta_k^2 \right].$$

5. DUAL SOMIGLIANA FORMULAE FOR EXTERIOR REGIONS

Figure 3 depicts a triple connected region A'_e bounded by the contours \mathcal{L}_o , \mathcal{L}_ε and the circle \mathcal{L}_R with radius ${}_eR$ and center O . Here \mathcal{L}_ε is the contour of the neighborhood A_ε of Q with radius R_ε while ${}_eR$ is sufficiently large so that the region bounded by \mathcal{L}_R covers both \mathcal{L}_o , and \mathcal{L}_ε . If ${}_eR \rightarrow \infty$ and $R_\varepsilon \rightarrow 0$ then clearly $A'_e \rightarrow A_e$.

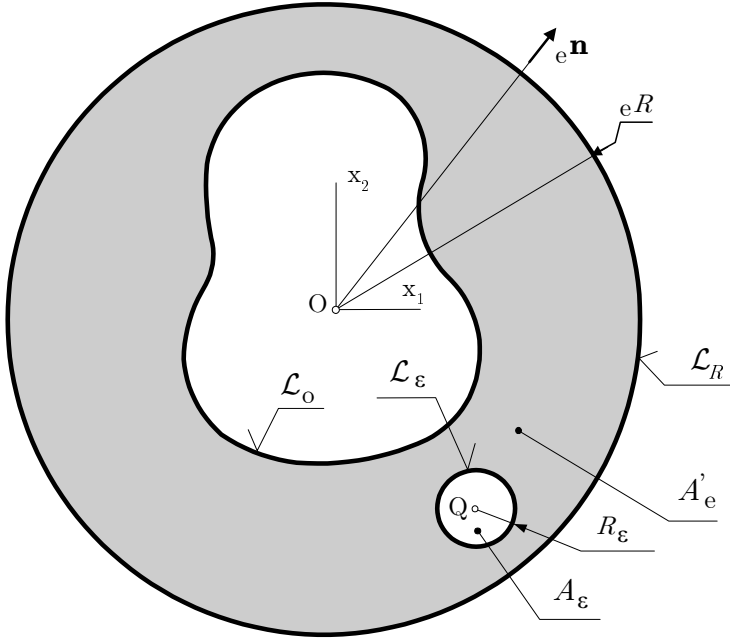


Figure 3.

We shall make the following assumptions:

1. The stresses are constant at infinity. Their values are denoted by

$$t_{11}(\infty), t_{12}(\infty) = t_{21}(\infty) \text{ and } t_{22}(\infty). \quad (5.1)$$

2. The rigid body rotation vanishes at infinity:

$$\varphi_3(\infty) = 0. \quad (5.2)$$

Let $u_l(M)$ and $\overset{*}{u}_l(M)$ be sufficiently smooth elastic states (dual displacements and rotation) on A_e . The corresponding dual stresses on the contour are denoted by

$$t_\lambda \quad \text{and} \quad \overset{*}{t}_\lambda$$

respectively. The equation

$$\begin{aligned} & \int_{A'_e} \left[u_r(M) \left(\overset{M}{\mathcal{D}}_{r,l} \overset{*}{u}_l(M) \right) - \overset{*}{u}_r(M) \left(\overset{M}{\mathcal{D}}_{r,l} u_l(M) \right) \right] dA_M = \\ & = \oint_{\mathcal{L}_o} \left[u_\lambda(\overset{\circ}{M}) \overset{*}{t}_\lambda(\overset{\circ}{M}) - \overset{*}{u}_\lambda(\overset{\circ}{M}) t_\lambda(\overset{\circ}{M}) \right] ds_{\overset{\circ}{M}} + \oint_{\mathcal{L}_\varepsilon} \left[u_\lambda(\overset{\circ}{M}) \overset{*}{t}_\lambda(\overset{\circ}{M}) - \overset{*}{u}_\lambda(\overset{\circ}{M}) t_\lambda(\overset{\circ}{M}) \right] ds_{\overset{\circ}{M}} \\ & \quad + \oint_{\mathcal{L}_R} \left[u_\lambda(\overset{\circ}{M}) \overset{*}{t}_\lambda(\overset{\circ}{M}) - \overset{*}{u}_\lambda(\overset{\circ}{M}) t_\lambda(\overset{\circ}{M}) \right] ds_{\overset{\circ}{M}} \quad (5.3) \end{aligned}$$

is the dual SOMIGLIANA identity (4.2) when it is applied to the triple connected region A'_e . Observe that M over a letter denotes that the corresponding derivatives are taken with respect to the coordinates of M .

Let again $\mathbf{u}_l^*(Q) = e_k(Q)\mathfrak{U}_{k\kappa}(M, Q)$, which is a non-singular elastic state of the plane in A'_e . We regard $\mathbf{u}_l(M)$ as a different elastic state in the region A_e . Further we assume that $\mathbf{u}_l(M)$ has the far field pattern (asymptotic behavior)

$$\mathbf{u}_\lambda(M) = \tilde{\mathbf{u}}_\lambda(M) = c_\lambda(\infty) + \varepsilon_{\kappa\rho 3}x_\rho t_{\lambda\kappa}(\infty), \quad (5.4a)$$

$$\mathbf{u}_3(M) = \tilde{\mathbf{u}}_3(M) = -\varphi_3(\infty) = 0. \quad (5.4b)$$

when x_β or equivalently M tends to infinity. Here $c_\lambda(\infty)$ is an arbitrary constant which can be set to zero.

Substituting the above quantities into the SOMIGLIANA identity (5.3) and taking into account that the surface integrals vanish we have

$$\begin{aligned} e_k(Q) \left\{ \oint_{\mathcal{L}_o} \left[\mathfrak{T}_{k\lambda}(\overset{\circ}{M}, Q)\mathbf{u}_\lambda(\overset{\circ}{M}) - \mathfrak{U}_{k\lambda}(\overset{\circ}{M}, Q)\mathfrak{t}_\lambda(\overset{\circ}{M}) \right] ds_{\overset{\circ}{M}} + \right. \\ \left. + \oint_{\mathcal{L}_e} \left[\mathfrak{T}_{k\lambda}(\overset{\circ}{M}, Q)\mathbf{u}_\lambda(\overset{\circ}{M}) - \mathfrak{U}_{k\lambda}(\overset{\circ}{M}, Q)\mathfrak{t}_\lambda(\overset{\circ}{M}) \right] ds_{\overset{\circ}{M}} + \right. \\ \left. + \oint_{\mathcal{L}_R} \left[\mathfrak{T}_{k\lambda}(\overset{\circ}{M}, Q)\mathbf{u}_\lambda(\overset{\circ}{M}) - \mathfrak{U}_{k\lambda}(\overset{\circ}{M}, Q)\mathfrak{t}_\lambda(\overset{\circ}{M}) \right] ds_{\overset{\circ}{M}} \right\} = 0 \quad (5.5) \end{aligned}$$

since

$$\mathfrak{t}_\kappa^*(\overset{\circ}{M}) = e_l(Q)\mathcal{T}_{l\kappa}(\overset{\circ}{M}, Q).$$

It is clear that one can omit $e_k(Q)$. Recalling the limit (4.8) we get

$$\begin{aligned} \mathbf{u}_k(Q) = \lim_{eR \rightarrow \infty} \oint_{\mathcal{L}_R} \left[\mathfrak{T}_{k\lambda}(\overset{\circ}{M}, Q)\mathbf{u}_\lambda(\overset{\circ}{M}) - \mathfrak{U}_{k\lambda}(\overset{\circ}{M}, Q)\mathfrak{t}_\lambda(\overset{\circ}{M}) \right] ds_{\overset{\circ}{M}} + \\ + \oint_{\mathcal{L}_o} \left[\mathfrak{T}_{k\lambda}(\overset{\circ}{M}, Q)\mathbf{u}_\lambda(\overset{\circ}{M}) - \mathfrak{U}_{k\lambda}(\overset{\circ}{M}, Q)\mathfrak{t}_\lambda(\overset{\circ}{M}) \right] ds_{\overset{\circ}{M}}. \quad (5.6) \end{aligned}$$

In order to establish the first dual SOMIGLIANA formula for the exterior region A_e we need to find the limit of the first integral on the right hand side.

In the following, our main objective is to prove that

$$I_k = \lim_{eR \rightarrow \infty} \oint_{\mathcal{L}_R} \left[\mathfrak{T}_{k\lambda}(\overset{\circ}{M}, Q)\mathbf{u}_\lambda(\overset{\circ}{M}) - \mathfrak{U}_{k\lambda}(\overset{\circ}{M}, Q)\mathfrak{t}_\lambda(\overset{\circ}{M}) \right] ds_{\overset{\circ}{M}} = \tilde{\mathbf{u}}_k(Q). \quad (5.7)$$

The proof uses the first dual SOMIGLIANA formula valid for inner regions and requires simple tools only.

Let us consider the simple connected region A_R bounded by the circle \mathcal{L}_R with radius eR and center at O . We shall assume that the point Q is an inner one.

It is clear that the dual displacements $\tilde{\mathbf{u}}_\kappa(M)$ and rotation field $\tilde{\mathbf{u}}_3(M)$ defined by equations (5.4a,b) are an elastic state of A_R with no body forces. The corresponding dual stresses on the contour are denoted by $\tilde{\mathfrak{t}}_\kappa(\overset{\circ}{M})$. It is also obvious that for any

elastic state of the region A_R one can apply the first dual SOMIGLIANA formula. Since $\tilde{u}_k(M)$ is an elastic state of the orthotropic inner region A_R we have

$$\tilde{u}_k(Q) = \oint_{\mathcal{L}_R} \left[\mathfrak{T}_{k\lambda}(\overset{\circ}{M}, Q) \tilde{u}_\lambda(\overset{\circ}{M}) - \mathfrak{U}_{k\lambda}(\overset{\circ}{M}, Q) \tilde{t}_\lambda(\overset{\circ}{M}) \right] ds_{\overset{\circ}{M}}. \quad (5.8)$$

If in addition we take into account the limits

$$\lim_{eR \rightarrow \infty} \mathfrak{U}_\lambda(\overset{\circ}{M}) = \tilde{u}_\lambda(\overset{\circ}{M}) \quad \text{and} \quad \lim_{eR \rightarrow \infty} \mathfrak{t}_\lambda(\overset{\circ}{M}) = \tilde{t}_\lambda(\overset{\circ}{M}), \quad (5.9)$$

then we find that the limit of the integral in question in equation (5.7) is really

$$\lim_{eR \rightarrow \infty} \oint_{\mathcal{L}_R} \left[\mathfrak{T}_{k\lambda}(\overset{\circ}{M}, Q) \mathfrak{u}_\lambda(\overset{\circ}{M}) - \mathfrak{U}_{k\lambda}(\overset{\circ}{M}, Q) \mathfrak{t}_\lambda(\overset{\circ}{M}) \right] ds_{\overset{\circ}{M}} = \tilde{u}_k(Q). \quad (5.10)$$

Consequently, the first dual SOMIGLIANA formula – modified to include a constant stress state at infinity – immediately follows from equations (5.6) and (5.7):

$$\mathfrak{u}_k(Q) = \tilde{u}_k(Q) + \oint_{\mathcal{L}_o} \mathfrak{U}_{k\lambda}(\overset{\circ}{M}, Q) \mathfrak{t}_\lambda(\overset{\circ}{M}) ds_{\overset{\circ}{M}} - \oint_{\mathcal{L}_o} \mathfrak{T}_{k\lambda}(\overset{\circ}{M}, Q) \mathfrak{u}_\lambda(\overset{\circ}{M}) ds_{\overset{\circ}{M}}. \quad (5.11)$$

If $Q = \overset{\circ}{M}$ is on \mathcal{L}_o , nothing changes concerning the limit of the integral taken on \mathcal{L}_R . Consequently

$$c_{\kappa\lambda}(\overset{\circ}{Q}) \mathfrak{u}_\lambda(\overset{\circ}{Q}) = \tilde{u}_k(\overset{\circ}{Q}) + \oint_{\mathcal{L}_o} \mathfrak{U}_{\kappa\lambda}(\overset{\circ}{M}, \overset{\circ}{Q}) \mathfrak{t}_\lambda(\overset{\circ}{M}) ds_{\overset{\circ}{M}} - \oint_{\mathcal{L}_o} \mathfrak{T}_{\kappa\lambda}(\overset{\circ}{M}, \overset{\circ}{Q}) \mathfrak{u}_\lambda(\overset{\circ}{M}) ds_{\overset{\circ}{M}}. \quad (5.12)$$

where $c_{\kappa\rho} = \delta_{\kappa\rho}/2$ if the contour is smooth at $\overset{\circ}{Q}$. This integral equation is that of the direct method (or the second dual SOMIGLIANA formula) for exterior regions.

If Q is inside the contour \mathcal{L}_o , i.e., in the region A_i , then it is easy to show that

$$0 = \tilde{u}_k(Q) + \oint_{\mathcal{L}_o} \mathfrak{U}_{k\lambda}(\overset{\circ}{M}, Q) \mathfrak{t}_\lambda(\overset{\circ}{M}) ds_{\overset{\circ}{M}} - \oint_{\mathcal{L}_o} \mathfrak{T}_{k\lambda}(\overset{\circ}{M}, Q) \mathfrak{u}_\lambda(\overset{\circ}{M}) ds_{\overset{\circ}{M}}. \quad (5.13)$$

which is the third SOMIGLIANA formula for exterior regions.

Recalling formula (4.14) for the stresses, it is easy to check that

$$\mathfrak{s}_m(Q) = \mathfrak{s}_m(\infty) + \oint_{\mathcal{L}_o} S_{m\lambda}(\overset{\circ}{M}, Q) \mathfrak{t}_\lambda(\overset{\circ}{M}) ds_{\overset{\circ}{M}} - \oint_{\mathcal{L}_o} D_{m\lambda}(\overset{\circ}{M}, Q) \mathfrak{u}_\lambda(\overset{\circ}{M}) ds_{\overset{\circ}{M}}. \quad Q \in A_e \quad (5.14)$$

6. CALCULATIONS OF THE STRESSES ON THE BOUNDARY

After solving the integral equations of the direct method (equation (4.12) for inner regions, equation (5.12) for exterior regions) we know the dual displacement vector u_κ (the stress functions) and the dual stress vector t_κ (displacement derivatives with respect to the arc coordinate s) on the contour. The next question is how to determine the stresses on the contour in terms of these quantities.

The calculations leading to the equation system that results in the stresses sought will be carried out in the coordinate system (x, y) . In this section we shall not apply indicial notations including the summation convention.

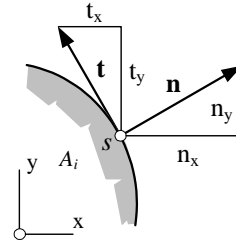


Figure 4.

It is clear from Figure 4 that

$$\frac{dx}{ds} = t_x = -n_y \quad \text{and} \quad \frac{dy}{ds} = t_y = n_x \tag{6.1}$$

If we recall formulae (2.1a,b) which give the stresses in terms of stress functions, we can write (indices 1 and 2 correspond to x and y , respectively):

$$\frac{d\mathcal{F}_x}{ds} = \frac{\partial \mathcal{F}_x}{\partial x} \frac{dx}{ds} + \frac{\partial \mathcal{F}_x}{\partial y} \frac{dy}{ds} = n_x \sigma_{xx} + n_y \tau_{xy} , \tag{6.2a}$$

$$\frac{d\mathcal{F}_y}{ds} = \frac{\partial \mathcal{F}_y}{\partial x} \frac{dx}{ds} + \frac{\partial \mathcal{F}_y}{\partial y} \frac{dy}{ds} = n_x \tau_{xy} + n_y \sigma_{yy} . \tag{6.2b}$$

On the basis the definition of the dual stresses (2.5b) we have

$$-t_x = \frac{du_x}{ds} = \frac{du_x}{dx} \frac{dx}{ds} + \frac{du_x}{dy} \frac{dy}{ds} = e_{xx} \frac{dx}{ds} + \frac{du_x}{dy} \frac{dy}{ds} \tag{6.3}$$

$$-t_y = \frac{du_y}{ds} = \frac{du_y}{dx} \frac{dx}{ds} + \frac{du_y}{dy} \frac{dy}{ds} = \frac{du_y}{dx} \frac{dx}{ds} + e_{yy} \frac{dy}{ds} . \tag{6.4}$$

Multiplying by $t_x = -n_y$ and $t_y = n_x$ throughout and combining the equations obtained from (6.3) and (6.4) we arrive at

$$n_y t_x - n_x t_y = e_{xx} \left(\frac{dx}{ds} \right)^2 + e_{yy} \left(\frac{dy}{ds} \right)^2 + \frac{dy}{ds} \frac{dx}{ds} \overbrace{\left(\frac{\partial u_x}{\partial y} + \frac{\partial u_y}{\partial x} \right)}^{2e_{xy}} \tag{6.5}$$

from which making use of the HOOKE law and the geometrical relations (6.1) we obtain

$$n_y t_x - n_x t_y = (n_y^2 s_{11} + n_x^2 s_{21}) \sigma_x - n_x n_y \frac{s_{66}}{2} \tau_{xy} + (n_y^2 s_{12} + n_x^2 s_{22}) \sigma_y . \tag{6.6}$$

Equations (6.2a,b) and (6.6) can be arranged in a matrix form

$$\begin{bmatrix} n_x & n_y & 0 \\ 0 & n_x & n_y \\ n_y^2 s_{11} + n_x^2 s_{21} & -n_x n_y \frac{s_{66}}{2} & n_y^2 s_{12} + n_x^2 s_{22} \end{bmatrix} \begin{bmatrix} \sigma_{xx} \\ \tau_{xy} \\ \sigma_{yy} \end{bmatrix} = \begin{bmatrix} d\mathcal{F}_x/ds \\ d\mathcal{F}_y/ds \\ n_y \mathbf{t}_x - n_x \mathbf{t}_y \end{bmatrix}. \quad (6.7)$$

Since the outer normal \mathbf{n} , the stress functions $\mathcal{F}_x, \mathcal{F}_y$ and the dual stresses $\mathbf{t}_x, \mathbf{t}_y$ are all known on the contour as soon as we have solved the integral equation of the direct method, solution of the above linear equations will result in the stress components sought.

7. EXAMPLES

A program has been written in Fortran 90 in order to solve the integral equations (4.12) and (5.12) of the direct method on inner and exterior regions numerically. We have applied quadratic boundary elements. Let n_{be} and n_{bn} be the number of boundary elements and that of the boundary nodes. Further let

$$\mathbf{u}_j = \begin{bmatrix} \mathbf{u}_1^j \\ \mathbf{u}_2^j \end{bmatrix} \quad \text{and} \quad \mathbf{t}_j = \begin{bmatrix} \mathbf{t}_1^j \\ \mathbf{t}_2^j \end{bmatrix} \quad j = 1, \dots, n_{bn} \quad (7.1)$$

be the matrices of the dual displacements and dual stresses at node j on the boundary.

Following the well-known procedure valid for the primal formulation – see for instance [9] – solution of the dual integral equation (4.12) can be reduced to the solution of the linear equations

$$\begin{bmatrix} \mathbf{h}_{11} & \mathbf{h}_{12} & \cdots & \mathbf{h}_{1n_{bn}} \\ \mathbf{h}_{21} & \mathbf{h}_{22} & \cdots & \mathbf{h}_{2n_{bn}} \\ \dots & \dots & \dots & \dots \\ \mathbf{h}_{n_{bn}1} & \mathbf{h}_{n_{bn}2} & \cdots & \mathbf{h}_{n_{bn}n_{bn}} \end{bmatrix} \begin{bmatrix} \mathbf{u}_1 \\ \mathbf{u}_2 \\ \dots \\ \mathbf{u}_{n_{bn}} \end{bmatrix} = \begin{bmatrix} \mathbf{b}_{11} & \mathbf{b}_{12} & \cdots & \mathbf{b}_{1n_{bn}} \\ \mathbf{b}_{21} & \mathbf{b}_{22} & \cdots & \mathbf{b}_{2n_{bn}} \\ \dots & \dots & \dots & \dots \\ \mathbf{b}_{n_{bn}1} & \mathbf{b}_{n_{bn}2} & \cdots & \mathbf{b}_{n_{bn}n_{bn}} \end{bmatrix} \begin{bmatrix} \mathbf{t}_1 \\ \mathbf{t}_2 \\ \dots \\ \mathbf{t}_{n_{bn}} \end{bmatrix} \quad (7.2)$$

where the 2×2 submatrices \mathbf{h}_{ij} and \mathbf{b}_{ij} are computed from the integrals

$$\hat{\mathbf{h}}_{ij} = \left[\sum_{e \in j} \int_{\mathcal{L}_e} \mathfrak{T}_{\kappa\lambda}(Q_i, \eta) N^{a(j,e)}(\eta) J(\eta) d\eta \right], \quad \mathbf{h}_{ij} = \begin{cases} \hat{\mathbf{h}}_{ii} + \mathbf{c}_{ii}, & \text{if } i = j \\ \hat{\mathbf{h}}_{ij}, & \text{if } i \neq j \end{cases} \quad (7.3)$$

$$\mathbf{b}_{ij} = \left[\sum_{e \in j} \int_{\mathcal{L}_e} \mathfrak{U}_{\kappa\lambda}(Q_i, \eta) N^{a(j,e)}(\eta) J(\eta) d\eta \right] \quad (7.4)$$

in which (a) the summation is to be carried out for those boundary elements having the nodal point j as their common nodal point; (b) i identifies the fixed nodal point

Q_i referred to as the collocation point; (c) $N^{a(j,e)}(\eta)$ is the a -th shape function for which $a(j,e)$ is the local number of the global nodal point j on element e ; (d) \mathbf{c}_{ii} is the matrix of $c_{\kappa\lambda}(Q_i)$ in equation (4.11); (e) $J(\eta)$ is the Jacobian. Equation system (7.2) can be rewritten as

$$\mathbf{H}\mathbf{u} = \mathbf{B}\mathbf{t} . \quad (7.5)$$

We remark that determination of the diagonal elements \mathbf{h}_{ii} , $i = 1, \dots, n_{bn}$ requires the computation of strongly singular integrals.

If the region under consideration is an exterior one then in accordance with integral equation (5.12) the right-hand side of equation (7.5) is to be supplemented by the term

$$\tilde{\mathbf{u}}^T = \left[\underbrace{\tilde{u}_1^1 \tilde{u}_2^1}_{\tilde{\mathbf{u}}_1^T} \mid \underbrace{\tilde{u}_1^2 \tilde{u}_2^2}_{\tilde{\mathbf{u}}_2^T} \mid \dots \mid \underbrace{\tilde{u}_1^{n_{bn}} \tilde{u}_2^{n_{bn}}}_{\tilde{\mathbf{u}}_{n_{bn}}^T} \right] \quad (7.6)$$

and takes the form

$$\mathbf{H}\mathbf{u} = \tilde{\mathbf{u}} + \mathbf{B}\mathbf{t} . \quad (7.7)$$

If the dual displacements (the stress functions) are constant the stresses and the strains vanish. If in addition we assume that the rotation φ^3 vanishes – this does not violate generality – then the dual stresses also vanish. Consequently

$$\sum_{j=1}^{2n_{bn}} H_{ij} = 0 \quad \text{from where} \quad H_{ii} = - \sum_{\substack{j=1 \\ (i \neq j)}}^{2n_{bn}} H_{ij} \quad i = 1, 2, \dots, 2n_{bn} \quad (7.8)$$

where H_{ij} is an element of the matrix \mathbf{H} . Making use of the equation above we can avoid the computation of strongly singular integrals for interior boundary value problems.

For an exterior region, the strongly singular integrals can be determined using an equation similar to equation (7.8), which we present here without proof:

$$H_{ii} = - \sum_{\substack{j=1 \\ (i \neq j)}}^{2n_{bn}} H_{ij} + 1 \quad i = 1, 2, \dots, 2n_{bn} . \quad (7.9)$$

We have solved one simple internal test problem and two external boundary value problems. First we consider a beam in pure bending (Figure 5), second the coordinate plane with a circular hole (Figure 6b.); third the coordinate plane with a rigid inclusion (Figure 6c.). The material is birch for which $s_{11} = 8.497 \times 10^{-5}$, $s_{12} = s_{21} = -6.11 \times 10^{-2}$, $s_{22} = 1.6999 \times 10^{-4}$ and $s_{66} = 1.456 \times 10^{-3} [mm^2/N]$.

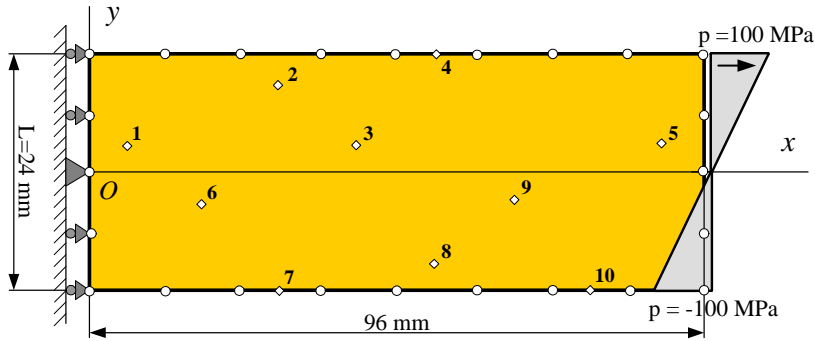


Figure 5.

The first problem has a closed form solution for the stresses:

$$\sigma_{xx} = 200y/L, \quad \sigma_{yy} = 0; \quad \tau_{xy} = 0.$$

The contour is divided into twenty elements of equal length as shown in Figure 6. Table 1 presents the computed results which are in close agreement with the accurate values.

Table 1.. Results for the pure bending of a beam

Pure bending: stresses at the inner - and contour points			
The point Selected	Stresses [MPa]		
	σ_{xx}	τ_{xy}	σ_{yy}
1 (6;3)	25.00023	0.000707695	-0.000186628
2 (30;9)	74.99414	0.000184937	-0.000164188
3 (42;3)	24.99820	-0.000128817	-0.000083552
4 (54;12)	100.02202	0.000000000	0.000000000
5 (90;3)	25.00023	0.000707695	-0.000186628
6 (18;-3)	-24.99898	-0.000708675	0.000120160
7 (30;-12)	-100.02220	0.000000000	0.000000000
8 (54;-9)	-74.99372	-0.000055471	0.000156285
9 (66;-3)	-24.99844	0.000398726	0.000092128
10 (78;-12)	-100.02223	0.000000000	0.000000000

For the exterior boundary value problems we shall assume that

$$\tau_{xy}(\infty) = \sigma_{yy}(\infty) = 0 \quad \text{and} \quad \sigma_{xx}(\infty) = p = \text{constant}$$

For completeness Figure 6a shows the region to use if we solve the integral equation of the direct method in its traditional form – see equation (4.9) – i.e. if the exterior region is replaced by a bounded one.

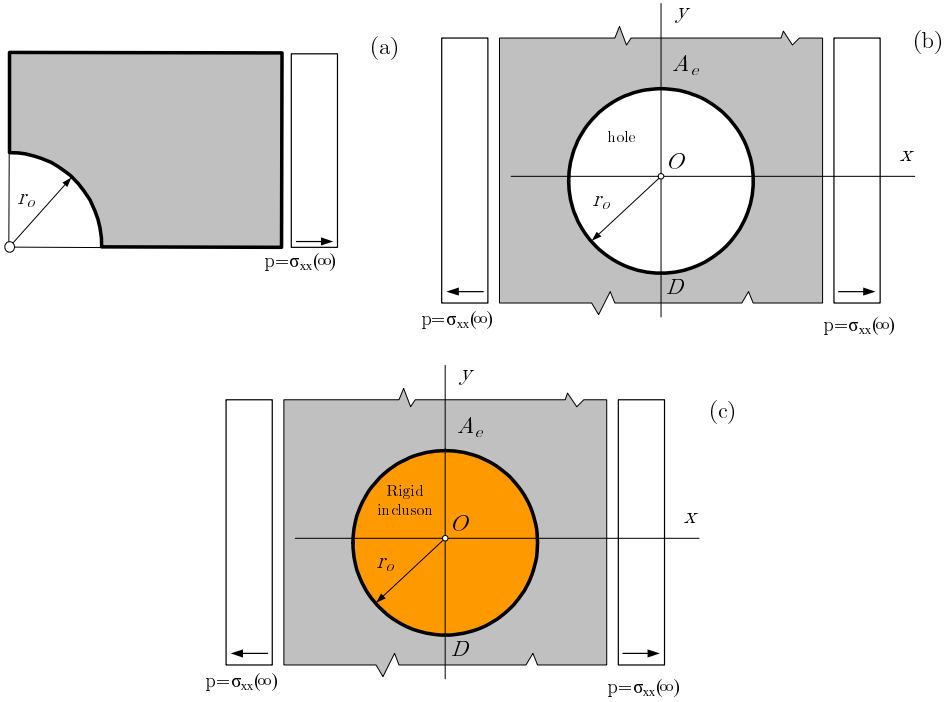


Figure 6.

LEKHTNISKI’s book [15] contains closed form solutions for the stresses on the boundary, as well as numerical values which can be found in Table 17 on page 197. In this paper we show the results as computed by solving the integral equation and the results taken from [15] – see Tables 2 and 3. We used a polar coordinate system, and the tables contain the quotients σ_θ/p for the plane with circular hole and σ_r/p , $\tau_{r\theta}/p$ and σ_θ/p for the plane with the rigid circular inclusion.

Table 2.. Results for the circular hole

Polar angle	Circular hole	
	σ_θ/p Lekhnitski [15]	
0°	-0.70744	-0.707
15°	-0.33928	-0.340
30°	0.06951	0.069
45°	0.40451	0.404
60°	0.96605	0.966
75°	2.57736	2.577
90°	5.45409	5.453

Table 3. Results for the rigid inclusion

Polar angle	Rigid kernel					
	σ_r/p		$\tau_{r\theta}/p$		σ_θ/p	
	Lekhnitski [15]		Lekhnitski [15]		Lekhnitski [15]	
0°	1.2363	1.237	0.0000	0.000	0.0444	0.044
15°	1.1558	1.156	-0.2999	-0.299	0.0936	0.093
30°	0.9364	0.937	-0.5188	-0.519	0.2701	0.270
45°	0.6370	<u>0.698</u>	-0.5986	-0.599	0.5158	0.516
60°	0.3377	0.338	-0.5181	-0.519	0.6990	0.699
75°	0.1188	0.119	-0.2987	-0.299	0.5627	0.564
90°	0.0389	0.039	0.0000	0.000	0.0028	0.003

We remark that the underlined value is mistaken in book [15].

8. CONCLUDING REMARKS

The present paper has dealt with the following issues:

1. We have presented the equations of plane elasticity for an orthotropic body in terms of stress functions of order one. We have also clarified what are the supplementary conditions of single valuedness for a class of mixed boundary value problems in the dual system of plane elasticity.
2. By applying Galorkin functions and following the procedure presented among others in book [14] by KUPRADZE we have derived the dual fundamental solutions of order one and two for plane problems of orthotropic bodies.
3. We have set up the dual Somigliana relations both for inner regions and for exterior ones. A constant stress state at infinity is a part of the formulation we have developed for exterior regions. The integral representation of the stresses has also been established.
4. Three simple boundary value problems (one for an interior region, the other two for the same exterior region) have been solved numerically in order to demonstrate the applicability of the solution algorithm.

We remark that the supplementary conditions of single valuedness should be incorporated into the algorithm if (a) the number of arcs on which tractions are prescribed is more than one or (b) if in addition to this the region under consideration is multiply connected. Work on these issues is in progress.

REFERENCES

1. TONTI, E.: A mathematical model for physical theories I. II. *Rendiconti Accademia Nazionale dei Lincei*, pp. 175–181; 351–356.
2. RIZZO, F. J. and SHIPPY, D. J.: A method for stress determination in plane anisotropic bodies. *Journal of Composite Materials*, **4**(1), (1970), 36–61.
3. RIZZO, F. J.: An integral equation approach to boundary value problems of classical elastostatics. *Q. J. Appl. Math.*, **25**, (1967), 83–95.

4. VABLE, M. and SIKARSKIE, D. L.: Stress analysis in plane orthotropic material by the boundary element method. *Int. J. Solids Structures*, **24**(1), (1988), 1–11.
5. SHIAH, Y. C. and TAN, C. L.: BEM treatment of two-dimensional anisotropic field problems by direct domain mapping. *Engineering Analysis with Boundary Elements*, **20**, (1997), 347–351.
6. SHIAH, Y. C. and TAN, C. L.: BEM treatment of three-dimensional anisotropic field problems by direct domain mapping. *Engineering Analysis with Boundary Elements*, **28**, (2004), 43–52.
7. HUANG, L., SUN, X., LIU, Y., and CEN, Z.: Parameter identification for two-dimensional orthotropic material bodies by the boundary element method. *Engineering Analysis with Boundary Elements*, **28**(2), (2004), 109–121.
8. BANARJEE, P. K. and BUTTERFIELD, R.: *Boundary Element Methods in Engineering Science*. Mir, Moscow, 1984.
9. BANARJEE, P. K.: *The Boundary Element Methods in Engineering*. McGraw-Hill, New York, 1994.
10. SZEIDL, G.: Kinematic admissibility of strains for same mixed boundary value problems in the dual system of micropolar theory of elasticity. *Journal of Computational and Applied Mechanics*, **1**(2), (2000), 191–203.
11. SZEIDL, G.: Boundary integral equations for plane problems in terms of stress functions of order one. *Journal of Computational and Applied Mechanics*, **2**(2), (2001), 237–261.
12. SZEIDL, G. and SZIRBIK, S.: *New Developments in the Boundary Element Method: Boundary Contour Method for Plane Problems in a Dual Formulation with Quadratic Shape Functions*, Chapter 14. Springer-Verlag, 2002.
13. SZEIDL, G.: *Problems of Continuum Mechanics in a Dual Formulation*. Dr. Sc. Thesis, Hungarian Academy of Sciences, 2005. (in Hungarian).
14. В. Д. Купрадзе: Методы потенциала в теории упругости. Физматгиз, Москва, 1963.
15. С. Г. Лехницки: Теория упругости анизотропного тела. Второе Издание, Наука, Москва, 1977.

ACCELERATION ANALYSIS OF RIGID BODY MOTION

ISTVÁN ECSEDI AND ATTILA BAKSA

Institute of Applied Mechanics, University of Miskolc

H-3515 Miskolc, Miskolc–Egyetemváros, Hungary

istvan.ecsedi@uni-miskolc.hu, attila.baksa@uni-miskolc.hu

[Received: February 26, 2015, Accepted: August 28, 2015]

*Dedicated to Professor Barna Szabó on the occasion of his eightieth birthday
and to Professor Imre Kozák on the occasion of his eighty-fifth birthday*

Abstract. The aim of this paper is to analyze some second order motion properties of rigid body motion. The existence of unique acceleration center is proven by means of vector-tensor algebra for the case when the vectors of angular velocity and of angular acceleration are linearly independent. The case when the vectors of angular velocity and of angular acceleration are linearly dependent is also considered. Explicit coordinate free relationships are derived for the position of the acceleration center and axis. A detailed analysis of the linear eigenvalue problem arising in the definition of acceleration axis is presented.

Mathematical Subject Classification: 70B10, 70B15

Keywords: rigid body motion, acceleration, acceleration center, acceleration axis

1. INTRODUCTION

Consider a rigid body b moving in general spatial motion with respect to a fixed reference frame $\{0; x, y, z\}$. Let $\boldsymbol{\omega}$ be the angular velocity of body b and let the points A and B be on body b with their velocities denoted by \mathbf{v}_A and \mathbf{v}_B , respectively. The velocity field of body b is formulated as [1, 2]

$$\mathbf{v}_B = \mathbf{v}_A + \boldsymbol{\omega} \times (\mathbf{r}_B - \mathbf{r}_A), \quad (1.1)$$

where \mathbf{r}_A and \mathbf{r}_B are the position vectors of points A and B relative to the fixed frame $\{0; x, y, z\}$ (Figure 1). In equation (1.1), the cross denotes the vectorial product of two vectors. It is known if

$$\mathbf{v}_A \cdot \boldsymbol{\omega} = 0 \quad \text{and} \quad \boldsymbol{\omega} \neq \mathbf{0}, \quad (1.2)$$

then there exists a set of points on body b which have zero velocity at the instant considered. The points which have zero velocity are called velocity center points; they are on a straight line which is parallel to the angular velocity vector $\boldsymbol{\omega}$ [1, 3]. We note that in equation (1.2) the dot between two vectors indicates their scalar product. Assuming that the condition formulated in equation (1.2) is satisfied, then

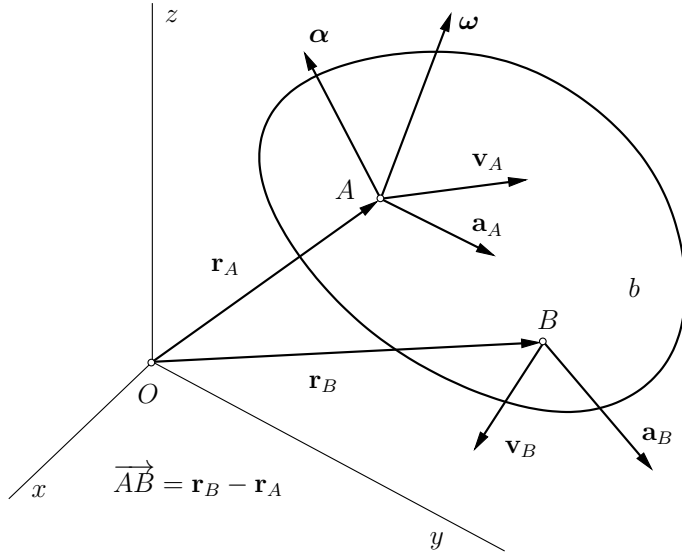


Figure 1. Rigid body in instantaneous general spatial motion.

the position of velocity center points is given by the formula

$$\mathbf{r}_C = \mathbf{r}_A + \frac{\boldsymbol{\omega} \times \mathbf{v}_A}{\omega^2} + p\boldsymbol{\omega} \quad -\infty < p < \infty. \quad (1.3)$$

Equation (1.3) gives the equation of the instantaneous axis of rotation [2, 3]. The validity of formula (1.3) can be checked by a direct substitution of equation (1.3) into equation (1.1).

Differentiation of equation (1.1) with respect to time leads to the formula of acceleration field

$$\mathbf{a}_B = \mathbf{a}_A + \boldsymbol{\alpha} \times (\mathbf{r}_B - \mathbf{r}_A) + \boldsymbol{\omega} \times (\boldsymbol{\omega} \times (\mathbf{r}_B - \mathbf{r}_A)), \quad (1.4)$$

where

$$\mathbf{a}_A = \frac{d\mathbf{v}_A}{dt}, \quad \mathbf{a}_B = \frac{d\mathbf{v}_B}{dt} \quad (1.5)$$

are the accelerations of points A and B (Figure 1), t is the time, $\boldsymbol{\alpha} = \frac{d\boldsymbol{\omega}}{dt}$ is the angular acceleration of body b .

The aim of this paper is to analyze two second order motion properties of rigid body motion, which are the acceleration center and acceleration axis. The concepts of acceleration center and of acceleration axis are borrowed from the book by Bottema and Roth [1] and a paper by Mohamed [4]. The existence of a unique acceleration center is proven from the case when $\boldsymbol{\omega}$ and $\boldsymbol{\alpha}$ are linearly independent vectors by the use of the method of vector and tensor algebra. An explicit coordinate-free relationships will be derived for the position of acceleration center and axis. The case when $\boldsymbol{\omega}$ and $\boldsymbol{\alpha}$ are linearly dependent vectors is also considered.

Martinez and Duffy [5] presents a review of papers dealing with the acceleration center. Martinez and Duffy gave the inverse of acceleration matrix introduced by Mohamed [4] but they did not cite Mohamed's paper [4]. In [5], a closed form expression for the inverse of the acceleration matrix in terms of the coordinates of $\boldsymbol{\omega}$ and $\boldsymbol{\alpha}$ is presented. Martinez and Duffy transformed the coordinate representation of the position vector of center of acceleration into a coordinate-free vectorial formula [5].

2. ACCELERATION CENTER

Denote Q the acceleration center of body b at the considered instant and let $\boldsymbol{\rho}$ be defined as $\boldsymbol{\rho} = \mathbf{r}_Q - \mathbf{r}_A$. According to the definition of acceleration center [1, 4, 5] we can write

$$\mathbf{a}_Q = \mathbf{0} = \mathbf{a}_A + \boldsymbol{\alpha} \times \boldsymbol{\rho} + \boldsymbol{\omega} \times (\boldsymbol{\omega} \times \boldsymbol{\rho}). \quad (2.1)$$

Two cases are treated. At first we assume that

$$\boldsymbol{\omega} \times \boldsymbol{\alpha} \neq \mathbf{0} \quad (2.2)$$

and then we investigate the existence of the center of acceleration when

$$\boldsymbol{\omega} \times \boldsymbol{\alpha} = \mathbf{0} \quad \text{and} \quad E = \omega^4 + \alpha^2 \neq 0. \quad (2.3)$$

If condition (2.2) holds then the vectors $\mathbf{a}_1 = \boldsymbol{\omega}$, $\mathbf{a}_2 = \boldsymbol{\alpha}$ and $\mathbf{a}_3 = \boldsymbol{\omega} \times \boldsymbol{\alpha}$ form a base of the 3D space.

In this case, we seek the position vector of point Q relative to point A as

$$\boldsymbol{\rho} = p_1\boldsymbol{\omega} + p_2\boldsymbol{\alpha} + p_3\boldsymbol{\omega} \times \boldsymbol{\alpha} \quad (\boldsymbol{\omega} \times \boldsymbol{\alpha} \neq \mathbf{0}). \quad (2.4)$$

Combination of equation (2.1) with equation (2.4) yields

$$p_1\boldsymbol{\alpha} \times \boldsymbol{\omega} + p_2\boldsymbol{\omega} \times (\boldsymbol{\omega} \times \boldsymbol{\alpha}) + p_3\{\boldsymbol{\alpha} \times (\boldsymbol{\omega} \times \boldsymbol{\alpha}) + \boldsymbol{\omega} \times [\boldsymbol{\omega} \times (\boldsymbol{\omega} \times \boldsymbol{\alpha})]\} = -\mathbf{a}_A. \quad (2.5)$$

Dot products of vector equation (2.5) with the vectors $\boldsymbol{\omega}$, $\boldsymbol{\alpha}$ and $\boldsymbol{\omega} \times \boldsymbol{\alpha}$ give

$$p_3(\boldsymbol{\omega} \times \boldsymbol{\alpha})^2 = -\mathbf{a}_A \cdot \boldsymbol{\omega}, \quad (2.6)$$

$$p_2(\boldsymbol{\omega} \times \boldsymbol{\alpha})^2 = \mathbf{a}_A \cdot \boldsymbol{\alpha}, \quad (2.7)$$

$$p_1(\boldsymbol{\omega} \times \boldsymbol{\alpha})^2 + p_3\omega^2(\boldsymbol{\omega} \times \boldsymbol{\alpha})^2 = \mathbf{a}_A \cdot (\boldsymbol{\omega} \times \boldsymbol{\alpha}). \quad (2.8)$$

Substitution of equation (2.6) into equation (2.8) leads to the equation

$$p_1(\boldsymbol{\omega} \times \boldsymbol{\alpha})^2 = \mathbf{a}_A \cdot (\boldsymbol{\omega} \times \boldsymbol{\alpha}) + (\mathbf{a}_A \cdot \boldsymbol{\omega})\omega^2. \quad (2.9)$$

The combination of equations (2.6), (2.7) and (2.9) with equation (2.4) gives the coordinate-free expression of the position vector of acceleration center Q relative to point A

$$\begin{aligned} \boldsymbol{\rho} = \frac{1}{(\boldsymbol{\omega} \times \boldsymbol{\alpha})^2} [(\mathbf{a}_A \cdot \boldsymbol{\alpha})\boldsymbol{\alpha} - (\mathbf{a}_A \cdot \boldsymbol{\omega})(\boldsymbol{\omega} \times \boldsymbol{\alpha}) + \\ + \{\mathbf{a}_A \cdot (\boldsymbol{\omega} \times \boldsymbol{\alpha}) + (\boldsymbol{\omega} \cdot \mathbf{a}_A)\omega^2\} \boldsymbol{\omega}]. \end{aligned} \quad (2.10)$$

By the use of the next identity

$$[(\boldsymbol{\omega} \times \boldsymbol{\alpha}) \times \boldsymbol{\omega}] \times \mathbf{a}_A = [\mathbf{a}_A \cdot (\boldsymbol{\omega} \times \boldsymbol{\alpha})] \boldsymbol{\omega} - (\mathbf{a}_A \cdot \boldsymbol{\omega}) \boldsymbol{\omega} \times \boldsymbol{\alpha} \quad (2.11)$$

we can write into a more compact form the expression of position vector $\boldsymbol{\rho}$ as

$$\boldsymbol{\rho} = \frac{1}{(\boldsymbol{\omega} \times \boldsymbol{\alpha})^2} [\{ (\boldsymbol{\omega} \times \boldsymbol{\alpha}) \times \boldsymbol{\omega} \} \times \mathbf{a}_A + (\boldsymbol{\alpha} \cdot \mathbf{a}_A) \boldsymbol{\alpha} + \omega^2 (\boldsymbol{\omega} \cdot \mathbf{a}_A) \boldsymbol{\omega}] . \quad (2.12)$$

Here, we note

$$(\boldsymbol{\omega} \times \boldsymbol{\alpha})^2 = \omega^2 \alpha^2 \sin^2 \gamma , \quad (2.13)$$

where γ is the angle formed by the vectors $\boldsymbol{\omega}$ and $\boldsymbol{\alpha}$ and we have

$$(\boldsymbol{\omega} \times \boldsymbol{\alpha})^2 = \omega^2 \alpha^2 - \omega^2 \alpha^2 \cos^2 \gamma = \omega^2 \alpha^2 - (\boldsymbol{\omega} \cdot \boldsymbol{\alpha})^2 , \quad (2.14)$$

$$\omega^2 = \boldsymbol{\omega} \cdot \boldsymbol{\omega} , \quad \alpha^2 = \boldsymbol{\alpha} \cdot \boldsymbol{\alpha} . \quad (2.15)$$

Mohamed [4] deduced a system of linear equations for the coordinates of vector $\boldsymbol{\rho}$ in a matrix form. The coefficient matrix of the unknown coordinates of $\boldsymbol{\rho}$ is called the “acceleration matrix” and it is shown by Mohamed [4], its determinant is opposite to $(\boldsymbol{\omega} \times \boldsymbol{\alpha})^2$. An explicit (closed) form of the inverse matrix of acceleration matrix was not presented by Mohamed [4].

Martinez and Duffy [5] gave the expression of inverse of acceleration matrix in terms of coordinates of $\boldsymbol{\omega}$ and $\boldsymbol{\alpha}$ by means of the symbolic algebra software MapleTM. Martinez and Duffy decomposed the inverse of the acceleration matrix into its symmetric and skew-symmetric parts and they interpreted these parts in the form of vector and scalar products respectively, and they obtained the vector formula (2.10) for the position of acceleration center [5]. Our approach does not use the coordinate representation of equation (2.1) in any Cartesian coordinate system to get the vector formula (2.10) for the acceleration center.

In the Appendix, the geometrical meaning of vectors

$$\boldsymbol{\rho}_1 = \frac{1}{(\boldsymbol{\omega} \times \boldsymbol{\alpha})^2} [(\mathbf{a}_A \cdot \boldsymbol{\alpha}) \boldsymbol{\alpha} - (\mathbf{a}_A \cdot \boldsymbol{\omega}) (\boldsymbol{\omega} \times \boldsymbol{\alpha})] \quad (2.16)$$

and

$$\boldsymbol{\rho}_2 = \frac{1}{(\boldsymbol{\omega} \times \boldsymbol{\alpha})^2} [\mathbf{a}_A \cdot (\boldsymbol{\omega} \times \boldsymbol{\alpha}) + (\boldsymbol{\omega} \cdot \mathbf{a}_A) \omega^2] \boldsymbol{\omega} \quad (2.17)$$

appearing in formula (2.10) is presented.

Next, we analyze the existence of acceleration center under the condition (2.3). In this case the angular velocity vector $\boldsymbol{\omega}$ and angular acceleration vector $\boldsymbol{\alpha}$ are not linearly independent, their vectors are parallel. We again start from equation (2.1) and equation (2.7). Let

$$\boldsymbol{\rho} = \boldsymbol{\rho}_0 + p \boldsymbol{\omega} , \quad (2.18)$$

be, where

$$\boldsymbol{\omega} \cdot \boldsymbol{\rho}_0 = 0 . \quad (2.19)$$

Inserting equation (2.18) into equation (2.1) we obtain

$$\boldsymbol{\alpha} \times \boldsymbol{\rho}_0 - \omega^2 \boldsymbol{\rho}_0 = -\mathbf{a}_A . \quad (2.20)$$

According to the condition (2.3) we have

$$\boldsymbol{\omega} = \omega \mathbf{e} , \quad \boldsymbol{\alpha} = \alpha \mathbf{e} , \quad (2.21)$$

where \mathbf{e} is the unit vector directed to parallel to the direction of $\boldsymbol{\omega}$ and $\boldsymbol{\alpha}$, thus we have $\omega = \boldsymbol{\omega} \cdot \mathbf{e}$, $\alpha = \boldsymbol{\alpha} \cdot \mathbf{e}$.

From equation (2.20) we get the condition of existence of acceleration center point which is

$$\mathbf{a}_A \cdot \mathbf{e} = 0 . \tag{2.22}$$

The conditions formulated in equations (2.21) and (2.22) are valid for instantaneous plane motion [2, 3]. We look for $\boldsymbol{\rho}_0$ in the form

$$\boldsymbol{\rho}_0 = p_1 \mathbf{a}_A + p_2 \mathbf{a}_A \times \mathbf{e} . \tag{2.23}$$

Scalar product equation (2.20) with the vectors \mathbf{a}_A and $\mathbf{a}_A \times \mathbf{e}$ gives the results

$$\alpha (\mathbf{a}_A \times \mathbf{e}) \cdot \boldsymbol{\rho}_0 - \omega^2 \boldsymbol{\rho}_0 \cdot \mathbf{a}_A = -\mathbf{a}_A^2 , \tag{2.24}$$

$$\alpha \boldsymbol{\rho}_0 \cdot \mathbf{a}_A + \omega^2 (\mathbf{a}_A \times \mathbf{e}) \cdot \boldsymbol{\rho}_0 = 0 . \tag{2.25}$$

On the other hand from equation (2.23) it follows that

$$p_1 \mathbf{a}_A^2 = \boldsymbol{\rho}_0 \cdot \mathbf{a}_A , \quad p_2 \mathbf{a}_A^2 = \boldsymbol{\rho}_0 \cdot (\mathbf{a}_A \times \mathbf{e}) . \tag{2.26}$$

Combination of equations (2.24), (2.25) with equations (2.26)_{1,2} gives

$$\omega^2 p_1 - \alpha p_2 = 1 , \tag{2.27}$$

$$\alpha p_1 + \omega^2 p_2 = 0 , \tag{2.28}$$

from which we have

$$p_1 = \frac{\omega^2}{\omega^4 + \alpha^2} , \quad p_2 = -\frac{\alpha}{\omega^4 + \alpha^2} . \tag{2.29}$$

Substitution of equations (2.29)_{1,2} into equation (2.23) yields the result

$$\boldsymbol{\rho}_0 = \frac{1}{\alpha^2 + \omega^4} [\omega^2 \mathbf{a}_A + \boldsymbol{\alpha} \times \mathbf{a}_A] . \tag{2.30}$$

It is evident the location of the acceleration centers, points having zero acceleration, with respect to point A under the conditions (2.3) is given by the formula

$$\boldsymbol{\rho} = \frac{1}{\alpha^2 + \omega^4} [\omega^2 \mathbf{a}_A + \boldsymbol{\alpha} \times \mathbf{a}_A] + p \mathbf{e} , \quad -\infty < p < \infty . \tag{2.31}$$

Equation (2.31) defines the line of acceleration centers [4].

3. ACCELERATION ELLIPSOID

According to Mohamed [4] the acceleration ellipsoid is defined as

$$|\mathbf{a}(\mathbf{R})| = |\boldsymbol{\alpha} \times \mathbf{R} + \boldsymbol{\omega} \times (\boldsymbol{\omega} \times \mathbf{R})| = M = \text{constant} \quad (M \geq 0) . \tag{3.1}$$

In equation (3.1), \mathbf{R} is the position vector of an arbitrary point P on body b relative to the center of acceleration, that is $\mathbf{R} = \overrightarrow{QP}$ and $\mathbf{a}(\mathbf{R}) = \mathbf{a}_P$. At first, we consider the case when $\boldsymbol{\omega}$ and $\boldsymbol{\alpha}$ are linearly independent, the condition (2.2) is valid. We introduce tensor \mathbf{A}_0 by the next prescription

$$\mathbf{A}_0 = \mathbf{1} \times \boldsymbol{\alpha} + \boldsymbol{\omega} \circ \boldsymbol{\omega} - \omega^2 \mathbf{1} , \tag{3.2}$$

where $\mathbf{1}$ is the unit tensor of 3D space and a circle between two vectors denotes their tensorial (dyadic) product. The definition of the scalar and vectorial product of a

vector with a tensor and the properties of dyadic product are given by Malvern [6], Mase et al. [7] and Lurje [8]. It is obvious

$$\mathbf{a}(\mathbf{R}) = \mathbf{A}_0 \cdot \mathbf{R}. \quad (3.3)$$

Here, \mathbf{A}_0 is a nonsingular tensor, since its determinant [6, 8]

$$\det \mathbf{A}_0 = \frac{(\mathbf{f}_1 \times \mathbf{f}_2) \cdot \mathbf{f}_3}{(\boldsymbol{\omega} \times \boldsymbol{\alpha})^2} \quad (3.4)$$

is non-zero, where

$$\mathbf{f}_1 = \mathbf{A}_0 \cdot \boldsymbol{\omega}, \quad \mathbf{f}_2 = \mathbf{A}_0 \cdot \boldsymbol{\alpha}, \quad \mathbf{f}_3 = \mathbf{A}_0 \cdot (\boldsymbol{\omega} \times \boldsymbol{\alpha}). \quad (3.5)$$

By a simple calculation we obtain

$$\mathbf{f}_1 = \boldsymbol{\alpha} \times \boldsymbol{\omega}, \quad \mathbf{f}_2 = \boldsymbol{\omega} (\boldsymbol{\omega} \cdot \boldsymbol{\alpha}) - \boldsymbol{\alpha} \boldsymbol{\omega}^2, \quad \mathbf{f}_3 = \boldsymbol{\alpha} \times (\boldsymbol{\omega} \times \boldsymbol{\alpha}) - \boldsymbol{\omega}^2 (\boldsymbol{\omega} \times \boldsymbol{\alpha}). \quad (3.6)$$

Inserting the results above obtained into equation (3.4) we have

$$\det \mathbf{A}_0 = -(\boldsymbol{\omega} \times \boldsymbol{\alpha})^2 \quad (3.7)$$

according to the result of Mohamed [4] since the tensor \mathbf{A}_0 is the tensorial representation of the acceleration matrix $\boldsymbol{\psi}$ introduced by Mohamed [4]. The tensor

$$\mathbf{A} = \mathbf{A}_0^T \cdot \mathbf{A}_0 \quad (3.8)$$

is a positive definite symmetric tensor since its determinant is positive

$$\det \mathbf{A} = (\boldsymbol{\omega} \times \boldsymbol{\alpha})^4 > 0, \quad (3.9)$$

and for an arbitrary \mathbf{x} vector we have

$$\mathbf{x}^T \cdot \mathbf{A} \cdot \mathbf{x} \geq 0. \quad (3.10)$$

We reformulate equation (3.1) as

$$\mathbf{R} \cdot \mathbf{A} \cdot \mathbf{R} = M^2. \quad (3.11)$$

This equation shows that the points whose acceleration vector has a given magnitude lie on an ellipsoid (acceleration ellipsoid). The center point and main axes of the acceleration ellipsoid for different value of M are the same. The common center point of acceleration ellipsoids is the acceleration center.

By a lengthy but elementary calculation starting from equation (3.2) and using the definition of \mathbf{A} we can derive the coordinate-free representation for \mathbf{A} as

$$\mathbf{A} = -\boldsymbol{\alpha} \times \mathbf{1} \times \boldsymbol{\alpha} + \boldsymbol{\omega} \circ (\boldsymbol{\omega} \times \boldsymbol{\alpha}) + (\boldsymbol{\omega} \times \boldsymbol{\alpha}) \circ \boldsymbol{\omega} - \boldsymbol{\omega}^2 \boldsymbol{\omega} \circ \boldsymbol{\omega} + \boldsymbol{\omega}^4 \mathbf{1}. \quad (3.12)$$

In the second case when $\boldsymbol{\omega}$ and $\boldsymbol{\alpha}$ are not linearly independent we have $\boldsymbol{\omega} = \omega \mathbf{e}$, $\boldsymbol{\alpha} = \alpha \mathbf{e}$ and we resolve the vector \mathbf{R} into two components as

$$\mathbf{R} = \mathbf{R}_0 + \mathbf{R}_1, \quad \mathbf{R}_0 \cdot \mathbf{e} = 0, \quad \mathbf{R}_1 \times \mathbf{e} = \mathbf{0}. \quad (3.13)$$

A simple calculation shows that

$$\mathbf{A}_0 = \alpha \mathbf{1} \times \mathbf{e} + \omega^2 \mathbf{e} \circ \mathbf{e} - \omega^2 \mathbf{1}, \quad (3.14)$$

$$\mathbf{A} = -\alpha^2 \mathbf{e} \times \mathbf{1} \times \mathbf{e} - \omega^4 \mathbf{e} \circ \mathbf{e} + \omega^4 \mathbf{1}, \quad (3.15)$$

$$\mathbf{A}_0 \cdot \mathbf{e} = \mathbf{0} \quad \text{and} \quad \mathbf{A} \cdot \mathbf{e} = \mathbf{0}, \quad (3.16)$$

$$\mathbf{R} \cdot \mathbf{A} \cdot \mathbf{R} = \mathbf{R}_0 \cdot \mathbf{A} \cdot \mathbf{R}_0 = (\alpha^2 + \omega^4) R_0^2 . \tag{3.17}$$

From equation (3.17) it follows that the points whose acceleration vector has a given magnitude M and $E = \alpha^2 + \omega^4 \neq 0$ are on a cylindrical surface.

The generators of this cylindrical surface are parallel to the vectors \mathbf{e} and the center point of its base circle is one of the acceleration center given by equation (2.31); the radius of base circle is

$$|\mathbf{R}_0| = \frac{|M|}{\sqrt{\alpha^2 + \omega^4}} . \tag{3.18}$$

It is obvious the normal vector of the plane of base circle is \mathbf{e} .

4. ACCELERATION AXIS

At first we compute the angle between the acceleration vector $\mathbf{a}_P = \mathbf{a}(\mathbf{R})$ and the position vector $\mathbf{R} = \overrightarrow{QP} = R\mathbf{q}$. Here, \mathbf{q} is a unit vector and its direction is parallel to the vector \mathbf{R} . It is evident that

$$\mathbf{a}(\mathbf{R}) = R\mathbf{a}(\mathbf{q}) , \quad \mathbf{a}(\mathbf{q}) = \mathbf{A}_0 \cdot \mathbf{q} . \tag{4.1}$$

Equation (4.1) shows that the acceleration vectors of the points of straight line determined by point Q and unit vector \mathbf{q} ($0 \leq R < \infty$) have same direction and their magnitudes are proportional with $R = |\overrightarrow{QP}|$. The angle between $\mathbf{a}(\mathbf{q})$ and \mathbf{q} is denoted by δ . A simple calculation gives for $\boldsymbol{\omega} \times \boldsymbol{\alpha} \neq \mathbf{0}$

$$\cos \delta = \frac{\mathbf{q} \cdot \mathbf{a}(\mathbf{q})}{|\mathbf{a}(\mathbf{q})|} = \frac{\mathbf{q} \cdot \mathbf{A}_0 \cdot \mathbf{q}}{\sqrt{\mathbf{q} \cdot \mathbf{A} \cdot \mathbf{q}}} = -\frac{(\boldsymbol{\omega} \times \mathbf{q})^2}{\sqrt{\mathbf{q} \cdot \mathbf{A} \cdot \mathbf{q}}} . \tag{4.2}$$

From equation (4.2) it follows that

$$\frac{\pi}{2} \leq \delta \leq \pi . \tag{4.3}$$

If $\boldsymbol{\omega} \times \boldsymbol{\alpha} = \mathbf{0}$ and $E = \alpha^2 + \omega^4 \neq 0$, then we have $\boldsymbol{\omega} = \omega\mathbf{e}$, $\boldsymbol{\alpha} = \alpha\mathbf{e}$ and we resolve \mathbf{q} into two components as

$$\mathbf{q} = \mathbf{q}_0 + q_1\mathbf{e} , \quad \mathbf{q}_0 \cdot \mathbf{e} = 0 , \quad q_0^2 + q_1^2 = 1 . \tag{4.4}$$

By a detailed computation which is based on equations (3.14) and (3.15) we obtain

$$\cos \delta = \frac{\mathbf{q} \cdot \mathbf{a}(\mathbf{q})}{|\mathbf{a}(\mathbf{q})|} = -\frac{\omega^2}{\sqrt{\alpha^2 + \omega^4}} |\mathbf{q}_0| , \quad 0 \leq |\mathbf{q}_0| \leq 1 . \tag{4.5}$$

The latter case is characterised by the equation (2.21), we consider one of the acceleration centers given by equation (2.31). Let $q_1 = 0$ be in equation (4.4); in this case we have $|\mathbf{q}_0| = 1$. The angle δ for points lying in that plane whose normal vector is \mathbf{e} and contains the chosen acceleration center ($q_1 = 0$) is as follows

$$\cos \delta = -\frac{\omega^2}{\sqrt{\alpha^2 + \omega^4}} . \tag{4.6}$$

Equation (4.6) it is a known result of plane kinematics [2, 3].

Next, we deal with the general 3D motion which is characterised by equation (2.2). For this case the acceleration axis is defined by the equation

$$\cos \delta = -1, \quad \delta = \pi. \quad (4.7)$$

All points P whose acceleration vectors are directed along the position vector $\mathbf{R} = \overrightarrow{QP}$ (Q is the acceleration center) are in a line which is called acceleration axis [1, 4]. Equation (4.7) can also be formulated as an eigenvalue problem

$$\mathbf{A}_0 \cdot \mathbf{R} = \mu \mathbf{R}. \quad (4.8)$$

At first we prove the real eigenvalues of tensor \mathbf{A}_0 are non-positive. From equation (4.8) it follows that

$$\mathbf{R} \cdot \mathbf{A}_0 \cdot \mathbf{R} = -(\boldsymbol{\omega} \times \mathbf{R})^2 = \mu R^2, \quad (4.9)$$

i.e.

$$\mu = -\frac{(\boldsymbol{\omega} \times \mathbf{R})^2}{R^2} \leq 0. \quad (4.10)$$

The next bound for the real eigenvalues of tensor \mathbf{A}_0 can be derived

$$-\omega^2 \leq \mu \leq 0 \quad (4.11)$$

by the use of (4.10) and

$$(\boldsymbol{\omega} \times \mathbf{R})^2 \leq \omega^2 R^2. \quad (4.12)$$

The scalar product of equation (4.8) with the vectors

$$\mathbf{a}_1 = \boldsymbol{\omega}, \quad \mathbf{a}_2 = \boldsymbol{\alpha}, \quad \mathbf{a}_3 = \boldsymbol{\omega} \times \boldsymbol{\alpha} \quad (4.13)$$

leads to a system of homogenous linear equations

$$\begin{bmatrix} -\mu & 0 & 1 \\ \boldsymbol{\alpha} \cdot \boldsymbol{\omega} & -(\mu + \omega^2) & 0 \\ -\alpha^2 & \boldsymbol{\alpha} \cdot \boldsymbol{\omega} & -(\mu + \omega^2) \end{bmatrix} \cdot \begin{bmatrix} X_1 \\ X_2 \\ X_3 \end{bmatrix} = \begin{bmatrix} 0 \\ 0 \\ 0 \end{bmatrix}. \quad (4.14)$$

for

$$X_1 = \boldsymbol{\omega} \cdot \mathbf{R}, \quad X_2 = \boldsymbol{\alpha} \cdot \mathbf{R}, \quad X_3 = (\boldsymbol{\omega} \times \boldsymbol{\alpha}) \cdot \mathbf{R}. \quad (4.15)$$

The condition of the zero value of the determinant of coefficient matrix of equation (4.14) yields the next characteristic equation for $s = \frac{\mu}{\omega^2}$

$$s^3 + 2s^2 + (1 + h^2)s + h^2 \sin^2 \gamma = 0, \quad (4.16)$$

where

$$h = \frac{\alpha}{\omega^2}. \quad (4.17)$$

A special coordinate representation of the angular velocity and angular acceleration vectors was used by Bottema and Roth to get the characteristic equation for μ [1]. It is very easy to point out that equation (4.16) is the same as which can be obtained from Bottema and Roth's result.

The discriminant of cubic equation (4.16) can be written in the form [9]

$$D = D_1 + D_2, \quad (4.18)$$

where

$$D_1 = \frac{1}{27} \left(h^2 - \frac{1}{3} \right)^3, \quad D_2 = \frac{1}{4} \left(h^2 \sin^2 \gamma - \frac{2}{3} h^2 - \frac{2}{27} \right)^2. \quad (4.19)$$

- For $D < 0$ there are three distinct real roots of equation (4.16). In this case three real acceleration axes exist.
- For $D > 0$, equation (4.16) has only one real root and two complex roots. In this case there is only one real acceleration axis and the other two are imaginary.
- For $D = 0$ the cubic equation (4.16) has three real roots and at least two are equal. If $D_1 = D_2 = 0$ then there are three equal real roots. For the case $D = 0$ and $D_1^2 + D_2^2 \neq 0$ there are two real acceleration axes. If $D_1^2 + D_2^2 = 0$ then there is only one real acceleration axis.

The direction of the acceleration axis is determined by the eigenvector \mathbf{R} corresponding to the eigenvalue $\mu = \omega^2 s$. We look for \mathbf{R} as

$$\mathbf{R} = \lambda_1 \boldsymbol{\alpha} \times (\boldsymbol{\omega} \times \boldsymbol{\alpha}) + \lambda_2 (\boldsymbol{\omega} \times \boldsymbol{\alpha}) \times \boldsymbol{\omega} + \lambda_3 (\boldsymbol{\omega} \times \boldsymbol{\alpha}). \quad (4.20)$$

The vectors

$$\mathbf{h}_1 = \boldsymbol{\alpha} \times (\boldsymbol{\omega} \times \boldsymbol{\alpha}), \quad \mathbf{h}_2 = (\boldsymbol{\omega} \times \boldsymbol{\alpha}) \times \boldsymbol{\omega}, \quad \mathbf{h}_3 = \boldsymbol{\omega} \times \boldsymbol{\alpha} \quad (4.21)$$

are linearly independent since

$$(\mathbf{h}_1 \times \mathbf{h}_2) \cdot \mathbf{h}_3 = |(\boldsymbol{\omega} \times \boldsymbol{\alpha})|^4 \neq 0. \quad (4.22)$$

Combination of equation (4.15) with equation (4.20) gives

$$\lambda_1 = \frac{X_1}{(\boldsymbol{\omega} \times \boldsymbol{\alpha})^2}, \quad \lambda_2 = \frac{X_2}{(\boldsymbol{\omega} \times \boldsymbol{\alpha})^2}, \quad \lambda_3 = \frac{X_3}{(\boldsymbol{\omega} \times \boldsymbol{\alpha})^2}. \quad (4.23)$$

The relationships between X_2 , X_3 and X_1 for $\mu \neq -\omega^2$ are as follows

$$X_2 = \frac{\boldsymbol{\alpha} \cdot \boldsymbol{\omega}}{\mu + \omega^2} X_1, \quad X_3 = \mu X_1. \quad (4.24)$$

In (4.24) X_1 is an arbitrary constant.

Let

$$X = \frac{X_1}{(\boldsymbol{\omega} \times \boldsymbol{\alpha})^2}. \quad (4.25)$$

The combination of equation (4.20) with equations (4.23), (4.24) and (4.25) gives the equation of acceleration axis for $\mu \neq -\omega^2$

$$\mathbf{R} = X \left[\boldsymbol{\alpha} \times (\boldsymbol{\omega} \times \boldsymbol{\alpha}) + \frac{\boldsymbol{\alpha} \cdot \boldsymbol{\omega}}{\mu + \omega^2} (\boldsymbol{\omega} \times \boldsymbol{\alpha}) + \mu (\boldsymbol{\omega} \times \boldsymbol{\alpha}) \right], \quad -\infty < X < \infty. \quad (4.26)$$

Next, the case of $\mu = -\omega^2$ is analyzed. For this case from equation (4.14) we obtain

$$\omega^2 X_1 + X_3 = 0 \quad (4.27)$$

$$\boldsymbol{\alpha} \cdot \boldsymbol{\omega} X_1 = 0 \quad (4.28)$$

$$-\alpha^2 X_1 + \boldsymbol{\alpha} \times \boldsymbol{\omega} X_2 = 0. \quad (4.29)$$

The existence of a nontrivial solution for X_1 , X_2 and X_3 which means that $X_1^2 + X_2^2 + X_3^2 \neq 0$, is

$$\boldsymbol{\alpha} \cdot \boldsymbol{\omega} = 0. \quad (4.30)$$

From equation (4.14) it follows that

$$X_1 = 0, \quad X_3 = 0, \quad X_2 = \boldsymbol{\alpha} \cdot \mathbf{R} = \text{arbitrary}, \quad (4.31)$$

and the equation of acceleration axis has the form

$$\mathbf{R} = \lambda \boldsymbol{\alpha} \quad -\infty < \lambda < \infty \quad (4.32)$$

according to equations (4.15) (and (4.31).

The existence of $\mu = -\omega^2$ under the conditions

$$\boldsymbol{\alpha} \times \boldsymbol{\omega} \neq 0 \quad \text{and} \quad \boldsymbol{\alpha} \cdot \boldsymbol{\omega} = 0 \quad (4.33)$$

can be derived from the solution of cubic equation (4.16) with substitution for $\gamma = \frac{\pi}{2}$. In this case we have following solution for s

$$s_1 = -1, \quad \mu_1 = -\omega^2, \quad (4.34)$$

$$s_2 = \frac{-1 + \sqrt{1 - 4h^2}}{2}, \quad \mu_2 = \frac{-\omega^2 + \sqrt{\omega^4 - 4\alpha^2}}{2}, \quad (4.35)$$

$$s_3 = \frac{-1 - \sqrt{1 - 4h^2}}{2}, \quad \mu_3 = \frac{-\omega^2 - \sqrt{\omega^4 - 4\alpha^2}}{2}, \quad (4.36)$$

In what follows the case of $D_1^2 + D_2^2 = 0$ will be considered. For this case we have

$$h^2 = \frac{1}{3}, \quad \sin^2 \gamma = \frac{8}{9}. \quad (4.37)$$

Substitution of results obtained above into the cubic equation (4.16) gives

$$s^3 + 2s^2 + \frac{4}{3}s + \frac{8}{27} = 0, \quad (4.38)$$

i.e.

$$(3s + 2)^3 = 0. \quad (4.39)$$

It is evident that if the conditions formulated in equation (4.37) are satisfied then

$$s_1 = s_2 = s_3 = -\frac{2}{3}, \quad \mu_1 = \mu_2 = \mu_3 = -\frac{2}{3}\omega^2. \quad (4.40)$$

Substitution of equation (4.40)₂ into equation (4.14) gives

$$X_3 = -\frac{2}{3}\omega^2 X_1, \quad X_2 = \pm \frac{\alpha}{\omega} X_1. \quad (4.41)$$

From the equations above obtained it follows that

$$\mathbf{n}_1 \cdot \mathbf{R} = 0, \quad \mathbf{n}_2 \cdot \mathbf{R} = 0, \quad (4.42)$$

where

$$\mathbf{n}_1 = \boldsymbol{\omega} \times \boldsymbol{\alpha} + \frac{2}{3}\omega^2 \boldsymbol{\omega}, \quad (4.43)$$

$$\mathbf{n}_2 = \boldsymbol{\alpha} - \frac{\alpha}{\omega} \boldsymbol{\omega} \quad \text{for} \quad \cos \gamma = \frac{1}{3}, \quad (4.44)$$

$$\mathbf{n}_2 = \boldsymbol{\alpha} + \frac{\alpha}{\omega} \boldsymbol{\omega} \quad \text{for} \quad \cos \gamma = -\frac{1}{3}. \quad (4.45)$$

The intersection of planes whose equations are given by (4.41) is a straight line, which is the real acceleration axis in the considered case. From equation (4.41) it follows that the equation of acceleration axis has the form

$$\mathbf{R} = \lambda(\mathbf{n}_1 \times \mathbf{n}_2) \quad -\infty < \lambda < \infty. \quad (4.46)$$

It is also worth noting that the eigenvalue μ cannot be zero or an imaginary number if $\boldsymbol{\omega} \neq \boldsymbol{\alpha} \neq \mathbf{0}$. The validity of this statement follows from equation (4.16). It is evident, if

$$\boldsymbol{\omega} \times \boldsymbol{\alpha} = \mathbf{0} \quad \text{and} \quad \alpha \neq 0 \quad (4.47)$$

then the acceleration axis does not exist, but for the case

$$\boldsymbol{\omega} \times \boldsymbol{\alpha} = \mathbf{0} \quad \text{and} \quad \alpha = 0, \quad \omega \neq 0 \quad (4.48)$$

we have

$$\mathbf{a}(\mathbf{q}) = \omega^2 \mathbf{e} \times [\mathbf{e} \times (\mathbf{q}_0 + q_1 \mathbf{e})] = -\omega^2 \mathbf{q}_0 \quad (4.49)$$

i.e., all the line segments \overline{QP} in the plane $q_1 = 0$ can be considered as an acceleration axis.

5. CONCLUSION

This paper deals with the analysis of the acceleration field of a rigid body in a general 3D spatial motion. Some results derived by Mohamed [4] are reformulated and analyzed in detailed forms. Explicit coordinate free relationships are presented for the position of the acceleration center and acceleration axis. A new proof is given to the vectorial formula of the acceleration center which was derived by Martinez and Duffy. Formulation and solution of problems are based on the well known relationships of rigid-body kinematics and the tools of vector–tensor algebra.

Acknowledgements. This research was carried out as part of the TAMOP 4.2.1.B-10/2/KONV-2010-0001 project with support by European Union, co-financed by European Social Fund.

APPENDIX A. REMARK TO THE FORMULA OF ACCELERATION CENTER

Let us consider the point X whose position vector relative to point A is (Figure 2)

$$\overrightarrow{AX} = \frac{1}{(\boldsymbol{\omega} \times \boldsymbol{\alpha})^2} [(\boldsymbol{\alpha} \cdot \mathbf{a}_A)\boldsymbol{\alpha} - (\boldsymbol{\omega} \cdot \mathbf{a}_A)(\boldsymbol{\omega} \times \boldsymbol{\alpha})] . \quad (A.1)$$

Application of equation (1.4) gives

$$\begin{aligned} \mathbf{a}_X &= \mathbf{a}_A + \boldsymbol{\alpha} \times \overrightarrow{AX} + \boldsymbol{\omega} \times (\boldsymbol{\omega} \times \overrightarrow{AX}) = \\ &= \mathbf{a}_A + \frac{1}{(\boldsymbol{\omega} \times \boldsymbol{\alpha})^2} [-(\boldsymbol{\omega} \cdot \mathbf{a}_A)\alpha^2 \boldsymbol{\omega} + (\boldsymbol{\alpha} \cdot \boldsymbol{\omega})(\boldsymbol{\omega} \cdot \mathbf{a}_A)\boldsymbol{\alpha} + \\ &\quad + (\boldsymbol{\omega} \cdot \boldsymbol{\alpha})(\boldsymbol{\alpha} \cdot \mathbf{a}_A)\boldsymbol{\omega} - \omega^2(\mathbf{a}_A \cdot \boldsymbol{\alpha})\boldsymbol{\alpha} + \omega^2(\boldsymbol{\omega} \cdot \mathbf{a}_A)\boldsymbol{\omega} \times \boldsymbol{\alpha}] . \quad (A.2) \end{aligned}$$

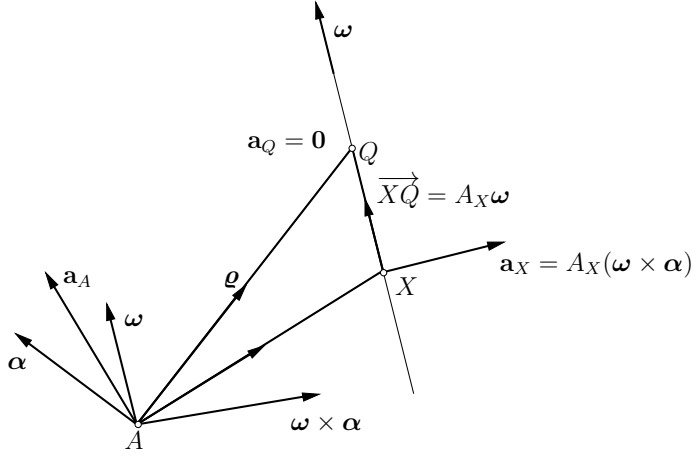


Figure 2. Determination of position of acceleration center

A simple computation shows that

$$\mathbf{a}_X \cdot \boldsymbol{\omega} = 0, \quad \mathbf{a}_X \cdot \boldsymbol{\alpha} = 0, \quad (\text{A.3})$$

$$\mathbf{a}_X \cdot (\boldsymbol{\omega} \times \boldsymbol{\alpha}) = \mathbf{a}_A \cdot (\boldsymbol{\omega} \times \boldsymbol{\alpha}) + (\mathbf{a}_A \cdot \boldsymbol{\omega})\omega^2. \quad (\text{A.4})$$

From equations (A.2), (A.3) and (A.4) it follows that

$$\mathbf{a}_X = A_X(\boldsymbol{\omega} \times \boldsymbol{\alpha}), \quad (\text{A.5})$$

where

$$A_X = \frac{1}{(\boldsymbol{\omega} \times \boldsymbol{\alpha})^2} [\mathbf{a}_A \cdot (\boldsymbol{\omega} \times \boldsymbol{\alpha}) + (\mathbf{a}_A \cdot \boldsymbol{\omega})\omega^2], \quad (\text{A.6})$$

The position vector of point Q relative to point X according to formula (2.11) is

$$\begin{aligned} \overrightarrow{XQ} &= \frac{1}{(\boldsymbol{\omega} \times \boldsymbol{\alpha})^2} [\{(\boldsymbol{\omega} \times \boldsymbol{\alpha}) \times \boldsymbol{\omega}\} \times \mathbf{a}_X + (\boldsymbol{\alpha} \cdot \mathbf{a}_X)\boldsymbol{\alpha} + \omega^2(\boldsymbol{\omega} \cdot \mathbf{a}_X)\boldsymbol{\omega}] = \\ &= \frac{A_X}{(\boldsymbol{\omega} \times \boldsymbol{\alpha})^2} \{(\boldsymbol{\omega} \times \boldsymbol{\alpha}) \times \boldsymbol{\omega}\} \times (\boldsymbol{\omega} \times \boldsymbol{\alpha}) = A_X\boldsymbol{\omega}, \end{aligned} \quad (\text{A.7})$$

that is

$$\overrightarrow{XQ} = A_X\boldsymbol{\omega} = \frac{1}{(\boldsymbol{\omega} \times \boldsymbol{\alpha})^2} [\mathbf{a}_A \cdot (\boldsymbol{\omega} \times \boldsymbol{\alpha}) + (\mathbf{a}_A \cdot \boldsymbol{\omega})\omega^2]. \quad (\text{A.8})$$

Comparing equation (2.10) with equations (A.1) and (A.8) we can write

$$\boldsymbol{\rho} = \overrightarrow{AQ} = \overrightarrow{AX} + \overrightarrow{XQ}, \quad (\text{A.9})$$

where $\boldsymbol{\rho}_1 = \overrightarrow{AX}$ and $\boldsymbol{\rho}_2 = \overrightarrow{XQ}$ are given by (A.1) and (A.8), respectively (Figure 2).

REFERENCES

1. O. BOTTEMA, B. ROTH, *Theoretical Kinematics*, North-Holland, Amsterdam, 1979.
2. I. H. GINSBERG, *Advanced Engineering Dynamics*, Cambridge University Press, Cambridge, 1995.
3. K. HUNT, *Kinematics Geometry of Mechanisms*, Oxford University Press, Oxford, 1978.
4. M. G. MOHAMED, Kinematics of rigid bodies in general spatial motion: second order motion properties, *Appl. Math. Modelling*, 21 (1997) 471–479.
5. J. M. R. MARTINEZ, J. DUFFY, Determination of the acceleration center of a rigid body in spatial motion, *Eur. J. Mech. A/Solids*, **17**, (1998), 969–977.
6. L. E. MALVERN, *Introduction to the Mechanics of Continuous Medium*, Prentice Hall, New York, 1969.
7. G. T. MASE, G. M. MASE, *Continuum Mechanics*, CRC Press, London, 1997.
8. A. I. LURJE, *Theory of Elasticity* (in Russian), Izd. Nauka, Moscow, 1970.
9. I. N. BRONSHTEIN, K. A. SEMENDYAYEV, G. MUISOL, H. MUCHLING, *Handbook of Mathematics*, Springer, Berlin, 2004.

ALWAYS CONVERGENT METHODS FOR SOLVING NONLINEAR EQUATIONS

AURÉL GALÁNTAI
Óbuda University
1034 Budapest, Bécsi út 96/b, Hungary
galantai.aurel@nik.uni-obuda.hu

[Received: August 03, 2015, Accepted: August 24, 2015]

Dedicated to Professor Barna Szabó on the occasion of his eightieth birthday

Abstract. We develop always convergent methods for solving nonlinear equations of the form $f(x) = 0$ ($f : \mathbb{R}^n \rightarrow \mathbb{R}^m$, $x \in B = \times_{i=1}^n [a_i, b_i]$) on continuous space curves that are lying in B . Under the only assumption that f is continuous these methods have a kind of monotone convergence to the nearest zero on the given curve, if it exists, or the iterations leave the region in a finite number of steps. Depending on the selection of the curve these methods are always convergent in the previous sense. In the paper we also investigate the selection of curves and also provide numerical test results that indicate the feasibility of the suggested methods.

Mathematical Subject Classification: 65H05, 65H20

Keywords: Always convergent methods, nonlinear equations, space-filling functions, α -dense curves

1. INTRODUCTION

Targonszky [1] investigated the following problem:

Let $f : \mathbb{C} \rightarrow \mathbb{C}$ be continuous in the closed domain

$$S = \{z \in \mathbb{C} : |z| \leq K, \varphi_0 \leq \arg z \leq \varphi_1\}$$

and assume that $f(0) \neq 0$. Let

$$\omega(\delta) = \sup_{\substack{z_1, z_2 \in S \\ |z_1 - z_2| \leq \delta}} |f(z_1) - f(z_2)|$$

be the modulus of continuity of f and let $\rho : [0, \infty) \rightarrow [0, \infty)$ be a continuous and strictly monotone increasing function so that

$$\rho(0) = 0, \quad \rho(\delta) \geq \omega(\delta) \quad (\delta > 0), \quad \lim_{\delta \rightarrow \infty} \rho(\delta) = \infty.$$

Furthermore assume that $\gamma > 0$ is a constant such that $\gamma K \leq 1$. Let $F : [0, \infty) \rightarrow [0, \infty)$ be any continuous and strictly monotone decreasing function such that

$$F(0) = 1, \quad F(x) \geq \frac{1}{1+x} \quad (x > 0).$$

Let

$$\psi(z) = zF(\gamma\rho^{-1}(|f(z)|)). \quad (1.1)$$

Observe that for $z \neq 0$, $z = \psi(z)$ if and only if $f(z) = 0$. For any $0 \neq z \in S$, $f(z) \neq 0$, define the iteration sequence

$$z_0 = z \quad (1.2)$$

$$z_{i+1} = \psi(z_i), \quad i = 0, 1, \dots \quad (1.3)$$

Theorem 1. ([1]). *The iteration is always convergent in the following sense: (i) If the line segment $\{tz \in \mathbb{C} : 0 < t \leq 1\}$ contains no zero of f , then $z_i \rightarrow 0$; (ii) If the line segment contains at least one zero of f , then z_i tends to the zero that is nearest to z .*

Theorem 2. ([1]). *The line segment $\{tz \in \mathbb{C} : 0 < t \leq 1\}$ contains no zero of f , if and only if the series $\sum_{n=0}^{\infty} z_i$ is convergent.*

Denote by $\text{Lip}_M\beta$ ($0 < \beta \leq 1$) those functions for which

$$\|f(x) - f(y)\| \leq M \|x - y\|^\beta \quad (x, y \in D \subset D(f)). \quad (1.4)$$

$\text{Lip}\beta$ denotes the set of those functions that are $\text{Lip}_M\beta$ for some constant $M \geq 0$.

If $f \in \text{Lip}_L\beta$ ($L > 0$), then $\omega(f; \delta) = \rho(\delta) = L\delta^\beta$ can be chosen. Thus $\rho^{-1}(x) = (x/L)^{1/\beta}$ and the iteration function (1.1) takes the form

$$\psi(z) = zF\left(\gamma\left(\frac{|f(z)|}{L}\right)^{\frac{1}{\beta}}\right). \quad (1.5)$$

It is interesting to note that Beauzamy [2] investigated the direct paths from 0 to the zeros of polynomials P , that is the sets $\{P(tz_j) : 0 \leq t \leq 1\}$, where z_j is a zero of $P(z)$ (where P is normalized so that $P(0) = 1$). He showed that there is always a zero towards which the direct path declines near 0, that is $|P(tz_j)| < |P(0)|$ if t is small enough. However, starting with degree 5, there are polynomials for which no direct path constantly remains below the altitude 1. Observe that Targonszky's method approaches the zero from above.

Also note that algorithm (1.2)–(1.3) works with any function f that is continuous on the compact set S . The weak point of the algorithm is, however, its behavior at zero. There is no indication if f has no zero on the line segment, while the algorithm makes infinitely many iterations.

In this paper we extend Targonszky's method for solving nonlinear equations in more general environments. In Section 2 we analyze and generalize some of its properties. Then we develop some classes of iteration methods with better convergence

behavior. Using the new results we suggest always convergent iteration schemes for solving nonlinear equations of the form

$$f(x) = 0 \quad (f : \mathbb{R}^n \rightarrow \mathbb{R}^m, x \in B = \times_{i=1}^n [a_i, b_i]), \tag{1.6}$$

where f is continuous on B . These methods work on continuous curves lying in B and exhibit a kind of monotone convergence to the nearest zero on the given curve, if it exists, or the iterations leave the region in a finite number of steps. The convergence is assured under continuity and its rate is estimated in many cases. The suggested curves are space-filling curves and/or α -dense curves.

Definition 3. Let $r : [0, 1] \rightarrow [0, 1]^n$ ($n \geq 2$) be a continuous mapping. The curve $x = r(t)$ ($t \in [0, 1]$) is space-filling if r is surjective.

Given a space-filling curve $r : [0, 1] \rightarrow [0, 1]^n$ and the hyperrectangle (or box) $B = \times_{i=1}^n [a_i, b_i]$, the mapping

$$h_i(t) = (b_i - a_i)r_i(t) + a_i, \quad i = 1, \dots, n$$

clearly fills up the whole hyperrectangle B .

Space-filling curves are used in many areas ([3], [4], [5], [6]). Their use in optimization was first suggested by Butz [7], [8], followed by Strongin and others (see, e.g. [9], [3], [6]). The use of Hilbert's space-filling functions for solving nonlinear systems was also suggested by Butz [10] and also later by Hlawka [11].

Definition 4. Let $I = [a, b] \subset \mathbb{R}$ be an interval and $B = \times_{i=1}^n [a_i, b_i] \subset \mathbb{R}^n$ be a rectangle. The map $x : I \rightarrow B$ is an α -dense curve, if for every $x \in B$, there exists a $t \in I$ such that $\|x(t) - x\| \leq \alpha$.

The concept and use of α -dense curves in optimization was suggested and applied by Cherruault and Guillez (see, e.g. [12], [13] or [14]).

In Section 6 we analyze and select space-filling and α -dense functions. In Section 8 we test some of the new methods on a set of test problems in order to see the feasibility of the suggested algorithms.

2. AN ANALYSIS OF TARGONSKY'S METHOD

There are two key elements of Targonszky's method. One is the iteration formula, the other is a kind of Lipschitz property.

For the first element, we can reformulate the Targonszky method in the following way. Set $z_i = zt_i$ ($t_i \in (0, 1]$). Then iteration function (1.1) can be replaced by

$$\psi(t) = tF(\gamma\rho^{-1}(|f(zt)|)), \tag{2.1}$$

where function $tF(y)$ has the following properties:

(i) $tF(y)$ is strictly monotone increasing in t and strictly monotone decreasing in y ;

(ii) For $t > 0$ and $y > 0$, $tF(y) < t$;

(iii) For $t > 0$, $tF(y) = t$ if and only if $y = 0$.

In the next two sections we generalize this iteration method and also derive particular formulae.

The second element is that if f has a zero $z^* = zt^* \in \{tz \in \mathbb{C} : 0 < t \leq 1\}$, then $\gamma\rho^{-1}(|f(zt)|)$ satisfies a kind of Lipschitz property

$$\gamma\rho^{-1}(|f(zt)|) \leq \frac{|t - t^*|}{t^*}.$$

From the proof of Theorem 1 it seems that the latter property is the quintessential element of Targonszky's method. It can be formulated more generally as follows.

Lemma 5. *Assume that $f \in C[a, b]$, $\omega(\delta) = \omega(f; \delta)$ is its modulus of continuity, $\rho : [0, \infty) \rightarrow [0, \infty)$ is a strictly monotone increasing function such that $\rho(0) = 0$, $\rho(x) \geq \omega(x)$ for $x \in [0, b - a]$ and $\lim_{x \rightarrow \infty} \rho(x) = \infty$. Assume that f has a zero $\xi \in [a, b]$. Then*

$$\rho^{-1}(|f(x)|) \leq |x - \xi| \quad (x \in [a, b]).$$

Proof. Since $|f(x)| = |f(x) - f(\xi)| \leq \omega(|x - \xi|) \leq \rho(|x - \xi|)$ and ρ^{-1} is also strictly monotone increasing we have $\rho^{-1}(|f(x)|) \leq |x - \xi|$. □

If $f \in \text{Lip}_M\beta$, then $\rho(\delta) = \omega(f; \delta) = M\delta^\beta$ can be chosen. If f is not Lipschitz β for some β ($0 < \beta \leq 1$), then we can use the following result (for the proof, see Efimov [15]).

Theorem 6. *(S.B. Stechkin). For each modulus of continuity $\omega(\delta)$, $0 \leq \delta \leq b - a$, there is a concave modulus of continuity $\omega_1(\delta)$ with the property*

$$\omega(\delta) \leq \omega_1(\delta) \leq 2\omega(\delta), \quad 0 \leq \delta \leq b - a. \tag{2.2}$$

Function ω_1 is called the least concave majorant of ω . It is easy to see that for $f \not\equiv 0$, either ω_1 is strictly monotone on $[0, b - a]$ or it is strictly increasing on some interval $[0, c]$ and becomes constant on $[c, b - a]$.

In order to get a proper ρ we can take any continuous and strictly monotone increasing function $g(x)$ that satisfies $g(0) = 0$, $g(x) \geq x$, and $\lim_{x \rightarrow \infty} g(x) = \infty$. Then the function

$$\rho(x) = \begin{cases} g(x + \omega_1(x)), & 0 \leq x \leq b - a \\ g(x + \omega_1(b - a)), & x > b - a \end{cases}$$

will satisfy the requirements for ρ . For example, $g(x) = e^x - 1$ is such a function.

Assume that $T \subset \mathbb{R}^n$ is a closed and bounded region and $f : \mathbb{R}^n \rightarrow \mathbb{R}^m$ is a continuous function on T . The modulus of continuity of f is defined by

$$\omega(\delta) = \omega(f; \delta) = \sup_{\substack{x_1, x_2 \in T \\ \|x_1 - x_2\| \leq \delta}} \|f(x_1) - f(x_2)\| \quad (0 \leq \delta \leq \text{diam}(T)), \tag{2.3}$$

where $\text{diam}(T)$ is the diameter of the compact region T . It is clear that $\omega(\delta)$ is monotone decreasing.

For other properties, Kolodii and Khil'debrand [16] proved the following results:

(i) $\omega(\delta)$ is continuous from the right;

(ii) $\omega(\delta)$ is continuous from the left if and only if T satisfies the following condition A: for any $\delta > 0$ and any points $x, y \in T$, $x \neq y$, there are points $x', y' \in T$ such that $\|x' - x\| < \delta$, $\|y' - y\| < \delta$ and $\|x' - y'\| < \|x - y\|$;

(iii) $\omega(\delta)$ is continuous if and only if T satisfies condition A;

(iv) ω is subadditive if and only if T is convex.

Note that any region T satisfying condition A is connected. It is also obvious that if T is convex, then it satisfies condition A.

Lemma 7. *Assume that $T \subset \mathbb{R}^n$ is a closed, bounded and convex region and $f : \mathbb{R}^n \rightarrow \mathbb{R}^m$ is continuous on T . Let ω_f denote the modulus of continuity of f on T . Let Γ be any continuous curve that lays in T , that is $\Gamma = \{r(t) : 0 \leq t \leq \tau\} \subset T$. Denote its modulus of continuity by ω_r . Assume that $\rho_f, \rho_r : [0, \infty) \rightarrow [0, \infty)$ are continuous and strictly monotone increasing functions so that*

$$\rho_f(0) = 0, \quad \rho_f(\delta) \geq \omega_f(\delta) \quad (\delta \in [0, \text{diam}(T)]), \quad \lim_{\delta \rightarrow \infty} \rho_f(\delta) = \infty \quad (2.4)$$

and

$$\rho_r(0) = 0, \quad \rho_r(\delta) \geq \omega_r(\delta) \quad (\delta \in [0, \tau]), \quad \lim_{\delta \rightarrow \infty} \rho_r(\delta) = \infty \quad (2.5)$$

hold, respectively. If $f(r(t))$ has a zero ξ on the curve Γ , that is $f(r(\xi)) = 0$ for some $\xi \in [0, \tau]$, then

$$\rho_r^{-1} \left(\rho_f^{-1} (\|f(r(t))\|) \right) \leq |t - \xi| \quad (t \in [0, \tau]). \quad (2.6)$$

Proof. Since

$$\|f(r(t))\| = \|f(r(t)) - f(r(\xi))\| \leq \omega_f(\|r(t) - r(\xi)\|) \leq \rho_f(\|r(t) - r(\xi)\|),$$

we have

$$\rho_f^{-1} (\|f(r(t))\|) \leq \|r(t) - r(\xi)\| \leq \omega_r(|t - \xi|) \leq \rho_r(|t - \xi|)$$

and

$$\rho_r^{-1} \left(\rho_f^{-1} (\|f(r(t))\|) \right) \leq |t - \xi|.$$

□

Assume that $f \in \text{Lip}_{L_f} \beta$ ($0 < \beta \leq 1$). Then $\omega_f(\delta) \leq L_f \delta^\beta$ and we can select $\rho_f(\delta) = L_f \delta^\beta$ and $\rho_f^{-1}(\delta) = \left(\frac{\delta}{L_f}\right)^{1/\beta}$. Similarly, if curve Γ is $\text{Lip}_{L_r} \mu$ ($\mu \in (0, 1]$), that is

$$\|r(s) - r(t)\| \leq L_r |s - t|^\mu \quad (t, s \in [0, \tau]), \quad (2.7)$$

then $\omega_r(\delta) \leq L_\Gamma \delta^\mu$ and so we can take $\rho_r(\delta) = L_\Gamma \delta^\mu$ and $\rho_r^{-1}(\delta) = \left(\frac{\delta}{L_\Gamma}\right)^{1/\mu}$. Thus $\rho_r^{-1}(\rho_f^{-1}(\delta)) = \frac{1}{L_\Gamma^\mu} \left(\frac{\delta}{L_f}\right)^{\frac{1}{\mu\beta}}$ and in the case of a zero $\xi \in [0, \tau]$, we have the estimate

$$\rho_r^{-1} \rho_f^{-1} (\|f(r(t))\|) = \frac{1}{L_\Gamma^\mu} \left(\frac{\|f(r(t))\|}{L_f} \right)^{\frac{1}{\mu\beta}} \leq |t - \xi| \quad (t \in [0, \tau]). \tag{2.8}$$

In Targonszky's case $r(t) = t$ for which $\mu = 1$, $L_\Gamma = |z|$.

Corollary 8. *Assume that both f and Γ are bi-Hölder, that is*

$$k_f \|x - y\|^\beta \leq \|f(x) - f(y)\| \leq L_f \|x - y\|^\beta \quad (x, y \in T) \tag{2.9}$$

and

$$k_\Gamma |s - t|^\mu \leq \|r(s) - r(t)\| \leq L_\Gamma |s - t|^\mu \quad (s, t \in [0, \tau]). \tag{2.10}$$

If $f(r(t))$ has a zero ξ on the curve Γ , that is $f(r(\xi)) = 0$ for some $\xi \in [0, \tau]$, then

$$\left(\frac{k_\Gamma}{L_\Gamma}\right)^{\frac{1}{\mu}} \left(\frac{k_f}{L_f}\right)^{\frac{1}{\alpha\beta}} |t - \xi| \leq \rho_r^{-1} \rho_f^{-1} (\|f(r(t))\|) \leq |t - \xi|. \tag{2.11}$$

Proof. Since

$$k_f k_\Gamma^\beta |t - \xi|^{\mu\beta} \leq \|f(r(t))\| \leq L_f L_\Gamma^\beta |t - \xi|^{\mu\beta}$$

we have

$$\rho_r^{-1} \left(\left[\frac{k_f k_\Gamma^\beta |t - \xi|^{\mu\beta}}{L_f} \right]^{1/\beta} \right) \leq \rho_r^{-1} \rho_f^{-1} (\|f(r(t))\|) \leq \rho_r^{-1} (L_\Gamma |t - \xi|^\mu) = |t - \xi|.$$

By definition

$$\rho_r^{-1} \left(\left[\frac{k_f k_\Gamma^\beta |t - \xi|^{\mu\beta}}{L_f} \right]^{1/\beta} \right) = \left(\frac{k_\Gamma}{L_\Gamma}\right)^{\frac{1}{\mu}} \left(\frac{k_f}{L_f}\right)^{\frac{1}{\alpha\beta}} |t - \xi|,$$

and so we have the two-sided bound

$$\left(\frac{k_\Gamma}{L_\Gamma}\right)^{\frac{1}{\mu}} \left(\frac{k_f}{L_f}\right)^{\frac{1}{\alpha\beta}} |t - \xi| \leq \rho_r^{-1} \rho_f^{-1} (\|f(r(t))\|) \leq |t - \xi|. \tag{2.12}$$

□

If $\Gamma \subset \mathbb{R}$ is an interval, that is $r(t) = t$, then $k_\Gamma = L_\Gamma = 1$, $\mu = 1$, $\rho_r(t) = t$ and

$$\left(\frac{k_f}{L_f}\right)^{\frac{1}{\beta}} |t - \xi| \leq \rho_r^{-1} \rho_f^{-1} (\|f(r(t))\|) \leq |t - \xi|. \tag{2.13}$$

3. A GENERAL CLASS OF ITERATION METHODS

We investigate iteration methods of the form

$$x_{i+1} = F(x_i, \varphi(x_i))$$

for solving real equation $f(x) = 0$ on the interval $[a, 1]$ ($[a, 1] \subset [0, 1]$, $f \in C[a, 1]$). The selection of interval $[0, 1]$ is only for convenience. We assume that $F(x, y) = x \Leftrightarrow y = 0$ ($x \geq a$), $F(x, y) > x$ or $F(x, y) < x$ for $y > 0$, $\varphi(x) \geq 0$ and $\varphi(x) = 0 \Leftrightarrow f(x) = 0$. We also assume that $y \geq 0$ and $y := \varphi(x) \leq |x - \xi|$, if a zero ξ of f exists in the interval $[a, 1]$. Both F and φ are continuous, $F(x, y)$ is strictly monotone increasing in x and strictly monotone in y . We separately investigate the case when $a = 0$ and $F(0, y) = 0$ may occur for some $y > 0$.

Theorem 9. *Assume that*

- (a) $F(x, y)$ is continuous in $[a, 1] \times [0, \infty)$;
- (b) $x \geq a$, $F(x, y) = x \Leftrightarrow y = 0$;
- (c) $F(x, y) < x$ ($x \in [a, 1]$, $y > 0$);
- (d) For $x > \xi$ ($x, \xi \in [a, 1]$) and $0 \leq y \leq x - \xi$, $F(x, y) \geq \xi$.
- (e) $F(x, y)$ is strictly monotone increasing in x , and strictly monotone decreasing in y ;

Assume further that $\varphi(x) \geq 0$, $\varphi(\xi) = 0 \Leftrightarrow f(\xi) = 0$ and if a root $\xi \in [a, 1]$ exists, then $\varphi(x) \leq |x - \xi|$. Let $x_0 = 1$ and assume that $\varphi(1) > 0$. Define

$$x_{i+1} = F(x_i, \varphi(x_i)) \quad (i = 0, 1, 2, \dots). \tag{3.1}$$

Then $\{x_i\}$ is a strictly monotone decreasing sequence that converges to ξ_{\max} if a root exists in $[a, 1]$. If no root exists, then the sequence $\{x_i\}$ leaves the interval $[a, 1]$ in a finite number of steps.

Proof. If $\varphi(x_i) > 0$, then $x_{i+1} < x_i$ by (c). If $\varphi(x_i) = 0$ then $x_{i+1} = x_i$ by (b). Assume that $x_i > \xi_{\max}$. Then $\varphi(x_i) \leq x_i - \xi_{\max}$ and $x_{i+1} = F(x_i, \varphi(x_i)) \geq \xi_{\max}$ by (d). Hence the sequence $\{x_i\}$ can not pass the zero ξ_{\max} . Since $\{x_i\}$ is a monotone decreasing sequence bounded from below, it has a limit point x^* so that $\xi_{\max} \leq x^* = F(x^*, \varphi(x^*))$. Hence $x^* = \xi_{\max}$. If there is no zero in $[a, 1]$, then $x - F(x, \varphi(x)) \geq m > 0$ ($x \in [a, 1]$) by (c). Hence $x_{i+1} \leq x_i - m$ and for a large enough i , $x_i < a$. □

Corollary 10. *If for $x > \xi$ ($x, \xi \in [a, 1]$) and $0 \leq y \leq x - \xi$,*

$$F(x, y) \geq \xi + \kappa_2(x - \xi) \quad (0 < \kappa_2 < 1), \tag{3.2}$$

and $\varphi(x)$ is such that $\varphi(x) \leq |x - \xi|$ ($x \in [a, b]$), then the speed of convergence is at best linear.

Proof. Since $0 \leq \varphi(x_i) \leq x_i - \xi$, the assumption implies

$$x_{i+1} - \xi_{\max} = F(x_i, \varphi(x_i)) - \xi_{\max} \geq \kappa_2(x_i - \xi_{\max}),$$

which proves this. □

Corollary 11. *If for $x > \xi$ ($x, \xi \in [a, 1]$) and $0 \leq \theta(x - \xi) \leq y \leq x - \xi$,*

$$\xi + \kappa_1(x - \xi) \geq F(x, y) \quad (3.3)$$

holds with constant $0 < \kappa_2 < \kappa_1 < 1$, and $\varphi(x)$ is such that $\theta|x - \xi| \leq \varphi(x) \leq |x - \xi|$ ($x \in [a, b]$), then the convergence speed is linear.

Proof. The assumption implies $\theta(x_i - \xi_{\max}) \leq \varphi(x_i) \leq x_i - \xi_{\max}$ and

$$\kappa_1(x_i - \xi_{\max}) \geq x_{i+1} - \xi_{\max} \geq \kappa_2(x_i - \xi_{\max}).$$

□

If $a = 0$ and $F(x, y) = x$ is possible for $y > 0$ and $x = 0$, then what we can prove is prove definitely less.

Theorem 12. *Assume that*

- (a) $F(x, y)$ is continuous in $[0, 1] \times [0, \infty)$;
- (b) $x > 0$, $F(x, y) = x \Leftrightarrow y = 0$;
- (c) $F(x, y) < x$ ($x \in (0, 1]$, $y > 0$);
- (d) For $x > \xi$ ($x, \xi \in [0, 1]$) and $0 \leq y \leq x - \xi$, $F(x, y) \geq \xi$.
- (e) $F(x, y)$ is strictly monotone increasing in x , and strictly monotone decreasing in y ;

Assume further that $\varphi(x) \geq 0$, $\varphi(\xi) = 0 \Leftrightarrow f(\xi) = 0$ and if a root $\xi \in [0, 1]$ exists, then $\varphi(x) \leq |x - \xi|$. Let $x_0 = 1$ and assume that $\varphi(1) > 0$. Define

$$x_{i+1} = F(x_i, \varphi(x_i)) \quad (i = 0, 1, 2, \dots). \quad (3.4)$$

Then $\{x_i\}$ is a strictly monotone decreasing sequence that converges to ξ_{\max} if a root exists in $[0, 1]$. If no root exists, then the sequence $\{x_i\}$ either converges to 0 or leaves the interval $[0, 1]$ in a finite number of steps.

Proof. If $\varphi(x_i) > 0$, then $x_{i+1} < x_i$ by (c). If $\varphi(x_i) = 0$ then $x_{i+1} = x_i$ by (b). Assume that $x_i > \xi_{\max}$. Then $\varphi(x_i) \leq x_i - \xi_{\max}$ and $x_{i+1} = F(x_i, \varphi(x_i)) \geq \xi_{\max}$ by (d). Hence the sequence $\{x_i\}$ can not pass the zero ξ_{\max} . Since $\{x_i\}$ is a monotone decreasing sequence bounded from below, it has a limit point x^* so that $\xi_{\max} \leq x^* = F(x^*, \varphi(x^*))$. Hence $x^* = \xi_{\max}$. If there is no zero in $[0, 1]$, then we have two possible cases: $x_i \geq 0$ for all i or $x_{i_0} < 0$ holds for some integer $i_0 > 0$. If $x_i \geq 0$ for all i and we have no zero in $[0, 1]$, then $x_i \rightarrow 0$ must hold. □

Remark 13. *The result is different from the previous one. The Targonszky case indicates that problems with $a = 0$ if $F(0, y) = 0$ may happen for $y > 0$. The two corollaries of the previous theorem also hold.*

Theorem 14. *Assume that*

- (a1) $F(x, y)$ is continuous in $[a, 1] \times [0, \infty)$;
- (b1) $x \geq a$, $F(x, y) = x \Leftrightarrow y = 0$;
- (c1) $F(x, y) > x$ ($x \in [a, 1]$, $y > 0$);
- (d1) For $x < \xi$ ($x, \xi \in [a, 1]$) and $0 \leq y \leq \xi - x$, $F(x, y) \leq \xi$;
- (e1) $F(x, y)$ is strictly monotone increasing both in x and y .

Assume further that $\varphi(x) \geq 0$, $\varphi(\xi) = 0 \Leftrightarrow f(\xi) = 0$ and if a root $\xi \in [a, 1]$ exists, then $\varphi(x) \leq |x - \xi|$. Let $x_0 = a$ and assume that $\varphi(a) > 0$. Define

$$x_{i+1} = F(x_i, \varphi(x_i)) \quad (i = 0, 1, 2, \dots). \tag{3.5}$$

Then $\{x_i\}$ is a strictly monotone increasing sequence that converges to ξ_{\min} if a root exists in $[a, 1]$. If no root exists, then the sequence $\{x_i\}$ leaves the interval $[a, 1]$ in a finite number of steps.

Proof. If $\varphi(x_i) > 0$, then $x_{i+1} > x_i$ by (c1). If $\varphi(x_i) = 0$ then $x_{i+1} = x_i$ by (b1). Assume that $x_i > \xi_{\max}$. Then $\varphi(x_i) \leq \xi_{\min} - x_i$ and $x_{i+1} = F(x_i, \varphi(x_i)) \leq \xi_{\min}$ by (d1). Hence the sequence $\{x_i\}$ cannot pass the zero ξ_{\min} . Since $\{x_i\}$ is a monotone increasing sequence bounded from above, it has a limit point x^* so that $\xi_{\min} \geq x^* = F(x^*, \varphi(x^*))$. Hence $x^* = \xi_{\min}$. If there is no zero in $[a, 1]$, then $F(x, \varphi(x)) - x \geq m > 0$ ($x \in [a, 1]$) by (c1). Hence $x_{i+1} \geq x_i + m$ and for a large enough i , $x_i > 1$. □

Corollary 15. *If for $x < \xi$ ($x, \xi \in [a, 1]$) and $0 \leq y \leq \xi - x$,*

$$F(x, y) \leq \xi - \lambda_2 (\xi - x) \quad (0 < \lambda_2 < 1), \tag{3.6}$$

and $\varphi(x)$ is such that $\varphi(x) \leq |x - \xi|$ ($x \in [a, b]$), then the speed of convergence is at best linear.

Proof. The assumption implies

$$\xi_{\min} - x_{i+1} = \xi_{\min} - F(x_i, \varphi(x_i)) \geq \lambda_2 (\xi_{\min} - x_i),$$

which proves this. □

Corollary 16. *If for $x < \xi$ ($x, \xi \in [a, 1]$) and $0 \leq \theta(\xi - x) \leq y \leq \xi - x$,*

$$\xi - \lambda_1 (\xi - x) \leq F(x, y) \tag{3.7}$$

holds with constants $0 < \lambda_2 < \lambda_1 < 1$, and φ is such that $\theta|x - \xi| \leq \varphi(x) \leq |x - \xi|$ ($x \in [a, 1]$), then the convergence speed is linear.

Proof. The assumption implies $\theta(\xi_{\min} - x_i) \leq \varphi(x_i) \leq \xi_{\min} - x_i$ and

$$\lambda_2 (\xi_{\min} - x_i) \leq \xi_{\min} - x_{i+1} \leq \lambda_1 (\xi_{\min} - x_i).$$

□

For certain cases $a = 0$ is possible. For $F(x, y) = x(1 + y)$ the iteration does not start from $x_0 = 0$.

4. SOME ITERATION FUNCTIONS

Using requirements (a)-(e), (a1)-(e1) and various assumptions on the form of $F(x, y)$ such as

$$F(x, y) = g(x)h(y),$$

$$F(x, y) = g(x) + h(y),$$

and

$$F(x, y) = \frac{\alpha + \beta x + \gamma y}{a + bx + cy}$$

we derived the iteration functions (d-1)-(d-3), (i-1)-(i-3) given in the following tables. These tables also contain iteration functions (d-4), (i-4) that are direct generalizations of method [17] (see, also [18], [19]). It is assumed that function U is strictly monotone increasing, and both U and U^{-1} are Lipschitz with $L_{U^{-1}} < 1$ and $L_U > 1$.

For the error constants $\kappa_1, \kappa_2, \lambda_1$ and λ_2 we have to assume the existence of a zero ξ .

	monotone decreasing case	κ_2	κ_1
(d-1)	$F(x, y) = \frac{x}{1+y}$	$(1 - \xi) / 2 \geq 0$	$1 - \theta\xi \leq 1$
(d-2)	$F(x, y) = x - \frac{1}{P}y \quad (P \geq 1)$	$1 - \frac{1}{P} \geq 0$	$1 - \frac{\theta}{P} < 1$
(d-3)	$F(x, y) = \frac{px+qy}{p+wy}$ $(p > 0, W \geq 0, q < 0, p \geq W - q)$	$\frac{p-w+q}{p+w} \geq 0$	$\frac{p-\theta(w\xi-q)}{p} < 1$
(d-4)	$F(x, y) = U^{-1}(U(x) - y)$	$1 - L_{U^{-1}}$	$1 - \frac{\theta}{L_U}$

	monotone increasing case	λ_2	λ_1
(i-1)	$F(x, y) = x(1+y)$	$1 - x \geq 0$	$1 - \theta x \leq 1$
(i-2)	$F(x, y) = x + \frac{1}{P}y \quad (P \geq 1)$	$1 - \frac{1}{P} \geq 0$	$1 - \frac{\theta}{P} < 1$
(i-3)	$F(x, y) = \frac{px+qy}{p+wy} \quad (p \geq q > w \geq 0)$	$\frac{p-(q-w\xi)}{p+w} \geq 0$	$\frac{p-\theta(q-w\xi)}{p} < 1$
(i-4)	$F(x, y) = U^{-1}(U(x) + y)$	$1 - L_{U^{-1}}$	$1 - \frac{\theta}{L_U}$

Formulae (d-1) and (d-2) are special cases of (d-3). Case (d-1) is Targonszky's formula and $F(x, y) = x \Leftrightarrow y = 0$ holds only for $x > 0$.

Formula (i-2) is a special case of (i-3). For (i-1), $F(x, y) = x \Leftrightarrow y = 0$ holds only for $x > 0$.

If $U(x) = Px + q$, then $U^{-1}(x) = \frac{x-q}{P}$ and $U^{-1}(U(x) \pm y) = x \pm \frac{1}{P}y$. In this case formulae (d-2) and (i-2) are special cases of subclasses (d-4) and (i-4).

While the determination of error constants for cases (1)-(3) is rather straightforward, cases (d-4)-(i-4) require some argument. Here we exploit the strict monotonicity of U and U^{-1} as follows. For $x > \xi$,

$$U^{-1}(U(x) - y) - \xi \geq \kappa_2(x - \xi) \Leftrightarrow U(x) - y \geq U(\xi + \kappa_2(x - \xi)) \Leftrightarrow$$

$$U(x) - U(\xi + \kappa_2(x - \xi)) > \frac{1}{L_{U^{-1}}}(1 - \kappa_2)(x - \xi) \geq x - \xi \geq y$$

holds if $\frac{1}{L_{U^{-1}}}(1 - \kappa_2) \geq 1$. This gives the error constant $\kappa_2 \leq 1 - L_{U^{-1}}$. Also we have

$$\begin{aligned} \kappa_1(x - \xi) \geq F(x, y) - \xi &\Leftrightarrow U(\kappa_1(x - \xi) + \xi) \geq U(x) - y \Leftrightarrow \\ U(x) - U(\kappa_1(x - \xi) + \xi) &\leq L_U(x - \xi - \kappa_1(x - \xi)) \\ &= L_U(1 - \kappa_1)(x - \xi) \leq \theta(x - \xi) \leq y, \end{aligned}$$

that is if $L_U(1 - \kappa_1) \leq \theta$, which leads to $\kappa_1 \geq 1 - \frac{\theta}{L_U}$.

Derivation of (i-4) error constants is similar. Note that in case (d-3) $\kappa_2 > 0$, if $p > W - q$. Similarly in case (i-3) $\lambda_2 > 0$ if $p > q$.

5. ITERATION METHODS FOR GENERAL EQUATIONS

Here we study equations of the form

$$f(x) = 0 \quad (f : \mathbb{R}^n \rightarrow \mathbb{R}^m, x \in T = \times_{i=1}^n [a_i, b_i]), \tag{5.1}$$

where f is continuous on the (compact) rectangle/hyperinterval T , and each of the cases $n = m$, $n < m$ and $n > m$ is possible.

Assume that a continuous curve $\Gamma = \{r(t) : 0 \leq t \leq 1\} \subset T$ is given. We seek for the solution of $f(x) = 0$ on the curve Γ , that is the solution of equation

$$f(r(t)) = 0 \quad (t \in [0, 1]), \tag{5.2}$$

which is equivalent to the real equation

$$\|f(r(t))\| = 0 \quad (t \in [0, 1]). \tag{5.3}$$

Taking any iteration method $t_{i+1} = F(t_i, \varphi(t_i))$ of Section 3 with

$$\varphi(t) = \rho_r^{-1} \left(\rho_f^{-1} (\|f(r(t))\|) \right) \tag{5.4}$$

we have an always convergent iteration method that either solves the equation on the curve Γ or leaves Γ in a finite number of steps.

One can easily reformulate Theorems 9, 12 and 14 and their respective Corollaries. We just do this with Theorem 9.

Theorem 17. *Assume that $f : \mathbb{R}^n \rightarrow \mathbb{R}^m$ is continuous on the rectangle $T = \times_{i=1}^n [a_i, b_i]$ and $\Gamma = \{r(t) : 0 \leq t \leq 1\} \subset T$ is a continuous curve. Let ω_f and ω_r be the modulus of continuity of f on T and Γ on $[0, 1]$, respectively. Assume that $\rho_f, \rho_r : [0, \infty) \rightarrow [0, \infty)$ are continuous and strictly monotone increasing functions so that*

$$\rho_f(0) = 0, \quad \rho_f(\delta) \geq \omega_f(\delta) \quad (\delta \in [0, \text{diam}(T)]), \quad \lim_{\delta \rightarrow \infty} \rho_f(\delta) = \infty \tag{5.5}$$

and

$$\rho_r(0) = 0, \quad \rho_r(\delta) \geq \omega_r(\delta) \quad (\delta \in [0, \tau]), \quad \lim_{\delta \rightarrow \infty} \rho_r(\delta) = \infty \tag{5.6}$$

hold, respectively. Furthermore assume that

- (a) $F(x, y)$ is continuous in $[a, 1] \times [0, \infty)$;
- (b) $x \geq a, F(x, y) = x \Leftrightarrow y = 0$;

(c) $F(x, y) < x$ ($x \in [a, 1], y > 0$);

(d) For $x > \xi$ ($x, \xi \in [a, 1]$) and $0 \leq y \leq x - \xi$, $F(x, y) \geq \xi$.

(e) $F(x, y)$ is strictly monotone increasing in x , and strictly monotone decreasing in y ;

Define $\varphi(t) = \rho_r^{-1}(\rho_f^{-1}(\|f(r(t))\|))$ ($t \in [a, 1]$). Let $t_0 = 1$ and assume that $\varphi(1) > 0$. Define

$$t_{i+1} = F(t_i, \varphi(t_i)) \quad (i = 0, 1, 2, \dots). \quad (5.7)$$

Then $\{t_i\}$ is a strictly monotone decreasing sequence that converges to ξ_{\max} if a root ξ of $\|f(r(t))\| = 0$ exists in $[a, 1]$. If no root exists, then the sequence $\{t_i\}$ leaves the interval $[a, 1]$ in a finite number of steps.

If Γ is a space-filling curve, then we clearly have the always convergence property. Butz [10] suggested using the Hilbert curve, while Hlawka [11] suggested using the Schoenberg curve.

If the selected curve Γ is not space-filling, the algorithm may fail to find a zero. However the space-filling functions used in practice are only approximations to the true ones, and do not have the space-filling property. Hence in practice we are forced to use approximate curves.

6. SELECTION OF CURVES

6.1. Space-filling curves. The first examples of space-filling functions were given by Peano in 2D and 3D and were followed by several other space-filling functions constructed by Hilbert, Lebesgue, Sierpinski, Schoenberg and many others (see, e.g. Singh [20], Sagan [21], Bader [22]). There are plenty of space-filling or Peano-type curves that are applied in a variety of fields (see, e.g. Strongin-Sergeyev [3], Zumbusch [4], Bebendorf [5], Sergeyev et al. [6]). The most often applied space-filling function is the Hilbert function (for definition, see, e.g. [21], Butz [7], [23], [3], [4], [6]).

Lemma 18. *The Hilbert mapping $r_H : [0, 1] \rightarrow [0, 1]^n$ is space-filling, nowhere differentiable and $\text{Lip}_K \mu$ with $K = 2\sqrt{n+3}$ and $\mu = 1/n$:*

$$\|r_H(s) - r_H(t)\| \leq K |s - t|^{1/n} \quad (s, t \in [0, 1]). \quad (6.1)$$

For a proof, see, e.g. [4] (p. 96). Other n -dimensional space-filling functions that are $\text{Lip} \frac{1}{n}$ are the Peano and Sierpiński curves (see [4] p. 101).

Buckley [24] proved that there exist 2D space-filling curves f that are $\text{Lip} \frac{1}{2}$, but no such curve is $\text{Lip} \mu$ for $\mu > 1/2$. Hence for $n = 2$, the Lipschitz/Hölder-exponent of the Hilbert curve is the best possible. However the estimate of Lipschitz constant $K = 2\sqrt{5} \approx 4.4721$ is not the sharpest result. Bauman [25] proved that $K = 2\sqrt{5}$ can be replaced by $K = \sqrt{6} = 2.4495$. For a more refined characterization of the smoothness properties of space-filling functions, see Jaffard-Nicolay [26].

Most of the space-filling functions are defined by a possibly recursive geometric process [21]. Any evaluation of the function at a point requires building up a good

approximation to the whole function. We however need only to estimate the function at certain points.

From this point of view, Schoenberg’s space filling-function [27], [28] is different, as it is defined by absolutely convergent series that can be evaluated at any point. Define function p as

$$p(t) = \begin{cases} 0, & 0 \leq t \leq 1/3 \\ 3t - 1, & 1/3 \leq t \leq 2/3 \\ 1, & 2/3 \leq t \leq 4/3 \\ 5 - 3t, & 4/3 \leq t \leq 5/3 \\ 0, & 5/3 \leq t \leq 2 \end{cases} \tag{6.2}$$

and extend it periodically by $p(t + 2) = p(t)$ ($t \in \mathbb{R}$). Note that $0 \leq p(t) \leq 1$ for any $t \in \mathbb{R}$. Also we have $|p(s) - p(t)| \leq 3|s - t|$ ($s, t \in [0, 2]$), which extends to $|p(s) - p(t)| \leq 3|s - t|$ ($s, t \geq 0$).

The two-dimensional space-filling curve of Schoenberg [27] is defined by

$$r_{\text{Sch}}(t) = [x(t), y(t)]^T \quad (t \in [0, 1]), \tag{6.3}$$

where

$$x(t) = \frac{1}{2} \sum_{k=0}^{\infty} \frac{p(3^{2k}t)}{2^k}, \quad y(t) = \frac{1}{2} \sum_{k=0}^{\infty} \frac{p(3^{2k+1}t)}{2^k}. \tag{6.4}$$

Steele [29] proved that Schoenberg’s 2D curve is Lipschitz α with $\alpha = \frac{1}{2 \log_2 3} \approx 0.31546$ (see also Jaffard-Nicolay [26]).

For general finite dimensional spaces Hlawka [11] extended Schoenberg’s functions [27], [28]. The n -dimensional Schoenberg space-filling curve $r : [0, 1] \rightarrow [0, 1]^n$ is defined by

$$r_j(t) = \sum_{k=0}^{\infty} \frac{1}{2^{k+1}} p(3^{nk+j-1}t) \quad (j = 1, \dots, n). \tag{6.5}$$

Using the proof of Steele [29] we estimate the Lipschitz exponent and also the Lipschitz constant.

Lemma 19. *The n -dimensional Schoenberg curve is $\text{Lip}_L \alpha$ with $\alpha = \frac{1}{\log_2 3^n}$ and Lipschitz constant $L \leq 3^{2n} / \sqrt{2}$.*

Proof. We can write

$$\begin{aligned} |r_j(s) - r_j(t)| &\leq \frac{1}{2} \sum_{k=0}^{\ell} \frac{|p(3^{nk+j-1}s) - p(3^{nk+j-1}t)|}{2^k} + \frac{1}{2} \sum_{k=\ell+1}^{\infty} \frac{2}{2^k} \\ &\leq \frac{3^j |s - t|}{2} \sum_{k=0}^{\ell} \left(\frac{3^n}{2}\right)^k + \frac{1}{2^{\ell+1}} \end{aligned}$$

$$= \frac{3^{n+j} |s - t|}{2(3^n - 2)} \left(\frac{3^n}{2}\right)^\ell + \frac{1}{2^{\ell+1}}$$

Select ℓ so that

$$-\frac{\log_2 |s - t|}{\log_2 3^n} < \ell \leq -\frac{\log_2 |s - t|}{\log_2 3^n} + 1.$$

Then

$$|r_j(s) - r_j(t)| \leq \frac{1}{2} \left(\frac{3^{2n+j}}{3^n - 2} + 1\right) |s - t|^{\frac{1}{\log_2 3^n}}$$

and

$$\|r(s) - r(t)\|_2^2 \leq \left[\frac{1}{4} \sum_{j=1}^n \left(\frac{3^{2n+j}}{3^n - 2} + 1\right)^2\right] |s - t|^{\frac{2}{\log_2 3^n}}. \tag{6.6}$$

A simple calculation yields the estimates for $n \geq 2$ and $1 \leq j \leq n$,

$$\frac{3^{2n+j}}{3^n - 2} + 1 \leq \frac{4}{3} 3^{n+j}$$

and

$$\frac{1}{4} \sum_{j=1}^n \left(\frac{3^{2n+j}}{3^n - 2} + 1\right)^2 \leq \frac{1}{2} 3^{2n} (3^{2n} - 1).$$

Hence we obtain the estimate

$$\|r(s) - r(t)\|_2 \leq \frac{3^{2n}}{\sqrt{2}} |s - t|^{\frac{1}{\log_2 3^n}}.$$

□

A direct substitution into formula (6.6) gives a somewhat better result. For example for $n = 2$ and $n = 3$, we obtain $L = 55.54$ (vs $3^4/\sqrt{2} = 57.276$) and $L = 417.95$ (vs. $3^6/\sqrt{2} = 515.48$, respectively. Note however that

$$\lim_{n \rightarrow \infty} \frac{\frac{1}{4} \sum_{j=1}^n \left(\frac{3^{2n+j}}{3^n - 2} + 1\right)^2}{\frac{1}{2} 3^{4n}} = \frac{9}{16}.$$

Note that the n -dimensional Lebesgue space-filling curve is also $\text{Lip}_{\frac{1}{\log_2 3^n}}$ (see [4] p.108). Both curves are based on the Cantor set and closely related (see, e.g. [27], [4], [26], [30]).

6.2. Alpha-dense curves. The idea of α -dense curves comes from the Alienor method of optimization and it is due to Cherruault and Guillez (see, e.g. [12], [13]). The theory and application of α -dense curves is summarized in the monograph by Cherruault and Mora [14].

Definition 20. Let $I = [a, b] \subset \mathbb{R}$ be an interval and $B = \times_{i=1}^n [a_i, b_i] \subset \mathbb{R}^n$ be a rectangle. The map $x : I \rightarrow B$ is an α -dense curve, if for every $x \in B$, there exists a $t \in I$ such that $\|x(t) - x\| \leq \alpha$.

There are many α -dense curves (see, e.g. [14]). Particularly we mention two curves:

$$x_i(t) = \frac{1}{2}(1 - \cos(\omega_i 2\pi t)), \quad i = 1, \dots, n \tag{6.7}$$

by Cherruault and

$$x_1(t) = t, \tag{6.8}$$

$$x_i(t) = \frac{1}{2}(1 - \cos(\sigma^{i-1} 2\pi t)), \quad i = 2, \dots, n \tag{6.9}$$

by Mora.

Note that approximations of space-filling curves are also α -dense curves for some α . For 2D, the n th approximating polygon of the Hilbert curve is α -dense with $\alpha \leq \sqrt{2}/2^{2n}$, while for 3D, $\alpha \leq \sqrt{3}/2^{3n}$ (see, e.g. Sagan [21]).

Mora [31] gave a characterization of the connection between space-filling curves and α -dense curves.

The α -dense curves are not space-filling functions. Hence for any small $\alpha > 0$, the solver can fail. This may happen, however, with the approximate space-filling functions as well.

However it is easy to evaluate/compute α -dense curves and they may be smooth enough. It is a disadvantage that the known constructions are such that their Lipschitz constant grows to infinity, while $\alpha \rightarrow 0$.

We use the following class of α -dense curves.

Assume that $f_i : [0, 1] \rightarrow [0, 1]$ ($i = 1, \dots, n$) are continuous functions such that for each $i = 1, 2, \dots, n$, $\text{Range}(f_i) = [0, 1]$ and f_i is periodically extended to \mathbb{R} with period 1. Also assume that there exist constants $L_i > 0$ and $0 < \beta_i \leq 1$ such that

$$|f_i(x) - f_i(y)| \leq L_i |x - y|^{\beta_i} \quad (x, y \in [0, 1]) \tag{6.10}$$

hold for $i = 1, 2, \dots, n$. Define the curve $x : [0, 1] \rightarrow [0, 1]^n$ by

$$x_i(t) = f_i(\omega_i t), \quad i = 1, \dots, n, \tag{6.11}$$

where ω_i 's are positive integers such that $\omega_{i+1} = \sigma_i \omega_i$ with $\sigma_i \in \mathbb{N}$ and $\sigma_i \geq 1$.

It is clear that $x_i(t)$ is periodic with period $T_i = 1/\omega_i$. Note that $T_i = \sigma_i T_{i+1}$.

Lemma 21. *The density of curve (6.11) is*

$$\alpha \leq \left(\sum_{i=1}^n \frac{L_i^2}{(\sigma_i^{\beta_i})^2} \right)^{1/2} \tag{6.12}$$

Proof. Choose any point $a \in [0, 1]^n$. We estimate the distance between a and the curve $x(t)$. There exists $t_1 \in \left[0, \frac{1}{\omega_1}\right]$ such that $x_1(t_1) = a_1$. There is a unique integer

$0 \leq k_1 \leq \sigma_1 - 1$ such that $t_1 \in I_1 = \left[\frac{k_1}{\omega_2}, \frac{1+k_1}{\omega_2} \right]$. Note that for any $t \in I_1$,

$$|x_1(t) - a_1| = |f_1(\omega_1 t) - f_1(\omega_1 t_1)| \leq L_1 (\omega_1 |t - t_1|)^{\beta_1} \leq \frac{L_1}{\sigma_1^{\beta_1}}.$$

There exists $t_2 \in \left[0, \frac{1}{\omega_2} \right]$ such that $x_2(t_2) = a_2$. There is a unique integer $0 \leq k_2 \leq \sigma_2 - 1$ such that $t_2 \in \left[\frac{k_2}{\omega_3}, \frac{1+k_2}{\omega_3} \right]$. For any $t \in \left[\frac{k_2}{\omega_3}, \frac{1+k_2}{\omega_3} \right]$,

$$|x_2(t) - a_2| = |f_2(\omega_2 t) - f_2(\omega_2 t_2)| \leq L_2 (\omega_2 |t - t_2|)^{\beta_2} \leq \frac{L_2}{\sigma_2^{\beta_2}}.$$

Define $I_2 = \left[\frac{k_1}{\omega_2} + \frac{k_2}{\omega_3}, \frac{k_1}{\omega_2} + \frac{1+k_2}{\omega_3} \right]$. Since $\frac{1+k_2}{\omega_3} \leq \frac{1}{\omega_2}$, $I_2 \subset I_1$. The periodicity assumption implies that for $t \in I_2$,

$$|x_2(t) - a_2| \leq L_2 (\omega_2 |t - t_2|)^{\beta_2} \leq \frac{L_2}{\sigma_2^{\beta_2}}$$

also holds. Assume that for $j \geq 2$, we have the interval

$$I_j = \left[\sum_{i=1}^j \frac{k_i}{\omega_{i+1}}, \frac{1}{\omega_{j+1}} + \sum_{i=1}^j \frac{k_i}{\omega_{i+1}} \right] \subset I_{j-1}$$

such that for $t \in I_j$, $|x_j(t) - a_j| \leq L_j / \sigma_j^{\beta_j}$ holds. There exists $t_{j+1} \in \left[0, \frac{1}{\omega_{j+1}} \right]$ such that $x_{j+1}(t_{j+1}) = a_{j+1}$. There is a unique integer $0 \leq k_{j+1} \leq \sigma_{j+1} - 1$ such that $t_{j+1} \in \left[\frac{k_{j+1}}{\omega_{j+2}}, \frac{1+k_{j+1}}{\omega_{j+2}} \right]$. For any $t \in \left[\frac{k_{j+1}}{\omega_{j+2}}, \frac{1+k_{j+1}}{\omega_{j+2}} \right]$,

$$|x_{j+1}(t) - a_{j+1}| \leq L_{j+1} (\omega_{j+1} |t - t_{j+1}|)^{\beta_{j+1}} \leq \frac{L_{j+1}}{\sigma_{j+1}^{\beta_{j+1}}}.$$

Define

$$I_{j+1} = \left[\sum_{i=1}^{j+1} \frac{k_i}{\omega_{i+1}}, \frac{1}{\omega_{j+2}} + \sum_{i=1}^{j+1} \frac{k_i}{\omega_{i+1}} \right].$$

Since $\frac{1+k_{j+1}}{\omega_{j+2}} \leq \frac{1}{\omega_{j+1}}$, $I_{j+1} \subset I_j$. By the periodicity of $x_{j+1}(t)$, for $t \in I_{j+1}$,

$$|x_{j+1}(t) - a_{j+1}| \leq L_{j+1} (\omega_{j+1} |t - t_{j+1}|)^{\beta_{j+1}} \leq L_{j+1} / \sigma_{j+1}^{\beta_{j+1}}.$$

Thus we have a sequence of intervals $I_n \subset I_{n-1} \subset \dots \subset I_1$ such that for any $t \in I_n$,

$$|x_j(t) - a_j| \leq \frac{L_j}{\sigma_j^{\beta_j}} \quad (j = 1, 2, \dots, n).$$

Hence the density of $x(t)$ is estimated by

$$\|x(t) - a\|_2^2 \leq \sum_{i=1}^n \frac{L_i^2}{(\sigma_i^{\beta_i})^2}. \quad (6.13)$$

□

Remark 22. Since σ_i is specified by $\omega_{i+1} = \sigma_i \omega_i$ for $i = 1, \dots, n - 1$, $\sigma_n \geq 1$ is our choice. If $L = L_j$, $\sigma_i = \sigma > 1$ and $\beta_i = 1$ ($i = 1, \dots, n - 1$), then we can select $\sigma_n = \sigma$ and so the density estimate becomes

$$\|x(t) - a\|_2 \leq \frac{\sqrt{n}L}{\sigma}. \tag{6.14}$$

If $f_1(t) = t$, $\omega_1 = 1$ and $L = L_j$, $\sigma_i = \sigma > 1$, $\beta_i = 1$ ($i = 2, \dots, n$), then

$$\|x(t) - a\|_2 \leq \frac{\sqrt{1 + (n - 1)L^2}}{\sigma}. \tag{6.15}$$

Remark 23. It is clear from the proof that for $f_1(t) = t$, we do not need its periodic extension to \mathbb{R} . It also follows that for $t_1 \neq t_2$, $x(t_1) \neq x(t_2)$, unlike in the case of space-filling functions.

If f_i is periodically extended to \mathbb{R} , then its Lipschitz constant may change.

Lemma 24. If f_i is continuously and periodically extended to \mathbb{R} , then

$$|f_i(s) - f_i(t)| \leq 2^{1-\beta_i} L_i |s - t|^{\beta_i} \quad (s, t \geq 0). \tag{6.16}$$

Proof. Assume that $\beta_i = 1$. If $s, t \in [k, k + 1]$ ($k \geq 0$ integer), then

$$|f_i(s) - f_i(t)| = |f_i(s - k) - f_i(t - k)| \leq L_i |s - t|,$$

which clearly extends to \mathbb{R} . Assume that $\beta_i < 1$. If $s, t \in [k, k + 1]$ ($k \geq 0$ integer), then

$$|f_i(s) - f_i(t)| = |f_i(s - k) - f_i(t - k)| \leq L_i |s - t|^{\beta_i}.$$

If, say $s > t$ and $s \in [k, k + 1]$, $t \in [j, j + 1]$ and $k \geq j + 1$, then by the periodicity and the continuity

$$|f_i(s) - f_i(t)| = |f_i(s) - f_i(k) + f_i(j + 1) - f_i(t)| \leq L_i \left(|s - k|^{\beta_i} + |j + 1 - t|^{\beta_i} \right).$$

Since x^{β_i} is concave, the Jensen inequality implies that

$$|s - k|^{\beta_i} + |j + 1 - t|^{\beta_i} \leq 2 \left(\frac{s - k + j + 1 - t}{2} \right)^{\beta_i} \leq 2 \left(\frac{s - t}{2} \right)^{\beta_i}$$

and

$$|f_i(s) - f_i(t)| \leq 2^{1-\beta_i} L_i |s - t|^{\beta_i}.$$

□

Corollary 25. Curve (6.11) satisfies the Lipschitz condition

$$\|x(t) - x(s)\|_2 \leq \left[\sum_{i=1}^n \left(2^{1-\beta_i} L_i \omega_i^{\beta_i} |s - t|^{\beta_i} \right)^2 \right]^{1/2} \quad (s, t \in [0, 1]). \tag{6.17}$$

Particularly, if $L = L_j$, $\sigma_i = \sigma > 1$ and $\beta_i = 1$ ($i = 1, \dots, n$), then

$$\|x(t) - x(s)\|_2 \leq \omega_1 L \left(\frac{\sigma^{2n} - 1}{\sigma^2 - 1} \right)^{1/2} |s - t| \quad (s, t \in [0, 1]). \tag{6.18}$$

If $f_1(t) = t$, $\omega_1 = 1$ and $L = L_j$, $\sigma_i = \sigma > 1$, $\beta_i = 1$ ($i = 2, \dots, n$), then

$$\|x(t) - x(s)\|_2 \leq \left(1 + L^2 \frac{\sigma^{2n} - \sigma^2}{\sigma^2 - 1}\right)^{1/2} |s - t| \quad (s, t \in [0, 1]). \quad (6.19)$$

7. COMPARISON WITH KNOWN METHODS

The use of space filling functions for solving nonlinear equations first appeared in Butz [10] and later in Hlawka [11]. In the context of the theory of uniform distributions Hlawka suggested a quadrature related method that uses Schoenberg's space-filling curve and is different from the present approach.

Butz [10] investigated the following problem

$$f(x) = 0 \quad (f : X \subset [0, 1]^n \rightarrow \mathbb{R}^N), \quad (7.1)$$

where X is nonempty and closed. Let $h : [0, 1] \rightarrow [0, 1]^n$ be a space-filling curve that satisfies the Lipschitz condition

$$\|h(t) - h(t + \Delta)\| \leq B(\Delta t, t) \leq M\Delta^{1/n} \quad (t, t + \Delta t \in [0, 1], \Delta t \geq 0), \quad (7.2)$$

where B is a nondecreasing function of Δt , and $B = 0$ if and only if $\Delta t = 0$.

Define

$$\bar{t}(X) = \min \{t : t \in [0, 1], h(t) \in X\} \quad (7.3)$$

and $\bar{x}(X) = h(\bar{t}(X))$.

Theorem 26. (Butz [10]) Assume that $\omega(x)$ is some function and $\gamma(x)$ is some continuous function such that for all $x \in [0, 1]^n$,

$$\omega(x) \geq \gamma(x) \geq 0 \quad (7.4)$$

with strict inequality on the right if $x \notin X$ and, if X is not empty,

$$\omega(x) \leq \|x - x'\| \quad (7.5)$$

for every $x' \in X$. Let $\{t^i, x^i\}$ be a sequence, where $t^0 = 0$ and $x^i = h(t^i)$ such that

$$t^{i+1} = \min \{1, t^i + \Delta t^i\}, \quad (7.6)$$

where $\Delta t^i \geq 0$ is such that

$$\omega(x^i) \geq B(\Delta t^i, t^i) \geq \min \left\{ \kappa, \frac{1}{2} \omega(x^i) \right\}, \quad (7.7)$$

where $\kappa > 0$ is some constant, with strict inequality on the left if $\omega(x^i) > 0$ ($x^i \notin X$). Then if X is not empty, $t^i \rightarrow \bar{t}(X)$ and $x^i \rightarrow \bar{x}(X)$ with $t^{i+1} > t^i$ for all i (unless $h(0) \in X$). If X is empty, $t^i = 1$ for finite i with $\omega(h(1)) > 0$.

Butz applies this result and Hilbert's space-filling function to solve equation

$$f(x) = 0 \quad (f : [0, 1]^n \rightarrow \mathbb{R}^N),$$

when X is the solution set, and it is assumed that for any solution $x^* \in X$,

$$|f_k(x)| \leq K_k \|x - x^*\| \quad (x \in [0, 1]^n, k = 1, \dots, N) \quad (7.8)$$

holds with positive constants K_k . Using

$$\omega(x) = \max_{1 \leq k \leq N} \frac{|f_k(x)|}{K_k} \quad (\leq \|x - x^*\|) \tag{7.9}$$

his algorithm (7.6) takes the form

$$t^{i+1} = t^i + \left(\frac{\omega(x^i)}{M} \right)^n \tag{7.10}$$

(for this see [10], p. 379).

Since $f_k(x) = 0 \Leftrightarrow f_k(x)/K_k = 0$, we can assume that equation $f(x) = 0$ is such that every $K_k = 1$. Then $\omega(x) = \max_k |f_k(x)| = \|f(x)\|_\infty$. Here $\rho_r(\delta) = M\delta^{1/n}$ and $\rho_f(\delta) = \delta$, $\rho_r^{-1}(\delta) = \left(\frac{\delta}{M}\right)^n$ and $\rho_f^{-1}(\delta) = \delta$. Hence

$$\rho_r^1(\rho_f^{-1}(\delta)) = \rho_r^{-1}(\delta) = \left(\frac{\delta}{M}\right)^n,$$

and

$$\rho_r^1(\rho_f^{-1}(\|f(r(t))\|)) = \left(\frac{\|f(r(t))\|}{M}\right)^n$$

Hence formula (7.10) clearly corresponds to iteration function (i-2) with $P = 1$.

8. NUMERICAL EXPERIMENTS

The purpose of testing is only to get some view about the feasibility and behavior of the suggested algorithms. It is clear that space-filling curves have no finite arclength and so the computation time to get the first zero on the curve (if it exists) can be arbitrarily high. The smooth α -dense curves have finite arclength that increases to infinity when $\alpha \rightarrow 0$.

8.1. The tested algorithms and curves. 1. Targonszky's extended formula ((d-1))

$$F(x, y) = \frac{x}{1 + y}.$$

2. Formula (d-2) with $P = 1$:

$$F(x, y) = x - y.$$

This formula corresponds to formula (7.10) of Butz.

3. Formula (d-3) with fixed parameters

$$F(x, y) = \frac{x - 0.5y}{1 + 0.5y}.$$

4. Formula (d-4) with $U(x) = (x + 2)^2$:

$$F(x, y) = \sqrt{(x + 2)^2 - y} - 2.$$

The tested curves were the Hilbert and Schoenberg space-filling-curves and the following α -dense curves: Cherruault curve with $\omega_i = \sigma^i$, Mora's curve, and three other curves of the form

$$x_1(t) = t$$

$$x_i(t) = f(\sigma^{i-1}t), \quad i = 2, \dots, n,$$

with $f(x) = p(2x)$ (Schoenberg's $p(x)$, identified as Schoenberg- α), $f(x) = 1 - |2x - 1|$ (identified as ADC1) and

$$f(x) = \begin{cases} \frac{3}{2}x + \frac{1}{2}, & 0 \leq x \leq 1/3 \\ 2 - 3x, & 1/3 \leq x \leq 2/3 \\ \frac{3}{2}x - 1, & 2/3 \leq x \leq 1 \end{cases}$$

(identified as ADC2).

For the computation of the 2D Hilbert curve we used the algorithm on page 52 of Bader [22] with $depth = 50$, that computes the points of the curve with an error proportional to $2^{-50} = 8.8818 \times 10^{-16}$. For 3D, we used a recursively generated approximate Hilbert curve with 2097152 points and density $\alpha \approx 0.0078$. The error of the used Schoenberg curve approximation is also proportional to $2^{-50} = 8.8818 \times 10^{-16}$.

The problem of exit or termination condition is well-known both from practical and theoretical points of view (see, e.g. Rice [32], Delahaye [33]). We set generally the condition

$$\|f(r(t_i))\| \leq tol \vee i = itmax,$$

which is not the most sophisticated exit condition.

It is reasonable to have the practical lower bound $\varphi(t_i) \geq \varepsilon_{machine}$ on the iterates t_i . For $f \in Lip_{L_f}\beta$ and $r \in Lip_{L_r}\mu$, this holds if and only if $\|f(r(t_i))\| \geq L_f L_r^\beta \varepsilon_{machine}^{\mu\beta}$. Hence the tol parameter has the lower bound $tol \geq L_f L_r^\beta \varepsilon_{machine}^{\mu\beta}$. Since each of the tested problems has $\beta = 1$, the lower bound changes to $tol \geq L_f L_r \varepsilon_{machine}^\mu$.

In double precision floating point arithmetic $\varepsilon_{machine} \approx 2.2204e - 016$. The following table indicates the values of constant $L_r \varepsilon_{machine}^\mu$ of the lower bound on tol .

curve	n=2	n=3
Hilbert	6.6640e - 008	2.9666e - 005
Schoenberg	6.6042e - 004	2.6310e - 001
Mora	6.9757e-013	6.9757e-010
Schoenberg- α	1.3323e-012	1.3323e-009
Cherruault	6.9757e-010	6.9757e-007
ADC1	4.4409e-013	4.4409e-010
ADC2	6.6613e-013	6.6613e-010

Note that the α -dense curve values are computed for $\sigma = 1000$ and these lower bound constants are better than those of the space-filling curves.

Another reasonable bound on the tolerance is the following. If there is a zero x^* of f and $x(t)$ is α -dense, then there must be a point t' that $\|x(t) - x^*\| \leq \alpha$. Hence if $f \in \text{Lip}_{L_f}\beta$, then

$$\|f(r(t'))\| \leq L_f \|r(t') - x^*\| \leq L_f \alpha.$$

Hence $tol \leq L_f \alpha$ seems to be a practical restriction because tol must be definitely less than $L_f \alpha$ to sort out the possible zero.

In comparison we give the density estimates of these curves as well ($\sigma = 1000$).

curve	n=2	n=3
Mora	0.0033	0.0046
Schoenberg- α	0.0061	0.0085
Cherruault	0.0044	0.0054
ADC1	0.0022	0.0030
ADC2	0.0032	0.0044

For the 2D test problems and $\sigma = 1000$, the bound $L_f \alpha$ is proportional to $1e-2$ except for the Powell problem No. 7 the Lipschitz constant of which is $1.7e+5$. In the case of 3D problems the smallest bounds are proportional also to $1e-2$. Hence the selection of $tol = 1e - 2$ seems appropriate (for similar tolerance, see also Butz [10]).

8.2. Test results. We tested the four methods on each curve and on each 2D test problems with $tol = 1e - 2$ and $itmax = 1e + 6$. The α -dense curves used the parameter $\sigma = 1000$. The test was carried out on a PC with Intel I7 processor and Matlab R2011b. A summary of the obtained results (average iteration/average precision) is contained in the following two tables, the first of which contains the best methods versus curves, while the second contains the best curves versus methods.

2D curve	best in iterations		best in precision	
	method	iteration	method	precision
Hilbert	(d-2)	1.0848e+004	(d-2)	3.1479e-001
Schoenberg	(d-1)	1e+6	(d-1)	9.0372e-001
Mora	(d-2)	1.4541e+004	(d-3)	3.1661e-001
Schoenberg- α	(d-2)	1.2754e+005	(d-1)	3.0483e-001
Cherruault- α	(d-2)	4.7817e+004	(d-3)	1.9037e-001
ADC1	(d-2)	1.1923e+004	(d-4)	1.9774e-001
ADC2	(d-2)	1.6164e+004	(d-4)	3.1686e-001

method	best in iterations		best in precision	
	curve	iteration	curve	precision
(d-1)	ADC2	3.7099e+004	Cherruault	1.9058e-001
(d-2)	Hilbert	1.0848e+004	Cherruault	1.9064e-001
(d-3)	Hilbert	1.4002e+004	Cherruault	1.9037e-001
(d-4)	ADC1	4.5867e+004	Cherruault	1.9065e-001

In fact, none of the methods solved test problem No. 7 and Schoenberg's space filling curve did perform poorly. On average, the other method-curve combinations performed acceptably. For 3D the situation became different. The next table contains the results (average iteration/average precision) of 3D test problems. Here we set $itmax = 1e + 8$.

curve	best in iterations		best in precision	
	method	iteration	method	precision
Mora	(d-2)	2.7581e+006	(d-3)	2.5842e+000
Schoenberg- α	(d-2)	1.1053e+007	(d-4)	5.1233e-001
Cherruault- α	(d-4)	4.1809e+006	(d-4)	1.5270e-001
ADC1	(d-2)	2.0374e+006	(d-1)	2.6802e+000
ADC2	(d-2)	7.1008e+006	(d-4)	6.0737e-002

The performances of the 3D Hilbert and Schoenberg curves were so poor that the results are not included in the table. The 3D Hilbert curve performed better; however, the achieved precision was limited due to the lack of computer memory and a more efficient 3D Hilbert-curve program that computes the coordinate values directly. It is seen that α -dense curves performed better and the best methods stopped under the exit condition $\|f(r(t_i))\| \leq tol$. The arguments of the previous subsection indicate that smaller tol would require smaller $\varepsilon_{machine}$, which can be obtained with multiple precision arithmetic.

In general, we can say that the proposed methods are working and feasible, although they are more expensive than the local methods. For higher dimension they require the use of multiple precision and more efficient curve computation other than those of [34], [35] and references cited therein.

9. APPENDIX

The test problems are taken from the Estonian test problem collection [36]. Whenever it is available we give the original source as well.

No. 1 (Yamamoto [37])

$$f_1(x) = x_1^2 + x_2^3,$$

$$f_2(x) = x_2^2$$

No. 2 (Powell [38])

$$f_1(x) = x_1 - 1,$$

$$f_2(x) = x_1x_2 - 1.$$

No. 3 (Yamamoto [37])

$$f_1(x) = x_1^3 + x_1x_2,$$

$$f_2(x) = x_2 + x_2^2.$$

No. 4 (Fuchs)

$$f_1(x) = x_1^2 - x_2^2 - 1,$$

$$f_2(x) = x_1^2 + x_2^2 - 4.$$

No. 5 (Brezinski [39])

$$f_1(x) = 0.5x_2^2 - 0.5,$$

$$f_2(x) = -x_2 + \sin(x_1) + \sin(x_2 - 1) + 1.$$

No. 6 (Bartish)

$$f_1(x) = x_1^2 + x_2^2 - 1,$$

$$f_2(x) = 0.75x_1^3 - x_2.$$

No.7 (Powell [38])

$$f_1(x) = 10000x_1x_2 - 1,$$

$$f_2(x) = \exp(-x_1) + \exp(-x_2) - 1.0001.$$

No. 8 (Boggs [40])

$$f_1(x) = x_1^2 - x_2 + 1,$$

$$f_2(x) = x_1 - \cos(0.5\pi x_2).$$

No. 9 (Brezinski [39])

$$f_1(x) = -x_1 + 0.5x_2^2 - 1.5,$$

$$f_2(x) = -x_2 + 0.605 \exp(1 - x_1^2) + 0.395.$$

No. 10 (Allgower-Georg [41])

$$f_1(x) = (x_1 - x_2^2)(x_1 - \sin(x_2)),$$

$$f_2(x) = (\cos(x_2) - x_1)(x_2 - \cos(x_1)).$$

No.11 (Yamamoto [37])

$$f_1(x) = x_1 + x_2 + x_3 - 1,$$

$$f_2(x) = 0.2x_1^3 + 0.5x_2^2 - x_3 + 0.5x_3^2 + 0.5,$$

$$f_3(x) = x_1 + x_2 + 0.5x_3^2 - 0.5.$$

No. 12 (Allgower-Georg [41])

$$f_1(x) = x_1^2 + 2x_2^2 - 4,$$

$$f_2(x) = x_1^2 + x_2^2 + x_3 - 8,$$

$$f_3(x) = (x_1 - 1)^2 + (2x_2 - \sqrt{2})^2 + (x_3 - 5)^2 - 4.$$

No. 13 (Brown-Conte)

$$\begin{aligned}f_1(x) &= 3x_1 + x_2 + 2x_3^2 - 3, \\f_2(x) &= -3x_1 + 5x_2^2 + 2x_1x_3 - 1, \\f_3(x) &= 25x_1x_2 + 20x_3 + 12.\end{aligned}$$

No. 14 (Babitsch)

$$\begin{aligned}f_1(x) &= x_1x_2 + x_2x_3 + x_1x_3 - 47, \\f_2(x) &= x_1^1 + x_2^2 - x_3^2, \\f_3(x) &= (x_3 - x_1)(x_3 - x_2) - 2.\end{aligned}$$

REFERENCES

1. TARGONSKY, G.: An always convergent iteration process. *Acta Mathematica Hungarica*, **4**(1-2), (1953), 119–126.
2. BEAUZAMY, B.: On the paths to the zeros of a polynomial. *J. of Inequal. & Appl.*, **4**, (1999), 83–89.
3. SERGEYEV, Y. D. and STRONGIN, R. G.: *Global Optimization with Non-Convex Constraints*. Springer, 2000.
4. ZUMBUSCH, G.: *Parallel Multilevel Methods: Adaptive Mesh Refinement and Loadbalancing*. B.G. Teubner, Stuttgart-Leipzig-Wiesbaden, 2003. ISBN: 3-519-00451-8.
5. BEBENDORF, M.: *Hierarchical Matrices*. Springer, 2008.
6. SERGEYEV, Y. D., STRONGIN, R. G., and LERA, D.: *Introduction to Global Optimization Exploiting Space-Filling Curves*. Springer, 2013.
7. BUTZ, A. R.: Space filling curves and mathematical programming. *Information and Control*, **12**, (1968), 314–330.
8. BUTZ, A. R.: Convergence with Hilbert's space filling curve. *Journal of Computer and System Sciences*, **3**, (1969), 128–146.
9. STRONGIN, R. G.: On the convergence of an algorithm for finding a global extremum. *Engineering Cybernetics*, **11**(4), (1973), 549–555.
10. BUTZ, A. R.: Solutions of nonlinear equations with space filling curves. *Journal of Mathematical Analysis and Applications*, **37**, (1972), 451–383.
11. HLAWKA, E.: Über eine Klasse von Näherungspolygonen zur Peanokurve. *Journal of Number Theory*, **43**, (1993), 93–108.
12. CHERRUAULT, Y.: *Mathematical Modelling in Biomedicine*. D. Reidel Publishing Company, Dordrecht, Holland, 1986.
13. GUILLEZ, A.: Alienor, fractal algorithm for multivariable problems. *Mathl Comput. Modelling*, **14**, (1990), 245–247.
14. CHERRUAULT, Y. and MORA, G.: *Optimisation Globale. Théorie des courbes α -denses*. Economica, Paris, 2005. ISBN 2-7178-5065-1.
15. EFIMOV, A. V.: Linear methods of approximating continuous periodic functions. *Mat. Sb. (N.S.)*, **54**(96), (1961), 51–90. (in Russian).

16. KOLODII, I. M. AND KHIL'DEBRAND, F.: Some properties of the modulus of continuity. *Mat. Zametki*, **9**(5), (1971), 495–500. Also in *Mathematical Notes*, **9**(5), (1971), 285–288.
17. GALÁNTAI, A. and ABAFFY, J.: Always convergent iteration methods for nonlinear equations of Lipschitz functions. *Numer. Algor.*, **69**, (2015), 443–453. DOI 10.1007/s11075-014-9905-1.
18. ABAFFY, J. and FORGÓ, F.: Globally convergent algorithm for solving nonlinear equations. *J. Optim. Theory App.*, **77**, (1993), 291–304.
19. PIETRUS, A.: A globally convergent method for solving nonlinear equations without the differentiability condition. *Numerical Algorithms*, **13**, (1996), 60–76.
20. SINGH, A. N.: The theory and construction of non-differentiable functions. *Lucknow University Studies, Lucknow India*, **No. I**.
21. SAGAN, H.: *Space-filling Curves*. Springer, 1994.
22. BADER, M.: *Space-Filling Curves An Introduction with Applications in Scientific Computing*. Springer, 2013.
23. BUTZ, A. R.: Alternative algorithms for Hilbert's space-filling curve. *IEEE Transactions on Computers*, pp. 424–426.
24. BUCKLEY, S.: Space-filling curves and related functions. *Irish Mathematical Society Bulletin*, **36**, (1996), 9–18.
25. BAUMAN, K. E.: The dilation factor of the Peano-Hilbert curve. *Mathematical Notes*, **80**(5), (2006), 609–620.
26. JAFFARD, S. and NICOLAY, S.: Pointwise smoothness of space-filling functions. *Applied and Computational Harmonic Analysis*, **26**, (2009), 181–199.
27. SCHOENBERG, I. J.: On the Peano curve of Lebesgue. *Bulletin of American Mathematical Society*, **44**, (1938), 519.
28. SCHOENBERG, I. J.: *Mathematical Time Exposures*. The Mathematical Association of America, 1994.
29. STEELE, J. M.: *Seedlings in the theory of shortest paths*. in GRIMMETT, G. and WELSH, D. (eds): *Disorder in Physical Systems: A volume in Honor of J. M. Hammersley*. Cambridge University Press, London, 1990, pp. 277–306.
30. TAN, Y.: The construction of Lebesgue space-filling curve. *Southeast Asian Bulletin of Mathematics*, **36**, (2012), 883–890.
31. MORA, G.: The Peano curves as limit of α -dense curves. *Rev. R. Acad. Cien. Serie A. Mat.*, **99**(1), (2005), 23–28.
32. RICE, J. E.: *Numerical Methods*. McGraw-Hill, 1983.
33. DELAHAYE, J. P.: *Sequence Transformations*. Springer, 1988.
34. BREINHOLT, G. and SCHIERZ, C.: Algorithm 781: Generating Hilbert's space-filling curve by recursion. *ACM Transactions on Mathematical Software*, **24**(2), (1998), 184–189.
35. JIN, G. and MELLOR-CRUMLEY, J.: SFCGen: A framework for efficient generation of multi-dimensional space-filling curves by recursion. *ACM Transactions on Mathematical Software*, **31**(1), (2005), 120–148.

36. ROOSE, A., KULLA, V., LOMP, M. and MERESSO, T. (eds): *Test Examples of Systems on Nonlinear Equations, Version 3-90*. Estonian Software and Computer Service Company, Tallinn, 1990.
37. YAMAMOTO, N.: Newton's method for singular problems and its applications to boundary value problems. *J. Math. Tokushima Univ.*, **17**, (1983), 27–88.
38. POWELL, M. J. D.: *A FORTRAN Subroutine for solving systems of nonlinear algebraic equations*. in RABINOWITZ, P. (ed.): *Numerical Methods for Nonlinear Algebraic Equations*. Gordon and Breach Science Publisher, 1970, pp. 115–161.
39. BREZINSKI, C.: *Algorithmes d'accélération de la convergence*. Étude numérique. Editions Technip. Paris, 1978. ISBN 2-7108-0341-0.
40. BOGGS, P. T.: The solution of nonlinear systems of equations by a-stable integration techniques. *SIAM Journal on Numerical Analysis*, **8**(4), (1999), 767–785.
41. ALLGOWER, E. L. and GEORG, K.: *Relationships between Deflation and Global Methods in the Problem of Approximating Additional Zeros of a System of Nonlinear Equations*, in EAVES, B. C., GOULD, F. J., PEITGEN, H. O. and TODD, M. J. (eds): *Homotopy Methods and Global Convergence*. Plenum Press, New York, 1983. pp. 31–42.

PORTABLE TENT STRUCTURE DESIGNS FOR FLOOD PROTECTION

RÓBERT NAGY AND ZSOLT GÁSPÁR

Department of Structural Mechanics, Faculty of Civil Engineering
Budapest University of Technology and Economics
Műgyetem rkp. 3, 1111 Budapest, Hungary
robert.nagy@mail.bme.hu, gaspar@ep-mech.me.bme.hu

[Received: July 22, 2015, Accepted: September 30, 2015]

*Dedicated to Professor Barna Szabó on the occasion of his eightieth birthday
and to Professor Imre Kozák on the occasion of his eighty-fifth birthday*

Abstract. In this paper, we present two simple arrangements of portable tent structures for flood protection. In the first, an inflated cylinder lifts the top of the textile as the water level rises, while in the second the textile supporting the water pressure of the tide is hung on a steel framework and is filled with water previously. We give a numerical solution for the nonlinear system of equations of the compatibility and equilibrium conditions, and also present a complete analytic solution to the boundary value problem of the shape of an inextensible, weightless, prismatic textile, similar to the sessile drop problem. After discussing the mechanical behavior of the structures, different geometries capable of withstanding a certain water height are determined by a software developed for this specific purpose enabling the design for optimum. Furthermore, the basic rules of thumb are also formulated, aiding the preliminary conceptual design.

Mathematical Subject Classification: 65H05, 65B99

Keywords: Portable tent, flood protection, sessile drop, elastica, nonlinear pendulum, analytic solution

1. INTRODUCTION

Due to climate change, peak water levels more and more often exceed the height of the existing artificial embankment dams, causing ever increasing difficulties in flood-prone, inhabited areas near regulated rivers. Since the most common current emergency measures involve laying sandbags thus requiring considerable manpower, new methods are desired. In the first two chapters we present two possible alternatives, being fast and easy not only to transport but to construct as well, while in the last chapter we summarize the parametric representation of the directrix shape of a weightless, inextensible, prismatic membrane loaded by static water pressure, and we also derive the closed form equation of the area between the curve and an arbitrary vertical line. These formulations involve computationally burdensome elliptic

functions and their inverses; therefore, solving directly the governing boundary value problem by a numerical algorithm is also a good alternative.

2. FIRST ARRANGEMENT

The international Inflater project [1], managed by the MFKK Invention and Research Center and funded by the EU 7th Framework Programme, aimed to develop novel, affordable mobile flood defense systems. One of the many possibilities presented there involves a self-erecting textile. As participants, we developed a computer program capable of determining the static and geometric properties of the structure [2]. The detailed description of the algorithm and the analysis of the structural behavior are given in this section.

2.1. Geometry. This portable structure, mounted on the vertical crown of the existing embankment dam, solely consists of tensile elements. The first component is an inflated cylinder of radius r with diaphragms dividing its length into several cells and an additional active monitoring system for over-pressure control. The second is a sheet of impermeable textile skirt attached to a generatrix of the cylinder. The third component involves several tie-backs of length l welded to the same generatrix at equal distances along the length of the dam. The latter two are anchored to the foundation, a common fixed point on the horizontal crown of the embankment dam. A representative equilibrium cross-section is depicted in Fig. 1. We describe the setup in the x-y coordinate system. The main input parameters of the structure geometry are the BCDA textile section length (l_{BCDA}), the AB tie-back length (l_{AB}), the inflated cylinder radius (r), and the supported water level above crown level (h).

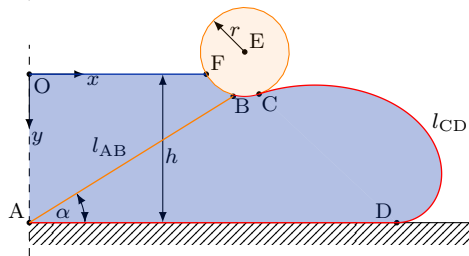


Figure 1. Cross-section of the 1st arrangement

2.2. Behavior of the structure. Initially the structure lies on the ground and is erected as the floating cylinder filled with air lifts the top of the textile with the rising water level, while the tie-back – capable of letting the water through – prevents the whole structure from collapsing. To avoid leakage, diaphragms and an electronic monitoring system are applied. The sufficiency of the anchorage at point A, although a critical issue of the general stability, is not addressed here.

2.3. Assumptions.

- The cross-section of the structure shows only negligible alterations in the longitudinal direction based on three-dimensional finite element simulation results, therefore it is sufficient to examine only the cross section in planar deformation state after linearly distributing the concentrated tie-back forces along directrix B.
- The over-pressure inside the inflated cylinder is high enough to maintain the circular cross-section, thus we handle it as a rigid body.
- The dimensions l_{BCDA} , l_{AB} , and r are constant, that is, all elements have tensile stiffness large enough for the loads to cause negligibly small strains.
- The weight of the textile, the tie-back, and the cylinder are negligible compared to the loads they bear.

2.4. Theoretical background. The internal forces and the equilibrium geometry of the arrangement are determined by a system of four nonlinear transcendental equations. The first two express the equilibrium of the cylinder, while the other two state the geometric compatibility of the textile.

2.4.1. Loads on the cylinder. Fig. 2 shows the loads acting on the inflated cylinder. These are:

1. T , the specific tensile force from the tie-back,
2. S , the specific force from the textile tangential to the cylinder, and
3. $p(\xi)$ the pressure from the water normal to the cylinder.

We describe the conformation of the whole arrangement by four parameters:

1. α , the inclination of the tie-back from the horizontal,
2. β , the angle between the horizontal and the BE line connecting the end of the tie-back and the center of the cylinder,
3. δ , the angle between the BE line and the CE line connecting the point where the textile separates from the cylinder and the center point, and
4. T , the specific force in the tie-back.

In terms of these parameters the coordinates of the center of the cylinder (E) are

$$x_E = l_{AB} \cos \alpha + r \cos \beta, \quad y_E = h - l_{AB} \sin \alpha - r \sin \beta, \quad (2.1)$$

the coordinates of the point where the canvas separates from the cylinder (C) are

$$x_C = x_E - r \cos(\beta + \delta), \quad y_C = y_E + r \sin(\beta + \delta), \quad (2.2)$$

the inclination of the tangent of the textile from the horizontal at point C is

$$\varphi_C = \frac{\pi}{2} - \beta - \delta, \quad (2.3)$$

the inclination of the FE line connecting the point where the water level intersects the cylinder and the center of the cylinder from the horizontal is

$$\gamma = -\arcsin \frac{y_E}{r}, \quad (2.4)$$

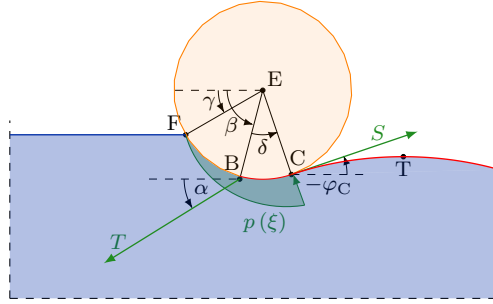


Figure 2. Parameters for the load calculation of the inflated cylinder

and the water pressure on the cylinder expressed as a function of the polar angle (ξ) measured counterclockwise from the horizontal is

$$p(\xi) = \rho g r (\sin \xi - \sin \gamma), \quad (2.5)$$

where $\rho = 1000 \text{ kg/m}^3$ is the density of the water and $g = 9.81 \text{ m/s}^2$ is the gravitational acceleration.

2.4.2. *Equilibrium of the cylinder.* The specific tensile force in the textile yields from the moment equilibrium at point E:

$$S = T \sin(\beta - \alpha). \quad (2.6)$$

The two projections of the force equilibrium equation are:

$$\begin{aligned} \int_{\gamma}^{\beta+\delta} p(\xi) r \cos \xi \, d\xi - T \cos \alpha + S \cos \varphi_C &= 0, \\ - \int_{\gamma}^{\beta+\delta} p(\xi) r \sin \xi \, d\xi + T \sin \alpha - S \sin \varphi_C &= 0, \end{aligned} \quad (2.7)$$

which after integration and substitution of (2.3) and (2.6) lead to the first two transcendental condition equations:

$$\begin{aligned} f_1(\alpha, \beta, \delta, T) &= T [\sin(\beta - \alpha) \sin(\beta + \delta) - \cos \alpha] + \\ &+ \rho g r^2 \left[\frac{\cos^2 \gamma + 3 \sin^2 \gamma - \cos 2(\beta + \delta)}{4} - \sin \gamma \sin(\beta + \delta) \right] = 0, \\ f_2(\alpha, \beta, \delta, T) &= T [\sin(\beta - \alpha) \cos(\beta + \delta) + \sin \alpha] + \\ &+ \rho g r^2 \left[\frac{\gamma - \beta - \delta}{2} + \frac{\sin 2(\beta + \delta) + \sin 2\gamma}{4} + \sin \gamma \cos(\beta + \delta) \right] = 0, \end{aligned} \quad (2.8)$$

where γ is determined via (2.4) and (2.1).

2.4.3. *Geometric compatibility of the textile.* The remaining two condition equations:

$$\begin{aligned} f_3(\alpha, \beta, \delta, T) &= l_{\text{BCDA}} - \delta \cdot r - l_{\text{CD}} - x_{\text{D}} = 0, \\ f_4(\alpha, \beta, \delta, T) &= h - y_{\text{D}} = 0, \end{aligned} \quad (2.9)$$

where l_{CD} , x_{D} , and y_{D} are calculated through (4.15), (4.20), and (4.9)₂, respectively, stem from the compatibility conditions of the textile, whose loaded shape determination is described in Section 4.

2.4.4. *The nonlinear system of equations.* To summarize (2.8) and (2.9), we write:

$$\mathbf{f}(\mathbf{x}) = 0, \quad \text{where } \mathbf{f} = \begin{bmatrix} f_1 \\ f_2 \\ f_3 \\ f_4 \end{bmatrix}, \quad \text{and } \mathbf{x} = \begin{bmatrix} \alpha \\ \beta \\ \delta \\ T \end{bmatrix}. \quad (2.10)$$

We solve (2.10) by a target code applying the Jacobi method implemented in MATLAB 2011a (The MathWorks Inc., Natick, Massachusetts, United States). As stated in (4.7), to find a physically admissible solution that prevents the textile from rising above water level, that is, to prevent inflection in the directrix, the domain of \mathbf{f} is restricted so that the Eötvös number exceeds the critical value of 1.

2.5. Analysis of the structure.

2.5.1. *Water level elevation.* As an illustration, the equilibrium geometries of the arrangement $l_{\text{AB}} = 1.1$ m, $l_{\text{BCDA}} = 3.1$ m, $r = 0.2$ m are shown in the frames of Fig. 3 for water level rising by 10 centimeters. The corresponding specific tensile force increases in the tie-back (T) and in the textile (S), along with the tie-back inclination (α), are shown in Fig. 4.

2.5.2. *Maximal supported water level.* The maximal supported water level h is a function of l_{AB} , l_{BCDA} , and r together describing the geometry of a given arrangement. This extremal state is defined by $\gamma = -\pi/2$. We first consider the value of r as given and instead of δ we choose φ_{C} as the independent variable, constraining $y_{\text{C}} = r(1 + \cos \varphi_{\text{C}})$. To reach the desired $h = y_{\text{D}}$, which due to (4.7)₁ and (4.9)₂ is smaller than

$$h_{\text{max}} = \sqrt{\frac{2r^2(1 + \cos \varphi_{\text{C}})^2}{1 - \cos \varphi_{\text{C}}}}, \quad (2.11)$$

S is found from (4.9)₂ to be

$$S = \frac{\rho g (h^2 - y_{\text{C}}^2)}{2(1 + \cos \varphi_{\text{C}})}. \quad (2.12)$$

φ_{C} uniquely describes F_x and F_y , the components of the water pressure resultant as shown in Fig. 5 and in (2.13):

$$F_x = \frac{\rho g r^2}{2} (1 + \cos \varphi_{\text{C}})^2, \quad F_y = \frac{\rho g r^2}{2} [\varphi_{\text{C}} - \pi + \sin \varphi_{\text{C}} (2 + \cos \varphi_{\text{C}})]. \quad (2.13)$$

Through the equilibrium of the cylinder, the tie-back position is determined via

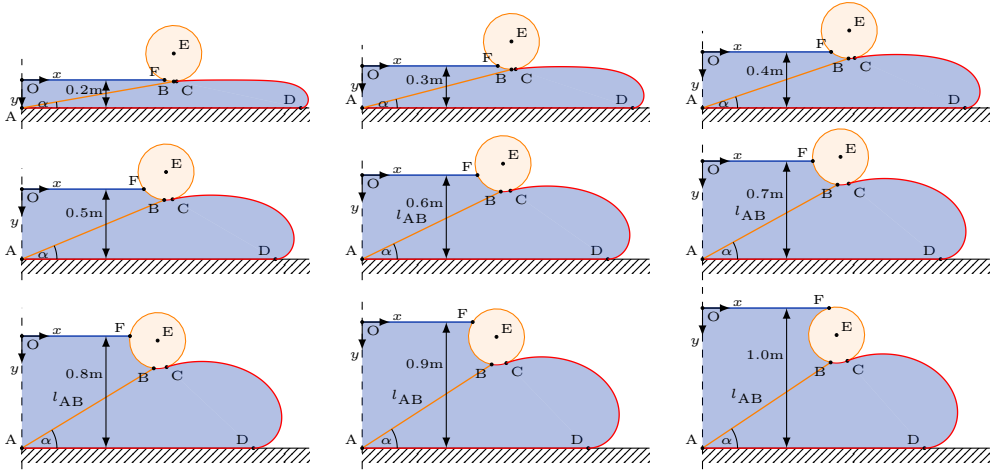


Figure 3. Frames of the equilibrium geomery of the arrangement $l_{AB} = 1.1$ m, $l_{BCDA} = 3.1$ m, $r = 0.2$ m in case of the water level rising by 10 cm in each step.

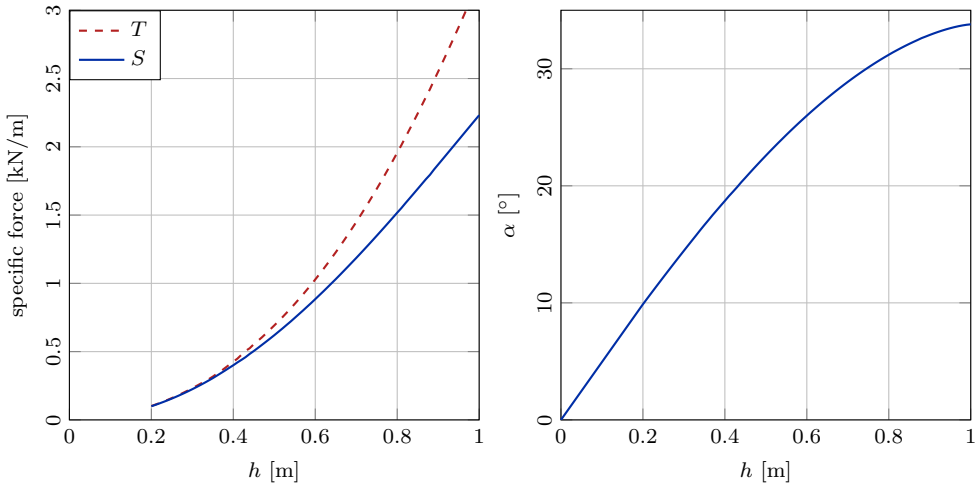


Figure 4. Specific tensile forces in the tie-back (T) and in the textile (S) (left), and the tie-back inclination (α) as a function of the rising water level (h)

$$\alpha = \arctan \frac{-S \sin \varphi_C - Fy}{S \cos \varphi_C + Fx}, \quad \beta = \alpha + \arcsin \frac{Fy \cos \alpha + Fx \sin \alpha}{Fy \cos \varphi_C - Fx \sin \varphi_C}, \quad (2.14)$$

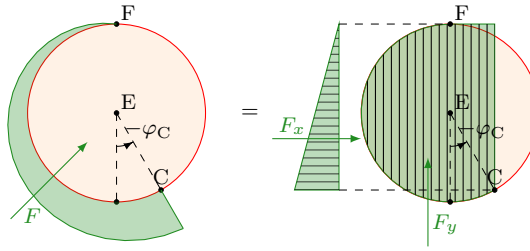


Figure 5. Decomposition of the water pressure resultant exerted on the cylinder in case of the highest possible supported water level

yielding the tie-back and textile lengths:

$$l_{AB} = \frac{h - r(1 + \sin \beta)}{\sin \alpha}, \quad l_{BCDA} = \delta \cdot r + l_{CD} + x_D, \quad (2.15)$$

where δ , l_{CD} and x_D are calculated via (2.3), (4.15) and (4.20), respectively.

2.6. Preliminary design.

We have now the possible geometric parameters characterizing the extremal design state of the structure. For a given r , their relation describes a surface in the three-dimensional (l_{AB} , l_{BCDA} , h) space, the contours of which are shown in Fig. 6 by blue lines, where it becomes possible to optimize the cost of the arrangement. Usually the textile length is to be minimized, both for financial reasons, and because the top of the existing dam it is going to be placed on offers a limited space, consequently the optimal designs are extremal points of the level lines forming the red curve also shown in Fig. 6. Agreeing upon this condition, we present the design method to define a geometry which is capable of withstanding a water height h :

1. We assume that h includes the uncertainty of the water level and the surface wave amplitudes as well. Hence reducing the problem to a quasi-static investigation.
2. As Fig. 7 shows, the tie-back and textile lengths decrease radically with the increasing cylinder radius, the critical design parameter, chosen to be the highest feasible value.
3. l_{AB} and l_{BCDA} are concluded from Fig. 7.
4. S and T , the specific textile and tie-back forces are found from Fig. 8.
5. For designing the anchorage foundation, the tie-back inclination angle is shown in Fig. 9.

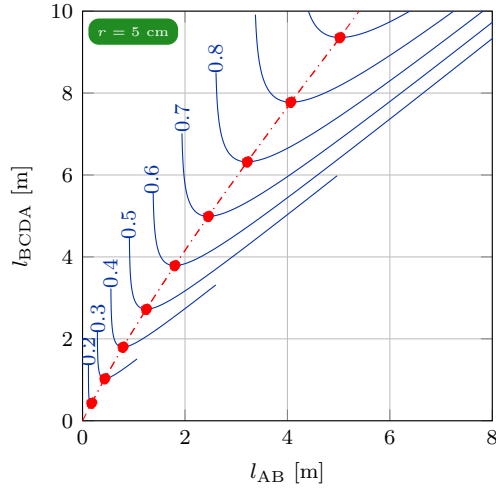


Figure 6. Blue level lines of the maximal supported water level, h [m] for a given cylinder radius ($r = 5$ cm); red curve is the optimal choice of the geometric parameters.

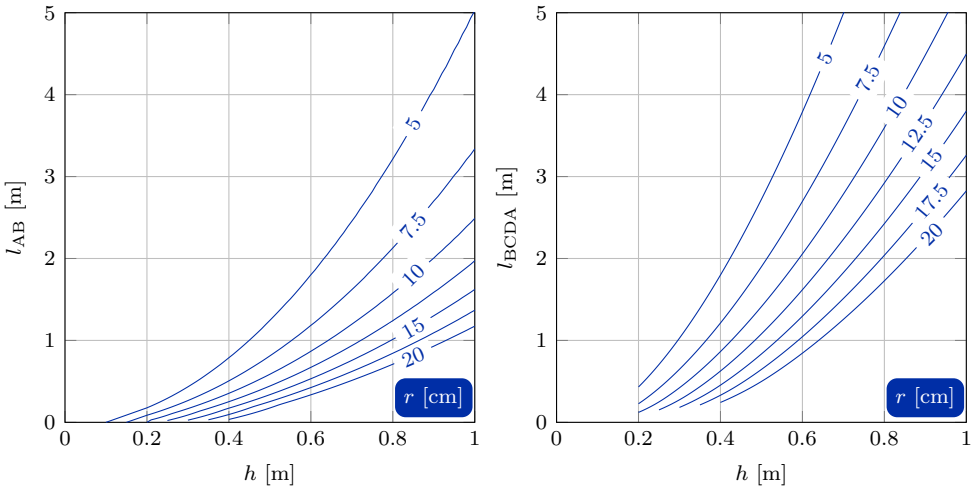
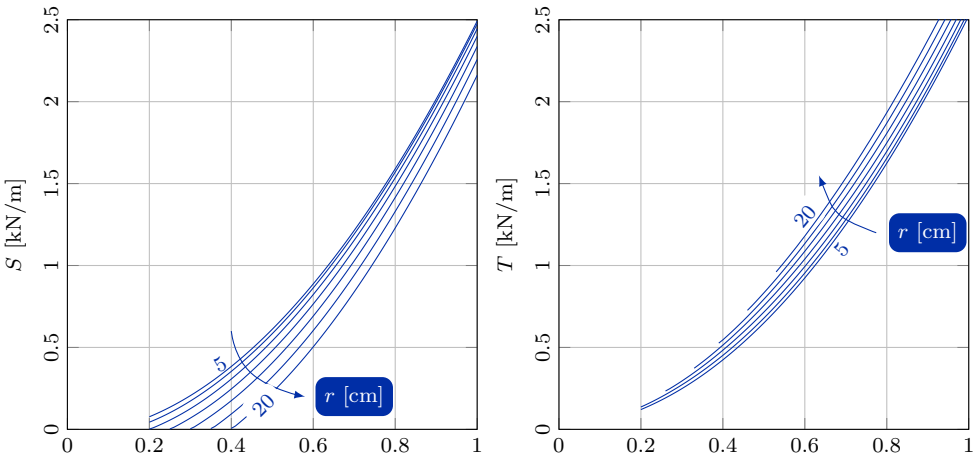


Figure 7. Tie-back and textile lengths as functions of the cylinder radius and maximal supported water level



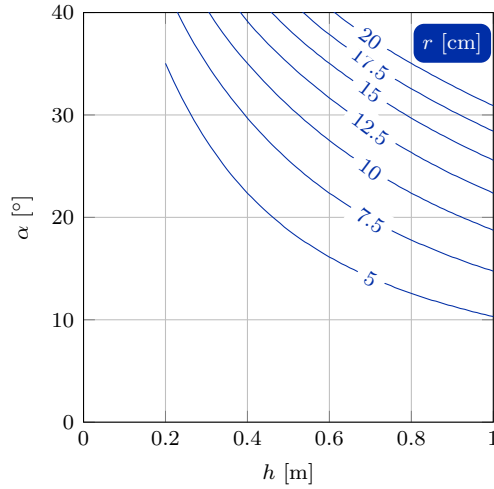


Figure 9. Extremal tie-back inclination angle as functions of the cylinder radius and maximal supported water level

3. SECOND ARRANGEMENT

The second scenario is invoked to life by the Airdome-Mobildam Kft. who approached us to analyze the structure presented in this chapter. Similarly to the first problem, we give here the shape and the specific forces of the textile and the reaction forces on the supports.

3.1. Geometry. This arrangement, also mounted on the crown, consists of an impermeable textile channel attached to a steel framework. A representative loaded cross-section solely of the textile in the plane of a frame position is presented in Fig. 10. The textile of cross-sectional length L is suspended on the framework at height H along two fixed directors, B_1 and B_2 at a vertical distance d from each other. The inner water height is h_i , the supported tidal water height over the crown is h_s .

3.2. Behavior of the structure. Initially the unloaded textile is hanging on the supporting framework at points B_1 and B_2 . During the fill-up, water is pumped inside the textile from the rising tide of the river, gradually erecting the yet symmetric structure. The rising supported water level deforms the structure violating the symmetry. At this stage, the weight of the water infill acts as a gravity retaining wall.

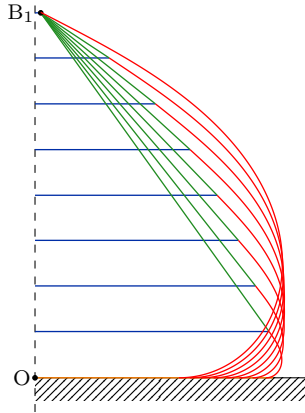


Figure 11. Unloaded, erected textile shape during the fillup process with internal water level rising by 20 centimeters

where $l_{C_1D_1}$ and x_{D_1} are found from (4.15) and (4.20), respectively. Based on the restriction on the Hamiltonian of the system ($H_0 < 0$ see Section 4.2), or – in a mechanically more expressive form – the horizontal equilibrium of a textile section, the viable values of S_1 are taken from $(S_{1,\min}, \infty)$, where

$$S_{1,\min} = \frac{\rho g h_i^2}{4}. \tag{3.3}$$

We obtain the solution of (3.2) by the bisection method, consequently this unbounded interval is transformed to the bounded interval of $s_1 \in (0, 1]$ by introducing

$$s_1 = \frac{S_{1,\min}}{S_1}. \tag{3.4}$$

3.4.2. *Design parameters.* For calculating the necessary strength and stability of the frame the support force components are to be determined. In case of our example we illustrate them in Fig. 12 in terms of the internal water level elevation.

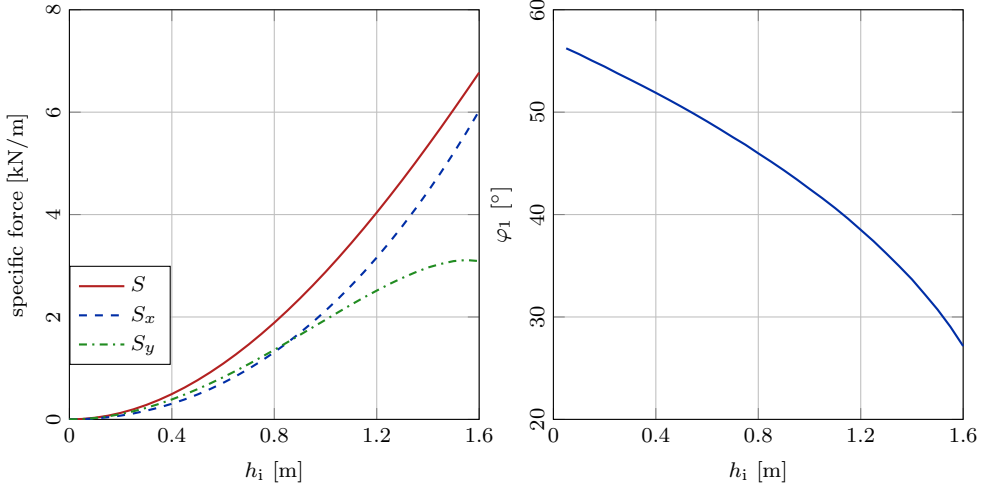


Figure 12. Specific tensile forces and its components in the textile (left), and initial inclination of the textile (right) as functions of the rising internal water level

3.5. Loaded geometry. The textile still remains smooth, stretches straight in segment B_2C_2 , leans against the ground in ED_1 , takes the loaded shape defined in Chapter 4 in segment C_2D_2 , and forms a circle section in D_2E , the radius (R) and central angle (ϕ) of which is:

$$R = \frac{S_2}{\varrho g (h_i - h_s)}, \quad (3.5)$$

$$\phi = \arccos \frac{R - h_s}{R}.$$

3.5.1. Governing equation. The geometric compatibility for a given h_i and h_s is again met by adjusting S_2 in the cross-sectional length error:

$$f_2(S_1) = 2 \left(\frac{H - h_i}{\sin \varphi_2} + l_{C_2D_2} + R\phi + x_{D_2} - R \sin \phi \right) - L = 0, \quad (3.6)$$

where $l_{C_2D_2}$ and x_{D_2} are found by evaluating at $\varphi = \pi - \phi$ the functions (4.13) and (4.19), respectively. Similarly to the unloaded case, the solution is obtained by the bisection method, thus the unbounded interval of $S_2 \in (S_{2,\min}, \infty)$, where

$$S_{2,\min} = \frac{\varrho g (h_i^2 - h_s^2)}{4} \quad (3.7)$$

is transformed to the bounded interval of $s_2 \in (0, 1]$ by introducing

$$s_2 = \frac{S_{2,\min}}{S_2}. \quad (3.8)$$

3.6. Rise of the supported water level. Once the desired internal water level is reached, its volume (found from (4.21) and shown in Fig. 13) does not change throughout the increasing loading of the tide. Numerically, after the two internal

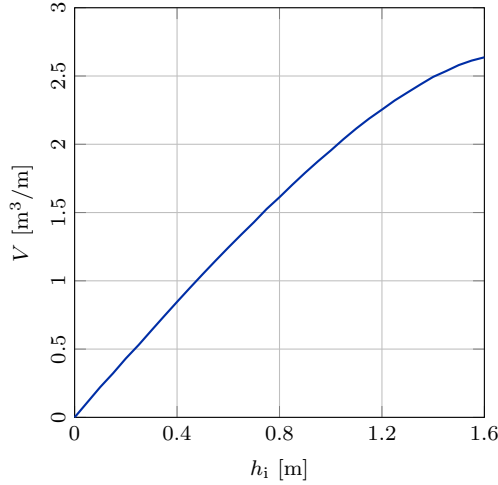


Figure 13. Specific volume of the infill against its rising level

iteration of S_1 and S_2 for the geometric compatibility of the two sides, an outer bisection iteration adjusts h_i to match the volume requirement:

$$f_3(h_i) = 2V(\varphi_C, \pi, S) - V(\varphi_{C_1}, \pi, S_1) + V(\varphi_{C_2}, \varphi_{D_2}, S_2) + \frac{R^2\phi}{2} - \frac{R^2 \sin 2\phi}{4} + R(1 - \cos \phi)(x_{D_2} - R \sin \phi) = 0, \tag{3.9}$$

where V is defined in (4.21), arguments with indice 1 and 2 represent the free and the loaded side, respectively while the symmetric unloaded geometry is referred to by subscripts without any index. Fixing the infill volume at the value when $h_i = 1.3$ m in the unloaded state, the increasing h_s deforms the cross-section shown in the frames of Fig. 14. Fig. 15 depicts the tension (S_2) in the loaded textile decreasing with h_s .

3.7. Conclusions.

- The structure acts as a gravity retaining wall.
- The symmetry of the erected structure is violated by the supported tidal water pressure.
- Counter-intuitively, instead of pushing the structure away from the riverbed, the external water pulls it closer due to the uplift.
- The internal water level decreases, although insignificantly (by 5 cm in the presented example, see Figure 15, where the specific tensile force becomes zero at $h_s = 1.25$ cm).

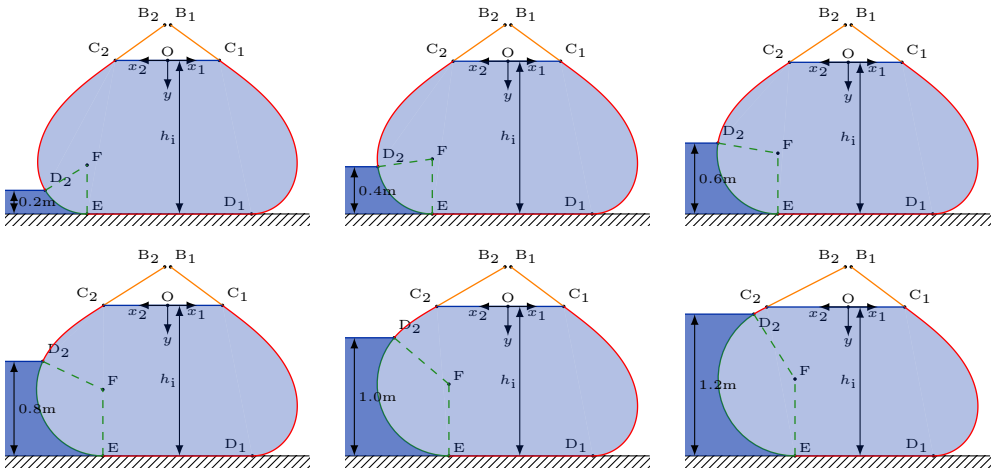


Figure 14. Frames of the structure deformation as the supported water level rises by 20 centimeters

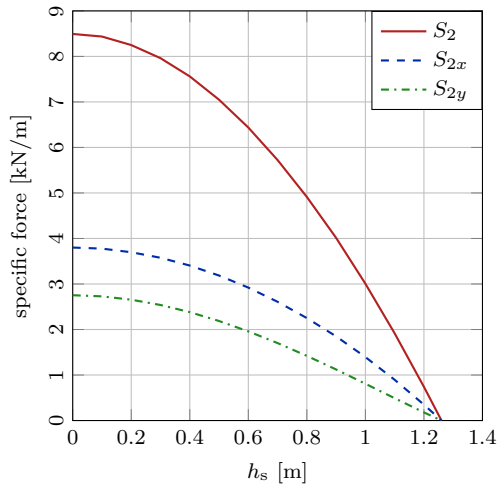


Figure 15. Specific tensile force and its components in the textile loaded by the rising supported water level

- The textile tension in the supporting side decreases to zero as h_s reaches h_i , when the supporting textile loosens and its shape becomes undefined.
- The properties of the side away from the river depend only on the internal water level, which is virtually unaltered, thus its shape and tension agrees with the unloaded state.

- $h_s = h_i$ is the critical state from stability point of view, when total load of the tide acts only on the outer textile part, while the balancing tension in the other side of the textile is missing.

3.8. Preliminary design. The preliminary design for an expected $h_{s,max}$ starts with prescribing H and d for the framework and t , the necessary minimal length where the textile touches the ground at the time of the maximal tidal level to prevent the river flooding out and to provide the overall stability of the structure; and results in the critical design force descriptors from the point of view of the framework: S_1 , the specific force in the outer textile part and φ_{C_1} , the inclination of the textile tangent at point C_1 . In Figure 16, we present the design charts supporting this simplified work-flow. We consider the limit case when $h_i = 1.25h_{s,max}$, and assume that $H = h_i$. Having been agreed upon the safety ratio of 1.25 and infill ratio of 1, the designer chooses a suitable t , adjusts it by d and from the left graph on Figure 16 the necessary cross-sectional textile length is obtained alongside with S_1 as is φ_{C_1} from the chart on the right. For a given H , the increase in L causes a decrease in both S_1 and φ_{C_1} , thus not only because of the limited space available and cost efficiency reasons, but because of overall structural stability issues, the shortest L is to be chosen meeting the criterion on t .

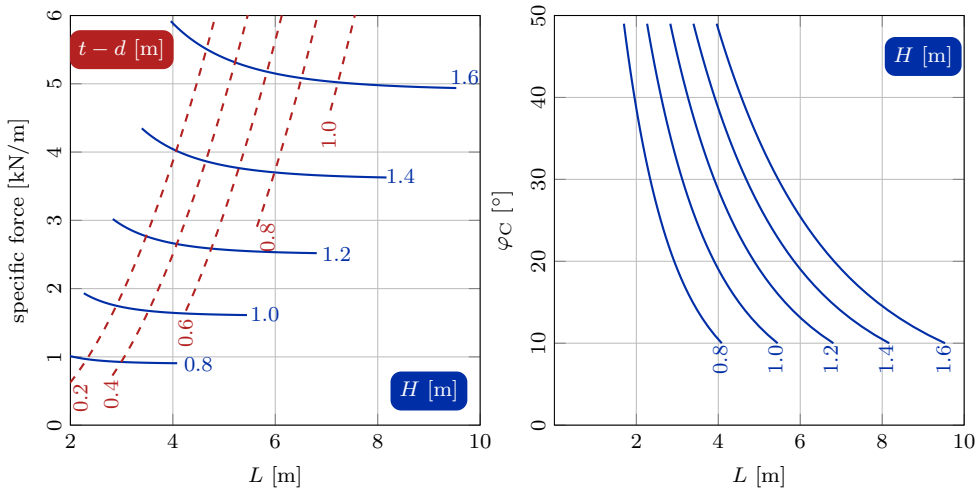


Figure 16. Dependence of the specific force in the outer textile part (S_1) (left) and the inclination of the textile tangent from the vertical at point C_1 (φ_{C_1}) (right) on the cross-sectional textile length (L) and the framework height (H) when the supported water height (h_s) is $0.8H$

4. SHAPE OF THE LOADED TEXTILE SECTION

Consider a prismatic, weightless, inextensible textile supporting static water pressure, the cross-section of which is shown in Fig. 17, where the water level is at $y = 0$. In this section we give the parametric functional description of this directrix (in the following referred to as fiber) shape and the closed form equation of the V area between the curve and the y axis. For similar structures, such as closed pressurized geomembrane tubes c.f. [3] for the elastic case, [4] for stacked arrangement, [5] for infill with liquids of different density, [6] for compressible subgrade soil; or [7] for liquid filled nonlinearly elastic shells.

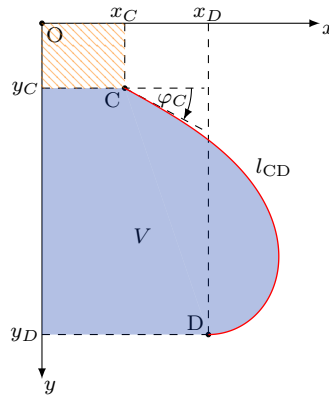


Figure 17. Boundary value problem of the textile shape loaded by static water pressure

4.1. Initial value problem. The initial value problem of ordinary differential equations describing the fiber shape is given by

$$\begin{aligned} x' &= \cos \varphi, & x(0) &= x_C, \\ y' &= \sin \varphi, & y(0) &= y_C, \\ \varphi' &= \frac{\rho g}{S} y, & \varphi(0) &= \varphi_C, \end{aligned} \quad (4.1)$$

where x and y are the horizontal and vertical coordinates respectively, φ is the inclination of the tangent from the positive x axis in clockwise direction. ρ is the water density, g is the gravitational acceleration, S is the specific tensile force in the fiber, and prime denotes the derivative with respect to the arc length parameter (λ). The first two equations are the compatibility conditions and the third is the tangential equilibrium statement. Since the fiber weight is negligible and the water pressure is normal to the curve, the equilibrium condition in the normal direction prescribes the specific tension (S) in the fiber being constant. By eliminating y from the last two

ODEs of (4.1), we simplify the problem to

$$\varphi'' = \omega^2 \sin \varphi, \quad \varphi'(0) = \omega^2 y_C, \quad \varphi(0) = y_C, \quad \omega^2 = \frac{\rho g}{S}, \quad (4.2)$$

which is analogous to the nonlinear pendulum equation [8] except the sign change. The same equation governs the elastica [9] and capillarity problems and if we consider S to be the surface tension, we arrive at the problem of sessile drops.

4.2. The first integral. We can define the corresponding Lagrangian:

$$L = \varphi'^2 + 4\omega^2 \sin^2 \frac{\varphi}{2}, \quad (4.3)$$

which does not depend explicitly on the arch-length, thus following Noether's theorem [10] we construct a conserved quantity:

$$H = \varphi'^2 - 4\omega^2 \sin^2 \frac{\varphi}{2} = \text{const.} \quad (4.4)$$

This – speaking in mechanical terms – states the horizontal equilibrium of a textile section. At a certain depth the first term is proportional to the horizontal hydrostatic load resultant, the second is proportional to the horizontal tensile force in the textile, resulting in the alternate form of (4.4):

$$\tilde{H} = \frac{\rho g y^2}{2} + S \cos \varphi = \text{const.} \quad (4.5)$$

In the followings we work with the form of (4.4). This translational symmetry, analogous to the energy or the Hamiltonian of the pendulum moving in conservative field, suggests scrutinizing the periodic phase space and its two qualitatively different trajectories DTCD ($0 < H = \text{const.}$) and SUVS ($0 > H = \text{const.}$) separated by the dash-dotted separatrix ($H = 0$) in Fig. 18. We introduce two constants:

$$H_0 = \omega^4 y_C^2 - H_p \sin^2 \frac{\varphi_C}{2}, \quad H_p = 4\omega^2, \quad (4.6)$$

which correspond to the total energy and the maximal potential energy of the pendulum, respectively.

In case of the first arrangement (Chapter 2), we allow only the curves above the upper separatrix since it restricts the y coordinate to be positive, that is the fibre does not rise above the water level, and has no inflection, which is the only physically acceptable scenario, analogous to the overturning pendulum. The necessary criterion is $H_0 > 0$, which yields an inequality constraint to the boundary conditions given by

$$y_C > y_l, \quad \text{where} \quad y_l = \sqrt{\frac{2(1 - \cos \varphi_c) S}{\rho g}}, \quad \text{or} \quad (4.7)$$

$$Eo > 1, \quad \text{where} \quad Eo = \frac{\rho g y_c^2}{2(1 - \cos \varphi_c) S}.$$

Here y_l is the capillarity length and Eo is the Eötvös number both measuring the relationship between the gravity and surface tension effects, and are extensively used

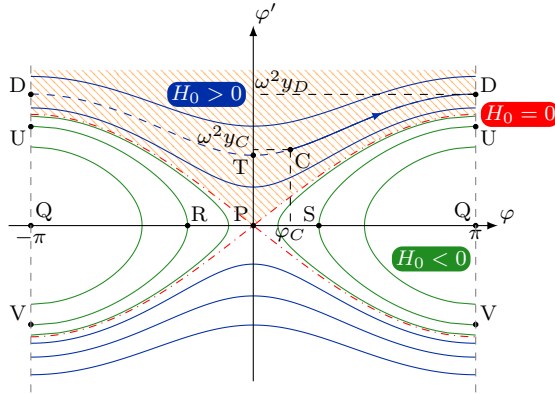


Figure 18. Phase space of the Hamiltonian

for analyzing capillarity phenomena such as the shape of pendant or sessile drops [11]. Now we are able to determine

$$y(\varphi) = \sqrt{y_C^2 + \frac{4}{\omega^2} \left(\sin^2 \frac{\varphi}{2} - \sin^2 \frac{\varphi_C}{2} \right)}, \tag{4.8}$$

which gives us the maximal and minimal textile heights denoted by points D and T in the phase space:

$$\begin{aligned} y_T &= \sqrt{y_C^2 - \frac{2}{\omega^2} (1 - \cos \varphi_C)}, \\ y_D &= \sqrt{y_C^2 + \frac{2}{\omega^2} (1 + \cos \varphi_C)}. \end{aligned} \tag{4.9}$$

In case of the second arrangement (Chapter 3), analogous to the oscillating pendulum, the only viable curves are between the separatrices ($H_0 < 0$) with initial conditions $\varphi' = 0$ and $\varphi > 0$, turning around the relations in (4.7), but leaving (4.8) unaltered.

4.3. Elliptic functions. In the followings we use the definition of Legendre’s elliptic integrals (4.10) and the Jacobi functions (4.11). These are the incomplete elliptic integrals of the first (F) and second (E) kind; the Jacobi amplitude (am), the sinus amplitudinis (sn), and cosinus amplitudinis (cn) functions:

$$F(\varphi|A) = \int_0^\varphi \frac{d\phi}{\sqrt{1 - A \sin^2 \phi}}, \tag{4.10}$$

$$E(\varphi|A) = \int_0^\varphi \sqrt{1 - A \sin^2 \phi} \, d\phi,$$

$$\begin{aligned} \text{am}(\lambda|A) &= F^{-1}(\lambda|A), \\ \text{sn}(\lambda|A) &= \sin[\text{am}(\lambda|A)], \\ \text{cn}(\lambda|A) &= \cos[\text{am}(\lambda|A)], \end{aligned} \tag{4.11}$$

4.4. Parametric description of the fiber. In the first scenario $H_p = 4\omega^2 > 0$, $H_0 > 0$, and $\varphi' > 0$; in the second $H_0 < -H_p \sin^2(\varphi_C/2) < 0$ and $\varphi' > 0$ since $\varphi \in [\varphi_C, \pi]$. Consequently, for both arrangements (4.4) results in the ODE:

$$\varphi' = \sqrt{H_0 + H_p \sin^2 \frac{\varphi}{2}}, \tag{4.12}$$

and its solutions:

$$\lambda(\varphi) = \text{sign}(H_0) \frac{2}{\sqrt{H_0}} \text{F}\left(\frac{\varphi}{2} | A\right) - \lambda_C, \quad \text{and} \quad \varphi(\bar{\lambda}) = 2\text{am}(\bar{\lambda} | A), \quad \text{where} \tag{4.13}$$

$$\bar{\lambda} = \text{sign}(H_0) \frac{\sqrt{H_0}}{2} (\lambda + \lambda_C), \quad \lambda_C = \text{sign}(H_0) \frac{2}{\sqrt{H_0}} \text{F}\left(\frac{\varphi_C}{2} | A\right), \quad A = -\frac{H_p}{H_0}. \tag{4.14}$$

Hence the length of the CD curve is

$$l_{\text{CD}} = \text{sign}(H_0) \frac{2}{\sqrt{H_0}} \left[\text{F}\left(\frac{\varphi_D}{2} | A\right) - \text{F}\left(\frac{\varphi_C}{2} | A\right) \right]. \tag{4.15}$$

Substituting (4.13)₂ into (4.8) gives

$$y(\bar{\lambda}) = \sqrt{y_C^2 + \frac{4}{\omega^2} \left[\text{sn}^2(\bar{\lambda} | A) - \sin^2 \frac{\varphi_C}{2} \right]}. \tag{4.16}$$

Merging (4.2)₁ and (4.13)₂, we get

$$x' = \cos [2\text{am}(\bar{\lambda} | A)] = 1 - 2\text{sn}^2(\bar{\lambda} | A), \tag{4.17}$$

and its solution

$$\begin{aligned} x(\bar{\lambda}) = x_C + \frac{4H_0 + 2H_p}{\sqrt{H_0}H_p} (\bar{\lambda} - \bar{\lambda}_C) + \\ + \frac{4\sqrt{H_0}}{H_p} \{ \text{E} [\text{am}(\bar{\lambda}_C | A) | A] - \text{E} [\text{am}(\bar{\lambda} | A) | A] \}, \end{aligned} \tag{4.18}$$

where $\bar{\lambda}_C = \sqrt{H_0}\lambda_C/2$, or in terms of φ

$$\begin{aligned} x(\varphi) = x_C + \text{sign}(H_0) \frac{4H_0 + 2H_p}{\sqrt{H_0}H_p} \left[\text{F}\left(\frac{\varphi}{2} | A\right) - \text{F}\left(\frac{\varphi_C}{2} | A\right) \right] + \\ + \text{sign}(H_0) \frac{4\sqrt{H_0}}{H_p} \left[\text{E}\left(\frac{\varphi_C}{2} | A\right) - \text{E}\left(\frac{\varphi}{2} | A\right) \right]. \end{aligned} \tag{4.19}$$

We also give the x coordinate of point D:

$$x_D = x_C + l_{\text{CD}} \frac{H_p + 2H_0}{H_p} + \text{sign}(H_0) \frac{4\sqrt{H_0}}{H_p} \left[\text{E}\left(\frac{\varphi_C}{2} | A\right) - \text{E}\left(\frac{\varphi_D}{2} | A\right) \right]. \tag{4.20}$$

4.5. Enclosed area. The area between the y axis and the curve, when $\varphi \in [\varphi_C, \varphi_D]$ (shaded area in Fig. 17), can be deduced using Green's theorem, partial integration, variable change, (4.16) and (4.1)_{1,3} in this order, as shown in (4.21).

$$\begin{aligned}
 V(\varphi_C, \varphi_D, S) &= \int_{y_C}^{y_D} x \, dy = \int_0^{l_{CD}} xy' \, d\lambda = [xy]_C^D - \int_0^{l_{CD}} x'y \, d\lambda = \\
 &= [xy]_C^D - \int_{\varphi_C}^{\varphi_D} \frac{x'y}{\varphi'} \, d\varphi = x_D y_D - x_C y_C - \int_{\varphi_C}^{\varphi_D} \frac{\cos \varphi y}{\omega^2 y} \, d\varphi = \\
 &= x_D y_D - x_C y_C - \frac{1}{\omega^2} \int_{\varphi_C}^{\varphi_D} \cos \varphi \, d\varphi = \\
 &= x_D y_D - x_C y_C + (\sin \varphi_C - \sin \varphi_D) \frac{S}{\rho g}.
 \end{aligned} \tag{4.21}$$

4.6. Conclusion. In this section we derived the parametric functional description of the cross-sectional shape and the explicit function of the enclosed area of an inextensible weightless prismatic textile subjected to water pressure loading and constant specific tensile force with known initial point coordinates (x_C, y_C) and prescribed initial tangent line inclination (φ_C) . As a summary, we give here the most important equations of the fiber position:

$$\begin{aligned}
 x(\varphi) &= x_C + \text{sign}(H_0) \frac{4H_0 + 2H_p}{\sqrt{H_0 H_p}} \left[F\left(\frac{\varphi}{2} \middle| A\right) - F\left(\frac{\varphi_C}{2} \middle| A\right) \right] + \\
 &\quad + \text{sign}(H_0) \frac{4\sqrt{H_0}}{H_p} \left[E\left(\frac{\varphi_C}{2} \middle| A\right) - E\left(\frac{\varphi}{2} \middle| A\right) \right], \\
 y(\varphi) &= \sqrt{y_C^2 + \frac{4S}{\rho g} \left(\sin^2 \frac{\varphi}{2} - \sin^2 \frac{\varphi_C}{2} \right)},
 \end{aligned} \tag{4.22}$$

and the area enclosed by the y axis and the curve:

$$V(\varphi) = xy - x_C y_C + (\sin \varphi_C - \sin \varphi) \frac{S}{\rho g}, \tag{4.23}$$

the parameter (φ) being the inclination angle.

REFERENCES

1. Inflater project. 2015, URL <http://inflater.eu/>. [Online; accessed 19-March-2015].
2. ADANY, S., BOCSKAI, Z., GALASKO, G., GÁSPAR, Z., LAKATOS, E., LENGYEL, A., and NAGY, R.: *INFLATER Handbook: Half time report*, chap. Mechanical structure design, pp. 121–167. Springer Verlag, Budapest University of Technology and Economics, Geotechnical Department, I. Nagy, t. huszak edn., 2013.
3. ANTMAN, S. S. and SCHAGERL, M.: Slumping instabilities of elastic membranes holding liquids and gases. *International Journal of Non-Linear Mechanics*, **40**(8), (2005), 1112–1138.
4. CANTRE, S.: Geotextile tubes – analytical design aspects. *Geotextiles and Geomembranes*, **20**(5), (2002), 305–319.

5. MALIK, J. and SYSALA, S.: Analysis of geosynthetic tubes filled with several liquids with different densities. *Geotextiles and Geomembranes*, **29**(3), (2011), 249–256.
6. GUO, W., CHU, J., and YAN, S.: Effect of subgrade soil stiffness on the design of geosynthetic tube. *Geotextiles and Geomembranes*, **29**(3), (2011), 277–284.
7. KOLESNIKOV, A.: Equilibrium of an elastic spherical shell filled with a heavy fluid under pressure. *Journal of applied mechanics and technical physics*, **51**(5), (2010), 744–750.
8. OCHS, K.: A comprehensive analytical solution of the nonlinear pendulum. *European Journal of Physics*, **32**(2), (2011), 479.
9. LEVIEN, R.: The elastica: a mathematical history. *Electrical Engineering and Computer Sciences University of California at Berkeley*.
10. NOETHER, E.: Invariante variationsprobleme. *Nachrichten von der Gesellschaft der Wissenschaften zu Göttingen, mathematisch-physikalische Klasse*, **1918**, (1918), 235–257.
11. DE GENNES, P., BROCHARD-WYART, F., and QUERE, D.: *Capillarity and Wetting Phenomena: Drops, Bubbles, Pearls, Waves*. Springer, 2004, ISBN 9780387005928.

ANALYSIS OF STEADY WEAR PROCESSES FOR PERIODIC SLIDING

ISTVÁN PÁCZELT

Institute of Applied Mechanics, University of Miskolc
H-3515 Miskolc, Miskolc–Egyetemváros, Hungary
mechpacz@uni-miskolc.hu

ZENON MROZ

Institute of Fundamental Technological Research, A. Pawińskiego 5B, 02-106 Warsaw,
Poland
zmroz@ippt.pl

ATTILA BAKSA

Institute of Applied Mechanics, University of Miskolc
H-3515 Miskolc, Miskolc–Egyetemváros, Hungary
attila.baksa@uni-miskolc.hu

[Received: June 14, 2015, Accepted: September 2, 2015.]

*Dedicated to Professor Barna Szabó on the occasion of his eightieth birthday
and to Professor Imre Kozák on the occasion of his eighty fifth birthday*

Abstract. The relative sliding motion of two elastic bodies in contact induces wear process and contact shape evolution. The transient process at the constant relative velocity between the bodies tends to a steady state occurring at fixed contact stress and strain distribution. This state corresponds to a minimum of the wear dissipation power. The optimality conditions of the functional provide the contact stress distribution and the wear rate compatible with the rigid body punch motion. The present paper is devoted to analysis of wear processes occurring for periodic sliding of contacting bodies, assuming cyclic steady state conditions for mechanical fields. From the condition of the rigid body wear velocity a formula for summarized contact pressure in the periodic steady state is derived. The optimization problem is formulated for calculation of the contact surface shape induced by wear in the steady periodic state.

Mathematical Subject Classification:

Keywords: steady wear process, periodic sliding, unilateral contact, p-version of finite element method, shape optimization

1. INTRODUCTION

The wear process on the frictional interface of two bodies in a relative sliding motion induces shape evolution. In many practical industrial applications it is very important to predict the form of wear shape and contact stresses. Usually the simulation of the

contact shape evolution is performed by numerical integration of the modified Archard wear rule expressed in terms of the relative slip velocity and contact pressure.

For cases of monotonic sliding motion the minimization of the wear dissipation power provided the contact pressure distribution and rigid body wear velocities directly without time integration of the wear rule until the steady state is reached, cf. [1, 2, 3, 4]. (The steady state is reached when the contact stress is fixed with respect to the moving contact domain and the rigid body wear velocity is constant in time. The quasi-steady wear state is reached for the stress distribution dependent on a slowly varying contact domain $S_c(t)$. It is important, that in general contact conditions the vector of wear rate is not normal to the contact surface and has tangential component [1]. A fundamental assumption was introduced, namely, *in the steady state the wear rate vector is collinear with the rigid body wear velocity of a sliding body, allowed by boundary constraints.*

In [1] a new idea of the wear rate vector and new form of the wear dissipation power was presented. This new principle was applied in the analysis of the steady wear states in disk and drum brakes.

Next, this approach was extended in [2] by the authors of previous analysis to specification of steady-state contact shapes with account for coupled wear and thermal distortion effects. The wear rule was assumed as a non-linear relation of wear rate to shear stress and relative sliding velocity. The analysis of wear of disks and drum brakes was presented with account for the thermal distortion effect.

In [3] the improved numerical analysis of the thermo-elastic contact coupled with wear process was developed. The coupled thermo-mechanical problem has been numerically treated by applying the operator split technique. For larger values of relative sliding velocities and moving frictional heat fluxes the thermal analysis requires application of upwind technique. Neglecting temperature dependence of material parameters, it was concluded that the contact pressure distribution in the steady-state is not affected by temperature field, but the contact surface shape reached in the wear process strongly depends on the thermal distortion. A brake system with different shoes support was investigated, deriving the contact pressure distribution also for the steady wear state.

In [4] the numerical analysis of coupled thermo-elastic steady wear regimes was presented: wear analysis of a punch translating on an elastic strip and wear induced by a rotating punch on a toroidal surface. The wear and friction parameters were assumed as fixed or temperature dependent. The incremental procedure for temperature dependent parameters was established. Three transverse friction models were discussed accounting for the effect of wear debris motion. It was demonstrated, that the contact pressure distribution depends only on the transformed wear velocities, friction coefficient and wear parameter b , and is not dependent on relative velocity and wear parameter $\tilde{\beta}_i$ (see (1)). The contact conformity condition was defined. In the cases of wear of punch and wear of two bodies the contact pressure distribution in the steady state is governed by the relative rigid body motion induced by wear. On the other hand, when only wear of substrate takes place, the contact pressure

distribution is specified from the contact conformity condition and depends on the elastic moduli of contacting bodies. In literature there are numerous works dealing with fretting problems when in the contact domain both adhesion and slip sub-regions can develop, [5, 6, 7, 8, 9]. The periodic contact sliding was treated in some papers, cf. [10, 11].

The extension of variational method is presented for the case of multi-zone contact problems for steady wear states in [12] which both transient and steady states have been analyzed.

Paper [13] was aimed at extending the results of previous analyses [1, 2, 3, 4] of steady state conditions to cases of periodic sliding of contacting bodies, assuming the existence of cyclic steady state conditions. In the time integration it was assumed that contact pressure distribution is fixed during the semi-cycle and varies discontinuously during sliding reversal in consecutive semi-cycles. The p -version of the finite element method is well suited for solving the contact problems with high accuracy, using the blending technique for approximation of the shape. Wear prediction was made in the brake system by using the averaging technique of results from monotonic motions. The contact pressure distribution has been derived in the discretized form for 3 cases using the Green functions. *Case 1*: wear of both punch and substrate, *Case 2*: wear of substrate only, *Case 3*: wear of punch only.

In particular, the body B_1 can be regarded as a punch translating and rotating relative to the substrate.

Several classes of wear problems can be distinguished and discussed for specified loading and support conditions for two bodies in the relative sliding motion: *Class 1*: The contact zone S_c is fixed on one of sliding bodies (like punch) and translates on the surface of the other body (substrate). The rigid body wear velocity is compatible with the specified boundary conditions. The steady state condition is reached when the contact pressure distribution corresponds to the wear rate proportional to the rigid body velocity [2, 3]. The relative velocity between the bodies is constant in time. *Class 2*: Similarly as for Class 1 the contact zone S_c is fixed but the wear process occurs for periodic sliding motion. *Class 3*: Similarly as for Class 1 the relative velocity is constant, but the load is periodic in time. *Class 4*: Similarly as for Class 2 the contact zone is fixed, but the wear process reaches the steady state for periodic load and periodic sliding motion (for instance in braking process). In the case *Class 1* from minimization of the wear dissipation power it is easy to derive the formulae for contact pressure distribution [2, 3]. Paper [6] presents the analysis of wear for the case of periodic sliding of contacting bodies, assuming cyclic steady state conditions with account for the heat generation at the contact surface. In particular, the body B_1 can be regarded as a punch translating and rotating relative to the substrate B_2 .

It is assumed that strains are small and the materials of the contacting bodies are linearly elastic. In discretization of the contacting bodies for the displacement and temperature determination, the p -version of finite elements was used, [13, 14], assuring fast convergence of the numerical process and providing a high level accuracy of geometry for shape optimization.

The specific examples are related to the analysis of punch wear induced by reciprocal sliding along a rectilinear path on an elastic strip. The external loads acting on the punch are not symmetric. Specifying the steady state contact pressure distributions for an arbitrarily constrained punch, it is noted that the pressure at one contact edge vanishes, and the maximal pressure is reached at the other edge. It was shown that by summarizing pressure values for consecutive semi-cycles, the resulting distribution is obtained that corresponds to a rigid body displacement of punch. The analysis of the same example with account for heat generation demonstrates that the thermal distortion affects essentially the contact shape and the transient contact pressure distribution [15]. However, it was shown that in the steady wear state for reciprocal sliding, the contact pressure reaches the same distribution as that obtained for the case of neglect of heat generation, but the steady state contact shapes are different.

In the case of periodic sliding motion, the steady state cyclic solution should be specified and the averaged pressure in one cycle and the averaged wear velocity can be determined from the averaged wear dissipation in one cycle. In our investigation between the bodies it was assumed that the stick zone no longer exists and the whole contact zone undergoes sliding. The tangential stress can then be directly calculated from the contact pressure and the coefficient of friction.

2. WEAR RULE AND WEAR RATE VECTOR

The modified Archard wear rule [1] specifies the wear rate $\dot{w}_{i,n}$ of the i -th body in the normal contact direction. Following the previous work [1, 2] it is assumed that

$$\dot{w}_{i,n} = \beta_i (\tau_n)^{b_i} \|\dot{\mathbf{u}}_\tau\|^{a_i} = \beta_i (\mu p_n)^{b_i} \|\dot{\mathbf{u}}_\tau\|^{a_i} = \beta_i (\mu p_n)^{b_i} v_r^{a_i} = \tilde{\beta}_i p_n^{b_i} v_r^{a_i}, \quad i = 1, 2 \quad (1)$$

where μ is the friction coefficient, β_i , a_i , b_i are the wear parameters, $\tilde{\beta}_i = \beta_i \mu^{b_i}$, $v_r = \|\dot{\mathbf{u}}_\tau\|$ is the relative tangential velocity between the bodies, constrained by the boundary conditions.

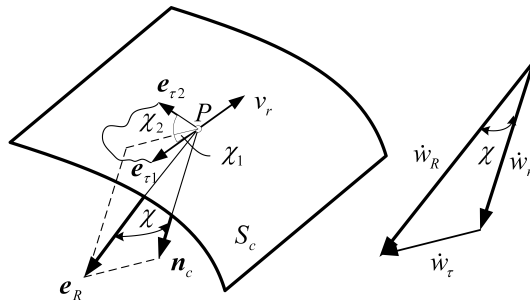


Figure 1. Reference frame and wear rate vectors on the contact surface S_c . Coaxiality rule of $\dot{\mathbf{w}}_R$ and \mathbf{e}_R .

The shear stress at the contact surface is expressed in terms of the contact pressure p_n by the Coulomb friction law $\tau_n = \mu p_n$. In general contact conditions the wear rate vector $\dot{\mathbf{w}}_i$ is not normal to the contact surface and results from the constraints imposed on the rigid body motion of punch B_1 . Introducing the local reference triad

\mathbf{e}_{τ_1} , \mathbf{e}_{τ_2} , \mathbf{n}_c on the contact surface S_c (see Figure 1), where \mathbf{n}_c is the unit normal vector, directed into body B_2 , \mathbf{n}_i is the unit surface normal of the i -th body, \mathbf{e}_{τ_1} is the unit tangent vector coaxial with the sliding velocity and \mathbf{e}_{τ_2} is the transverse unit vector, the wear rate vectors of bodies B_1 and B_2 are

$$\dot{\mathbf{w}}_1 = -\dot{w}_{1,n} \mathbf{n}_c + \dot{w}_{1,\tau_1} \mathbf{e}_{\tau_1} + \dot{w}_{1,\tau_2} \mathbf{e}_{\tau_2}, \quad \dot{\mathbf{w}}_2 = \dot{w}_{2,n} \mathbf{n}_c - \dot{w}_{2,\tau_1} \mathbf{e}_{\tau_1} - \dot{w}_{2,\tau_2} \mathbf{e}_{\tau_2}. \quad (2)$$

The contact traction on S_c can be expressed as follows [3]

$$\mathbf{t}^c = \mathbf{t}_1^c = -\mathbf{t}_2^c = -p_n^\pm \boldsymbol{\rho}_c^\pm, \quad \boldsymbol{\rho}_c^\pm = \mathbf{n}_c \pm \mu \mathbf{e}_{\tau_1} + \mu_d \mathbf{e}_{\tau_2} \quad (3)$$

where $\boldsymbol{\rho}_c^\pm$ specifies the orientation and magnitude of traction \mathbf{t}^c with reference to the contact pressure p_n and μ_d is the transverse friction coefficient. The sign + in (2) corresponds to the case when the relative tangential velocity is $\dot{\mathbf{u}}_\tau = \dot{\mathbf{u}}_\tau^{(2)} - \dot{\mathbf{u}}_\tau^{(1)} = -\|\dot{\mathbf{u}}_\tau\| \mathbf{e}_{\tau_1} = -v_r \mathbf{e}_{\tau_1}$ with the corresponding shear stress acting on the body B_1 along $-\mathbf{e}_{\tau_1}$. The fundamental coaxially rule was stated by Páczelt and Mróz [1, 2, 3, 4], namely: in the steady state the wear rate vector $\dot{\mathbf{w}}_R$ is collinear with the rigid body wear velocity vector $\dot{\boldsymbol{\lambda}}_R$, thus

$$\dot{\mathbf{w}}_R = \dot{w}_R \mathbf{e}_R, \quad \mathbf{e}_R = \frac{\dot{\boldsymbol{\lambda}}_R}{\|\dot{\boldsymbol{\lambda}}_R\|} = \frac{\dot{\boldsymbol{\lambda}}_F + \dot{\boldsymbol{\lambda}}_M \times \Delta \mathbf{r}}{\|\dot{\boldsymbol{\lambda}}_F + \dot{\boldsymbol{\lambda}}_M \times \Delta \mathbf{r}\|}, \quad (4)$$

where $\Delta \mathbf{r}$ is the position vector. The coaxiality rule is illustrated in Figure 1. The normal and tangential wear rate components now are

$$\dot{w}_n = \dot{w}_R \cos \chi, \quad \dot{w}_\tau = \dot{w}_R \sin \chi = \dot{w}_n \tan \chi \quad (5)$$

where χ is the angle between \mathbf{n}_c and \mathbf{e}_R . The wear rate components in the tangential directions are

$$\dot{w}_{\tau_1} = \dot{w}_R \sin \chi \cos \chi_1, \quad \dot{w}_{\tau_2} = \dot{w}_R \sin \chi \sin \chi_1 \quad (6)$$

where the angle χ_1 is formed between the projection of $\dot{\mathbf{w}}_R$ on S_c and \mathbf{e}_{τ_1} as shown in Figure 1. Let us note that the sliding velocity $v_r = \|\dot{\mathbf{u}}_\tau\|$ is specified from the boundary conditions and the wear velocity vectors $\dot{\boldsymbol{\lambda}}_F$ and $\dot{\boldsymbol{\lambda}}_M$ should be determined from the solution of a specific problem. In the analysis of sliding wear problems the elastic term of relative sliding velocity is usually neglected.

3. STEADY STATE CONDITIONS FOR MONOTONIC MOTION

It has been shown in [1, 2] that the steady state conditions for monotonic motion can be obtained from minimization of the wear dissipation power subject to equilibrium constraints for body B_1 . The wear dissipation power for the case of wear of two bodies equals

$$D_w = \sum_{i=1}^2 \left(\int_{S_c} (\mathbf{t}_i^c \cdot \dot{\mathbf{w}}_i) \, dS \right) = \sum_{i=1}^2 C_i. \quad (7)$$

The global equilibrium conditions for the body B_1 can be expressed as follows

$$\mathbf{f} = - \int_{S_c} \boldsymbol{\rho}_c^\pm p_n^\pm dS + \mathbf{f}_0 = \mathbf{0}$$

$$\mathbf{m} = - \int_{S_c} \Delta \mathbf{r} \times \boldsymbol{\rho}_c^\pm p_n^\pm dS + \mathbf{m}_0 = \mathbf{0}$$
(8)

where \mathbf{f}_0 and \mathbf{m}_0 denote the resultant force and moment acting on the body B_1 . The formula for contact pressure at steady wear state can be found in papers [1, 2, 4] and for multi-contact zone cases the contact pressure's formula can be found in [12].

4. WEAR DISSIPATION IN PERIODIC MOTION AND SUMMED PRESSURE IN PERIODIC STEADY WEAR STATE

In this section we shall analyse the wear process induced by the reciprocal strip translation. It is assumed that only the punch undergoes wear (see Figure 2), that is in our case $\tilde{\beta}_1 \neq 0, \tilde{\beta}_2 = 0$.

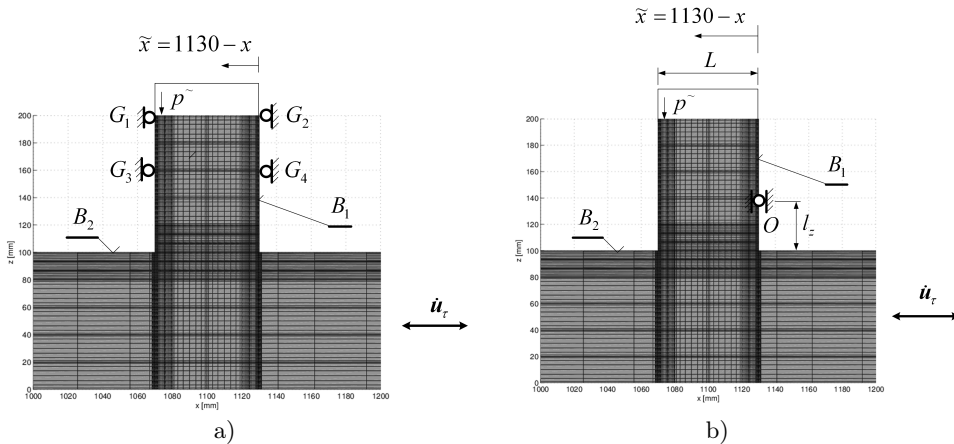


Figure 2. Periodic sliding on the contact interface between punch and strip. The number of finite elements in body 1 along the x direction is 8, and in vertical z direction is 7. The lines are drawn through the Lobatto integral coordinates.

In the analysis the contact pressure distribution is assumed as fixed during semi-cycle and varies discontinuously during sliding reversal in consecutive semi-cycle. The temperature distribution varies continuously during each cycle period [15]. The coupled thermo-mechanical problem was solved by the operator split technique [16]. The wear effect is calculated incrementally by applying the Archard type wear rule (1). The wear is accumulated at the end of half period of motion, so the contact pressure is fixed (at the iteration level), and the transient heat conduction problem is next solved for the given temperature field at the beginning of half period.

The steady state contact pressure distribution in the wear process induced by periodic sliding does not depend on the value of wear factor $\tilde{\beta}_1$ nor generated temperature field, but the wear induced contact surface shape is strongly affected.

During the steady periodic response the wear increment accumulated during one cycle should be compatible at each point $x \in S_c$ with the rigid body punch motion.

The wear dissipation work for periodic motion is

$$E_w = \frac{1}{2} \sum_{i=1}^2 \int_0^{T_*/2} \left(\int_{S_c^{(i)}} (\mathbf{t}_i^{c+} \cdot \dot{\mathbf{w}}_i^+) dS \right) d\tau + \frac{1}{2} \sum_{i=1}^2 \int_{T_*/2}^{T_*} \left(\int_{S_c^{(i)}} (\mathbf{t}_i^{c-} \cdot \dot{\mathbf{w}}_i^-) dS \right) d\tau \tag{9}$$

where \mathbf{t}_i^{c+} , \mathbf{t}_i^{c-} is the contact traction vector and $\dot{\mathbf{w}}_i^+$, $\dot{\mathbf{w}}_i^-$ is the wear velocity of the i -th body in the progressive and reciprocal motion direction, T_* is the period of sliding motion, $T_* = 2\pi/\omega$.

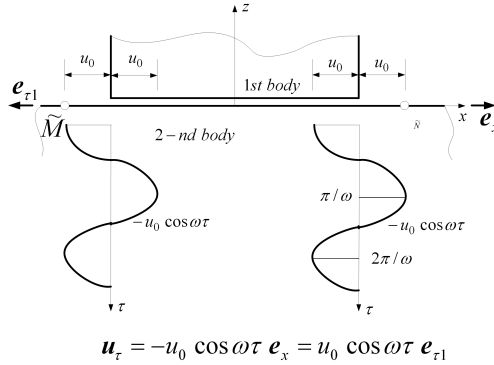


Figure 3. The wear process occurring on the contact interface between punch and strip translating with the relative velocity $v_r = u_0 \omega \sin \omega \tau$, $\mathbf{u}_\tau = -v_r \mathbf{e}_{\tau 1}$. The segment $\tilde{M}\tilde{N}$ of the substrate takes part in the wear process.

In our case the tangential velocity of body 2 is (see Figure 3):

$$\dot{\mathbf{u}}_\tau = \dot{\mathbf{u}}_\tau^{(2)} - \dot{\mathbf{u}}_\tau^{(1)} = u_0 \omega \sin \omega \tau \mathbf{e}_x = -u_0 \omega \sin \omega \tau \mathbf{e}_{\tau 1} = -v_r \mathbf{e}_{\tau 1} \tag{10}$$

with the corresponding shear stress acting on the body B_1 along $-\mathbf{e}_{\tau 1}$. The integral of the relative velocity between the bodies is

$$\int_0^{T_*/2} v_r d\tau = \int_{T_*/2}^{T_*} v_r d\tau = 2u_0. \tag{11}$$

In view of the wear rule (1) the wear dissipation for the punch of Figure 2 is

$$E_w = \frac{1}{2} \sum_{i=1}^1 \int_0^{T_*/2} \left(\int_{S_c^{(1)}} p_n^+ \dot{w}_{1,n}^+ dS \right) d\tau + \frac{1}{2} \sum_{i=1}^1 \int_{T_*/2}^{T_*} \left(\int_{S_c^{(1)}} p_n^- \dot{w}_{1,n}^- dS \right) d\tau \tag{12}$$

and for $\tilde{\beta}_1 \neq 0$, $\tilde{\beta}_2 = 0$, $a_1 = b_1 = 1$ there is

$$\frac{E_w}{2u_0 \tilde{\beta}_1} = \int_{S_c^{(1)}} \{ (p_n^+)^2 + (p_n^-)^2 \} dS = \frac{E_w^+}{2u_0 \tilde{\beta}_1} + \frac{E_w^-}{2u_0 \tilde{\beta}_1}. \quad (13)$$

In the steady wear state E_w reaches a minimum value. Let us note that p_n^+ and p_n^- are not uniformly distributed at the contact interface. Taking the coordinate $\tilde{x} = 1130 - x$ it can be stated that $p(x) = p(\tilde{x})$ during the consecutive semi-cycles of reciprocal sliding.

It is very important, that during the steady wear periodic state the wear increment accumulated during one cycle should be compatible at each point $p(x) = p(\tilde{x})$ with the rigid body punch motion. The main idea for derivation of the wear increment and summed pressure for 2D system with cylindrical contact surface is collected in the Appendix.

Assume the rigid body wear velocities for left (-) and right (+) directions of the substrate in the following

$$\dot{\lambda}_F^- = -\dot{\lambda}_F^- \mathbf{e}_z, \quad \dot{\lambda}_M^- = \dot{\lambda}_M^- \mathbf{e}_y, \quad \dot{\lambda}_F^+ = -\dot{\lambda}_F^+ \mathbf{e}_z, \quad \dot{\lambda}_M^+ = -\dot{\lambda}_M^+ \mathbf{e}_y. \quad (14)$$

Thus the velocities at an arbitrary point at punch, Figure 2b, are $-(\dot{\lambda}_F^+ + \dot{\lambda}_M^+ \tilde{x})\mathbf{e}_z$, or $-(\dot{\lambda}_F^- - \dot{\lambda}_M^- \tilde{x})\mathbf{e}_z$. The displacements resulting from this velocities are

$$-(\Delta\lambda_F^+ + \Delta\lambda_M^+ \tilde{x})\mathbf{e}_z \quad \text{and} \quad -(\Delta\lambda_F^- - \Delta\lambda_M^- \tilde{x})\mathbf{e}_z \quad (15)$$

where

$$\Delta\lambda_{F,M}^+ = \int_0^{T_*/2} \dot{\lambda}_{F,M}^+ dt, \quad \Delta\lambda_{F,M}^- = \int_{T_*/2}^{T_*} \dot{\lambda}_{F,M}^- dt.$$

Thus, the total wear accumulated during one sliding cycle is

$$\Delta w_n = \Delta w_n^+ + \Delta w_n^- = (\Delta\lambda_F^- + \Delta\lambda_F^+) - (\Delta\lambda_M^- - \Delta\lambda_M^+) \tilde{x} \quad (16)$$

This value of wear can be calculated from the wear law supposing $\tilde{\beta}_1 \neq 0$, $\tilde{\beta}_2 = 0$, $a_1 = b_1 = 1$, thus according to (A.12)

$$\Delta w_n = \Delta w_n^+ + \Delta w_n^- = Q (p_n^+ + p_n^-) = 2 Q p_m = Q p_\Sigma \quad (17)$$

where

$$p_m = (p_n^+ + p_n^-)/2 = p_\Sigma/2 \quad \text{and} \quad Q = \tilde{\beta}_1 \int_0^{T_*/2} \|\dot{\mathbf{u}}_\tau\| dt.$$

Comparing (16) and (17), it is seen that the distribution of the sum of contact pressure values of consecutive semi-cycles must be a linear function of position, thus

$$p_m = p_m^C + p_m^L \tilde{x} \quad (18)$$

that is

$$\Delta w_n = \Delta w_n^+ + \Delta w_n^- = (\Delta \lambda_F^- + \Delta \lambda_F^+) - (\Delta \lambda_M^- - \Delta \lambda_M^+) \tilde{x} = \tilde{\beta}_1 \int_0^{T_*} \|\dot{\mathbf{u}}_\tau\| dt \cdot 2 (p_m^C + p_m^L \tilde{x}),$$

where $\Delta \lambda_{F,M}^\pm$ is the increment of rigid body wear velocities in the half period time. Using the equilibrium equations for summed loads, the summed pressure for the steady wear state is determined as

$$p_m^C = \frac{F_0}{S_c} - \frac{3F_0(-L + 2\tilde{x}_F)}{L S_c}, \quad p_m^L = \frac{6F_0(-L + 2\tilde{x}_F)}{L^2 S_c}, \tag{19}$$

$$p_\Sigma = 2p_m = p_n^+ + p_n^- = 2(p_m^C + p_m^L \tilde{x})$$

where \tilde{x}_F is the coordinate of the resultant load $F_0 = F_0(p^\sim)$. For non-negativity of p_m there should be $L/2 \leq \tilde{x}_F \leq 2L/3$. At $\tilde{x}_F = L/2$ the results of [5, 6] are obtained. Here S_c is the area of contact zone.

The wear increment in one period equals (note that the contact pressure is fixed in half period)

$$\Delta w_{1,n} = \tilde{\beta}_1 [p_n^+ + p_n^-] (u_0 \omega) \int_0^{T_*/2} |\sin \omega \tau| d\tau \tag{20}$$

which using (11) provides the simple relation

$$\Delta w_{1,n} = \tilde{\beta}_1 [p_n^+ + p_n^-] 2u_0 = Q p_\Sigma \tag{21}$$

where $Q = \tilde{\beta}_1 2u_0$ and the averaged wear rate in one period equals

$$\bar{w}_{1,n} = \frac{\Delta w_{1,n}}{T_*} = \frac{\tilde{\beta}_1 [p_n^+ + p_n^-]}{T_*} 2u_0. \tag{22}$$

If the rigid body wear velocity $\lambda_M^+ = \lambda_M^- = 0$, (at the supports see Figure 2a), then in the steady periodic wear regime the uniform wear increment is accumulated during full cycle at each point of the contact zone and the following condition should be satisfied

$$p_n^+ + p_n^- = 2p_m = const. \tag{23a}$$

Remark: If $a_1 = 1$ $b = b_1 \neq 1$ then in a periodic steady state there must be

$$(p_n^+)^b + (p_n^-)^b = 2(p_m)^b = const2 \tag{23b}$$

where p_m is the contact pressure at the centre of the punch contact zone, at $x = 1100$. Because at $x = 1070$, $p_n^- = 0$ the contact pressure is

$$p_n^+(x = 1070) = 2^{1/b} p_m \tag{23c}$$

At the other perimeter at $x = 1130$ it holds that $p_n^+ = 0$ and

$$p_n^-(x = 1130) = 2^{1/b} p_m. \tag{23d}$$

Performing time integration of the wear rate rule for $a_1 = b_1 = 1$ during the one half period, the wear increment is calculated in the following way

$$\Delta w_{1,n}^{(j)} = \int_{t_p}^{t_p+T_*/2} \tilde{\beta}_1 p_n^{(j)}(\tau) u_0 \omega |\sin \omega \tau| d\tau \cong \tilde{\beta}_1 p_n^{(j)}(t_p + T_*/2) \int_0^{T_*/2} u_0 \omega |\sin \omega \tau| d\tau \tag{24}$$

where t_p is the time of start of the half period, $p_n^{(j)} = p_n^{(j)}(t_p + T_*/2)$.

The accumulated wear at the end of half period at the iterational step j equals

$$w_{1,n}^{(j)}(t_p + T_*/2) = w_{1,n}(t_p) + \Delta w_{1,n}^{(j)} = w_{1,n}(t_p) + \tilde{\beta}_1 p_n^{(j)} 2 u_0 \tag{25}$$

or in other notation

$$w_{1,n}^{(j)}(t_p + T_*/2) = {}^{t_p+T_*/2}w_{1,n}^{(j)} = {}^{t_p}w_{1,n} + \Delta w_{1,n}^{(j)}. \tag{26}$$

This j type iterational process is repeated until $j = J$ when the following convergence criterion for contact shape is satisfied, thus

$$e_w = 100 \left| \int_{S_c} ({}^{t_p}g + \Delta w_{1,n}^{(j)}) dS - \int_{S_c} ({}^{t_p}g + \Delta w_{1,n}^{(j-1)}) dS \right| / \int_{S_c} ({}^{t_p}g + \Delta w_{1,n}^{(j-1)}) dS \leq \leq 0.01. \tag{27}$$

Here ${}^{t_p}g$ is the initial gap at the beginning of the half period.

Remark: If $a_1 = 1, b = b_1 \neq 1$ then the wear increment during the one half period is

$$\Delta w_{1,n}^{(j)} = \tilde{\beta}_1 \left(p_n^{(j)} \right)^b 2 u_0. \tag{28}$$

In practical calculations the iterative scheme of contact pressure and wear shape correction can be modified after k half cycles, so we can write

$${}^{t_p+kT_*/2}w_{1,n} = {}^{t_p}w_{1,n} + k\Delta w_{1,n}^{(j)}. \tag{29}$$

In our case choosing the extrapolation factor k in the following way:

for the numerical steps $n \leq 50, k = 1$; for $50 < n \leq 100, k = 5$ and when $n > 100$, then $k = 10$.

The number of the half periods in the interval then is

$$\begin{aligned} 50 \leq n \leq 100 & \quad n_{hp} = 50 + (n - 50) \cdot 5, \\ n \geq 100 & \quad n_{hp} = 300 + (n - 100) \cdot 10. \end{aligned} \tag{30}$$

5. EXAMPLES

5.1. Example 1: wear of punch induced by periodic sliding of the substrate.

Let us analyze the wear of punch (Body 1) shown in Figure 2. We would like to examine two types of constraints, one when the punch can move only in the vertical direction (see Figure 2a), and second when the punch has additional rotation around a pin (see Figure 2b). The point M in the punch has coordinates: $x = 1070, z = 100$.

The following geometric parameters are assumed: the punch width is $L = 60$ mm, its height is $h = 100$ mm, the thickness of punch and strip is $t_{th} = 10$ mm.

The wear parameters are: $\tilde{\beta}_1 = 1.25\pi \cdot 10^{-8}$, $\tilde{\beta}_2 = 0$, $a_1 = 1$, $b_1 = 1$, the coefficient of friction is $\mu = 0.25$. The horizontal displacement of the substrate is $u_\tau = -u_0 \cos \omega \tau$, where $u_0 = 1.5$ mm, $\omega = 10$ rad/s, τ is the time. The material parameters are presented in Table 1.

Table 1. Mechanical parameters of two materials

	Young modulus MPa	Poisson ratio	Material density kg/m ³
Material 1 (steel)	2.0×10^5	0.30	7800
Material 2 (composite)	1.3×10^5	0.23	846

The upper parts of the punch and strip are assumed to be made of the same materials, (Material 1, see Table 1). The lower punch portion of height 20 mm is characterized by the parameters of Material 2, see Table 1).

5.1.1. *Symmetric load.* The punch is loaded on the upper boundary $z = 200$ mm by the uniform pressure $p^\sim = 16.666$ MPa corresponding to the resultant vertical force $F_0 = 10.0$ kN.

The wear parameter is $b = 1$. This problem was analyzed with no account for heat generation in [13], and with account for heat generation in [15]. The numerical results of paper [13] are collected in Table 2 and in Figure 4 for $l_z = 40$ mm.

Let us denote the contact pressure for the punch of Figure 2a by $p_n(\dot{\lambda}_F)$, for the punch of Figure 2b for $l_z = 20$ and $l_z = 40$ by $p_n(\dot{\lambda}_F, \dot{\lambda}_M, l_z = 20)$ and $p_n(\dot{\lambda}_F, \dot{\lambda}_M, l_z = 40)$, respectively.

After time integration of the Archard wear rule the contact pressures at the point M are collected in Table 2 versus the numerical time steps n for different punch constraints.

It is clear that convergence to the pressure 33.333 MPa proceeds for all cases of constraints. In the case $l_z = 40$ mm the evolution of the shape and contact pressure is demonstrated in Figure 4.

Because the loading distribution is symmetric, the distribution of the pressure and shape is also symmetric. The optimal solutions (marked by ...) corresponds to the monotonic relative motion. Also it is observed, that after $n \geq 1500$, the pressure distribution does not change and the contact profile is preserved, moving along the punch axis like a rigid line. In this case $\Delta\lambda_F^- = \Delta\lambda_F^+$, $\Delta\lambda_M^- = \Delta\lambda_M^+$, that is in the wear process the accumulated punch wear is the same during each period, the pressure distribution is $p_m = p_m^C = p^\sim$, and the summed pressure $p_\Sigma = p_n^+ + p_n^- = 2p_m = 2p^\sim$.

Table 2. Mechanical parameters of two materials

n	no. of half period n_{hp}	$p_n(\dot{\lambda}_F)$	$p_n(\dot{\lambda}_F, \dot{\lambda}_M, \ell_z = 20)$	$p_n(\dot{\lambda}_F, \dot{\lambda}_M, \ell_z = 40)$
1	1	$0.14841933E + 03$	$0.10087461E + 03$	$0.13837226E + 03$
50	50	$0.11470731E + 03$	$0.87926576E + 02$	$0.10745308E + 03$
100	300	$0.69721237E + 02$	$0.57950338E + 02$	$0.67301651E + 02$
200	1300	$0.46654939E + 02$	$0.41195687E + 02$	$0.46039272E + 02$
300	2300	$0.40931186E + 02$	$0.36462991E + 02$	$0.40376545E + 02$
400	3300	$0.37501127E + 02$	$0.35565594E + 02$	$0.37620120E + 02$
500	4300	$0.36392637E + 02$	$0.34548895E + 02$	$0.36225178E + 02$
600	5300	$0.35307986E + 02$	$0.33997961E + 02$	$0.35262677E + 02$
700	6300	$0.34768942E + 02$	$0.33713578E + 02$	$0.34696425E + 02$
800	7300	$0.34330459E + 02$	$0.33562469E + 02$	$0.34205548E + 02$
900	8300	$0.34008547E + 02$	$0.33456073E + 02$	$0.33905548E + 02$
1000	9300	$0.33529593E + 02$	$0.33394566E + 02$	$0.33758886E + 02$
1100	10300	$0.33568957E + 02$	$0.33358149E + 02$	$0.33445945E + 02$
1500	15300	$0.33403968E + 02$	$0.33307992E + 02$	$0.33345945E + 02$
1700	16300	$0.33372654E + 02$	$0.33304515E + 02$	$0.33335945E + 02$

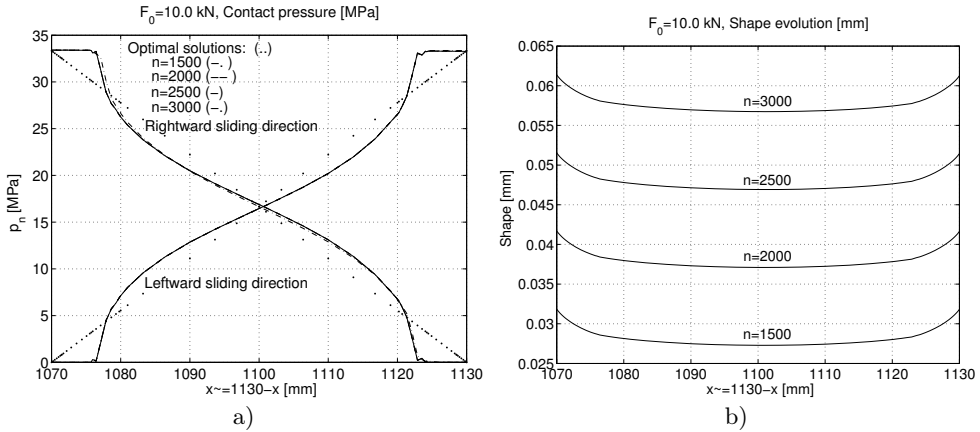


Figure 4. a) Contact pressure at different time steps and sliding directions, b) Evolution of shape of punch for reciprocal motion, $l_z = 40$ mm, the load $p \sim = 16.666$ MPa and resultant force's coordinate is $\tilde{x}_F = L/2$.

The wear parameter is $b \neq 1$. Let us investigate the periodic wear process at $\tilde{\beta}_1 = 1.25\pi\mu^{0.2}10^{-8}$, $\tilde{\beta}_2 = 0$, and $a_1 = 1$, $b = b_1 = 1.2$, $\mu = 0.25$. The displacement of body 2 is: $u = -u_0 \cos\omega\tau$, where $u_0 = 1.5$ mm, $\omega = 10$ rad/s.

Performing time integration of (1) we see that after the number of half periods ($n \geq 1100$) $n_{hp} \geq 10300$ the wear process reaches its steady state. In this case the value $2(p_m)^b = \text{const}2 = 61.48$, where $p_m = 17.369$ MPa, $p_n^+ = p_n^- = 30.948$ MPa.

Comparing the contact pressure and shape of punch in the steady state, we see that the pressure for $b = 1.2$ at the border of contact zone is lower than that for $b = 1$, and at the centre of the punch the pressure is higher. The contact shape for $b = 1.2$ is shown by the curve placed above that predicted for $b = 1$ cf. Figure 5. On the other hand, for the case $b = 0.8$, the contact pressure is higher than that for $b = 1$ at the perimeters points, and the contact shape curve is lower than that for $b = 1$. It also is noted that for the wear parameter value $\tilde{\beta}_1 = 1.25 \pi \mu^{-0.2} 10^{-8}$ which is smallest, the steady state is reached at $n = 2500$. Then the pressure in the centre is $p_m = 15.886$ MPa, the value $2(p_m)^b = const_2 = 18.274$, the pressure at the perimeter points are $p_n^+ = p_n^- = 37.806$ MPa and calculated value is $(p_n^+)^b = (p_n^-)^b = 18.283$. The calculation error $100 \left[(p_n^+)^b - 2(p_m)^b \right] / 2(p_m)^b = 0.0055$ is very small. Also $p_n^+(x = 1070) = 2^{1/b} p_m$, $p_m = 15.8954$ MPa.

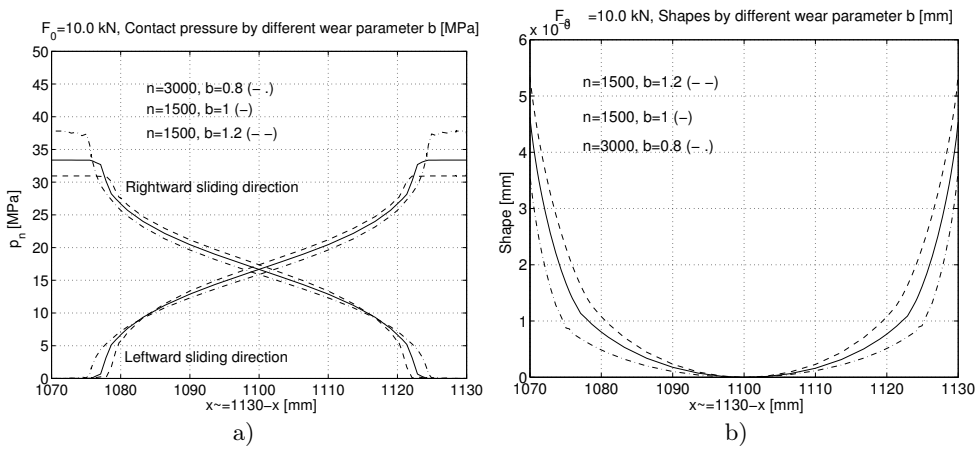


Figure 5. The effect of the wear parameter b on the periodic steady wear state, a) distribution of the contact pressure, b) contact shape of punch. (maximal shape function ordinate is $6 \mu\text{m}$).

5.1.2. *Non-symmetric load.* Let us now analyze the case of eccentric load when the resultant vertical force equals $F_0 = 10$ kN and its position coordinate is in the interval $L/2 = 30 \leq \tilde{x}_F \leq 2L/3 = 40$.

The first case. The pressure $p \sim 20$ MPa is applied in the interval $10 \leq \tilde{x} \leq 60$. The resultant position coordinate is $\tilde{x}_F \leq 35$ mm. This load case represents the variant 2. The results are presented in Figures 6. Figures 6a,c demonstrate the pressure at different numbers of half cycles and Figures 6b,d present the summed pressure $p_\Sigma = p_n^+ + p_n^- = 2p_m$. It is seen that after $n \geq 1000$ the summed pressure practically does not change. Its distribution is presented by a linear function. A small oscillation is observed because in the solution of the contact problem the positional technique has not been used [17]. In our calculation it is required, that the gap in point $x = 1130$ mm of the contact zone is fixed during consecutive iterations. The contact shapes are shown in Figure 7a,b. If the pin height is $l_z = 20$ mm, the obtained pressure

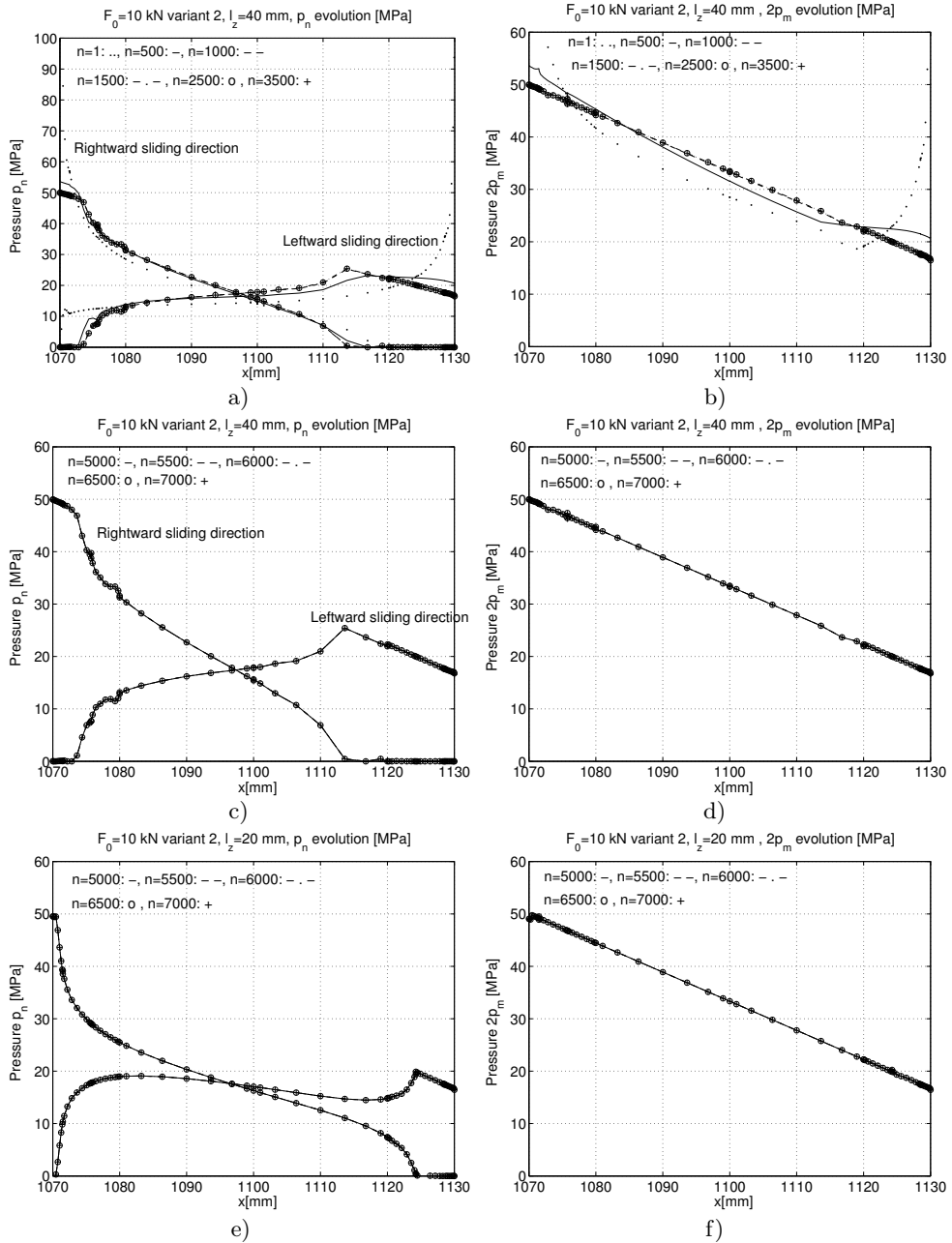


Figure 6. Periodic wear process for the load variant 2: a), c), e) evolution of pressures, b), d), f) evolution of the summed pressure $p_\Sigma = 2p_m$.

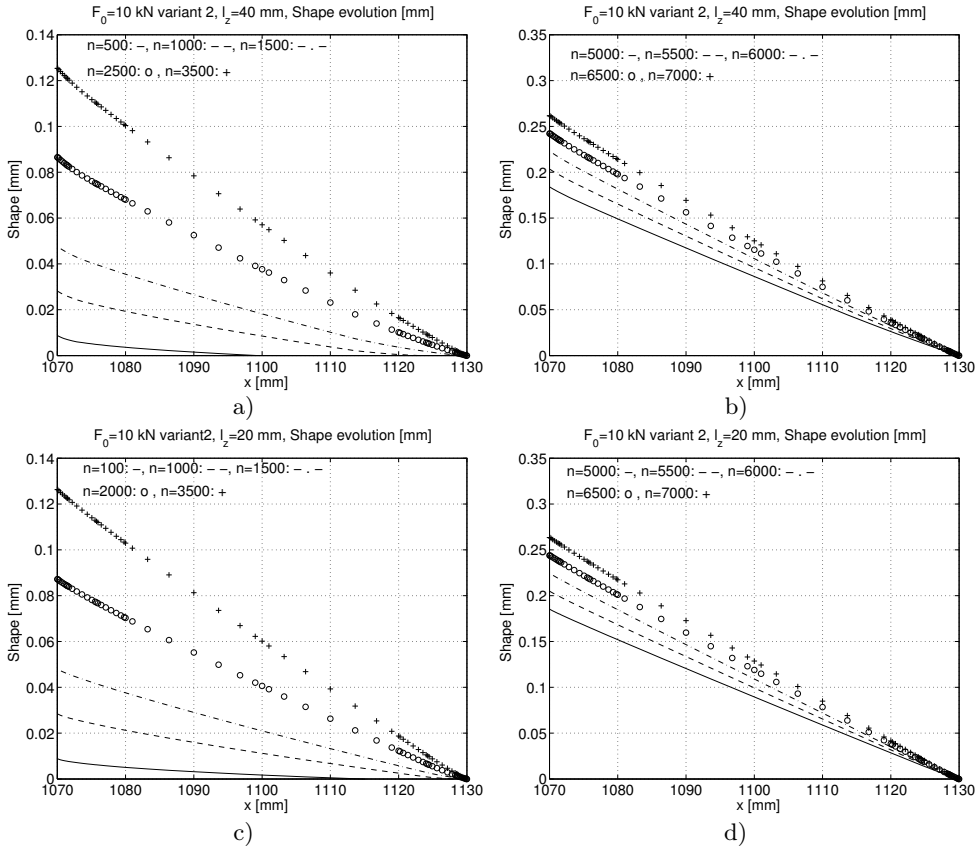


Figure 7. Evolution of contact shapes for periodic wear process at the load variant 2: a), c), $n = 100 - 3500$, b), d) $n = 5000 - 7000$.

distribution is shown in Figure 6e, and the summed pressure is shown in Figure 6f. The contact shapes are presented in Figures 7c,d. Because in the equation for summed pressure (19) the height l_z is absent, the summed pressures for $l_z = 20$ mm, and $l_z = 40$ mm must be the same. This fact is also demonstrated by the numerical time integration results (compare Figures 6d and 6f).

The second case. The pressures $p_1^{\sim} = 25$ MPa, $p_2^{\sim} = 12.5$ MPa act in the intervals: $p_1^{\sim}: 30 \leq \tilde{x} \leq 60$, $p_2^{\sim}: 10 \leq \tilde{x} \leq 30$. The resultant vertical force is $F_0 = 10$ kN, the resultant position coordinate is $\tilde{x}_F \leq 37.5$ mm. This load case corresponds to variant 3.

The pressure distribution can be seen in Figures 8a,c the summed pressure in Figures 8b,d. The maximum of the pressure is higher than before, because the resultant coordinate \tilde{x}_F is larger with 2.5 mm. In this case the high pressure at the border of contact domain very quickly decreases. For the periodic steady wear state the maximum of the pressure can be calculated from the summed pressure, which is predicted without time integration! For each half period the contact gap has been specified.

For the rightward sliding direction the maximum of the contact pressure is on the left border of contact zone, but for the leftward sliding direction the maximum is in the interior of the contact zone.

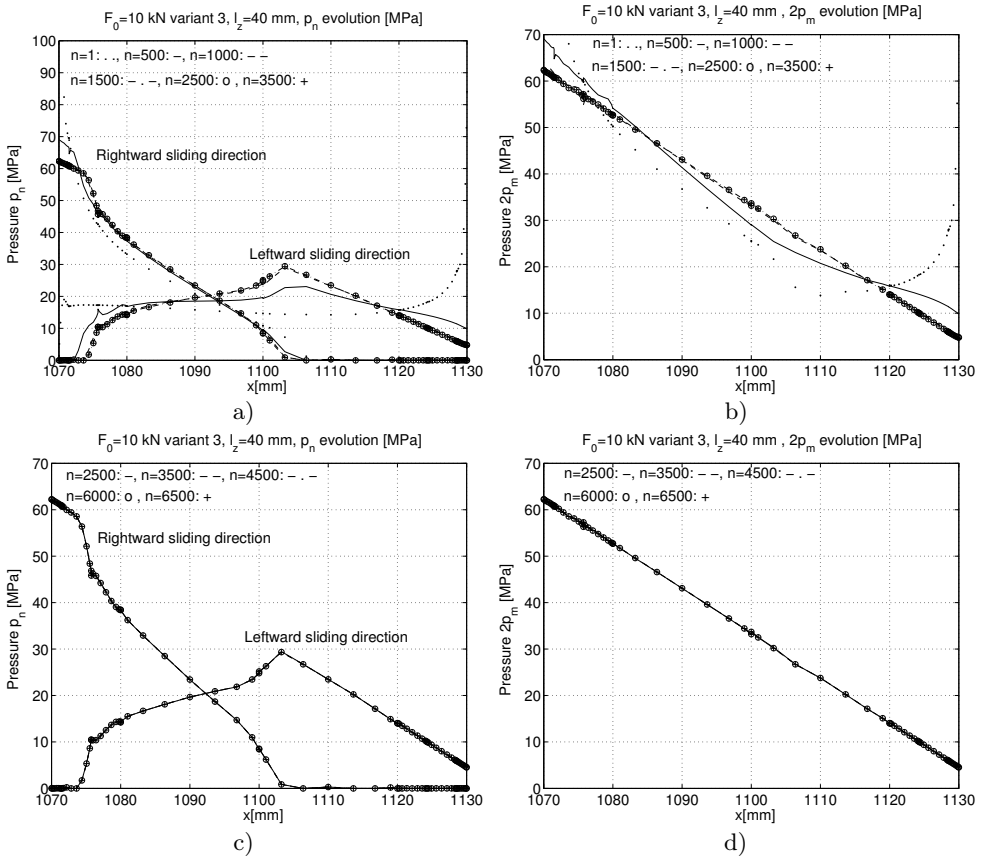


Figure 8. Periodic wear process for the load variant 3: a), c) evolution of the pressures, b), d) evolution of the summed pressure $p_\Sigma = 2p_m$.

The wear is larger for the loading variant 3 than for the variant 2. However, the character of wear process is the same. The shape evolution is presented in Figures 9a,b.

5.2. Example 2: Periodic steady wear state for brake system. Consider the periodic tangential relative displacement of body B_2 (disk) with respect to body B_1 in the direction e_τ

$$\mathbf{u}_\tau = u_0 \cos \omega T \mathbf{e}_\tau \quad (31)$$

where u_0 and ω are the amplitude and angular velocity of the motion.

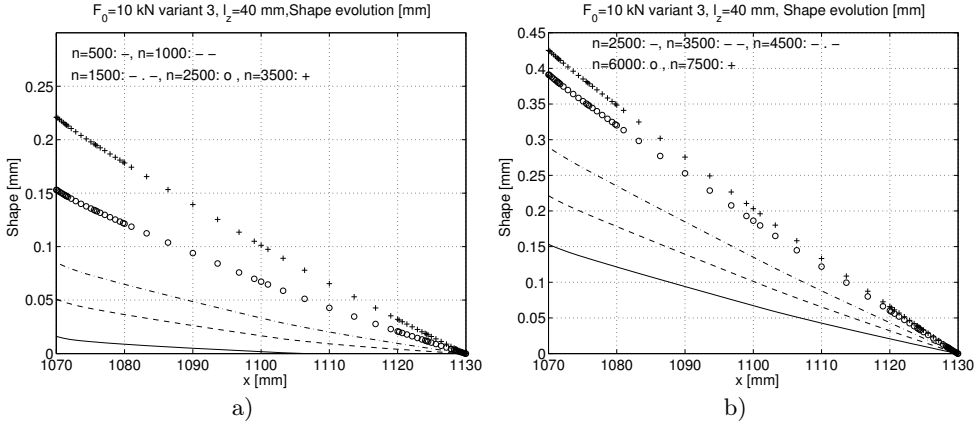


Figure 9. Evolution of the contact shapes for periodic wear process at the load variant 3: a) $n = 500 - 3500$, b) $n = 2500 - 7500$.

The relative sliding velocity and the cycle period are

$$\dot{\mathbf{u}}_{\tau} = -u_0 \omega \sin \omega \tau \mathbf{e}_{\tau} = -v_{\tau} \mathbf{e}_{\tau} \quad (32a)$$

$$v_{\tau} = \|\dot{\mathbf{u}}_{\tau}\| = |\omega u_0 \sin \omega \tau| = |v_0 \sin \omega \tau|, \quad T_* = \frac{2\pi}{\omega}, \quad v_0 = \omega u_0 \quad (32b)$$

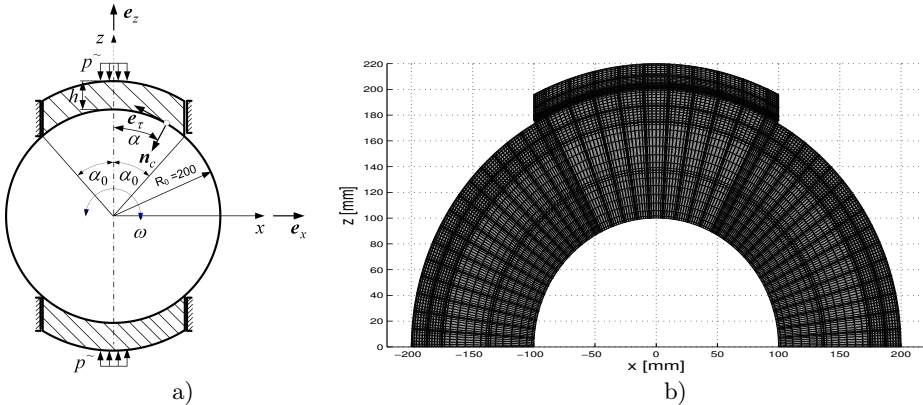


Figure 10. Brake system, a) $\alpha_0 = 30^\circ$, the resultant force $F_0 = 10$ kN, thickness of bodies $t_{th} = 10$ mm; b) finite element mesh of the half part of the system, number of contact elements are 11, number of elements in radial direction is 4, the p -version of the finite elements have $p = 8$ polynomial degree. The liners are drawn through the Lobatto integral coordinates.

The shoe (body B_1) is loaded by the force $\mathbf{F}_0 = -F_0 \mathbf{e}_z$. In our case $F_0 = 10$ kN. The Lagrangian multiplier $\dot{\lambda}_F$ represent the vertical wear velocity.

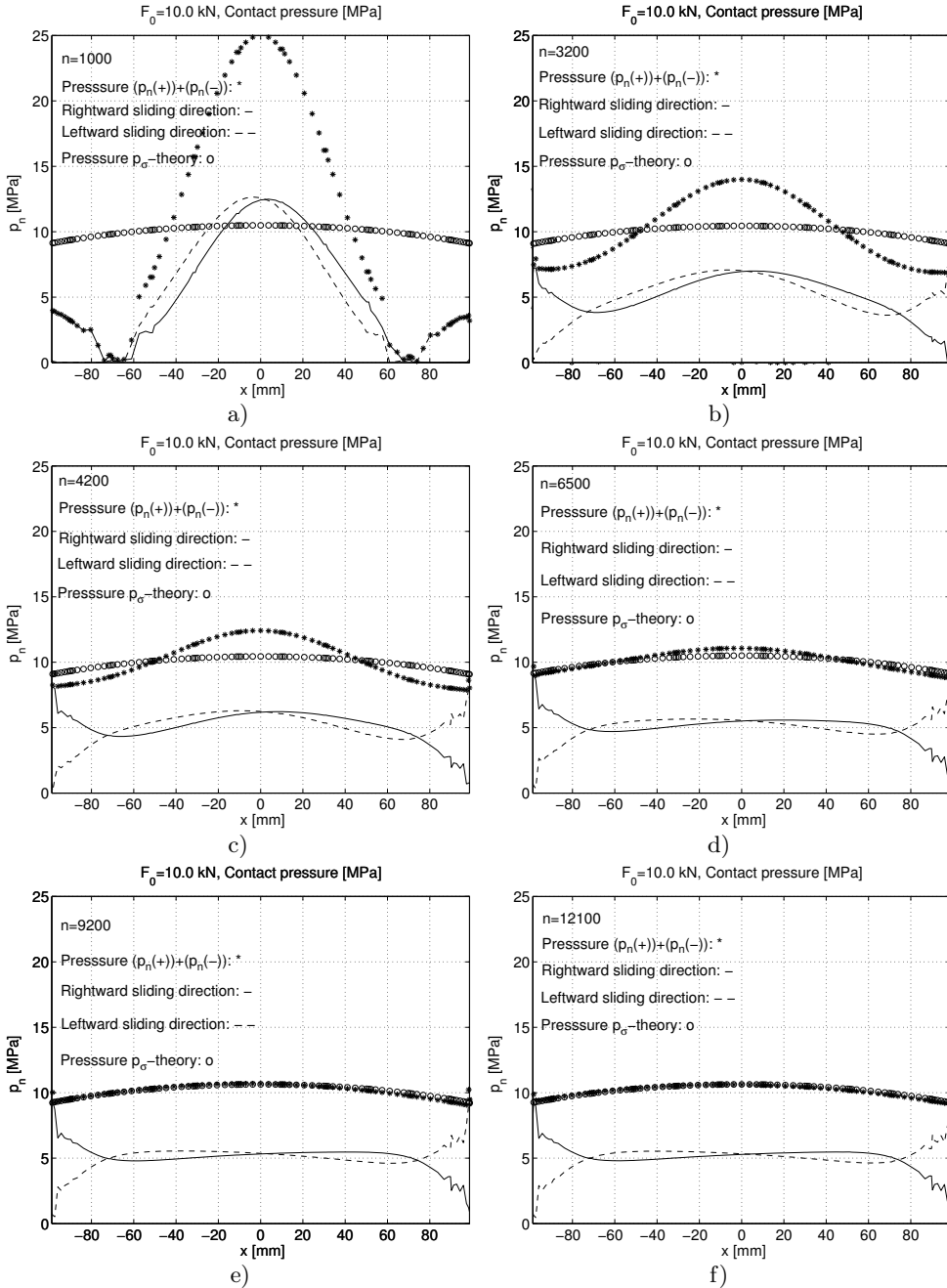


Figure 11. Contact pressure and summed pressure ($p_\Sigma = p_\sigma - theory$) distribution at different time steps.

It is easy to calculate the average normal wear rate for body 1. (The normal wear vector is $\dot{\mathbf{w}}_{1,n} = -\dot{w}_{1,n} \mathbf{n}_c$)

$$\bar{\dot{w}}_{1,n} = \frac{1}{T_*} \int_0^{T_*} \tilde{\beta}_1 p_n^b v_r^{a_1} d\tau = \frac{\tilde{\beta}_1 p_n^b}{T_*} \int_0^{T_*} v_r^{a_1} d\tau = \tilde{\beta}_1 p_n^b \bar{v}_r^{a_1} \quad (33)$$

The vertical average wear rate is

$$\bar{\dot{w}}_R = \bar{\dot{w}}_{1,n} / \cos \alpha \quad (34)$$

In view of (32)-(34), the average vertical wear rate in one period equals

$$\bar{\dot{w}}_R = \frac{1}{\cos \alpha} \frac{\tilde{\beta}_1 [p_n^{+b} + p_n^{-b}]}{T_*} (u_0 \omega)^{a_1} \int_0^{T_*/2} |\sin \omega \tau|^{a_1} d\tau \quad (35a)$$

which for $a_1 = b = 1$ provides the relation

$$\bar{\dot{w}}_R = \frac{1}{\cos \alpha} \frac{\tilde{\beta}_1 [p_n^+ + p_n^-]}{T_*} 2u_0, \quad \Delta w_R = \bar{\dot{w}}_R T_* = \frac{1}{\cos \alpha} (p_n^+ + p_n^-) \tilde{\beta}_1 2u_0 \quad (35b)$$

where Δw_R is the vertical wear increment for one motion cycle.

Let us note that p_n^+ and p_n^- are not uniformly distributed on the contact interface. To assure the uniform wear increment Δw_R accumulated during full cycle at each point of the contact zone, the following condition should be satisfied according to results of (A.20) in Appendix

$$\Delta w_R = \frac{\Delta w_{1,n}}{\cos \alpha} = \frac{Q p_\Sigma}{\cos \alpha} = Q 2 p_m^C = const \quad (36)$$

where

$$p_\Sigma = p_n^+ + p_n^- = 2p_m = 2p_m^C \cos \alpha, \quad Q = \tilde{\beta}_1 2u_0 \quad (37)$$

The wear parameters are $\tilde{\beta}_1 = 0.5\pi \cdot 10^{-8}$, $\tilde{\beta}_2 = 0$, $a_1 = b_1 = 1$. The sliding parameters are $u_0 = 1.5$ mm, $\omega = 10$ rad/s. Using time integration of the wear rule in the usual way, the obtained contact pressure evolution is demonstrated in Figure 11 at the beginning of numerical steps $n = 1000$. The number of the half periods are calculated by (10).

With increasing number of cycles condition (37) is progressively better satisfied, see Figure 11. Here $p_\Sigma = p_\Sigma(\alpha) = (p_n^+ + p_n^-) = 2p_m^C \cos \alpha$. At $n = 4200$, $p_\Sigma(0) = 12.42$ MPa, at $n = 6500$ $p_\Sigma(0) = 11.67$ MPa, at $n = 7200$ $p_\Sigma(0) = 10.93$ MPa, at $n = 8700$ $p_\Sigma(0) = 10.71$ MPa, at $n = 9200$ $p_\Sigma(0) = 10.69$ MPa, at $n = 10000$ $p_\Sigma(0) = 10.66$ MPa and at $n = 12100$ $p_\Sigma = 10.62$ MPa, that is $n \Rightarrow \infty$ $p_\Sigma(0) = 2p_m^C$. The value of $p_\Sigma(0)$ as the function of n is demonstrated in Figure 12. At the beginning of the wear process the drop of pressure $p_\Sigma(0)$ is very high, next it exponentially decreases to the value $p_\Sigma(0) = 2p_m = 10.57$ MPa. This value is calculated from (A.15).

The evolution of the contact shape is also interesting. In the initial phase the wear is high in the middle contact portion, and next the shape tends to its steady form which translates vertically as a rigid line, see Figure 13.

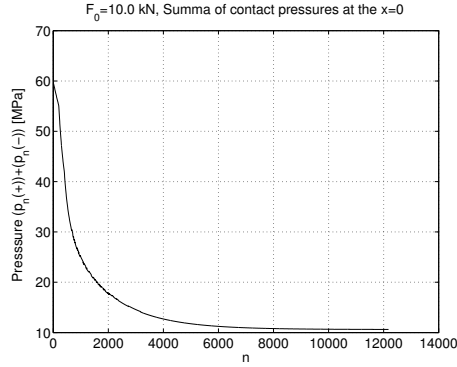


Figure 12. Satisfying the constraint of uniform vertical wear increment.

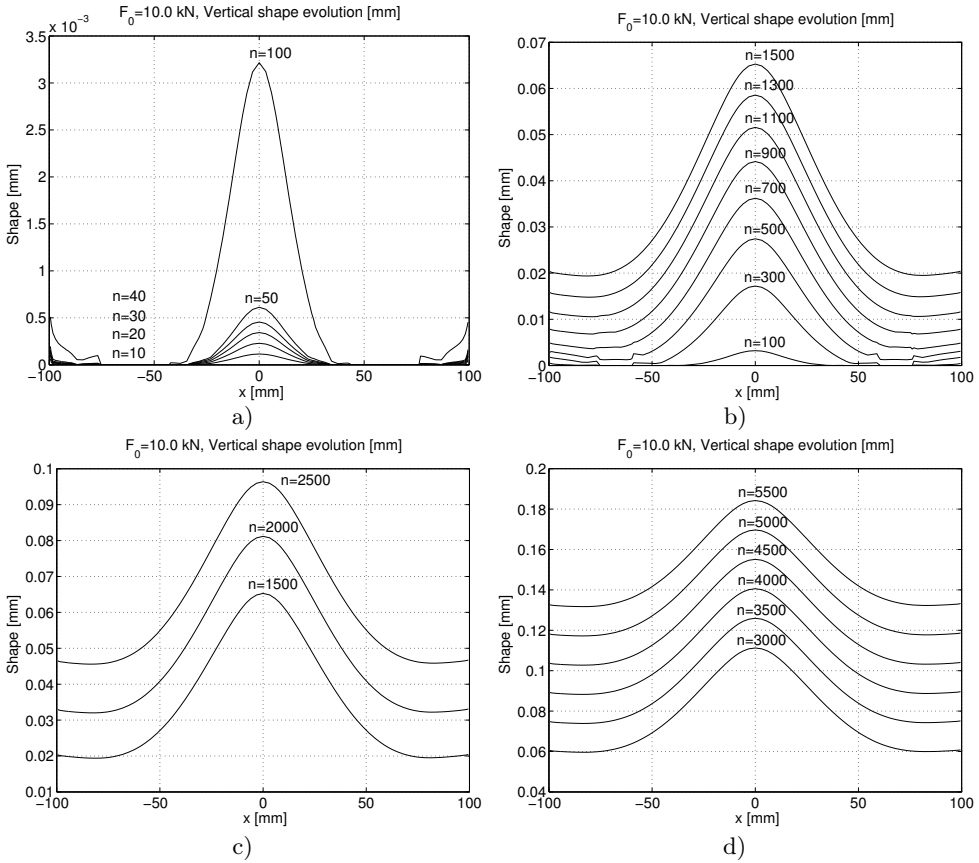


Figure 13. Evolution of contact shape in the wear process.

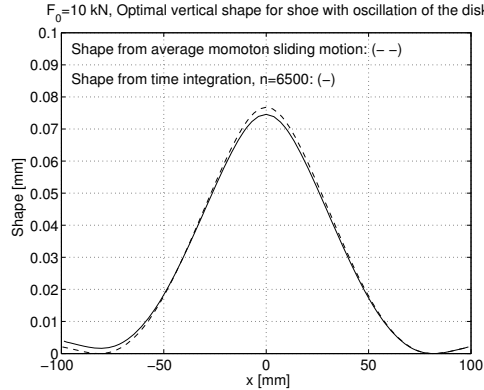


Figure 14. Prediction of contact shape from the averaged monotonic sliding motion between the shoe and disk.

The averaging technique for prediction of the shape form [13] provides an overestimated wear form, see Figure 14. In [13] it was demonstrated that the shape does not depend on the coefficient of friction. At the centre point the averaged shape function has the value 0.07503 mm, and the shape function obtained by time integration of the wear rule has the value 0.07456 mm. The error is less than 1%. A small asymmetry has been found from time integration.

6. OPTIMIZATION PROBLEM

6.1. Specification of the initial wear form. Let us analyze the wear of punch (Body 1) shown in Figure 2a. We would like to find the steady contact shape for periodic motion using the results of monotonic strip sliding in the leftward or rightward direction and develop a new optimization technique. The punch now is allowed to execute a rigid body wear velocity $\dot{\lambda}_F$ [13, 15] which is normal to the contact interface. The optimal pressure for steady wear state is uniform, $p_n^+ = p_n^- = p^\sim$. The calculation of the initial gap that is the wear shape is performed by loading separately each body by the optimal contact pressure and friction stress. In this case the bodies are not allowed for the rigid body motion in the vertical direction. For monotonic sliding the equation requiring the total contact gap to vanish specifies the wear gap g , thus

$$d = u_n^{(2)} - u_n^{(1)} - \lambda_F + g = 0 \quad (38)$$

where the rigid body wear velocity of the punch is known from the stationary condition, so that $\lambda_F = \dot{\lambda}_F t_s$, where t_s is the selected time instant specifying initiation of the steady state. The steady state shapes can be found in Figure 15 where at leftward sliding it is set: $g(x = 1070) = 0$, and at rightward sliding: $g(x = 1130) = 0$.

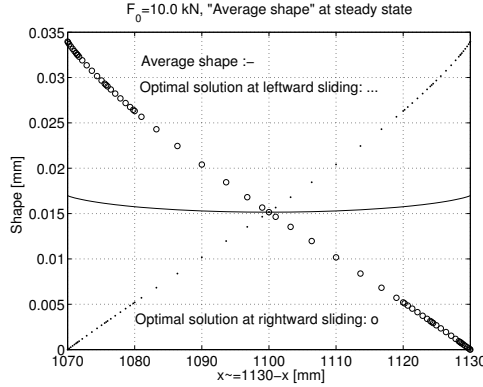


Figure 15. Shapes for the steady wear states induced by the strip monotonically translating in leftward or rightward directions. The average shape is $Shape^{(a)}$

Denoting by $shape^{(l)}$, $shape^{(r)}$ the resulting wear shape curves during the leftward and rightward monotonic sliding (see Figure 15), assume the shape curve for reciprocal

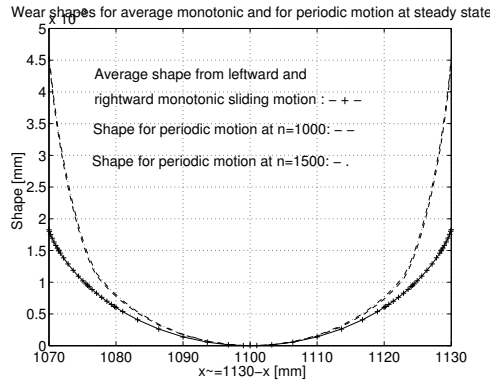


Figure 16. Prediction of the wear shape for periodic wear process from the results of monotonic sliding. The average shape is $Shape^{(a)}$

sliding to be approximated by the sum of monotonic shape curves, thus

$$Shape^{(a)} = shape^{(l)} + shape^{(r)} - 2 \cdot shape^{(l)}(x = 1100) \tag{39}$$

where the last term specifies the translation of the curve along the z-axis in order to obtain the zero value at the mid contact point (see Figure 16). It is seen that the prediction is not close to the actual wear form at the contact edges. It is also noted that shapes at $n = 1000$ and $n = 1500$ are practically the same, so the wear process has reached its steady state at $n = 1000$.

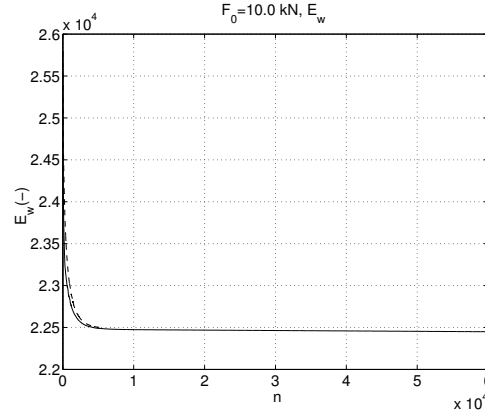


Figure 17. Evolution of the wear dissipation $E_w^-/2u_0\tilde{\beta}_1 = \int_{S_c} (p_n^-)^2 dS$

The evolution of the wear dissipation energy for one cycle is plotted in Figure 17. The continuous line corresponds to the leftward, and the dotted line to the rightward sliding direction of the substrate. The wear dissipation energy very quickly decreases and tends to its minimum level.

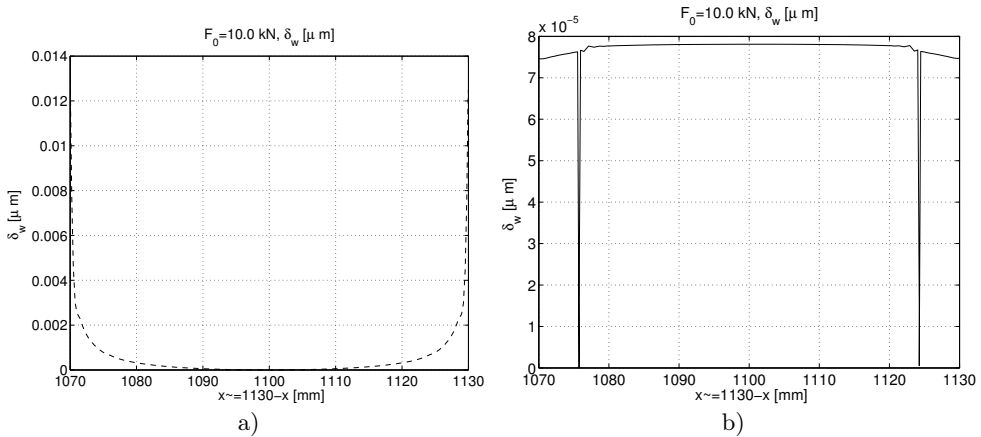


Figure 18. $\delta w = \Delta w_{1,n} - \min \Delta w_{1,n} = (\Delta w_{1,n}^+ + \Delta w_{1,n}^-) - \min(\Delta w_{1,n}^+ + \Delta w_{1,n}^-)$ at different time periods, a) at the beginning of the wear process, b) in the steady state.

Theoretically calculating the value

$$\delta w = \Delta w_{1,n} - \min \Delta w_{1,n} \quad (40)$$

it is expected that in the steady state it must vanish. Here δw is the wear difference after one sliding period. In Figure 18 the evolution of δw is shown at the beginning of the wear process (a), and at the periodical steady state (b). In the initial period of the wear process, δw is ~ 100 time greater than that at the steady state. In the

steady state it reaches a stabilized small value. It seems to be impossible to reduce δw to zero in the numerical calculation process.

6.2. Solution of the optimization problem using splines. In view of the preceding analysis, the following optimization problem can be stated for calculation of the wear shape

$$\min_{g_n} \{ \max \delta w = \Delta w_{1,n \max} - \Delta w_{1,n \min} \mid p_n^\pm \geq 0, d_n^\pm \geq 0, \\ p_n^\pm d_n^\pm = 0, \tau_n^+ = \mu p_n^+, \tau_n^- = -\mu p_n^-, \mathbf{f} = \mathbf{0}, \mathbf{m} = \mathbf{0} \} \quad (41)$$

where $\Delta w_{1,n \max}, \Delta w_{1,n \min}$ are the maximum and minimum values of wear attained in one cycle, $\mathbf{f} = \mathbf{0}, \mathbf{m} = \mathbf{0}$ are the punch equilibrium equations.

The global equilibrium conditions for the body B_1 can be expressed as (8).

According to Signorini contact conditions in the normal direction the contact pressure must be positive in the contact zone and distance after deformation between the bodies must also be positive, thus

$$d_n^\pm = u_n^{(2)\pm} - u_n^{(1)\pm} + g_n \geq 0 \quad (42)$$

where $u_n^{(i)} = \mathbf{u}^{(i)} \cdot \mathbf{n}_c$ is the normal displacement of the i -th body, g_n is the initial gap (shape of body 1 in the periodic steady state which is not given, but must be found in the optimization process). The Signorini conditions for the whole period then are

$$p_n^\pm d_n^\pm = 0, p_n^\pm \geq 0, d_n^\pm \geq 0. \quad (43)$$

The objective function can be stated as: $I_{\delta w} = \int_{S_c} \delta w dS$, or $I_{\delta w} \cdot \max \delta w$. The steady state condition then is $I_{\delta w} = 0$, also $\max \delta w = 0$. Numerically this extremum cannot be reached. In our examples it is found that $I_{\delta w} \cdot \max \delta w \sim 10^{-6}$.

6.2.1. *First step in the solution of the optimization problem* (41). The optimization problem is solved in two steps.

A. First we take the average shape for monotonic motions [5], see Figure 16(-+) line, to build a cubic spline for the next points:

	x mm	Shape mm
1	0.10700000E+04	0.18265000E-02
2	0.10707500E+04	0.16335910E-02
3	0.10715000E+04	0.14934270E-02
4	0.10736300E+04	0.11869800E-02
5	0.10757500E+04	0.95190000E-03
6	0.10778800E+04	0.76108000E-03
7	0.10800000E+04	0.60226500E-03
8	0.10900000E+04	0.13810000E-03
9	0.11000000E+04	0.00000000E-00
10	0.11136300E+04	0.26240500E-03
11	0.11200000E+04	0.60244000E-03
12	0.11221300E+04	0.76135000E-03
13	0.11242500E+04	0.95234000E-03
14	0.11263800E+04	0.11876850E-02
15	0.11285000E+04	0.14945845E-02
16	0.11292500E+04	0.16349025E-02
17	0.11300000E+04	0.18279500E-02

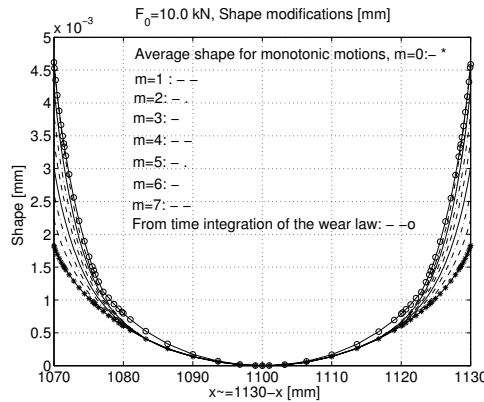


Figure 19. Shape modification specified with 9-th polynomial order.

B. Then transform the data in the following way

$$\begin{aligned} \Delta \cdot m \cdot (x - 1100)^q / (L/2)^q & \quad \text{for } x \leq 1100, \\ \Delta \cdot m \cdot (-x + 1100)^q / (L/2)^q & \quad \text{for } x > 1100. \end{aligned} \tag{44}$$

We take $q = 9$, $\Delta = 0.0004$ mm, $m = 1, 2, \dots, 7$. This procedure is named polynomial iteration. The shapes are demonstrated in Figure 19. In this figure the curve obtained from time integration of the wear rule (- - o) is presented. It is seen that the approximation curve at $m = 7$ is lower than the curve (- - o). That is, the spline approximation must be modified.

6.2.2. *Second step in the solution of the optimization problem* (41). In the second step we suppose that the new wear function can be approximated by the Taylor series

$$\delta w = \delta w^{(0)} + \sum_{j=1}^{16} \frac{\partial (\delta w)}{\partial a_j} \Delta a_j \tag{45}$$

that is we can calculate the spline parameters a_j

The derivative $\partial(\delta w)/\partial a_j$ is determined in the numerical way, so that

$$\frac{\partial(\delta w)}{\partial a_j} \approx \frac{\delta w(a_1^{(0)}, \dots, a_j^{(0)} + \Delta_s, \dots, a_{16}^{(0)}) - \delta w^{(0)}}{\Delta_s} \tag{46}$$

In our case $\Delta_s = 0.00002$.

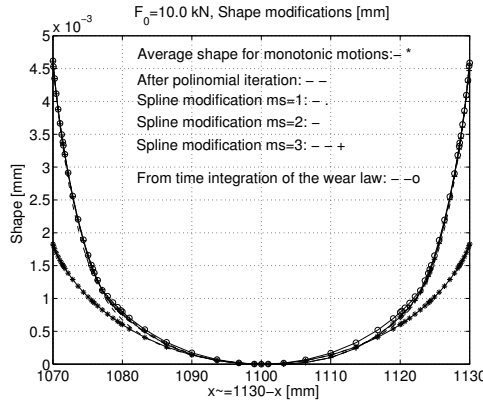


Figure 20. Shape modification specified by spline modification.

For each j the contact problem must be solved and the wear is calculated for one sliding period. For the control of the condition $\delta w = 0$, 16 point zones in the contact domain are taken, and using the Raphson iteration technique, new spline point coordinates can easily be found:

$$a_j^{new} = a_j^{(0)} + \Delta a_j \tag{47}$$

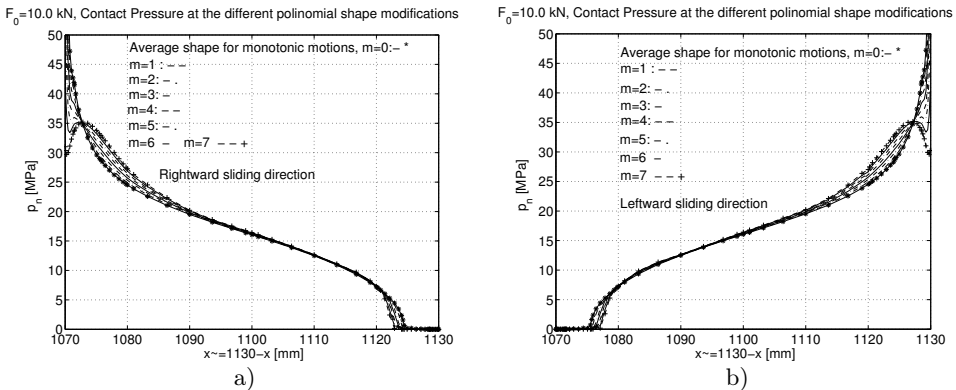


Figure 21. Contact pressure evolution due to different polynomial shape modifications, a) for rightward sliding motion, b) for leftward sliding motion.

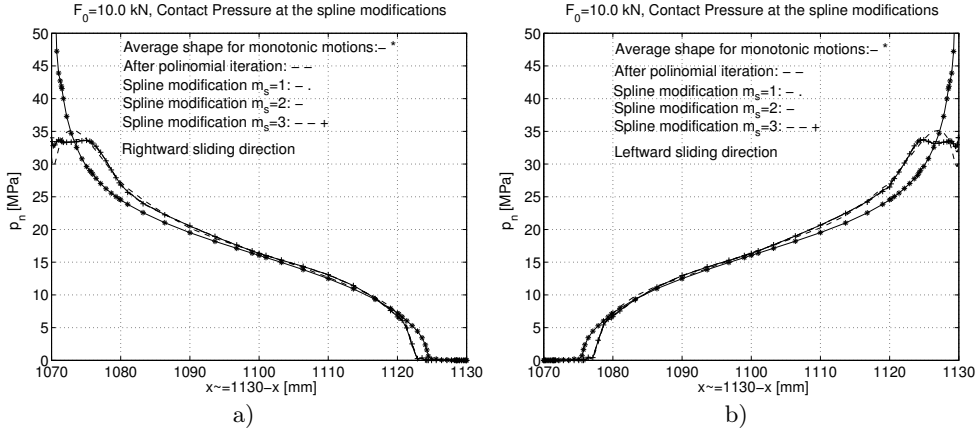


Figure 22. Contact pressure evolution due to spline modifications, a) for rightward sliding motion, b) for leftward sliding motion.

where the algebraic system is

$$\left[\frac{\partial(\delta w)_i}{\partial a_j} \right]_{i,j=1,16} \begin{bmatrix} \Delta a_1 \\ \vdots \\ \Delta a_j \\ \vdots \\ \Delta a_{16} \end{bmatrix} = - \begin{bmatrix} \delta w_1 \\ \vdots \\ \delta w_j \\ \vdots \\ \delta w_{16} \end{bmatrix}^{(0)} \quad (48)$$

Using this technique, after $m_s = 1, 2, 3$ spline modifications we obtain a nice result, see Figure 20. The calculated shape is practically the same as that obtained from time integration. The contact pressure distributions are presented in Figures 21 and 22. When the averaged monotonic shape is applied, the contact pressure has a high value at the perimeter points changing with the sliding direction, see Figure 21. After polynomial iteration the pressure value is lower than that in the steady state, see in Figure 21, lines $(-+)$. After the end of the second step, the pressure exhibits a very small oscillation, so the optimal solution is very close to the numerically specified result (see Figure 22). It can be concluded that the recommended optimization process provides correct results.

6.3. Solution of the optimization problem by applying the penalty technique. The objective function can be presented in a different form, using the pressure constraint in the periodic steady wear state. Define the pressure difference for the rigid body wear velocity $\dot{\lambda}_F^\pm \neq 0$, $\dot{\lambda}_M^\pm = 0$ (see (23a))

$$\Delta p_n = p_n^+ + p_n^- - 2p_m \quad (49)$$

If $\Delta p_n = 0$ at each point of contact zone, then the corresponding contact shape is correct. If not, then the shape must be modified. Using the idea of penalty technique [18], we can write

$$\Delta p_n = p_n^+ + p_n^- - 2p_m = c_n(u_n^+ + g_n^+ + u_n^- + g_n^-) - 2p_m \quad (50)$$

where g_n^+ and g_n^- are the shapes (gaps) at the end of the + or - sliding direction, c_n is the penalty parameter used for the normal contact problem.

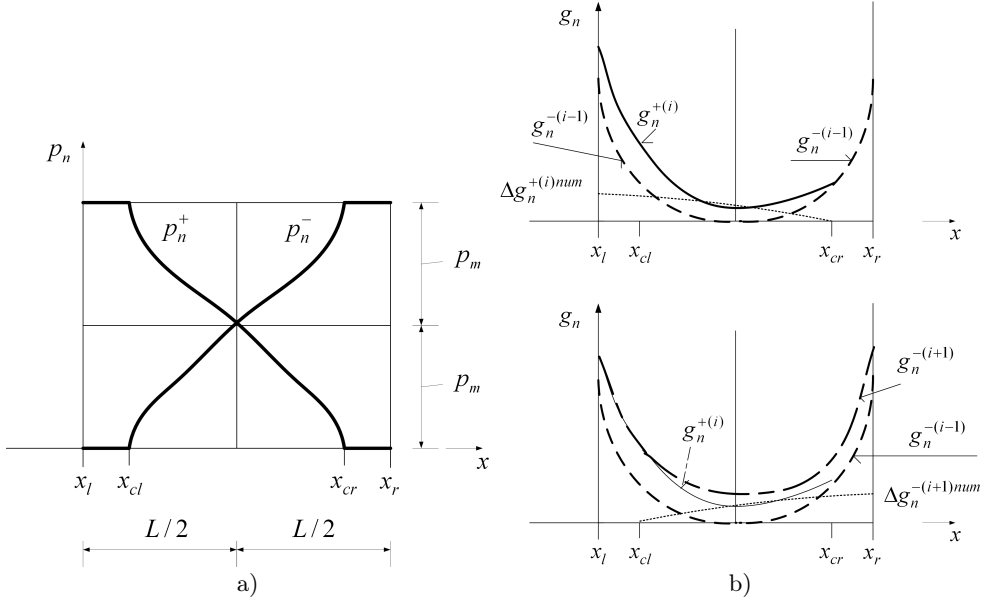


Figure 23. Contact pressure distribution and shape evolution. a) p_n at steady state, b) shape modification in the i -th (+ direction sliding) and $(i + 1)$ -th (- direction sliding) iterative step

If $\Delta p_n \neq 0$ the shape must be changed, that is instead of (50) it can be written

$$\Delta p_n^\pm = p_n^+ + p_n^- - 2p_m = c_n(u_n^+ + g_n^\mp + u_n^- + g_n^\pm) + c\Delta g_n^\pm - 2p_m \quad (51)$$

The optimizational problem can be written in the following form

$$\min_{g_n} \left\{ \int_{S_c} \frac{1}{2} (p_n^+ + p_n^- - 2p_m)^2 dS \mid p_n^\pm \geq 0, d_n^\pm \geq 0, p_n^\pm d_n^\pm = 0, \right. \\ \left. \tau_n^+ = \mu p_n^+, \tau_n^- = -\mu p_n^-, \text{ Equilibrium equations for punch} \right\} \quad (52)$$

where the minimum of (52) provides the contact pressure distribution satisfying (49) for $\Delta p_n = 0$. The shear stress τ_n^\pm acts on the contact surface of Body 1 in the direction of x -axis.

For solution of the minimization problem (52) a special iterative process is recommended. In each step the Signorini contact conditions: $p_n^\pm d_n^\pm = 0$, $p_n^\pm \geq 0$, $d_n^\pm \geq 0$, and the Coulomb dry friction law $\tau_n^+ = \mu p_n^+$, $\tau_n^- = -\mu p_n^-$ must be satisfied in the solution of contact problem and next the modified contact shape should be determined. The shape modification is taken from equation (51).

Consider the half cycle i of the + sliding direction, next $i + 1$ of the - sliding direction and similarly the consecutive half cycle $i + 2$ for + sliding direction and $i + 3$ for - direction of sliding and so on.

According to Figure 23 in the interval $x_l \leq x \leq x_{cl}$ the contact pressures are $0 \leq p_n^+$, $p_n^- = 0$ in the interval $x_{cl} \leq x \leq x_{cr}$ the pressures are $0 \leq p_n^+$, $0 \leq p_n^-$ and in the interval $x_{cr} \leq x \leq x_r$ the pressures are $p_n^+ = 0$, $0 \leq p_n^-$.

Let us begin the i -th half cycle. Then

$$\Delta p_n^\pm = p_n^+ + p_n^- - 2p_m = c_n(u_n^+ + g_n^\mp + u_n^- + g_n^\pm) + c\Delta g_n^\pm - 2p_m \quad (53)$$

in the interval $x_l \leq x \leq x_{cl}$ because $g_n^{+(i)} = g_n^{-(i-1)} + \Delta g_n^{+(i)}$. It is supposed that in the right direction of sliding at the end of half cycle the new shape is modified by $\Delta g_n^{+(i)}$. The modification of the shape is

$$\frac{\Delta p_n^+}{c_n} - (u_n^{+(i)} + g_n^{-(i-1)}) = \Delta g_n^{+(i)} - \frac{2p_m}{c_n} = \Delta \tilde{g}_n^{+(i)}. \quad (54)$$

In the interval $x_{cl} \leq x \leq x_{cr}$ in right direction

$$\begin{aligned} \Delta p_n^+ &= p_n^{+(i)} + p_n^{-(i-1)} - 2p_m = \\ &= c_n(u_n^{+(i)} + g_n^{-(i-1)} + u_n^{-(i-1)} + g_n^{-(i-1)}) + c_n\Delta g_n^{+(i)} - 2p_m, \end{aligned} \quad (55)$$

$$\frac{\Delta p_n^+}{c_n} - (u_n^{+(i)} + u_n^{-(i-1)} + 2g_n^{(i-1)}) = \Delta g_n^{+(i)} - \frac{2p_m}{c_n} = \Delta \tilde{g}_n^{+(i)}. \quad (56)$$

For numerical calculation it is supposed that at the point x_{cr} of the contact domain the modification of the gap is equal to zero, that is $\Delta \tilde{g}_n^{+(i)} - \Delta \tilde{g}_n^{+(i)}(x_{cr}) = \Delta g_n^{+(i) num}$ and the new shape at the end of + direction motion is

$$g_n^{+(i)} = g_n^{-(i-1)} + \Delta g_n^{+(i) num}. \quad (57)$$

In the interval $x_{cr} \leq x \leq x_r$ in the left direction we have

$$\Delta p_n^- = p_n^{-(i+1)} - 2p_m = c_n(u_n^{-(i+1)} + g_n^{+(i)}) + c_n\Delta g_n^{-(i+1)} - 2p_m \quad (58)$$

that is

$$\frac{\Delta p_n^-}{c_n} - (u_n^{-(i+1)} + g_n^{+(i)}) = \Delta g_n^{-(i+1)} - \frac{2p_m}{c_n} = \Delta \tilde{g}_n^{-(i+1)} \quad (59)$$

and in the interval $x_{cl} \leq x \leq x_{cr}$ for the left direction there is

$$\begin{aligned} \Delta p_n^- &= p_n^{+(i)} + p_n^{-(i+1)} - 2p_m = \\ &= c_n(u_n^{+(i)} + (g_n^{-(i-1)} + \Delta g_n^{+(i)}) + u_n^{-(i+1)} + g_n^{+(i)}) + c_n\Delta g_n^{-(i+1)} - 2p_m \end{aligned}$$

where $g_n^{+(i)} = g_n^{-(i+1)} + \Delta g_n^{+(i)}$, thus

$$\Delta p_n^- = p_n^{+(i)} + p_n^{-(i+1)} - 2p_m = c_n(u_n^{+(i)} + u_n^{-(i+1)} + 2g_n^{+(i)}) + c_c\Delta g_n^{-(i+1)} - 2p_m \quad (60)$$

and

$$\frac{\Delta p_n^-}{c_n} - (u_n^{+(i)} + u_n^{-(i+1)} + 2g_n^{+(i)}) = \Delta g_n^{-(i+1)} - \frac{2p_m}{c_n} = \Delta \tilde{g}_n^{-(i+1)} \quad (61)$$

Science in point x_{cl} the modification of the gap is equal to zero

$$\Delta \tilde{g}_n^{-(i+1)} - \Delta \tilde{g}_n^{-(i+1)}(x_{cl}) = \Delta g_n^{-(i+1) num}$$

for numerical calculation the modification of the gap will be

$$g_n^{-(i+1)} = g_n^{+(i)} + \Delta g_n^{-(i+1) num} \quad (62)$$

Now repeat the calculations for the consecutive period

Right motion:

$$x_l \leq x \leq x_{cl} \quad \frac{\Delta p_n^+}{c_n} - (u_n^{+(i+2)} + g_n^{-(i+1)}) = \Delta g_n^{+(i+2)} - \frac{2p_m}{c_n} = \Delta \tilde{g}_n^{+(i+2)} \quad (63)$$

$$x_{cl} \leq x \leq x_{cr} \quad \frac{\Delta p_n^+}{c_n} - (u_n^{+(i+2)} + g_n^{-(i+1)} + u_n^{-(i+1)} + g_n^{-(i+1)}) = \Delta g_n^{+(i+2)} - \frac{2p_m}{c_n}$$

$$\frac{\Delta p_n^+}{c_n} - (u_n^{+(i+2)} + u_n^{-(i+1)} + 2g_n^{-(i+1)}) = \Delta g_n^{+(i+2)} - \frac{2p_m}{c_n} = \Delta \tilde{g}_n^{+(i+2)} \quad (64)$$

Left motion

$$x_{cr} \leq x \leq x_r \quad \frac{\Delta p_n^-}{c_n} - (u_n^{-(i+3)} + g_n^{+(i+2)}) = \Delta g_n^{-(i+3)} - \frac{2p_m}{c_n} = \Delta \tilde{g}_n^{-(i+3)} \quad (65)$$

$$x_{cl} \leq x \leq x_{cr} \quad \frac{\Delta p_n^-}{c_n} - (u_n^{+(i+2)} + g_n^{+(i+2)} + u_n^{-(i+3)} + g_n^{+(i+2)}) = \Delta g_n^{-(i+3)} - \frac{2p_m}{c_n}$$

$$\frac{\Delta p_n^-}{c_n} - (u_n^{+(i+2)} + u_n^{-(i+3)} + 2g_n^{+(i+2)}) = \Delta g_n^{-(i+3)} - \frac{2p_m}{c_n} = \Delta \tilde{g}_n^{-(i+3)} \quad (66)$$

where

$$\Delta \tilde{g}_n^{+(i+2)} - \Delta \tilde{g}_n^{+(i+2)}(x_{cr}) = \Delta g_n^{+(i+2) num}, \quad g_n^{+(i+2)} = g_n^{-(i+1)} + \Delta g_n^{+(i+2) num},$$

$$\Delta \tilde{g}_n^{-(i+3)} - \Delta \tilde{g}_n^{-(i+3)}(x_{cl}) = \Delta g_n^{-(i+3) num}, \quad g_n^{-(i+3)} = g_n^{+(i+2)} + \Delta g_n^{-(i+3) num}.$$

In this formulation for one period and $(i+2-i+3)$ -th steps, the change of the shape is

$$g_n^{-(i+3)} = g_n^{-(i+1)} + \Delta g_n^{+(i+2) num} + \Delta g_n^{-(i+3) num} \quad (67)$$

In the numerical calculation for each cycle, initially the shape at the point $x = 0.5(x_l + x_r)$, $z = 100$ is set to zero value, that is the shape is moved vertically to this point.

Example 1:

For determination of the shape in periodic steady state for the punch Figure 2a, let us apply the above iteration process. The initial shape is taken from the solution for averaged monotonic sliding. Using this initial form the proposed iteration procedure must be performed approximately for 500 iteration steps. The shape evolution is shown in Figure 24a. At the beginning the contact pressure has a high value at the borders of contact domain (see Figure 24b). After ~ 300 steps the shape is close to the steady periodic shape form (see Figure 24a). Practically after 500 steps the iterative procedure provides accurate prediction – see Figure 24d.

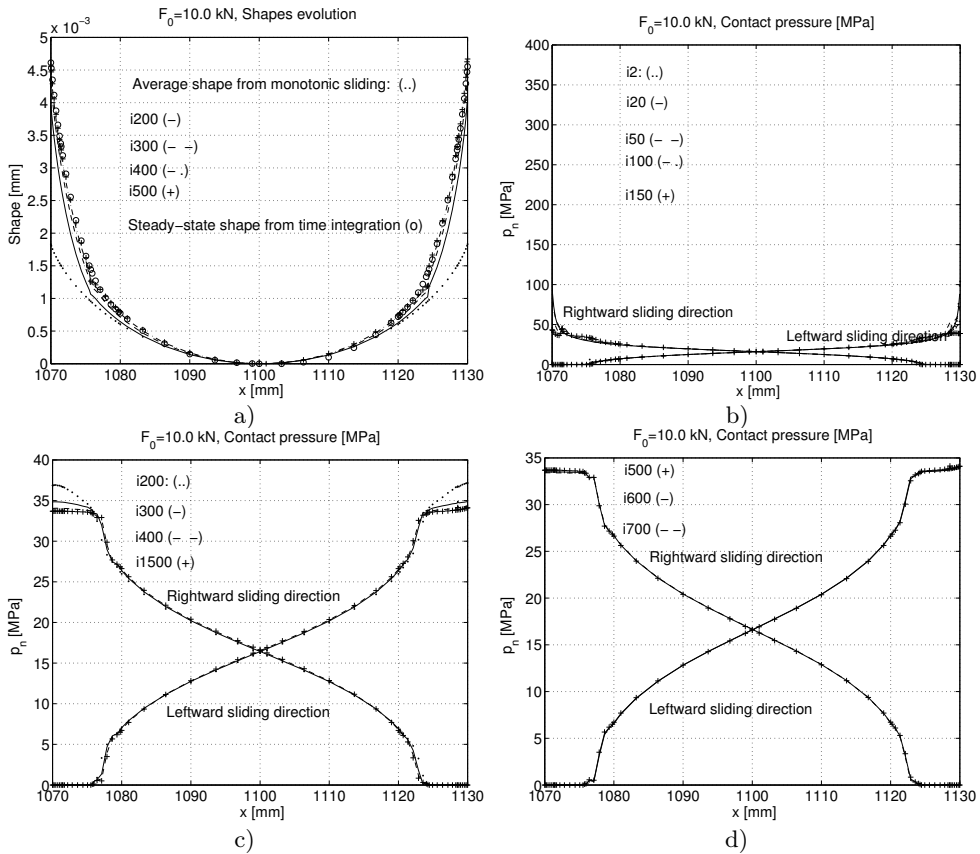


Figure 24. Determination of the shape for steady state periodic motion for construction Figure 19. a) Evolution of the shape in the iteration process, b)-d) evolution of the contact pressure.

Example 2:

In this example the punch constraint of Figure 2a is modified. The support is only placed at one point / pin at point ($x = 1030, z = 140$) – see Figure 2b. The initial shape is also taken from the result for averaged monotonic sliding, see Figure 25c with curve (...). To reach the steady state, approximately 300 iteration steps should be executed. Initially the contact pressure has a high value at the borders of contact domain. Figure 25e presents the sum of contact pressures which has a high value at the borders of contact zone in the beginning stage of the wear process. In the steady periodic state this sum is close to the $2p_m = 33.333$ MPa. After 200 steps the shape is close to the steady shape form (Figure 25d). Practically after 300 steps the distribution of contact pressure is fixed – see Figure 25b. The solution of the optimization problem (52) by penalty technique is characterized by the slow convergence, but the form of the contact shape can be determined with high accuracy.

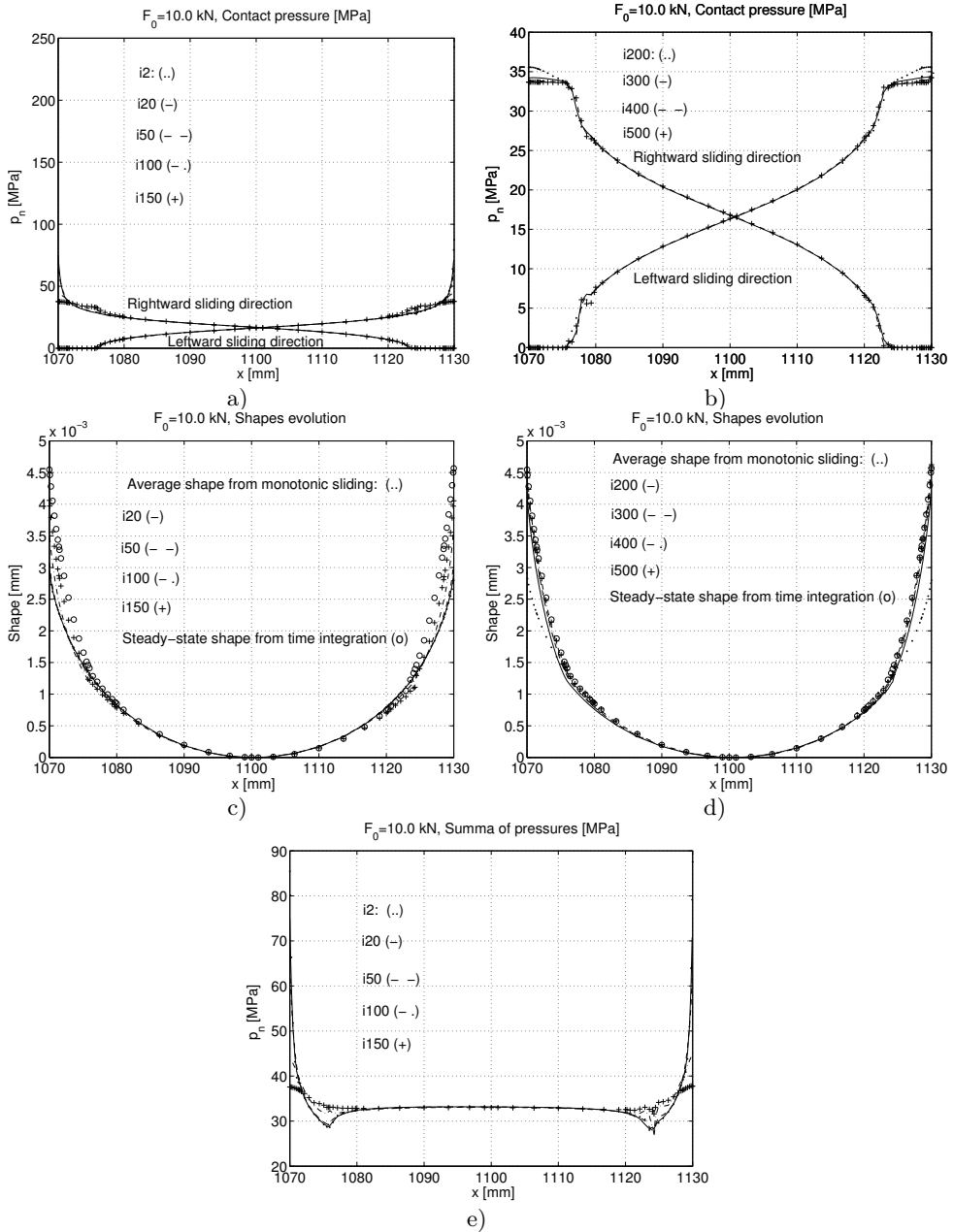


Figure 25. Optimization result for a plane punch with support at $l_z = 40$ mm. a) evolution of the contact pressure, b) contact pressure distribution near the steady state, c), d) evolution of the shape in the iteration process, e) evolution of the sum of contact pressures in the iteration process.

7. CONCLUSION

In our analysis the relative contact sliding displacements were considered and the partial slip displacements were neglected. The relative periodic sliding motion between contacting bodies induces a periodic steady wear state with different distributions of contact pressure during the leftward and rightward sliding directions. These pressure distributions cannot be specified from minimization of the wear dissipation in one sliding period. They are determined by solving the boundary value problem with imposed periodicity and contact compatibility conditions. On the other hand, the summed p_Σ contact pressure value for consecutive semi-cycles results from rigid body wear displacement of punch. In the steady periodic wear state the wear dissipation during one cycle reaches its minimum and specifies the summed contact pressure.

The specific examples presented in the paper illustrate the solution method for periodic wear states.

By solving the optimization problem (41) or (53), we can generate the shape and the contact pressure distributions with high accuracy without time integration of the wear rule for periodic sliding. The results of steady states for monotonic sliding provide fairly good simple predictions for shapes generated in the steady periodic wear states

APPENDIX A. PERIODIC SLIDING ALONG A CYLINDRICAL CONTACT SURFACE

Consider a 2D contact problem for fixed loads and periodically varying relative sliding velocity between two bodies interacting on a cylindrical contact surface, Figure 26. Body 1 (punch) is allowed to translate vertically in z -direction and rotate around y -axis located at point O. Body 2 (substrate) is a circular disc of radius R_0 executing periodic rotation through the angle $[+\alpha, -\alpha]$ with the relative velocity \dot{u}_τ , $v_r = \|\dot{\mathbf{u}}_\tau\|$. The wear rate in normal contact direction is specified is by the rule

$$\dot{w}_{i,n} = \beta_i v_r^{a_i} p_n^{b_i} \quad i = 1, 2 \tag{A.1}$$

It is assumed that during the steady periodic state the wear increment accumulated during one cycle should be compatible at each point $x \in S_c$ with the rigid body punch motion. Assume the rigid body wear velocities for left (-) and right (+) sliding directions of the substrate in the following form

$$\dot{\lambda}_F^- = -\dot{\lambda}_F^- e_z, \quad \dot{\lambda}_M^- = -\dot{\lambda}_M^- e_y, \quad \dot{\lambda}_F^+ = -\dot{\lambda}_F^+ e_z, \quad \dot{\lambda}_M^+ = \dot{\lambda}_M^+ e_y \tag{A.2}$$

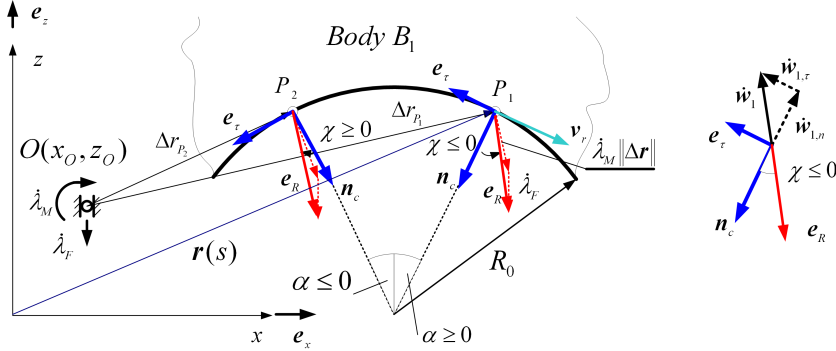


Figure 26. Body 1 can move as a rigid body in vertical direction and rotate around O. The wear velocity is not normal to the contact surface. Its direction \mathbf{e}_R is defined by the rigid body velocities $\dot{\lambda}_F^\pm$, $\dot{\lambda}_M^\pm$ according to (A.4).

Thus the velocities at an arbitrary point at punch are

$$\dot{\mathbf{w}}_R^+ = \dot{\lambda}_F^+ + \dot{\lambda}_M^+ \times \mathbf{r}_{OP}, \quad \dot{\mathbf{w}}_R^- = \dot{\lambda}_F^- + \dot{\lambda}_M^- \times \mathbf{r}_{OP} \quad (\text{A.3})$$

and the summed wear velocity for consecutive semi-cycles is

$$\dot{\mathbf{w}}_R = (\dot{\lambda}_F^+ + \dot{\lambda}_F^-) + (\dot{\lambda}_M^+ + \dot{\lambda}_M^-) \times \mathbf{r}_{OP} = -(\dot{\lambda}_F^+ + \dot{\lambda}_F^-) \mathbf{e}_z + (\dot{\lambda}_M^+ - \dot{\lambda}_M^-) \mathbf{e}_y \times \mathbf{r}_{OP} \quad (\text{A.4})$$

The displacement resulting from this velocity equals

$$\Delta \mathbf{w}_R = -(\Delta \lambda_F^+ + \Delta \lambda_F^-) \mathbf{e}_z + (\Delta \lambda_M^+ - \Delta \lambda_M^-) \mathbf{e}_y \times \mathbf{r}_{OP} = -\Delta \lambda_F \mathbf{e}_z + \Delta \lambda_M \mathbf{e}_y \times \mathbf{r}_{OP} \quad (\text{A.5})$$

where

$$\Delta \lambda_{F,M}^+ = \int_0^{T_*/2} \dot{\lambda}_{F,M}^+ dt, \quad \Delta \lambda_{F,M}^- = \int_{T_*/2}^{T_*} \dot{\lambda}_{F,M}^- dt.$$

The normal and tangential unit vector components are

$$\mathbf{n}_c = -\cos \alpha \mathbf{e}_z - \sin \alpha \mathbf{e}_x, \quad \mathbf{e}_\tau = \sin \alpha \mathbf{e}_z - \cos \alpha \mathbf{e}_x. \quad (\text{A.6})$$

Thus, the total wear in normal direction accumulated during one sliding cycle is

$$\Delta w_n = \Delta \mathbf{w}_R \cdot \mathbf{n}_c = \Delta \lambda_F \cos \alpha + \Delta \lambda_M [(x_P - x_O) \cos \alpha - (z_P - z_O) \sin \alpha] \quad (\text{A.7})$$

The wear velocity vector for two bodies is coaxial with rigid body wear velocity, that is

$$\dot{\mathbf{w}}_R = \dot{\mathbf{w}}_2 - \dot{\mathbf{w}}_1 \quad (\text{A.8})$$

Assuming $\tilde{\beta}_1 \neq 0$, $\tilde{\beta}_2 = 0$ (the material is removed only from Body 1), the wear velocity of Body 1 on the contact surface is expressed in the form

$$\dot{\mathbf{w}}_R = -\dot{\mathbf{w}}_1 = -(-\dot{w}_{1,n} \mathbf{n}_c + w_{1,\tau} \mathbf{e}_\tau), \quad \dot{w}_n = \dot{\mathbf{w}}_R \cdot \mathbf{n}_c = -\dot{\mathbf{w}}_1 \cdot \mathbf{n}_c = \dot{w}_{1,n} \quad (\text{A.9})$$

and its increment for one sliding period is

$$\Delta w_n = \Delta \mathbf{w}_R \cdot \mathbf{n}_c = -\Delta \mathbf{w}_1 \cdot \mathbf{n}_c = \Delta w_{1,n} \quad (\text{A.10})$$

In this way, the wear increment in normal direction can be calculated easily, thus

$$\Delta w_{1,n} = -\Delta \mathbf{w}_1 \cdot \mathbf{n}_c = \Delta \lambda_F \cos \alpha + \Delta \lambda_M [(x_P - x_O) \cos \alpha - (z_P - z_O) \sin \alpha] \quad (\text{A.11})$$

This value of wear can also be calculated from the wear rule, assuming $a_1 = b_1 = 1$, thus

$$\begin{aligned} \Delta w_{1,n} &= \Delta w_{1,n}^+ + \Delta w_{1,n}^- = \tilde{\beta}_1 \int_0^{T_*/2} \|\dot{\mathbf{u}}_\tau\| p_n^+ dt + \tilde{\beta}_1 \int_{T_*/2}^{T_*} \|\dot{\mathbf{u}}_\tau\| p_n^- dt \\ \Delta w_{1,n} &= \Delta w_{1,n}^+ + \Delta w_{1,n}^- = \tilde{\beta}_1 \int_0^{T_*/2} \|\dot{\mathbf{u}}_\tau\| dt (p_n^+ + p_n^-) = Q (p_n^+ + p_n^-) = Q 2p_m = Q p_\Sigma \end{aligned} \quad (\text{A.12})$$

where

$$p_m = (p_n^+ + p_n^-)/2 = p_\Sigma/2, \quad Q = \tilde{\beta}_1 \int_0^{T_*/2} \|\dot{\mathbf{u}}_\tau\| dt.$$

Comparing (A.11) and (A.12), it is seen that the distribution of the sum of contact pressure values of consecutive semi-cycles can be expressed as a function of position, thus

$$p_\Sigma/2 = p_m = p_m^C \cos \alpha + p_m^L [(x_P - x_O) \cos \alpha - (z_P - z_O) \sin \alpha] \quad (\text{A.13})$$

that is

$$\begin{aligned} \Delta w_{1,n} &= \Delta \lambda_F \cos \alpha + \Delta \lambda_M [(x_P - x_O) \cos \alpha - (z_P - z_O) \sin \alpha] = \\ &= \tilde{\beta}_1 \int_0^{T_*/2} \|\dot{\mathbf{u}}_\tau\| dt 2 \{ p_m^C \cos \alpha + p_m^L [(x_P - x_O) \cos \alpha - (z_P - z_O) \sin \alpha] \}. \end{aligned}$$

where $\Delta \lambda_{F,M}^\pm$ is the increment of rigid body wear velocities in the half period time, p_m^C, p_m^L are unknowns, which can be calculated from equilibrium equations.

The punch is assumed to be loaded by the resultant vertical load F_0 and the moment M_0 relative to the support point O . Using the equilibrium equations for summed loads, it can be written

$$0 = 2\mathbf{f}_0 + \int_{S_c} (\mathbf{t}^{c+} + \mathbf{t}^{c-}) dS \quad (\text{A.14a})$$

$$0 = 2\mathbf{m}_0 + \int_{S_c} \mathbf{r}_{OP} \times (\mathbf{t}^{c+} + \mathbf{t}^{c-}) dS \quad (\text{A.14b})$$

where

$$\mathbf{t}^{c+} = -p_n^+ \mathbf{n}_c - \mu p_n^+ \mathbf{e}_\tau, \quad \mathbf{t}^{c-} = -p_n^- \mathbf{n}_c + \mu p_n^- \mathbf{e}_\tau,$$

S_c is the area of contact zone, $\mathbf{f}_0 = -F_0 \mathbf{e}_z$, $\mathbf{m}_0 = M_0 \mathbf{e}_y$ resultant force and moment, respectively, of the specified loading. The projection of (A.14a) on \mathbf{e}_z gives

$$\begin{aligned}
 0 &= -2F_0 + \mathbf{e}_z \cdot \int_{S_c} (\mathbf{t}^{c+} + \mathbf{t}^{c-}) dS = \\
 &= -2F_0 + \int_{S_c} \{ (p_n^+ + p_n^-) \cos \alpha - \mu (p_n^+ - p_n^-) \sin \alpha \} t_{th} R_0 d\alpha
 \end{aligned}$$

or

$$0 = -2F_0 + \int_{S_c} \{ 2p_m \cos \alpha - \mu (p_n^+ - p_n^-) \sin \alpha \} t_{th} R_0 d\alpha. \tag{A.15}$$

The moment equilibrium equation has the form

$$\begin{aligned}
 0 &= 2\mathbf{m}_0 \cdot \mathbf{e}_y + \mathbf{e}_y \cdot \int_{S_c} \mathbf{r}_{OP} \times (\mathbf{t}^{c+} + \mathbf{t}^{c-}) dS = \\
 &= 2M_0 - \int_{S_c} 2p_m [(z_P - z_O) \sin \alpha - (x_P - x_O) \cos \alpha] t_{th} R_0 d\alpha + \\
 &\quad + \int_{S_c} \mu (p_n^+ - p_n^-) [(z_P - z_O) \cos \alpha + (x_P - x_O) \sin \alpha] t_{th} R_0 d\alpha \tag{A.16}
 \end{aligned}$$

where t_{th} is the disc and punch thickness.

We have two equations for calculation of p_m^C and p_m^L occurring in (A.13). For some cases we find a direct way to calculate these parameters.

Some remarks:

1. If $\dot{\lambda}_M = 0$, then $p_m = p_m^C \cos \alpha$ and in this case from (A.15) we find

$$p_m^C = F_0 / \int_{S_c} (\cos \alpha)^2 t_{th} R_0 d\alpha$$

2. If the contact surface is plane ($\alpha = 0$), then from (A.13) we have $p_m = p_m^C + p_m^L (x_P - x_O)$. The values of p_m^C and p_m^L can be calculated from (A.15) and (A.16): Using $dS = t_{th} R_0 d\alpha$ and $\Delta z = z_P - z_O = const$ we get that $\int_{S_c} \mu (p_n^+ - p_n^-) \Delta z dS = 0$ since

$$\mu \int_{S_c} (p_n^+ - p_n^-) \Delta z dS = \Delta z \mu \left(\int_{S_c} p_n^+ dS - \int_{S_c} p_n^- dS \right) = \Delta z (\mu F_0 - \mu F_0) = 0$$

Consequently the moment of the shear contact stress is equal to zero.

3. If in the integrals (A.15) and (A.16) the terms $\mu (p_n^+ - p_n^-)$ are negligible, then p_m^C and p_m^L can be calculated and can be regarded as the first approximations of exact values.

Assume the relative tangential displacement on the contact surface in the form $\mathbf{u}_\tau = u_0 \cos \omega t \mathbf{e}_\tau$. Then the relative velocity is $v_r = \|\dot{\mathbf{u}}_\tau\| = \omega u_0 \sin \omega t$.

The wear increment in one period equals (note that the contact pressure is fixed in half period)

$$\Delta w_{1,n} = \tilde{\beta}_1 [p_n^+ + p_n^-] (u_0 \omega) \int_0^{T_*/2} |\sin \omega \tau| d\tau \quad (\text{A.17})$$

which, using the equalities $\int_0^{T_*/2} v_r d\tau = \int_{T_*/2}^{T_*} v_r d\tau = 2u_0$, provides the simple relation

$$\Delta w_{1,n} = \tilde{\beta}_1 [p_n^+ + p_n^-] 2u_0 = Q p_\Sigma \quad (\text{A.18})$$

where $Q = \tilde{\beta}_1 2u_0$.

The averaged wear rate in one period equals

$$\bar{w}_{1,n} = \frac{\Delta w_{1,n}}{T_*} = \frac{\tilde{\beta}_1 [p_n^+ + p_n^-]}{T_*} 2u_0 = \frac{Q p_\Sigma}{T_*} \quad (\text{A.19})$$

If the rigid body wear velocity $\dot{\lambda}_M^+ = \dot{\lambda}_M^- = 0$, then $\dot{\lambda}_F^+ \neq 0$, $\dot{\lambda}_F^- \neq 0$, $p_m = p_m^C \cos \alpha$, $p_\Sigma = 2p_m = 2p_m^C \cos \alpha$ and

$$\Delta w_R = \frac{\Delta w_{1,n}}{\cos \alpha} = \frac{Q p_\Sigma}{\cos \alpha} = Q 2p_m^C = \text{const} \quad (\text{A.20})$$

that is in the steady periodic wear regime the uniform vertical (rigid body) wear increment is accumulated during full cycle at each point of the contact zone.

Acknowledgements. The present research was partially supported by the Hungarian Academy of Sciences, grants OTKA K67825 National Research, and Development and Innovation Office - NKFIH, K115701, and by project TÁMOP-4.2.1.B-10/2/KONV-2010-0001, TÁMOP-4.2.2/B-10/1-2010-0008.

REFERENCES

1. PÁCZELT, I. and MRÓZ, Z.: On the analysis of steady sliding wear process. *Tribology International*, **42**, (2009), 275–283.
2. PÁCZELT, I. and MRÓZ, Z.: Variational approach to the analysis of steady state thermo-elastic wear regimes. *Int. J. Num. Meth. Eng.*, **81**, (2010), 728–760.
3. MRÓZ, Z. and PÁCZELT, I.: Analysis of thermo-elastic wear problems. *J. Thermal Stresses*, **34-35**, (2011), 569–606.
4. PÁCZELT, I. and MRÓZ, Z.: Numerical analysis of steady thermo-elastic wear regimes induced by translating and rotating punches. *Computers and Structures*, **89**, (2011), 2495–2521.
5. GORYACHEVA, I. G., RAJEEV, P. T., and FARRIS, T. N.: Wear in partial slip contact. *J. Tribology*, **123**, (2001), 848–856.
6. MCCOLL, I. R., DING, J., and LEEN, S. B.: Finite element simulation and experimental validation of fretting wear. *Wear*, **256**, (2004), 1114–1127.
7. DING, J., LEEN, S. B., and MCCOLL, I. R.: The effect of slip regime on fretting wear-induced stress evolution. *Int. J. Fatigue*, **26**, (2004), 521–531.

8. FOUVRY, S., PAULIN, C., and LISKIEWICZ, T.: Application of an energy wear approach to quantify fretting contact durability: introduction of a wear energy capacity concept. *Tribology International*, **40**, (2007), 1428–1440.
9. FOUVRY, S., LISKIEWICZ, T., and PAULIN, C.: A global-local wear approach to quantify the contact endurance under reciprocating-fretting sliding conditions. *Wear*, **263**, (2007), 518–531.
10. PEIGNEY, U.: Simulating wear under cyclic loading by a minimization approach. *Int. J. Solids Struct.*, **41**, (2004), 6783–6799.
11. KIM, N. H., WON, D., BURRIS, D., HOLTKAMP, B., GESSEL, G. C., SWANSON, P., and SAWYER, W. G.: Finite element analysis and experiments of metal/metal wear in oscillatory contacts. *Wear*, **258**, (2005), 1787–1793.
12. PÁCZELT, I. and MRÓZ, Z.: On steady wear states for monotonic relative sliding of contacting bodies. *Key Engineering Materials*, **618**, (2014), 49–71.
13. PÁCZELT, I. and MRÓZ, Z.: Solution of wear problems for monotonic and periodic sliding with p-version of the finite element method. *Comput. Methods Appl. Mech. Engng.*, **249-252**, (2012), 75–103.
14. SZABÓ, B. and BABUSKA, I.: *Finite element analysis*. Wiley Interscience, New York, 1991.
15. PÁCZELT, I. and MRÓZ, Z.: Analysis of thermo-mechanical wear problems for reciprocal punch sliding. *Advances in Engineering Software*, **80**, (2015), 139–155.
16. ZAVARISE, G., WRIGGERS, P., and SCHREFLER, B.: On augmented lagrangian algorithms for thermomechanical contact problems with friction. *Int. J. Num. Meth. Eng.*, **38**, (1995), 2929–2949.
17. PÁCZELT, I., SZABÓ, B., and SZABÓ, T.: Solution of contact problem using the hp-version of the finite element method. *Comput. Math. Appl.*, **38**, (2000), 49–69.
18. OU, H., LU, B., CUI, Z. S., and LIN, C.: A direct shape optimization approach for contact problems with boundary stress concentration. *Journal of Mechanical Science and Technology*, **27**(9), (2013), 2751–2759.

Notes for Contributors

to the Journal of Computational and Applied Mechanics

Aims and scope. The aim of the journal is to publish research papers on theoretical and applied mechanics. Special emphasis is given to articles on computational mechanics, continuum mechanics (mechanics of solid bodies, fluid mechanics, heat and mass transfer) and dynamics. Review papers on a research field and materials effective for teaching can also be accepted and are published as review papers or classroom notes. Papers devoted to mathematical problems relevant to mechanics will also be considered.

Frequency of the journal. Two issues a year (approximately 80 pages per issue).

Submission of Manuscripts. Submission of a manuscript implies that the paper has not been published, nor is being considered for publication elsewhere. Papers should be written in standard grammatical English. The manuscript is to be submitted in electronic, preferably in pdf, format. The text is to be 130 mm wide and 190 mm long and the main text should be typeset in 10pt CMR fonts. Though the length of a paper is not prescribed, authors are encouraged to write concisely. However, short communications or discussions on papers published in the journal must not be longer than 2 pages. Each manuscript should be provided with an English Abstract of about 50–70 words, reporting concisely on the objective and results of the paper. The Abstract is followed by the Mathematical Subject Classification – in case the author (or authors) give the classification codes – then the keywords (no more than five). References should be grouped at the end of the paper in numerical order of appearance. Author’s name(s) and initials, paper titles, journal name, volume, issue, year and page numbers should be given for all journals referenced.

The journal prefers the submission of manuscripts in L^AT_EX. Authors should prefer the $\mathcal{A}\mathcal{M}\mathcal{S}$ -L^AT_EX article class and are not recommended to define their own L^AT_EX commands. Visit our home page for further details concerning the issue how to edit your paper.

For the purpose of refereeing the manuscripts should be sent either to Balázs Tóth (Balazs.TOTH@uni-miskolc.hu) or György SZEIDL (Gyorgy.SZEIDL@uni-miskolc.hu).

The eventual supply of an accepted for publication paper in its final camera-ready form will ensure more rapid publication. Format requirements are provided by the home page of the journal from which sample L^AT_EX files can be downloaded:

<http://www.mech.uni-miskolc.hu/jcam>

These sample files can also be obtained directly (via e-mail) from Balázs TÓTH (Balazs.TOTH@uni-miskolc.hu), upon request.

One issue of the journal and ten offprints will be provided free of charge and mailed to the correspondent author. Since JCAM is an open access journal each paper can be downloaded freely from the homepage of the journal.

The Journal of Computational and Applied Mechanics is abstracted in Zentralblatt für Mathematik and in the Russian Referativnij Zhurnal.

Secretariat of the Vice-Rector for Research and International Relations, University of Miskolc
Responsible for publication: Prof. Dr. Tamás Kékesi
Published by the Miskolc University Press under the leadership of Attila Szendi
Responsible for duplication: Works manager Erzsébet Pásztor
Number of copies printed: 75
Put to the Press on November 20, 2015
Number of permission: TNRT 2015-380-ME

HU ISSN 1586-2070

A Short History of the Publications of the University of Miskolc

The University of Miskolc (Hungary) is an important center of research in Central Europe. Its parent university was founded by the Empress Maria Teresia in Selmecebánya (today Banská Štiavnica, Slovakia) in 1735. After the first World War the legal predecessor of the University of Miskolc moved to Sopron (Hungary) where, in 1929, it started the series of university publications with the title *Publications of the Mining and Metallurgical Division of the Hungarian Academy of Mining and Forestry Engineering* (Volumes I.-VI.). From 1934 to 1947 the Institution had the name Faculty of Mining, Metallurgical and Forestry Engineering of the József Nádor University of Technology and Economic Sciences at Sopron. Accordingly, the publications were given the title *Publications of the Mining and Metallurgical Engineering Division* (Volumes VII.-XVI.). For the last volume before 1950 – due to a further change in the name of the Institution – *Technical University, Faculties of Mining, Metallurgical and Forestry Engineering, Publications of the Mining and Metallurgical Divisions* was the title.

For some years after 1950 the Publications were temporarily suspended.

After the foundation of the Mechanical Engineering Faculty in Miskolc in 1949 and the movement of the Sopron Mining and Metallurgical Faculties to Miskolc, the Publications restarted with the general title *Publications of the Technical University of Heavy Industry* in 1955. Four new series - Series A (Mining), Series B (Metallurgy), Series C (Machinery) and Series D (Natural Sciences) - were founded in 1976. These came out both in foreign languages (English, German and Russian) and in Hungarian.

In 1990, right after the foundation of some new faculties, the university was renamed to University of Miskolc. At the same time the structure of the Publications was reorganized so that it could follow the faculty structure. Accordingly three new series were established: Series E (Legal Sciences), Series F (Economic Sciences) and Series G (Humanities and Social Sciences). The latest series, i.e., the series H (European Integration Studies) was founded in 2001. The eight series are formed by some periodicals and such publications which come out with various frequencies.

Papers on computational and applied mechanics were published in the

Publications of the University of Miskolc, Series D, Natural Sciences.

This series was given the name Natural Sciences, Mathematics in 1995. The name change reflects the fact that most of the papers published in the journal are of mathematical nature though papers on mechanics also come out.

The series

Publications of the University of Miskolc, Series C, Fundamental Engineering Sciences

founded in 1995 also published papers on mechanical issues. The present journal, which is published with the support of the Faculty of Mechanical Engineering and Informatics as a member of the Series C (Machinery), is the legal successor of the above journal.



Journal of Computational and Applied Mechanics

Volume 10, Number 2 (2015)

Contents

Contributed Papers

László BARANYI, István PÁCZELT and György SZEIDL: Preface	105–112
Gabriella BOGNÁR and Zoltán CSÁTI: Numerical solution to boundary layer problem of non-Newtonian fluid flow over a moving surface	113–121
Edgár BERTÓTI: Comparative study of primal- and dual-mixed finite element models for cylindrical shells	123–146
Judit DUDRA and György SZEIDL: On the direct BEM formulation in the dual system of plane elasticity for orthotropic bodies	147–168
István ECSEDI and Attila BAKSA: Acceleration analysis of rigid body motion	169–181
Aurél GALÁNTAI: Always convergent methods for solving nonlinear equations	183–208
Róbert NAGY and Zsolt GÁSPÁR: Portable tent structure designs for flood protection	209–229
István PÁCZELT, Zenon MRÓZ and Attila BAKSA: Analysis of steady wear processes for periodic sliding	231–268